The role of the tumour suppressor *Nf1* in growth and metabolism of skeletal muscle cells

vorgelegt von
Dipl.-Biochem.
Julia Franke, geb. Grohmann
geb. in Bautzen

von der Fakultät III – Prozesswissenschaften
der Technischen Universität Berlin
zur Erlangung des akademischen Grades

Doktors der Naturwissenschaften
- Dr. rer. nat. -

genehmigte Dissertation

Promotionsausschuss:

Vorsitzender: Prof. Dr. Juri Rappsilber
Gutachter: Prof. Dr. Roland Lauster
Gutachter: Prof.Dr. Sigmar Stricker

Tag der wissenschaftlichen Aussprache: 21. November 2014

Berlin 2015

Diese Dissertation wurde in der Zeit vom 01.07.2010 bis zum 30.06.2014 in der Arbeitsgruppe von Prof. Dr. Stefan Mundlos am Max-Planck-Institut für Molekulare Genetik in Berlin angefertigt.

1. Gutachter: Prof. Dr. Roland Lauster
Institut für Biotechnologie
Medizinische Biotechnologie
Technische Universität Berlin
Gustav-Meyer-Allee 25
13355 Berlin

Tel.: 030/31472090
E-Mail: roland.lauster@tu-berlin.de

2. Gutachter: Prof. Dr. Sigmar Stricker
Institut für Chemie und Biochemie
Abteilung Biochemie
Freie Universität Berlin
Thielallee 63
14195 Berlin

Max-Planck-Institut für Molekulare Genetik
Ihnestraße 63-73
14195 Berlin

Tel.: 030/84131267
E-Mail: strick_s@molgen.mpg.de

Eidesstattliche Erklärung

Hiermit erkläre ich an Eides statt, dass ich die vorliegende Arbeit selbst angefertigt und keine anderen, als die hier angegebenen Hilfsmittel und Literaturquellen verwendet habe. Ich versichere, dass ich diese Arbeit weder in dieser noch in einer anderen Form bei einer anderen Prüfungsbehörde eingereicht habe.

Die hier vorgestellten Ergebnisse wurden noch nicht im Rahmen einer Publikation veröffentlicht.

Berlin, 31. Juli 2014

Table of contents

Chapter	Title		Page
1.	**Introduction**		**1**
1.1	Neurofibromatosis I is a multi-organ syndrome		1
	1.1.1	Neurofibromatosis I is a common genetic disorder	1
	1.1.2	Neurofibromatosis I affects multiple organs	1
	1.1.3	Neurofibromatosis I is caused by a loss of *NF1*	3
	1.1.4	The *NF1* gene product is a negative regulator of RAS signaling	3
	1.1.5	The Nf1Prx1 model recapitulates symptoms of neurofibromatosis I	5
1.2	Skeletal musculature is a multi-functional tissue		7
	1.2.1	Skeletal musculature is the biggest organ of the body	7
	1.2.2	Skeletal musculature consists of highly regular structures	8
	1.2.3	There are two main ways of energy production in skeletal muscles	11
	1.2.4	Skeletal muscle development is a multi-step process	13
1.3	Thesis objectives		16
2.	**Materials**		**17**
2.1	Instruments		17
2.2	Consumables		18
2.3	Chemicals		19
2.4	Molecular biology and biochemistry kits		22
2.5	Enzymes		22
2.6	Media and supplements for cell culture		22
2.7.	Buffers and solutions		23
2.8	Oligonucleotides		26
2.9	Size markers for analyses		29
2.10	Antibodies		29
2.11	Animals		31
2.12	Computer Software		32

3. Methods 33

3.1 Molecular biological methods 33
3.1.1 Genomic DNA isolation 33
3.1.2 Total RNA isolation from muscle tissue 33
3.1.3 Total RNA isolation from enriched osteocytes 34
3.1.4 Generation of cDNA 35
3. 1.5 Polymerase chain reaction (PCR) on genomic DNA 35
3.1.6 Semi-quantitative polymerase chain reaction (PCR) on genomic DNA 37
3.1.7 Quantitative polymerase chain reaction (qPCR) on cDNA 38
3.1.8 Agarose gel electrophoresis 38
3.1.9 Microarray gene expression analysis 39
3.1.10 Generation of RNA antisense probes for WM-ISH 39
3.1.11 RNA whole mount *in situ* hybridisation (WM-ISH) 41
3.2 Primary cell culture 41
3.2.1 Isolation of primary myoblasts and fibroblasts 41
3.2.2 Culturing of primary myoblasts and fibroblasts 42
3.2.3 Immunocytochemistry (ICC) of primary cells 43
3.2.4 Isolation, culturing and ICC of primary myotubes 43
3.3 Biochemical methods 44
3.3.1 Protein isolation from muscle tissue 44
3.3.2 Determination of protein concentration 44
3.3.3 SDS-PAGE according to Laemmli 44
3.3.4 Western blot (WB) 45
3.4 Histology 46
3.4.1 Animal sample preparation 46
3.4.2 Cryo sectioning of limb tissue 46
3.4.3 Immunohistochemistry (IHC) 47
3.4.4 Sdh staining 49
3.4.5 Single fibre isolation and processing 50
3.4.6 Sample preparation for electron microscopy on muscle tissue 51
3.4.7 Sample preparation for electron microscopy on cortical bone 52
3.5 Statistical evaluation 53
3.5.1 Standard error calculation 53

3.5.2 Student's t-test 53
3.5.3 ANOVA analysis for microarray evaluation 54

4. Results 55

4.1 Generation of knockout mice for a skeletal muscle specific loss of *Nf1* 55
4.1.1 mTmG mice show tissue specific activity of Lbx1_Cre, Myf5_Cre and HSA_Cre 55
4.1.2 *Nf1* is excised by Cre mediated recombination in Nf1Myf5, Nf1Lbx1 and Nf1HSA 56
4.2 Loss of *Nf1* results in a growth defect of skeletal muscles 59
4.2.1 Embryonic muscles of *Nf1* knockout mice do not show a growth defect 59
4.2.1.1 Embryonic Nf1Myf5 mice show no muscle patterning or growth defect 59
4.2.1.2 Embryonic myoblasts of the Nf1Lbx1 model do not show a reduced fusion rate 61
4.2.2 Fetal muscles of *Nf1* knockout mice show a growth defect 61
4.2.2.1 The size of fetal muscles in Nf1Lbx1 and Nf1Myf5 is decreased 61
4.2.3 Postnatal muscles of *Nf1* knockout mice show a growth defect 63
4.2.3.1 The size of muscles is decreased in NfMyf5 mice at P21 63
4.2.3.2 Size reduction of Nf1Myf5 muscles is not caused by a decrease in myofibre number 64
4.2.3.3 Size reduction of Nf1Myf5 muscles is caused by a decrease in myofibre size 65
4.2.3.4 Myofibre size reduction in Nf1Myf5 mice is dependent on the myofibre type 67
4.2.3.5 Nf1Myf5 do not show characteristics of degeneration and regeneration processes 68
4.2.3.6 Muscle and myofibre size reduction was persistent throughout age in Nf1Myf5 mice 69
4.2.3.7 The Nf1Myf5 muscle phenotype is progressive with age of mice 70
4.2.3.8 Fast twitch myofibre size reduction is due to a decreased myonuclear domain 71
4.2.3.9 Postnatal Nf1HSA mice do not show muscle size reduction 73

4.3 Loss of *Nf1* leads to defects in Pax7$^+$ cell development and differentiation 75
4.3.1 Loss of *Nf1* leads to altered numbers of Pax7$^+$ cells in Nf1Myf5 75
4.3.2 Fetal Pax7$^+$ cells of Nf1Myf5 mice show altered proliferation behaviour 77
4.3.3 Nf1Myf5 myofibres show characteristics of a disturbed differentiation process 79
4.4 Loss of *Nf1* leads to a metabolic muscle defect in postnatal mice 81
4.4.1 Loss of *Nf1* results in a switch of myofibre specific gene expression and metabolism 81
4.4.1.1 Nf1Myf5 mice show a switch in myofibre specific protein and gene expression 81
4.4.1.2 Nf1Myf5 mice show a shift towards mitochondrial oxidative metabolism 83
4.4.1.3 Nf1Myf5 mice show an increase in fatty acid beta oxidation 83
4.4.2 Loss of *Nf1* causes an increased activity of Ras downstream pathways in Nf1Myf5 85
4.4.3 *Nf1* depletion in osteocytes leads to defects similar to *Nf1* depletion in muscles: Evidence for a pleiotropic effect 86

5. Discussion 91

5.1 Generation of knockout mice for a muscle cell specific loss of *Nf1* 91
5.1.1 Distinction of muscle specific models to the Nf1Prx1 model 91
5.1.2 Cell specificity of the investigated mouse models 91
5.1.3 Critical evaluation of investigated mouse models 92
5.2 Loss of *Nf1* results in a growth defect of skeletal muscles 93
5.2.1 Embryonic muscles do not show a growth defect at E14.5 93
5.2.2 Fetal muscles show first signs of growth retardation at E18.5 94
5.2.3 Postnatal muscles of Nf1Myf5 show a growth reduction at P21 94
5.2.4 Adult muscles of Nf1Myf5 show a progressive size reduction at P156 95
5.2.5 The size reduction in Nf1Myf5 is due to a fibre size reduction 95
5.2.6 Postnatal Nf1HSA mice do not show a muscle size reduction 96
5.3 Loss of *Nf1* leads to defects in Pax7$^+$ cell development 96
5.4 Loss of *Nf1* leads to metabolic muscle defects 98

5.4.1 Loss of *Nf1* results in an alteration of fibre specific gene expression 98
5.4.2 Loss of *Nf1* results in a shift towards mitochondrial oxidative metabolism 99
5.4.3 The putative influence of metabolic shift on muscle mass and myogenesis in Nf1Myf5 100
5.5 Loss of *Nf1* causes an increased activity of Ras downstream pathways 103
5.6 *Nf1* depleted osteocytes show a pleiotropic effect to *Nf1* depleted muscles 105

6. Summary 107
Zusammenfassung (German version) 108

7. References 109

8. Abbreviations 127

9. Appendix 130
9.1 Acknowledgements 130
9.2 Publications 131

1. Introduction

The studies of this work are performed to elucidate the role of the neurofibromin protein in skeletal muscle cells. The results shall contribute to the general understanding of muscle cell development and reveal molecular mechanisms causing muscle defects associated with the disorder neurofibromatosis I.

1.1 Neurofibromatosis I is a multi-organ syndrome

1.1.1 Neurofibromatosis I is a common genetic disorder

Between two and three million people worldwide suffer from the hereditary disorder neurofibromatosis I (also called NF1, peripheral neurofibromatosis or von Recklinghausen disease). Its prevalence is one in 3000 to 3500 born children (Zhu et al., 2001). It is one of the most common hereditable disorders worldwide and affects more individuals than haemophilia (one in 5000 born boys) or Duchenne muscular dystrophy (one in 3600 born boys). Furthermore, NF1 is esteemed to be the most frequent hereditary tumour predisposition syndrome (Wimmer, 2005). However, there is no cure for NF1, which has tremendous consequences for the individual patient, society and health care system. Therapeutic management of NF1 is multidisciplinary (requires several specialists) and the average costs of treatment are about 970 € per affected individual per year (Wolkenstein et al., 2000).

The term neurofibromatosis is derived from its most obvious symptomatic manifestation: neurofiromas (Fig. 1.1). Friedrich Daniel von Recklinghausen coined the term neurofibroma in 1882 to describe a benign tumour of peripheral nerves (Dimitrova et al., 2008). Neurofibromas have a high tendency to become malignant. Therefore NF1 is defined as a tumour predisposition syndrome. Additionally, patients show developmental abnormalities in several organs that usually appear in childhood. Hence, NF1 is also defined as developmental disorder (Larizza et al., 2009).

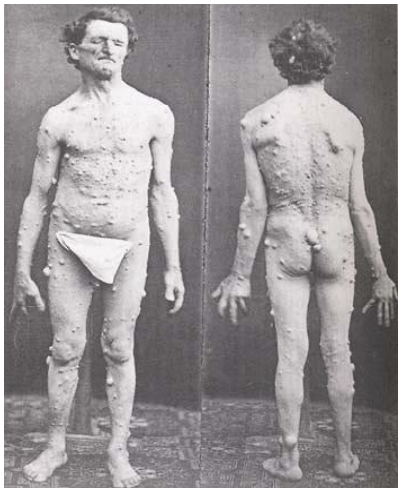

Fig. 1.1 Neurofibromatosis I patient
The photographs show the first patient described by von Recklinghausen in 1882. The patient displays numerous neurofibromas under his skin (Dimitrova et al., 2008).

1.1.2 Neurofibromatosis I affects multiple organs

NF1 is characterised by a broad spectrum of syndromes whereby skin and nervous system are affected the most. There is a very high variability in phenotypic expression and severity between patients.

Tab. 1.1 NHI diagnostic criteria for NF1 (Ferner et al., 2007)

- 6 or more café au lait macules (>0.5 cm in children or >1.5 cm in adults)
- 2 or more cutaneous/subcutaneous neurofibromas or one plexiform neurofibroma
- Axillary or groin freckling
- Optic pathway glioma
- 2 or more Lisch nodules (iris hamartomas seen on slit lamp examination)
- Bony dysplasia (sphenoid wing dysplasia, bowing of long bone ± pseudarthrosis)
- First degree relative with NF1

Over 50 % of patients are affected mildly. About 40 % have medical problems related to the disorder at some point during their life time. And only some of these require medical or surgical intervention (North, 1998). For diagnosis of NF1 seven criteria (Tab. 1.1) have been summarized by the NIH, two or more of which have to be fulfilled (Ferner et al., 2007). Prominent symptoms are, among others, characteristic skin lesions in the form of hyper pigmentation spots (café-au-lait maculae and freckling). However, the most common clinical manifestation is the development of neurofibromas (Cichowski and Jacks, 2001). Neurofibromas are benign tumours arising from the peripheral nerve sheet (Dimitrova et al., 2008). They consist of 60 - 80 % Schwann cells but also contain fibroblasts, fibroblast-derived perineurial cells, mast cells and axons (Peltonen et al., 1988; Krone et al., 1986). Neurofibromas have been subdivided into two broad categories: dermal and plexiform. Dermal neurofibromas are associated with a single peripheral nerve, while plexiform neurofibromas are associated with multiple nerve bundles (Yamamoto, 2004). About 10 % of the plexiform neurofibromas undergo transformation into a malignant peripheral nerve sheath tumour (MPNST; Mautner et al., 2003). Furthermore, NF1 patients are prone to develop a range of other tumours such as gliomas and pheochromocytomas, and may develop myeloid leukaemia. Although tumours are a relatively constant finding, a wide variety of skeletal deformations that occur in association with NF1 at a lower frequency had been described. These include scoliosis, vertebral dysplasia, short stature, sphenoid wing dysplasia and pseudarthrosis or bowing of long bones (Stevenson et al., 1999; Alwan et al., 2005). An alteration in bone structure and mineralisation is thought to cause long bone bowing, a high fracture risk and the development of pseudarthrosis (Stevenson et al., 1999; Alwan et al., 2005; Schindeler and Little, 2008; Riccardi, 2010). Less common abnormalities of the skeleton include osteosclerosis, lytic bone lesions, local overgrowth, abnormalities of the rib cage, genu varum/valgum, absence of the patella and syndactyly (Kolanczyk et al., 2007; Ruggieri et al., 1999). Skeletal deformations severely impair the mobility of NF1 patients. Additionally, a general tiredness (Samuelsson and Riccardi, 1989) and peripheral muscular weakness (Stevenson et al., 2012) aggravate patients' life. Decreased muscular force production has also been recently described in patients (Souza et al., 2009; Johnson et al., 2010; Johnson et al., 2012); and tibial lesions have been correlated to a reduced muscle mass (Fig. 1.2) in the lower leg (Stevenson et al., 2005; Kossler

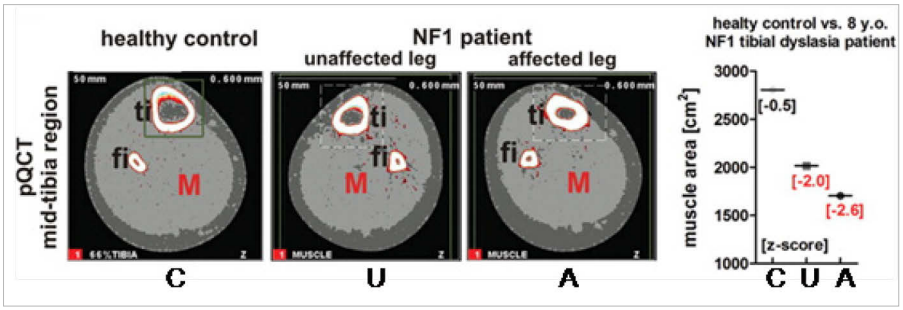

Fig. 1.2 Reduced muscular size in a neurofibromatosis I patient
Reduced muscle cross sectional area (light grey shading, red M) in the lower hind limb of an 8 - year - old NF1 patient with unilateral tibial dysplasia. Right panel: muscle cross sectional area measured with pQCT in the affected and unaffected extremity of the patient, and in the extremity of a healthy control. Muscle area in both the tibial dysplasia - affected leg and unaffected leg is reduced compared to the control (Kossler et al., 2011). C = control, U = unaffected, A = affected, ti = tibia, fi = fibula.

et al., 2011). Young children with NFl may demonstrate poor muscle tone and motor coordination, including impairment of balance and manual dexterity (North, 1998). Furthermore, general problems with gross motor coordination, falling and ataxia have been reported (Tonsgard, 2006). Whereas a lot of research is performed on NF1 tumourgenesis, the correlation between lesions of the neuronal system, muscles and skeleton has not been evaluated yet.

1.1.3 Neurofibromatosis I is caused by a loss of *NF1*

Neurofibromatosis I is an autosomal dominant hereditable syndrome. It is caused by mutations in the gene *NF1* (chromosome 17q11.2). This includes nonsense, missense or splice site mutations caused by base pair or sequence deletions, insertions and substitutions, respectively. In 90 % of all cases these mutations lead to a loss-of-function of the *NF1* gene product neurofibromin (Friedman et al., 1999). So far, no correlation could be found between the type of mutation and the expression of NF1 symptoms. It has been theorized that some of the symptoms emanate from haploinsufficency from the mono-allelic loss of *NF1* present in all patients, others are caused by second-hit mutations and loss of heterozygosity in somatic cells (Cichowski and Jacks, 2001). Neurofibromatosis I patients are heterozygous for a *NF1* mutation whilst homozygous loss-of-function leads to lethal cardiovascular malformations at early stages in development (Ismat et al., 2006). Half of the NF1 patients inherited the mutated allele from one of their parents (Friedman et al., 1999) and the rest carry *de novo* mutations. The high frequency of new mutations is due to the large size of the *NF1* gene. It is about ten times as large as an average gene, which makes it predisposed to mutation hotspots. *NF1* is spanning approximately 287 kb and consisting of 60 exons. According to the symptoms of neurofibromatosis I, *NF1* is considered to be a tumour suppressor gene as well as a histogenesis control factor (Hölzel et al., 2010; Riccardi, 2000).

1.1.4 The *NF1* gene product is a negative regulator of RAS signalling

The *NF1* gene encodes for the cytoplasmic protein neurofibromin. It has been found attached to the plasma membrane (Malhotra and Ratner, 1994), attached to the actin cytoskeleton and in the cell nucleus (Li et al., 2001). Although it is ubiquitinously expressed, it is mainly found in neurons, glia cells, Swann cells and melanocyts (Stocker et al., 1995). Furthermore its expression has been detected in skeletal muscle cells (Gutmann et al., 1991).
The neurofibromin protein is composed of 2818 amino acids. In man and mouse, the sequences of neurofibromin are identical in more than 98 % of all amino acids (Bernards et al., 1993). Its molecular weight is about 220 kDa (Marchuk et al., 1991). Four functional domains were indentified in neurofibromin (Fig. 1.3): a cysteine-serine rich domain (CSRD), a GTPase activating protein domain (GAP), a pleckstrin homologue like domain (PH) and a sec14 domain (Sec) (Xu et al., 1990; Aravind et al., 1999; Tokuo et al., 2001; D'Angelo et al., 2006). The CSRD domain contains constitutive phosphorylated amino acid residues necessary for the stability of neurofibromin. It was suggested, that the CSRD domain is phosphorylated by protein kinase A (PKA; Izawa et al., 1996; Tokuo et al., 2001). The biological relevance of this modification

remains unknown. The Sec and PH domains are thought to act as a functional unit. The activity of the Sec domain seems to be regulated by binding of a phospholipid ligand to the PH domain, and thus both domains potentially play a role in the membrane anchorage of neurofibromin (D'Angelo et al., 2006). The GTPase activating protein (GAP) domain shows homologies to the functional domains in the four known GTP proteins: Ira1, Ira2 (S. cerevisiae), GAP1 (D. melanogaster) and p120RASGAP (mammals; Dasgupta and Gutmann, 2003). *In vitro* and *in vivo* studies confirmed a GAP activity of neurofibromin towards the RAS p21 proteins (Xu et al., 1990).

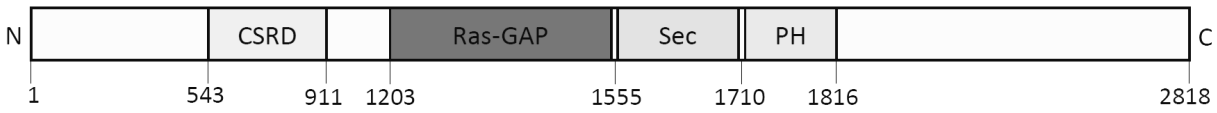

Fig. 1.3 Protein domains of neurofibromin
The schematic diagram represents a scheme of the location of the four protein domains of neurofibromin. The numbers below the scheme refer to the amino acids from the N-terminal (N) end to the C-terminal (C) end (Wegener 2009, Diplomarbeit).

RAS is a monomeric small guanine nucleotide binding protein (G protein) and plays an essential role in the transduction of extracellular signals to the cell nucleus. Signal transduction is initiated by the binding of a growth factor to its cognate transmembrane receptor. RAS thereby acts as a molecular switch regulating cellular processes like differentiation, proliferation, growth, apoptosis and senescence (Marshall, 1995b; Clark and Hynes, 1996; Serrano et al., 1997; Bonni et al., 1999; Gille and Downward, 1999). RAS can be present in two states: an inactive (bound to GDP/guanosine diphosphate) or an active (bound to GTP/guanosine triphosphate) state (Fig.1.4). Guanine nucleotide exchange factors (GEFs) activate RAS by facilitating the dissociation of GDP from RAS, which can then bind to a GTP molecule. On the other hand, GTPase activating proteins, like neurofibromin, enhance the hydrolization of GTP to GDP by RAS proteins, thus silencing RAS signalling (Lindquist, 2011; Martin et al., 1990; Cichowski and Jacks, 2001). Mutations in *NF1* lead to a loss of function of neurofibromin, therefore silencing of RAS is diminished. This can have tremendous consequences for a cell and the whole organism such as increased cell proliferation and predisposition to tumour formation.

Fig. 1.4 Schematic diagram of the RAS activation and deactivation cycle
RAS proteins cycle between an inactive (GDP - bound) and an active (GTP - bound) state. RAS is activated by guanine nucleotide exchange factors (GEFs), which stimulate the exchange of GDP for GTP, and inactivated by GTPase activating proteins (GAPs) that bind to RAS and stimulate its intrinsic GTPase activity (Lindquist, 2011).

The GTP-bound RAS activates several intracellular pathways. The most prominent one is the MAPK (mitogen-activated protein kinase) signalling pathway, a serine/threonine phosphorylation cascade. RAS directly activates a serine/threonine kinase (MAP-kinase-kinase-kinase, MAPKKK), which then phosphorylates a MAP-kinase-kinase (MAPKK), which in turn activates a MAP-kinase (MAPK; Fig. 1.5). The phosphorylated MAP-kinase is able to interact with several transcription factors (e.g. c-MYC, c-FOS, CREB, NF-kB),

with the elongation factors eIF4E and MAPs (microtubule associated proteins) as well as other proteins (Steelman et al., 2011) involved in proliferation, differentiation and survival processes. There are three known MAP cascades. Mitogenic activation is implemented via RAF-MEK1/2-ERK1/2, that regulate growth, proliferation and differentiation. Cell stress is activating the p38 MAPKα/β pathway leading to inflammatory responses, apoptosis, differentiation or growth. Stress, UV light or an osmotic shock can activate the third cascade: the JNK (cJun N-terminal kinase) pathway. The RAS cascades (Fig. 1.5) are initiated by signalling ligands like EGF (epidermal growth factor) or FGF (fibroblast growth factor). They bind to the extracellular domain of their specific plasma membrane receptor and induce the dimerisation of this receptor. Thereby a phosphorylation of intracellular receptor tyrosine residues and an interaction with adaptor molecules (SHC, SHP-2 and GRB2) is initiated. GRB2 binds to SOS1 and forms a GTP bound active RAS complex. This complex interacts with the first protein kinase RAF. The kinase gets phosphorylated and in turn activates MEK (MAP/ERK kinase). MEK phosphorylates both forms of ERK (extracellular signal regulated kinase), ERK1 (p44) and ERK2 (p42). The cascade ends by signal transduction to the nucleus where the transcription of target genes is regulated (Jorge et al., 2009).

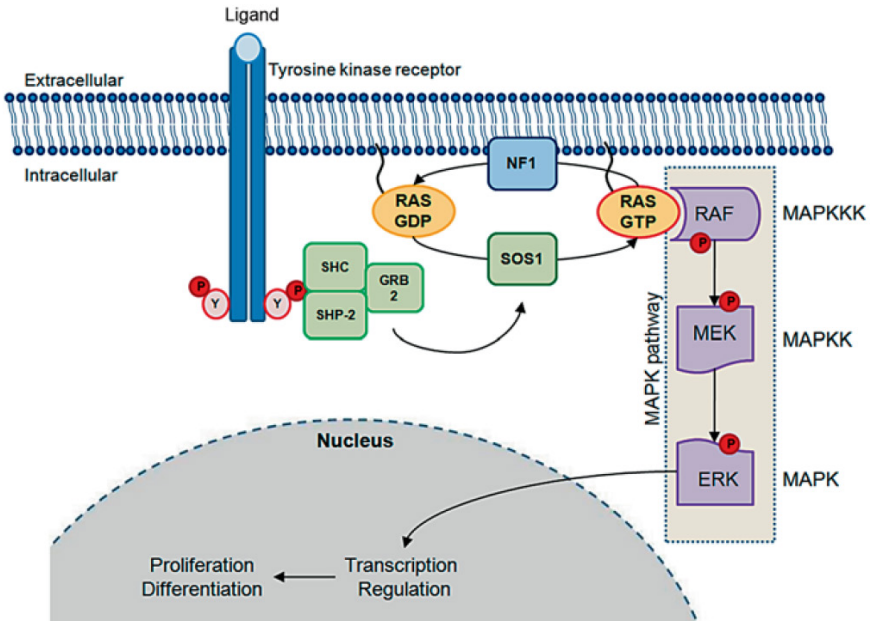

Fig. 1.5 Schematic diagram of the RAS signal transduction pathway
Growth factors bind to a receptor tyrosine kinase (RTK) resulting in receptor dimerisation and binding of adaptor molecules. The adaptor molecules initiate interaction of the guanine nucleotide exchange factors (GEF) SOS1 with RAS leading to a three phasic phosphorylation cascade (RAF-MEK-ERK). At the end transcription factors get activated by ERK leading to regulation of cellular processes like proliferation and differentiation. SHC = Src homology 2 domain containing, SHP-2 = Src homology region 2 phosphatase 2, GRB2 = growth factor receptor bound protein 2, SOS1 = son of sevenless 1, RAS = rat sarcoma, RAF = rapid fibrosarcoma, MEK = MAP/ERK-Kinase, ERK = extracellular signal-regulated kinase (Jorge et al., 2009).

1.1.5 The Nf1Prx1 model recapitulates symptoms of neurofibromatosis I

NF1 patients show increased levels of RAS activation through the loss of neurofibromin function (Bollag et al., 1996; Feldkamp et al., 1999). Studying neurofibromatosis I is difficult as disease severity and symptoms vary greatly between patients. Some of the symptoms emanate from *NF1* haploinsufficency, others are caused by second-hit mutations and loss of heterozygosity (Cichowski and Jacks, 2001). Depending on the cell lineages affected and the point in development when the second hit occurs patients can develop very different symptoms. Some of

the skeletal symptoms have been shown to be due to a loss of heterozygosity of *NF1*. Genetic analysis revealed bi-allelic inactivation of the *NF1* gene in pseudarthrosic tissue from NF1 patients (Stevenson et al., 2006) thus providing a starting point for studying musculoskeletal symptoms with the help of a mouse model.

Homozygous deletions of *Nf1* in the mouse model ($Nf1^{-/-}$) results in early embryonic lethality due to a cardiovascular defect (Brannan et al., 1994). However, heterozygous *Nf1* mice ($Nf1^{+/-}$) are phenotypical variable and only display few symptoms of neurofibromatosis I (Rizvi et al., 1999). Therefore both, $Nf1^{-/-}$ and $Nf1^{+/-}$, are not suited for the recapitulation of neurofibromatosis I. To investigate the role of *Nf1* in the development of skeletal elements of the limbs, a Cre/loxP based conditional knockout approach (Lobe and Nagy, 1998) was used which allows a time and tissue specific gene deletion. In this knockout technique a gene flanked (floxed gene) by the recognition sites (loxP sequences) of the enzyme Cre recombinase will be permanently excised from the genomic DNA by the Cre recombinase as soon as Cre starts being expressed. For the NF1 model, Cre recombinase transcribed under the control of a specific Prx1 limb enhancer was chosen (Kolanczyk et al. 2007). Prx1 is expressed in the early limb bud mesenchyme (Logan et al., 2002) resulting in inactivation of *Nf1* in all mesenchymal cells of the developing limb. To create the subject of study, two mouse strains have been crossed. The first strain carried two loxP sites in each of the *Nf1* alleles ($Nf1^{flox/flox}$). These sites have been placed before exon 41 and after exon 42 of *Nf1* (Zhu et al., 2001) as exon 41 is essential for Nf1 function (Brannan et al., 1994). The second strain carried a genomic construct with the Cre recombinase gene under control of the Prx1 enhancer ($Prx1^{Cre}$; Logan et al., 2002). By crossing of a homozygous $Nf1^{flox/flox}$ and a transgene $Nf1^{flox/+}$; $Prx1^{Cre}$ mouse exon 41 and 42 of *Nf1* have been excised in the offspring (Nf1Prx1). The first recombination could be seen in mesenchymal cells of Nf1Prx1 at 9.5 dpc (E9.5). Affected mesenchymal cell descendents are osteoblasts, chondrocytes, osteoclasts, bone marrow derived endothelial cells and skeletal muscle cells (Kolanczyk et al., 2007; Kossler et al., 2011). Similar to NF1 patients, Nf1Prx1 mice showed bowing of the tibia and diminished growth (Fig. 1.6A). Tibial bowing was caused by decreased stability of the cortical bone due to a high degree of porosity, decreased stiffness and reduction in the mineral content as well as hyperosteoidosis. Accordingly, osteoblasts showed an increase in proliferation and a decreased ability to differentiate and mineralize *in vitro*. Furthermore, Nf1Prx1 mice showed a fusion of the hip joints and other joint abnormalities which are not observed in neurofibromatosis I patients. Bone shaping and joint formation has been described to be dependent on load induction and muscle contraction (Sharir et al., 2011; Shwartz et al., 2012; Shwartz et al., 2013). Therefore skeletal muscle development was investigated in Nf1Prx1 as well. It was shown that *Nf1* gene

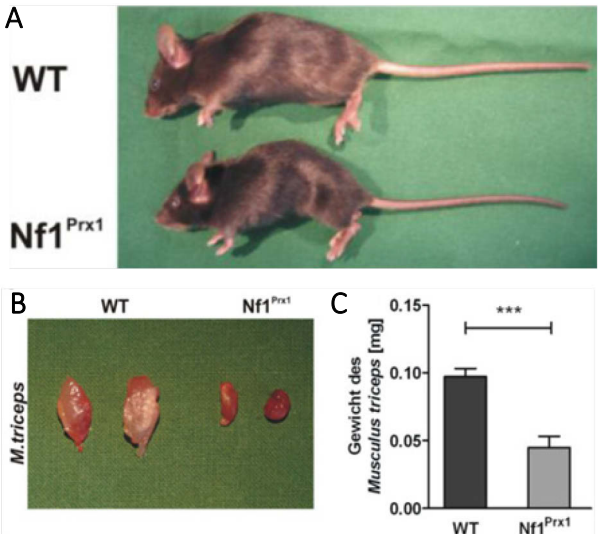

Fig. 1.6 The Nf1Prx1 mouse shows short stature and muscle size reduction

A Nf1Prx1 mice are smaller in size as control animals (WT) at P56. **B** Muscle size is reduced in Nf1Prx1 mice in comparison to control animals (WT) as shown for isolated triceps muscles of left and right forelimbs. **C** The reduction of muscle weight is significant for Nf1Prx1 animals in comparison to controls ($p \leq 0{,}001$) (modified after Kossler 2010, Dissertation).

inactivation in the early limb bud mesenchyme resulted in muscle dystrophy characterized by fibrosis, decreased muscle size and muscle weight (Fig. 1.6B and C) as well as a reduced number of muscle fibres and a decreased muscular force. This was caused by an early defect in myogenesis affecting the terminal differentiation of myoblasts between E12.5 and E14.5. The amount of muscle connective tissue increased starting from E14.5 when an enhanced proliferation of fibroblasts could be seen. These changes were accompanied by excessive Ras/Mapk pathway activation in connective tissue at E16.5. Additionally, muscle stem cells isolated from adult Nf1Prx1 mice showed impaired differentiation (Kossler et al., 2011). These results clearly demonstrated a requirement for neurofibromin for muscle formation and maintenance. This previously unrecognized function of *Nf1* might contribute to skeletal deformations and impaired fracture healing in NF1 patients. Furthermore, it may implicate an autonomous role for Nf1 in skeletal muscle cells. However, as *Nf1* is deleted in multiple cell species in Nf1Prx1 it is not possible to detect a putative muscle cell endogenous cause of the muscle defects. For elucidating the putative role of *Nf1* in skeletal muscle cells, more specific models need to be investigated.

1.2 Skeletal musculature is a multi-functional tissue

1.2.1 Skeletal musculature is the biggest organ of the body

Muscle is defined as soft tissue derived from the mesodermal layer of embryonic germ cells that can be found in most animals. The function of a muscle is to produce force and motion. This is realised by muscle cells that contract and thus changing cells length and shape. According to their function and anatomy there are three groups of muscles in vertebrates:

- smooth muscle
- cardiac muscle
- skeletal muscle

Smooth muscle is responsible for the contractility of hollow organs, e.g. stomach and intestines, as well as structures like blood vessels, bronchii and urethra; therefore responsible for the transport of e.g. food, blood and urine. Smooth muscle function is not under conscious control and therefore also termed “involuntary muscle”. Cardiac muscle is also an “involuntary muscle” found in the walls of the heart and is responsible for heart contractions. Unlike smooth muscle it is packed into highly regular arrangements of bundles and therefore called “striated”. Skeletal musculature is also “striated”. It can be found attached to bones via tendons and in contrast to the other muscles types, skeletal muscle is a “voluntary muscle” that is under the control of the somatic nervous system (Marieb and Hoehn, 2010; Schlossberg and Zuidema, 1997). Its function is the maintenance and changing of body posture as well as locomotion and movements of body parts. It comprises approximately 50 % of the body´s weight. Therefore, skeletal muscle constitutes the largest mass of cells in the body that have similar morphological and physiological properties (Kaneko et al., 1997). Skeletal muscles are considered to be organs and therefore their entirety forms the biggest organ of the body. Consequential, there are secondary functions like maintenance of body temperature through movement induced heat release or heat production and storage of nutrient reserves, especially proteins (Kettelhut et al., 1988). Furthermore, skeletal

muscle supports and shields internal organs and soft tissues and guards entrances and exits, for example of the digestive or urinary tracts. There are approximately 650 skeletal muscles in the human body (Poole, 1986) but an exact number is difficult to define as single muscles form groups, are directly connected and some muscles are not always present, such as palmaris longus. The first skeletal muscle cells are proposed to have evolved together with the nervous and digestive systems in a metazoan ancestor of ctenophores (comb jellyfish), cnidarians (jellyfish and polyps) and bilateria (Seipel and Schmid, 2005) about 700 millions of years ago (Erwin et al., 2011).

1.2.2 Skeletal musculature consists of highly regular structures

Each skeletal muscle consists of muscle tissue, nerve tissue, vascular tissue and connective tissue. Skeletal muscle cells (myofibres) are soft and fragile. The connective tissue provides them with support and protection and allows withstanding the forces of contraction. Connective tissue also provides pathways for the passage of blood vessels and nerves. Furthermore it transmits the force produced by the muscle cells to the tendons and cushions. It also serves as a reserve for nutrients and plays an important role in transmitting molecular signals to the myofibres (Sanes, 2003).

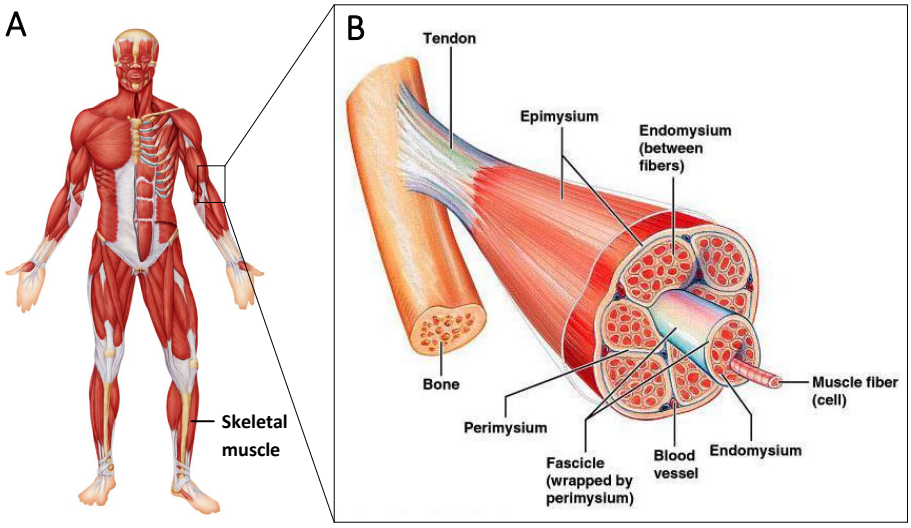

Fig. 1.7 Structure of skeletal musculature
A The human skeleton is covered by skeletal muscles (modified after: http://biology-pictures.blogspot.de). B Muscles are attached to bone via tendons. A muscle is encapsulated by epimysium and consists of fascicles (bundles of myofibres and endomysium) surrounded by perimysium (source: http://www.studyblue.com).

Skeletal muscles vary in size, shape and arrangement of fibres. They range from extremely tiny strands such as the stapedium muscle of the middle ear to large masses such as the muscles of the thigh. In some muscles the myofibres are parallel to the long axis of the muscle, in some they converge to a narrow attachment, and in some they are oblique. However, skeletal muscles share defined common structural characteristics. All muscles are attached to the skeleton via collagen-rich connective tissue units, the tendons (Fig 1.7). Muscles themselves are covered by a connective tissue layer called epimysium comprised primarily of collagen I and III. Within the epimysium hundreds, or even thousands, of myofibres are bundled together in fascicles and wrapped in another connective tissue covering called perimysium mainly composed of collagen I. The perimysium is the basic anchorage for tendons and contains blood vessels and nerves. Single myofibres are the basic unit of muscle tissue and are additionally encased by a connective tissue

layer called endomysium. Its primary components are collagens I and III (Gillies and Lieber, 2011). Between the endomysium and a myofibre is the muscle basement membrane, a connective tissue structure mainly composed of collagen IV and glycoproteins like Laminin A (Sanes, 2003). The side of the basement membrane facing the myofibres is directly linked to the myofibre membrane (sarcolemma), for example via integrin receptors or the dystroglycan complex, and it is referred to as the basal lamina (Gillies and Lieber, 2011). Although the basement membrane is considered to be distinct from endomysium, both are intimately connected to each other (Sanes, 2003).

A single myofibre is an elongated, multinucleated cell (syncytium) that may span the whole length of a muscle reaching a length of up to 40 cm (Lodish et al., 2000). The myofibre nuclei are located in the cell periphery whereas the cell centre is packed with compact bundles of contractile structures, the myofibrils. Myofibrils are arrays of repeating transverse units called sarcomeres, which are responsible for contraction. They consist of intercalated thick and thin filaments. Thin filaments are composed of skeletal actin with their ends embedded in a straining structure called Z disc. Thick filaments are bipolar filaments composed of myosin II. Myosin II molecules consist of two identical heavy chains and four light chains. Myosin II is a molecular motor that can move towards the ends of the thin filaments using energy form ATP hydrolysis thus producing contractions. These contractions are induced by increased cytosolic calcium ion (Ca^{2+}) concentrations. Ca^{2+} is stored in the sarcoplasmic reticulum, which surrounds myofibrils. Invaginations of the plasma membrane (sarcolemma), called transverse tubules, penetrate myofibres and built a connection to the myofibrils. Action potentials of neuromuscular junctions can travel down the transverse tubules and induce Ca^{2+} release from the sarcoplasmic reticulum thus inducing sarcomeric contractions. This mechanism is called electromechanical coupling (Walker and Schrodt, 1967).

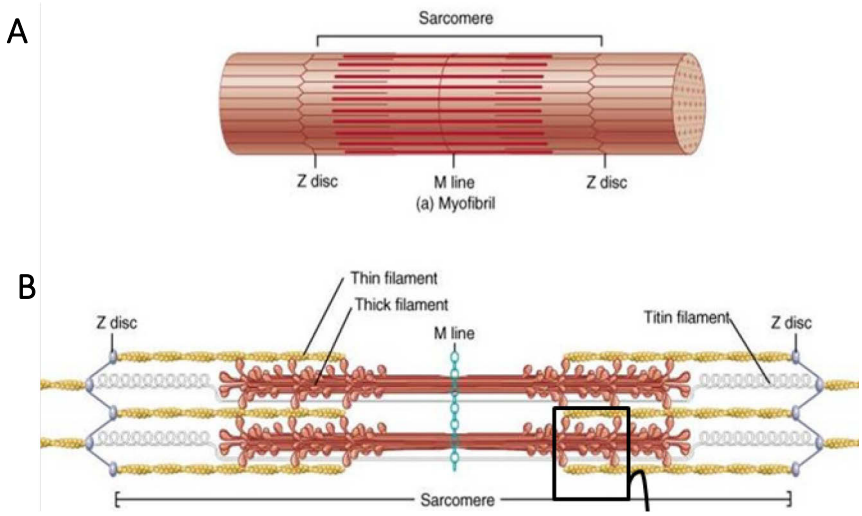

Fig. 1.8 Structure of a sarcomere
Sarcomeres are the transverse, functional units of a myofibril which in turn is the cytoplasmic contractile protein structure of a myofibre. **A** A scheme of a sarcomere shows its transverse structure composed of Z disc and M line. **B** A sarcomere consist of longitudinal thin (actin) and thick (myosin) filaments. Titin anchors myosin to the Z disc (source: http://trenchesofdis-covery.blogspot.de).

Adult muscle is composed of different myofibre types distinguished by their speed of contraction, fatigue resistance and metabolism. Different myofibre types allow the muscle to react to varying demands in performance. Myofibres can be divided into two main categories: type I or "slow twitch" fibres and type II or "fast twitch" fibres. The fast twitch fibres are further grouped according to their metabolism into three subcategories: fast oxidative or type IIa fibres, fast glycolytic or type IIb fibres and mixed type or IIx/d fibres (Galler et al., 1994).

Slow twitch fibres are mainly used to maintain posture while those with fast twitch characteristics are used in producing movement. Many of the contractile proteins within a fibre have multiple isoforms which are specific for different fibre types and correlate with their speed of contraction (Wigmore and Dunglison, 1998). So, each fibre type expresses a characteristic type of myosin heavy chain isoform that is responsible for their contractile characteristics. Slow twitch fibres express the slow myosin heavy chain isoform (MyHCI, encoded by the *Myh7* gene). Each fast twitch fibre subtype expresses a characteristic fast myosin heavy chain isoform (MyHCIIa, *Myh2* gene; MyHCIIx/d, *Myh1* gene or MyHCIIb, *Myh4* gene; Quiat et al., 2011). There are also fast twitch fibres that express a combination of the fast isoforms of myosin heavy chain (Galler et al., 1994).

Slow twitch fibres are sometimes called red fibres as they appear red due to high levels of myoglobin. Slow fibres tend to have more mitochondria and greater local capillary density. These fibres are more suited for endurance and are slow to fatigue because they use oxidative metabolism to generate ATP. But with each contraction they generate less force than fast twitch fibres. Fast twitch fibres are also called white fibres because of their low levels of myoglobin. Fast twitch fibres demonstrate a higher capability for electrochemical transmission of action potentials than slow fibres, as well as a quicker speed of Ca^{2+} release and uptake by the sarcoplasmic reticulum. The fast twitch fibres mainly rely on a short term, glycolytic system for energy transfer and can contract and develop tension at two to three times the rate of slow twitch fibres. Fast fibres generate short bursts of strength or speed more effectively than slow fibres, and so fatigue more quickly. The metabolism of fast fibres can be both: glycolytic or oxidative. Type IIb fibres function almost exclusively using glycolytic metabolism and have very few mitochondria. Type IIx fibres have more mitochondria and can function using oxidative or glycolytic metabolism depending on the current demands of the muscle. Type IIa fibres have a high number of mitochondria and use oxidative metabolism; they are however less enduring and are able to produce more force than slow fibres.

Individual muscles have characteristic proportions of myofibre types according to their physiological needs. In some muscles fibre types are distributed in a graded fashion with a higher proportion of fast fibres in more superficial regions, e.g. triceps brachii (Condon et al., 1990). Muscles predominantly composed of type II fibres are called 'fast' muscles, e.g. the extensor digitorum longus, while muscles with larger amounts of type I fibres are referred to as 'slow' muscles, e.g. the soleus. It is believed that the fibre type composition of the individual muscles is already established during embryonic myogenesis. *In vitro* experiments showed that primary myofibres are primed to become slow twitch fibres and secondary myofibres preferentially become fast twitch fibres (Dunglison et al., 1999). *In vivo,* it has been observed that all primary fibres become slow twitch fibres first and that some fibres later transform into fast twitch fibres during the fetal phase of myogenesis (Wigmore and Dunglison 1998). However, muscles show a high degree of plasticity after birth. Myofibres have been observed to possess the ability to change their fibre type *in vivo* and *in vitro* (Quiat et al., 2011; Termin et al., 1989). Changes in innervation patterns and functional demands have been implicated in this process (Termin et al., 1989; Rana et al., 2008; Ingalls, 2004). Also, RAS signalling has been shown to be involved in nerve activity dependent regulation of fibre type specific gene expression (Murgia et al., 2000). Furthermore, Ca^{2+} dependent activation of NFAT signalling has been proposed to be a trigger of fibre type transformation (Delling et al., 2000; Mu et al., 2007).

1.2.3 There are two main ways of energy production in skeletal muscles

For muscular performance, energy is needed. The breakdown of ATP into ADP or AMP and inorganic phosphate is the predominant source of cellular energy used to drive enzymatic reactions and to maintain cellular homeostasis (Ryall, 2013). The body is not able to effectively store ATP, thus storages get used up within a few seconds. Therefore, it is necessary to continually create ATP. In general, there are two major ways to convert nutrients to energy:

- aerobic or oxidative metabolism (with oxygen)
- anaerobic metabolism (without oxygen)

These pathways can be further divided. Most often it is a combination of energy systems that supply the fuel needed for exercise (Wilmore and Costill, 2005). Substrate (fats, carbohydrates, and proteins) and oxygen availability, as well as energy demand, can dictate the pathways used for ATP generation (Ryall, 2013).

Aerobic (oxidative) metabolism

Aerobic metabolism fuels most of the energy needed for long duration activity. It uses oxygen to convert nutrients to ATP. This system is slower than the anaerobic systems because it relies on the circulatory system to transport oxygen to the working muscles before it creates ATP. Aerobic metabolism is used primarily during endurance exercise, which is generally less intense and can continue for long periods of time (Wilmore and Costill, 2005). Aerobic metabolism takes place in the mitochondria via oxidative phosphorylation (OXPHOS). At the cellular level, free fatty acids and glucose are broken down into CoA-SAc (Acetyl-coenzyme A) in the presence of oxygen, via beta oxidation or glycolysis (Fig. 1.9). CoA-SAc in turn, enters the tricarboxylic cycle (TCA, also called citric acid or Krebs cycle), resulting in the reduction of NAD^+ to NADH, which is used to drive complex I (NADH dehydrogenase), and the production of succinate, which is used to drive complex II (succinate dehydrogenase) of the mitochondrial electron transport chain to generate ATP (Ryall, 2013).

Anaerobic metabolism

In the absence of oxygen, glucose is shunted away from the OXPHOS pathway, and ATP is instead generated via anaerobic glycolysis, a process leading to the conversion of pyruvate into lactate, instead of CoA-SAc (Fig. 1.9). Glycolysis is an inefficient method of generating ATP, as each molecule of glucose generates a net gain of two ATP molecules; in the OXPHOS pathway, 32 to 36 molecules of ATP are generated. Although it is relatively inefficient, glycolysis provides a number of important advantages for cells, including the ability to rapidly generate ATP in response to acute changes in energy demand (Pfeiffer et al., 2001) as well as generating the necessary glycolytic intermediates for the biosynthesis of new macromolecules via the pentose phosphate pathway (Ryall, 2013). Glycolysis takes place in the cytoplasm and creates ATP exclusively from carbohydrates, with lactic acid being a by-product. It provides energy by the (partial) breakdown of glucose without the need for oxygen. Anaerobic metabolism produces energy for short high-intensity bursts of activity lasting no more than several minutes before the

lactic acid build-up reaches a threshold known as the lactate threshold. Constituting fatigue makes it difficult to maintain such intensity.

For the first seconds of intense exercise the ATP-CP energy pathway (also called the phosphate system) supplies energy. It is used for short bursts of exercise. This pathway does not require oxygen. It first uses up any ATP stored in the muscle and then it uses creatine phosphate (CP) to re-synthesize ATP until the CP runs out. After the ATP and CP are used the body will move on to either aerobic metabolism or glycolysis to continue to create ATP (Wilmore and Costill, 2005).

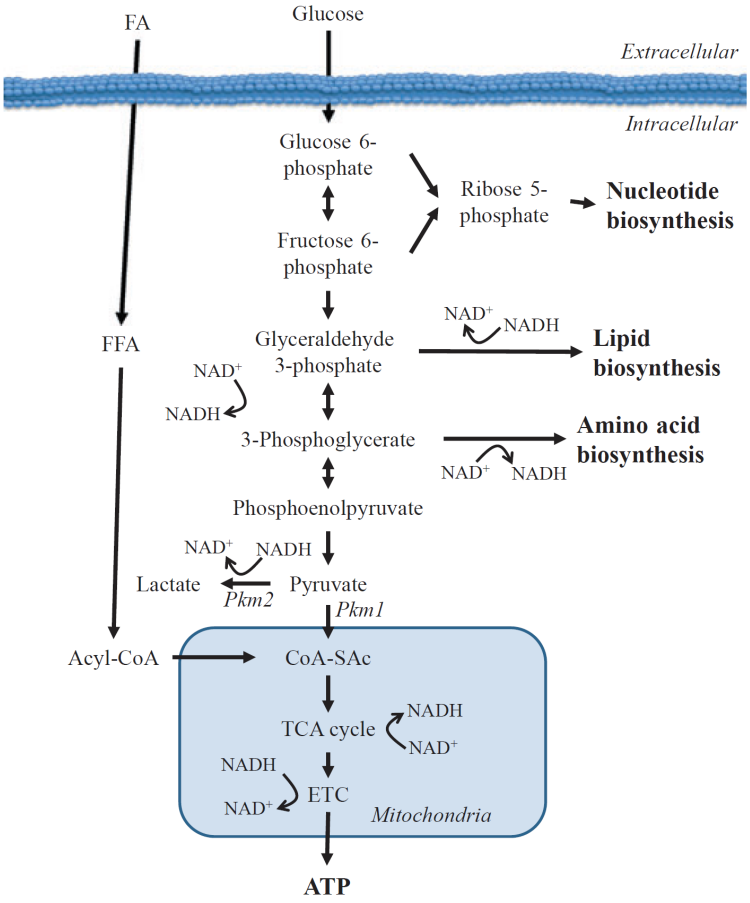

Fig. 1.9 The main metabolic pathways for ATP generation in skeletal muscle
Fatty acids and glucose serve as the two major energy substrates to generate ATP. Glutamine is a third substrate but is not explained here. Whereas both fatty acids and glucose can be used to generate ATP, only glucose can generate the glycolytic intermediates required for synthesis of nucleotides, lipids and amino acids. Nucleotides are generated from ribose 5-phosphate which is synthesized in the pentose phosphate pathway (also called the phosphogluconate pathway and the hexose monophosphate shunt). ETC = electron transport chain. ATP = adenosine triphosphate, FA = fatty acids, FFA = free fatty acids, Acyl-CoA = Acyl-coenzyme A, NAD^+ = nicotinamide adenine dinucleotide, NADH = reduced form of nicotinamide adenine dinucleotide, Pkm2 = muscle pyruvate kinase isoenzyme 2, Pkm1 = muscle pyruvate kinase isoenzyme 1, CoA-SAC = Acetyl-coenzyme A, TCA cycle = tricarboxylic cycle (Krebs cycle), ETC = electron transport chain (Ryall, 2013).

During exercise an individual is moving through all metabolic pathways. As exercise begins, ATP is produced via anaerobic metabolism. With an increase in breathing and heart rate, there is more oxygen available and aerobic metabolism begins and continues until the body cannot deliver oxygen quickly enough to generate ATP, and anaerobic metabolism sets in. Since this system is short-lived and lactic acid levels rise, the intensity cannot be sustained and the individual will need to decrease intensity. Nutrients get converted to ATP based upon the intensity and duration of activity, with carbohydrate as the main nutrient fuelling exercise of a moderate to high intensity, and fat providing energy during exercise that occurs at a lower intensity. As exercise intensity increases, carbohydrate metabolism takes over. It is more efficient than fat metabolism, but has limited energy stores. This stored carbohydrate (glycogen) can fuel about 2 hours of moderate to high level exercise. After that, glycogen depletion occurs (Wilmore and Costill, 2005).

1.2.4 Skeletal muscle development is a multi-step process

Skeletal musculature of vertebrates is divided into three groups according to its origin: craniofacial, epaxial and hypaxial musculature (Christ and Ordahl, 1995). Craniofacial muscles form from the unsegmented head mesoderm (Bothe and Dietrich, 2006). Musculature of the body comprises epaxial and hypaxial muscles and originate from the dermomyotome which is formed from the somites (Buckingham et al., 2003) whereby somites are segments of the paraxial mesoderm on either side of the neural tube and notochord of an embryo.
Development of muscles starts in the embryo and is termed myogenesis. There are four consecutive stages of myogenesis throughout life: embryonic, fetal, perinatal and adult myogenesis (Murphy and Kardon, 2011; Bentzinger et al., 2012) which will be explained in the following.

Embryonic myogenesis

In the embryonic stage of development the somites form along the anterior-posterior axis out of the paraxial mesoderm (bands of embryonic mesoderm adjacent to the notochord and neural tube). Molecular signals from the neural tube and adjacent tissue induce a polarisation within the somites (Fig. 1.10A). The ventral part of the somite, the sclerotome, will form the cartilage and bone of the vertebral column and ribs, whereas the dorsal part of the somite, the dermomyotome gives rise to the dermis of the back and to the skeletal muscles of the body and limbs (Buckingham et al., 2003). This process starts around day E8.5 in the mouse and is controlled by secreted signalling factors. Sonic hedgehog (Shh) is produced by the notochord and floor plate of the neural tube and induces the sclerotome at the medial side of the dermomyotome. Wingless proteins (Wnts) are expressed in the dorsal neural tube and the dorsal ectoderm. Together with Shh, Wnt signalling promotes myogenesis (Francis-West et al., 2003). Thus, the dermomyotome involutes to give rise to the dermatome (lateral, origin of the dermis) and the myotome (medial) which forms the epaxial musculature of the back. The dorso-lateral edge of the dermomyotome gives rise to muscles of the limbs, tongue, abdomen and diaphragm. Pre-myogenic cells from the dermomyotome are induced to delaminate by scatter factor and fibroblast growth factors (Fgfs) emanating from the lateral plate mesoderm and subsequently migrate distally into the limb bud. Scatter factor and Fgfs are also thought to control the migration process. The pre-myogenic cells express paired box 3 (Pax3) and the scatter factor receptor c-met which are needed for delamination. Furthermore, they express ladybird homeobox 1 (Lbx1) that is required for migration. The cells are not committed to myogenic differentiation as Bmps (bone morphogenic proteins) from the lateral plate mesoderm inhibit myogenic differentiation. Once within the limb bud, a subpopulation of pre-myogenic cells in the proximal limb bud starts to differentiate and express the myogenic regulatory genes myogenic factor 5 (Myf5) and myogenic differentiation factor 1 (MyoD; Buckingham et al., 2003; Fig.1.10B) These proteins are transcription factors of the myogenic regulatory factors (Mrf) family and markers of early myoblast differentiation (Ontell et al., 1995). The expression of MyoD pre-figures the prospective muscle pattern in the embryo. The onset of Mrf expression is regulated by growth factors produced by the limb bud. Cells committed to myogenesis are found towards the centre of the limb bud whilst the proliferative Pax3 expressing cells are found closer to the ectoderm. Bmp signalling from the ectoderm and

underlying mesenchyme, together with scatter factor in the mesenchyme and Fgfs in the AER (apical ectodermal rich), repress myogenic differentiation. After proliferation and initial differentiation, myoblasts differentiate terminally. This is marked by the expression of Mrf4 and Myogenin (transcription factors of the Mrf family). Terminally differentiated myoblasts fuse with each other to form multinucleated cells, embryonic myotubes. Myotubes express myosin heavy chain (MyHc) and skeletal actin and finally form myofibrils inside their cytoplasm (Duprez, 2002). In the following, further differentiated myoblasts fuse with multinucleated myotubes increasing their size. These myotubes give rise to the primary muscle fibres (myofibres; Fig. 1.10B). The appearance of these fibres is considered to be the end of embryonic myogenesis (Murphy and Kardon, 2011).

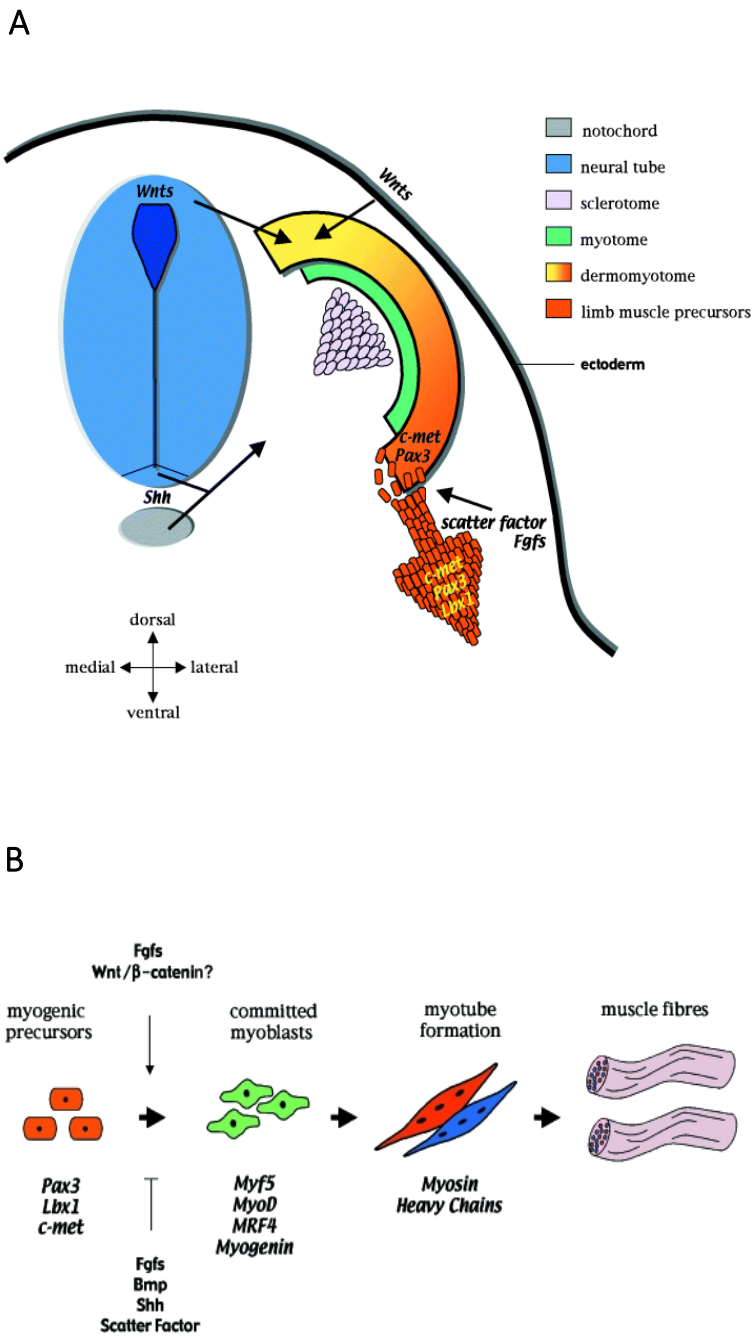

Fig. 1.10 The regulation of embryonic myogenesis

A The somite differentiates into sclerotome (light pink) and dermomyotome (orange-yellow). The sclerotome forms vertebrae and ribs. The dermomyotome forms muscles and the dermis. The dorso-medial edge of the dermomyotome (yellow) forms the myotome (green) and epaxial muscles of the back. The dorso-lateral region of the dermomyotome (orange) gives rise to the hypaxial muscles. At the limb level, premyogenic precursors delaminate and migrate distally into the developing limb bud (orange arrow). Molecular signals that control these events are Shh from the notochord (grey) and neural tube (blue), Wnt proteins from the dorsal neural tube and dorsal ectoderm. The premyogenic cells are induced to delaminate by scatter factor and Fgfs which are also thought to control migration. Premyogenic cells express Pax3, Lbx1 and c-met. They are not committed to myogenic differentiation due to repressive signals from the lateral plate mesoderm. B Muscle precursors of the limb initially express the transcription factors Pax3 and Lbx1 together with c-met. Commitment to myogenic differentiation is marked by the expression of the myogenic regulatory factors (Mrfs): Myf5, MyoD, Mrf4 and Myogenin. Subsequently, myoblasts terminally differentiate, fuse to myotubes and express myosin heavy chain. Later in development they form muscle fibres. (Buckingham et al., 2003).

Fetal myogenesis

During the transition from embryonic to fetal myogenesis, $Pax3^+$ muscle progenitors start to express paired box protein 7 (Pax7) and down-regulate Pax3. These $Pax7^+$ muscle progenitors proliferate and give rise to $Pax7^+$ fetal myoblasts that are responsible for muscle hypertrophy (increase in myofibre size) and hyperplasia (increase in myofibre number) during fetal development (Murphy and Kardon, 2011). Fetal myoblasts use existing primary myofibres as a template to fuse locally thereby forming secondary fibres (Fig 1.11). Fetal myoblasts have also been shown to fuse with the existing primary fibres in a process called myonuclear accretion. This further increases fibre size (Murphy and Kardon, 2011).

Perinatal myogenesis

Around birth, hypertrophy and hyperplasia of the muscles continues. Hyperplasia is thought to occur in early postnatal muscles at a lower degree as during the fetal growth and to stop at a certain point (White et al., 2010). During postnatal growth, $Pax7^+$ muscle precursors still proliferate and give rise to new myoblasts that will differentiate and fuse with their associated myofibres. $Pax7^+$ progenitors do now locate between the myofibres and the basal lamina (Fig. 1.11) and from this point on are sometimes referred to as satellite cells (muscle stem cells). However, it is a matter of debate whether they can be called satellite cells as they have not reached their characteristic quiescent state before the end of perinatal development. During postnatal growth the myofibres also undergo myonuclear accretion independent hypertrophy characterized by increased protein synthesis seen in the increase of the myonuclear domain. The myonuclear domain is defined as the cytoplasmic volume per nucleus in a cell and is thought to remain constant in fully grown muscles that are not exposed to varying physical demands (White et al., 2010). The number of $Pax7^+$ muscle progenitors steadily declines after birth until it reaches its lowest level at the end of perinatal growth and remains fairly constant during adulthood (White et al. 2010). The myonuclear accretion process follows the same pattern and steadily declines.

Adult myogenesis

After the perinatal phase myofibres continue their hypertrophic growth until they reach their adult size and the myonuclear domain stops increasing.
The $Pax7^+$ muscle progenitors stop proliferating and become quiescent at the transition from perinatal to adult development, which in the mouse occurs at postnatal day 21 (Duprez, 2010). $Pax7^+$ cells give rise to satellite cells (Fig. 1.11), stem cells of adult muscles. This marks the end of the perinatal and the beginning of the adult phase (Murphy and Kardon, 2011). It is hypothesized that satellite cells are responsible for muscle homeostasis (Zammit, 2008) and muscle regeneration after injury (Sambasivan et al., 2011).

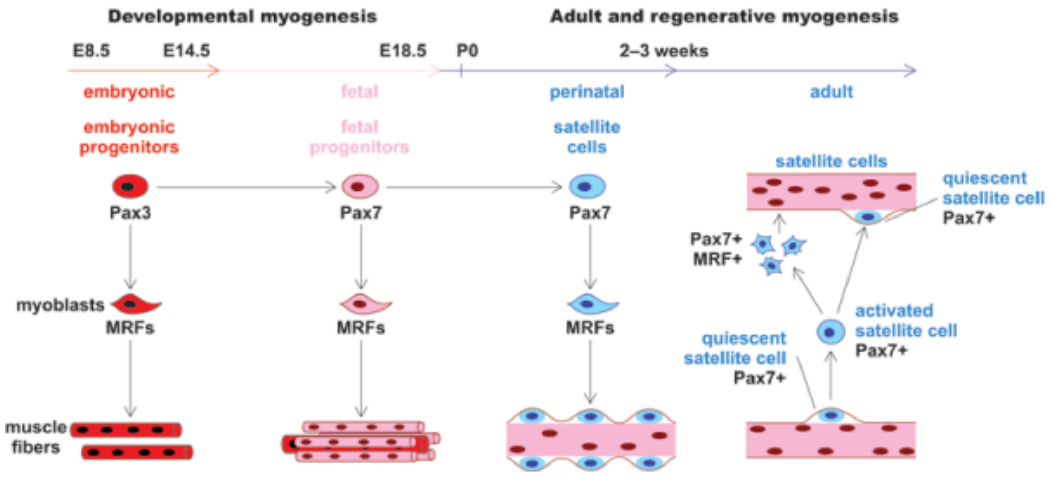

Fig. 1.11 Embryonic, fetal, perinatal and adult myogenesis in the mouse
Skeletal muscle is established in successive steps involving different types of muscle progenitors: embryonic Pax3$^+$ and fetal Pax7$^+$ progenitors during prenatal development, and satellite cells in the adult. Progenitor cells become myogenic by the expression of Mrfs. In the mouse, embryonic myogenesis occurs from E8.5 (embryonic day 8.5) to E14.5. From E14.5 to E18.5, fetal myogenesis allows muscle growth in the fetus. From E18.5, Pax7$^+$ cells and hypertrophy are responsible for perinatal growth. From three weeks postnatal, Pax7$^+$ cells are quiescent (satellite cells). Upon injury, satellite cells are activated, proliferate and differentiate to re-form the damaged muscle. During this process, a subset of satellite cells is used to renew the cell pool. Pax3 = Paired box protein 3 , Pax7 = Paired box protein 7, Mrfs = Myogenic regulatory factors (Duprez, 2010).

1.3 Thesis objectives

It has been reported that mutations in *NF1* and the resulting loss of function of its gene product neurofibromin cause defects in skeletal muscles in both humans and mice. Until now, however, the cellular pathomechanism is not explored.
For studying *Nf1* function during limb development, the Nf1Prx1 mouse model had been generated previously. It is a multi tissue knockout model and recapitulates several aspects of the disorder neurofibromatosis I, but it is not suited for elucidating the endogenous role of *Nf1* in muscle cells. Therefore, in this work a suitable mouse model for investigation of the internal role of *Nf1* in developing muscle cells should be established. For a better understanding of stage specific roles *Nf1* knockout models that differ in the initial time point of *Nf1* deletion should be generated. The subsequent characterisation of the mouse models via histological, immunochemical, molecular and biochemical approaches comprised the following objectives:

1. Description of the histological consequences of a *Nf1* deletion in four muscles of the forelimb and the hindlimb.
2. Estimation of the developmental stages and mechanisms *Nf1* is essential for.
3. Defining candidate signalling pathways deregulated by a knockout of *Nf1* in the developing muscle cell.
4. Comparison of the mouse phenotype with the symptoms of neurofibromatosis I patients and suggesting targets for therapy of musculoskeletal defects.

The results of this work shall contribute to the understanding of molecular mechanisms in myogenesis and reveal aspects of the NF1 muscular pathomechanism.

2. Materials

2.1 Instruments

Instrument	Type	Provider
Axio Cam	HRC and MRC5	Zeiss
Bead mill	TissueLyser LT	Quiagen
Binocular	MZ 12	Leica
Centrifuge	Biofuge pico	Thermo
Cryotome	HM 560 Cryo-Star	Microm
Disperser	UltraTurrax	IKA
Electric power supply		Peqlab
Electron microscope	120 kV Tecnai Spirit	FEI
ELISA Reader	Spectra Max 250	Molecular Devices
Fluorescence microscope	Axiovert 200M	Zeiss
Freezer	-20°C	Bosch
Freezer	-80 °C, Forma 906	Thermo
Fridge	4°C	Bosch
Gel electrophoresis equipment	Gel chamber, slides, combs	PeqLab
Heating block for tubes	Ori-Block OV 3	Techne
Heating plate	HI 1220	Leica
Laboratory car	FI1500	Fischer
Laminar flow clean bench	HERA safe	Kendro
Laser scanning microscope	LSM 700	Zeiss
Microscope	DMR HC	Leica
Microwave oven	900 Grill	Severin
Multi channel pipette	3 - 300 µl	Eppendorf
Optical film developer	Curix 60	Agfa-Gevaert AG
Oven	OV 2	Biometra
pH meter	MP220	Mettler
Pipetting aid	Pipettboy acu	ISS Intergra Bioscience
Real-Time PCR Cycler	Taqman 7500HT Fast	Applied Biosystems
Refrigerated centrifuge	Centrifuge 5417 R	Eppendorf
Rolling device	Roller Mixer SRT9	Stuart

Scale	F1500	Fischer
Scanning fluorescence microscope	Biorevo BZ9000	Keyence
Sequencing machine	Sequence Analyser 3100 AB	Applied Biosystems
Shaker	G10 Gyrotory	New Brunswick Scientific
Single channel pipettes	10 µl, 20 µl, 200 µl, 1 ml	Eppendorf
Sonificator	BioruptorTM NextGen	Diagenode
Thermal PCR Cycler	PCR System 2700	Applied Biosystems
Thermo shaker	Thermomixer compact 5350	Eppendorf
Ultramicrotome	Ultracut E	Reichert-Jung/Leitz
UV transilluminator with camera	E.A.S.Y	Herolab
UV-Vis spectrophotometer	NanoDrop ND-2000	Thermo Scientific
Vortex	Microspin FV-2400	Lab4you
Waterbath	D1	Haake fisions
Western blot chamber	Transblot Semi-Dry	Bio-Rad

2.2 Consumables

Material	**Type**	**Provider**
Autoclave tape	Comply	Steam
Cell culture plates	6-well; 12-well	TPPR
Cell culture plastic pipettes	StripetteR, 2 ml; 5 ml; 10 ml; 25 ml	CostarR
Cell strainer	20 µM	BD Bioscience
Cell strainer	100 µM	BD Bioscience
Conical-bottom tubes	15 ml; 50 ml	TPPR, Greiner
Cover slips	24 x 32 mm No.1	Marienfeld
Cryotome Blades	Sec35p Low Profile Blades	Microm
Glass pipettes	1 ml; 5 ml; 10 ml; 20 ml	FortunaR Germany
Glass slides	Superfrost plus	Thermo scientific
Glass slides, round	10 mm diameter	Roth
Laboratory aluminium foil	Rotilabo, 8 µm thickness	Roth
Laboratory gloves	Latex safety & comfort	Latech
Parafilm	Parafilm M	Pechinery
Pasteur pipette	3 ml	Brand Plastibrand

Pipette tips	10 µl	Gilson
Pipette tips	20 µl	DeckWorks
Pipette tips	200 µl	DeckWorks
Pipette tips	1 ml	DeckWorks
Reaction tubes	0,5 ml; 1,5 ml; 2 ml tubes	Eppendorf
Radiographic film	Super RX Fuji Rays Film	Hartenstein
Silica beads with indicator	Silica Gel Orange, 2 - 5 mm	Roth
Stainless steel beads	Grinding bead, 3 mm diameter	Labmarket GmbH
Sterile filters	Rotilabo, 0,22 µm; 0,45 µm	Roth
Sterile scalpels	Surgical disposable scalpels	B. Braun
Sterile syringes	One-way syringes Sterican	B. Braun
Transfer membrane	ImmobilonTM-P (0,45 µm)	Merck-Millipore
8-tube strip and caps	MicroAmp, 0,2 ml	Applied Biosystems
96-well plate	MicroAmp	Applied Biosystems
Whatman paper	Extra thick Blot Paper Criterion	Biorad

2.3 Chemicals

Chemical	**Provider**
Acetic acid	Merck-Millipore
Acetone	Merck-Millipore
Acrylamide mix 30 %, Rotiphorese Gel	Roth
Agarose	Invitrogen
Ammonium persulfate (APS)	Sigma-Aldrich
Ammonium sulphate $(NH)_4SO_4$	Gibco
Aqua bidest (A. bidest)	produced *in-house*
Bio-Rad Protein Assay	Biorad
Blocking Reagent BBR	Roche
Blocking Reagent powder	Perkin Elmer
BM purple AP substrate	Roche
Bovine serum albumin (BSA)	Sigma-Aldrich
5-Bromo-2`-deoxy-uridine (BrdU), 10 mM	Roche
Chloroform, pro analysis	Merck-Millipore
Complete Protease Inhibitor	Roche

Cresol red	Merck-Millipore
4', 6-diamidino-2-phenylindole (DAPI)	Invitrogen
Diethylpyrocarbonate (DEPC)	Sigma-Aldrich
Disodium hydrogen phosphate ($Na_2HPO_4 \cdot 12H2O$)	Merck-Millipore
Deoxyribonucleotide (dNTP) mix	Fermentas
Ethanol; pro analysis	Merck-Millipore
Ethidium bromide solution (10 mg/ml)	Roth
Ethylenediaminetetraacetic acid (EDTA)	Merck-Millipore
Fluoromount G	Southern Biotech
Formamide, pro analysis	Merck-Millipore
Glutaraldehyde (25 %)	Sigma-Aldrich
Glycine, pro analysis	Merck-Millipore
Heparin	Merck-Millipore
HEPES (4-(2-hydroxyethyl)-1-piperazineethanesulfonic acid)	Calbiochem
Hydromatrix	Micro-Tech-Lab
Hydroxide peroxide (30%)	Merck-Millipore
Isopentane	Roth
Isopropanol, pro analysis	Merck-Millipore
Lead citrate	Sigma-Aldrich
L-Glutamine	Cambrex
Lithium chloride	Sigma-Aldrich
Magnesium chloride ($MgCl_2$)	Merck-Millipore
β-Mercaptoethanol	Roth
Methanol, pro analysis	Merck-Millipore
Monopotassium phosphate (KH_2PO)	Merck-Millipore
NBT (nitrotetrazolium blue)	Sigma-Aldrich
Nonidet P40 (NP-40)	Fluka
Normal Horse Serum	Vector Laboratories
Oligonucleotides and oligonucleotide primer	Eurofins
Orange G	Merck-Millipore
Osmium tetroxide	Sigma-Aldrich
Osteosoft	Merck-Millipore
Paraformaldehyde (PFA)	Merck-Millipore
peqGold TriFast	peqLab
Phenylmethylsulfonyl fluoride (PMSF)	Sigma-Aldrich

PhosSTOP Phosphatase Inhibitor	Roche
Potassium chloride (KCl)	Merck-Millipore
Propylene oxide	Sigma-Aldrich
QuickExtract DNA Extraction Solution	Cambio
Sodium acetate	Merck-Millipore
Sodium bicarbonate ($NaHCO_3$)	Merck-Millipore
Sodium cacodylate buffer	Sigma-Aldrich
Sodium chloride (NaCl)	Merck-Millipore
Sodium citrate	Sigma-Aldrich
Sodium deoxycholate	Sigma-Aldrich
Sodium dodecyl sulfate (SDS)	Roth
Sodium dihydrogen phosphate ($NaH_2PO_4 \cdot 1H_2O$)	Merck-Millipore
Sodium fluoride (NaF)	Sigma-Aldrich
Sodium hydroxide (NaOH)	Merck-Millipore
Sodium pyrophosphate (NaPPi)	Sigma-Aldrich
Sodium succinate	Merck-Millipore
Sucrose	Merck-Millipore
SYBR Green PCR Master Mix, 2 x	Applied Biosystems
Tannin	Sigma-Aldrich
Target retrieval solution pH 6	DAKO
Target retrieval solution pH 9	DAKO
TEMED (N,N,N',N'-Tetramethylethane-1,2-diamine)	Invitrogen
Tetramisol	Merck-Millipore
TissueTek cryo embedding medium	Sakura
Tris base	Merck-Millipore
Triton X-100	Sigma-Aldrich
t-RNA (Typ III baker's yeast)	Sigma-Aldrich
Trypsin	Gibco
Tween20	Roth
Uranyl acetate	Sigma-Aldrich

2.4 Molecular biology and biochemistry kits

Kit	Provider
BCA Protein Assay Reagent Kit	Pierce
Big Dye V3.1 Sequencing Kit	Applied Biosystems
DIG RNA Labelling Kit	Roche
Gel-Out Gel Extraction Kit	A & A Biotechnology
Spurr Low-Viscosity Embedding Kit	Sigma-Aldrich
TaqMan Reverse Transcription Reagents Kit	Roche

2.5 Enzymes

Enzyme	Provider
Collagenase NB4 G	Serva
Collagenase type 1	Sigma-Aldrich
Collagenase type 4	Sigma-Aldrich
DNase I	Quiagen
Proteinase K	Boehringer Ingelheim
Reverse Transcriptase Superscript II	Invitrogen
RNase A	Sigma-Aldrich
Sp6 polymerase	Roche
T3 polymerase	Roche
T7 polymerase	Roche
Taq polymerase	Fermentas

2.6 Media and supplements for cell culture

Solution	Provider
Cell Recovery Solution (for matrigel cultures)	BD Bioscience
DMEM (inc. 4,5 g/l glucose)	BioWhittaker Cambrex
Dulbecco`s Phosphate Buffered Saline (DPBS)	Lonza
10 % Fetal calf serum (FCS)	Biochrom
Gentamycin 50 mg/ml	Life Technologies

Hanks Buffered Saline Solution (HBSS)	Biochrom AG
2 % L-glutamine	BioWhittaker Cambrex
Matrigel (Basement Membrane Matrix)	BD Bioscience
1 % Penicilline/streptomycine	BioWhittaker Cambrex

2.7 Buffers and solutions

Buffer/solution	**Components**
General	
DEPC-H_2O	0,1 % DEPC in A. bidest; incubate at 37 °C over night and autoclave
Loading dye for agarose gels 6 x	15 g sucrose; 0,175 g Orange G ad 50 ml A. bidest
PBS 10 x	80 g NaCl; 2 g KCl; 14,4 g Na_2PO_4; 2,4 g KH_2PO_4; ad 1 l A. bidest or DEPC-H_2O; pH 7.4
PBX 1 x	100 ml PBS (10 x), 0.1 % Triton X-100 ad 1 l A. bidest
PBST	1x PBS; 0,1 % Tween20
4 % PFA/PBS	40 g PFA ad 1 l 1 x PBS (dissolve by heating); pH 7.4
SDS buffer (DNA extraction liver)	0,85 % SDS; 17 mM EDTA; 170 mM NaCl; 17 mM Tris/HCl; pH 7.5; add 200 µg/ml proteinase K
TAE buffer	0,04 M Tris; 5 mM sodium acetate; 1 mM EDTA; pH 8
TBS buffer 10 x	300 ml 5 M NaCl; 100 ml 1 M Tris; ad 1 l DEPC-H_2O; pH 7.4
SDH staining	
Incubation medium	3 ml NBT solution; 4,5 ml sodium succinate; 4,5 ml phosphate buffer 100 mM
NBT solution	250 mg NBT solved in 100 ml A.bidest; stored light-protected at 4 °C
Phosphate buffer 100 mM	0,69 g $NaH_2PO_4 \cdot 1H_2O$; $Na_2HPO_4 \cdot 12H_2O$; ad 250 ml A. bidest; pH 7,4
Sodium succinate 0,2 M	5,4 g sodium succinate solved in 100 ml A. bidest; pH 7,4; stored at -20 °C

PCR

Cresol red solution	84,5 mg cresol red diluted in 100 ml T0,1E; store aliquots at -20°C
DNA polymerase PCR buffer 10 x	750 mM Tris HCl pH 8.8; 200 mM $(NH_4)_2SO_4$; 15 mM $MgCl_2$; ad A. bidest, filter sterile
10 x PCR buffer GS	45 ml Tris-HCl pH 8,8; 50 ml cresol red solution; 1,5 ml A. bidest; 3,5 ml 1 M $MgCl_2$; 1,454 g $(NH)_4SO_4$; store aliquots at -20°C
PCR buffer "dilute"	100 ml A. bidest; 50 ml T0,1E; 0,8125 ml cresol red solution; 50 µl 4 M NaOH; store aliquots at -20°C
Sucrose solution 1 M	121,1 g sucrose diluted in 350 ml A. bidest; store aliquots at -20°C
T0,1E	10 mM Tris pH 8,8; 0,1 mM EDTA

Whole Mount in situ hybridisation (WM-ISH)

Alkaline phosphatase (ALP) buffer	12 ml 5 M NaCl; 30 ml 1 M $MgCl_2$; 6 ml 10 % Tween20; 60 ml 1 M Tris pH 9.5; 300 mg tetramisol; ad 600 ml A. bidest
Blocking solution	10 % blocking reagent BBR in 1 x MABT
Formamide buffer (SSC/FA/T)	100 ml 20 x SSC; 500 ml formamide; 10 ml 10 % Tween20; ad 1 l A. bidest
Hybridisation buffer	25 ml formamide; 12,5 ml 20 x SSC; 25 µl heparin; 500 µl 10 % Tween20; ad 50 ml DEPC-H_2O
MABT 5 x	100 ml 1M maleic acid; 30 ml 5 M NaCl; 10 ml 10 % Tween20; ad 200 ml DEPC-H_2O
PBST/glycine	1 x PBST; 2 mg/ml glycine
PBST/tetramisol	500 mg tetramisol ad 1 l PBST
4 % PFA/0,2 % glutaraldehyde	50 ml 4 % PFA/PBS; 400 µl glutaraldehyde; 500 ml 0.5 M EDTA
Proteinase K buffer	1 ml Tris pH 7; 0,1 ml 0.5 M EDTA; ad 500 ml H2O-DEPC
RIPA buffer	2,5 ml SDS 10 %; 15 ml 5 M NaCl; 5 ml NP-40; 2,5g sodium deoxycholate; 1 ml 0,5 M EDTA; 25 ml 1 M Tris (pH 8) ad 500 ml DEPC-H_2O
RNase A solution	50 ml RNase solution; 500 µl 10 mg/ml RNaseA

RNase wash buffer 10 x	800 ml 5 M NaCl; 100 ml 1M Tris; 100 ml 0,5 M EDTA
SSC (saline-sodium citrate) 20 x	175,32 g/l (3 M) NaCl; sodium citrate: 88,23 g/l (0,3 M)
tRNA solution	10 mg t-RNA (Typ III baker's yeast) per 1 ml DEPC-H_2O; stored at -20 °C

Primary cell culture

Growing medium	DMEM; 1x gentamycin; 10 % FCS (445 ml DMEM, 5ml gentamycin, 50 ml FCS)
Matrigel 10 %	10 ml matrigel; 90 ml DMEM; store in aliquots at -20 °C

Protein isolation and western blot

Transfer buffer 1 x	100 ml 10 x transfer buffer, 200 ml MeOH ad 1 l A. bidest
Transfer buffer 10 x	29 g glycine; 58 g Tris base; 40 ml 10 % (w/v) SDS ad 1 l A. bidest
Protein loading dye 4 x	2 ml 1 M Tris; 4 ml glycerin; 2 ml 20 % (w/v) SDS; 400 µl 1 % brom phenol blue; 600 µl H2O, 1 ml β-mercaptoethanol; pH 7.5
Running buffer 5 x	25 mM Tris; 250 mM glycine; 0,1 % (w/v) SDS
Membrane lysis buffer	50 mM NaF; 30 mM NaPPi; 5 mM EDTA; 1% Triton-X 100; 1 x TBS; per 10 ml add 1 tablet Complete Protease Inhibitor and one tablet PhosSTOP Phosphatise Inhibitor; store aliquots at -80 °C
Stripping buffer	7,5 ml 1 M glycine, 2 ml 10 % (w/v) SDS/50 ml A. bidest; pH 2.5

Immunochemistry

TSA blocking solution	1 x PBS, 10 % normal horse serum, 5 mg/ml Blocking Reagent powder
Staining solution	1 x PBS, 0.03 % normal horse serum, 0.003 % BSA, 0.001 % Triton X-100

Single myofibre isolation

Collagenase solution	0.2 % collagenase type I in DMEM (for two EDL muscles: preparation of 2 ml of collagenase solution); filter through 0.22 µm sterile filter; pre-warm at 37 °C in a water bath 10

	min before EDL isolation. Aliquots of undiluted collagenase can be frozen at -20 °C for later use
Culture medium	Supplement DMEM with 20 % FBS, 1% chicken embryo extract and 1% penicillin/streptomycin. Filter through 0.22 µm filter before use
Washing medium	Supplement DMEM with 1 % penicillin/streptomycin; filter through 0.22 µm sterile filter before use
Staining solution	1 x PBS, 0.03 % horse serum, 0.003 % BSA, 0.001 % Triton X-100

Electron microscopy

EM fixing solution	2 % PFA/PBS, 2,5 % glutaraldehyde in 50 mM sodium cacodylate buffer
Reynold's lead citrate solution	1,33 g lead citrate; 1,76 g sodium citrate; 5 ml 1N NaOH; 30 ml A. bidest; stir for 10 minutes to dissolve and add additional 15 ml of distilled water; store solution for 3 to 6 months at 4 ºC

2.8 Oligonucleotides

Genotyping

Primer name	**Nucleotide sequence (5' → 3')**
Lbx1_Cre_fw	CGCCTTCCTCTCGCACCGTC
Lbx1_Cre_rev	GGCAGCCCGGACCGAC
mTmG_fw	CTCTGCTGCCTCCTGGCTTCT
mTmG_KO_rev	CGAGGCGGATCACAAGCAATA
mTmG_WT_rev	TCAATGGGCGGGGGTCGTT
Myf5_Cre_fw	CGTAGACGCCTGAAGAAGGTCAACCA
Myf5_Cre_KO_rev	ACGAAGTTATTAGGTCCCTCGAC
Myf5_Cre_WT_rev	CACATTAGAAAACCTGCCAACACC
Nf1_P1	CTTCAGACTGATTGTTGTACCTGA
Nf1_P2	CATCTGCTGCTCTTAGAGGAACA
Nf1_P3	ACCTCTCTAGCCTCAGGAATGA
Nf1_P4	TGATTCCCACTTTGTGGTTCTAAG

Unspecific_Cre _fw	GAGTGATGAGGTTCGCAAGA
Unspecific_Cre_rev	CTACACCAGAGACGGAAATC

Quantitative Real time PCR (qRT-PCR)

Primer name	**Forward; reverse primer nucleotide sequence (5' → 3')**
Acadl	GTAGCTTATGAATGTGTGCAACTC;
	GTCTTGCGATCAGCTCTTTCATTA
β-Actin	CGTGAAAAGATGACCCAGATCA;
	GGGACAGCACAGCCTGGAT
Akp2	ACTCAGGGCAATGAGGTCAC;
	CTGGTGGCATCTCGTTATCC
Acta1	CTGAGCGTGGCTATTCCTTC,
	AAGTCCAGGGCCACATAGC
Col II	CTTCAATTCAACATCCCCTTTTG;
	TCTACTTTTGAAGCTCGCATGCT
Cox1	ATCCCTTGACATCGTGCTTC;
	AGCAAACACTGCTCCCATTG
CS-1 (Myoz2)	CCATGCAGAATGGGAGAGTT
	GGTGCGATGTTCTCTGGATT
CyclinD1	TGCTGCAAATGGAACTGCTT;
	CGGCCAGGTTCCACTTGA
E11	AACAACCACAGGTGCTACTGG;
	CCTCTAAGGGAGGCTTCGTC
Fabp4	ATGAAATCACCGCAGACGAC;
	TCGACTTTCCATCCCACT TC
Gapdh	AACTTTGGCATTGTGGAAGG;
	CAGTCTTCTGGGTGGCAGTG
Gsk3b	AGAGCT GCAAGCCAGTGC;
	TGCCACTAC TGTGGTTACCTTG
Hadh	TGCTGTCAGGCACTTCGTATAAA;
	AAACCCGAAAGTGCAGCTCTAG
Maz	GACCACATGAGGTGCACAG;
	GCACAGCTTACACAGGATGC

Mc2-r	GTGACAAAGCCAAGGAGAGG;
	GGTGTTTGCCGTTGACTTAC
m-Cs	CCCAGGATACGGTCATGCA;
	GCAAACTCTCGCTGACAGGAA
Myf5	TGAGGGAACAGGTGGAGAAC;
	CTGTTCTTTCGGGACCAGAC
MyFastGl	GTGATTTCTCCTGTCACCTCTC;
	GGAGGACCGCAAGAACGTGCTGA
MyFastOx	ATGAGCTCCGACGCCGAG;
	TCTGTTAGCATGAACTGGTAGGCG
MyoD	AGCACTACAGTGGCGACTCA;
	GCTCCACTATGCTGGACAGG
Myogenin	CTACAGGCCTTGCTCAGCTC;
	AGATTGTGGGCGTCTGTAGG
MySlow	CCAGGGGCAAACAGGCATTCACT;
	CTTCCACTGGGCCACTTCACTGTT
Nd1	CCATTCTAATCGCCATAGCC;
	GCCGTATGGACCAACAATG
Nf1	ACTTGCGGAAACGGTGTTG;
	TGCCATCACCTCAGCTTTGATA
$Nfat_{c1}$	ATG TCT GCA ACG GGA AAC G;
	GGTACGTGAAACGCTGGTACT
$Nfat_{c2}$	GAC TGGACACGAAAAGCAACTG;
	TGAGTTGAGAATGAGGCTTTGGT
$Nfat_{c3}$	ATGCATTCTGGACAGCACTCAA;
	GCCTCCTTGGCCTGTACTTTG
$Nfat_{c4}$	CCCGCCTACCTTCAGTCTCTT;
	CCTCCATATTGATCACCAGGAAA
Pax7	CCGTGTTTCTCATGGTTGTG;
	GAGCACTCGGCTAATCGAAC
Pepck	TCTCTGATCCAGACCTTCCAA;
	GAAGTCCAGACCGTTATGCAG
Pgc-1	AACCACACCCACAGGATCAGA;
	TCTTCGCTTTATTGCTCCATGA

Ppar g	TTTTCCGAAGAACCATCCGAT;
	ACAAATGGTGAT TTGTCCGTTG
Rcan1	CCTGACATAGAAACCCTGCTG;
	CTGGAAGGTGGTGTCCTTGT
Runx2	CCGTGGCCTTCAAGGTTGT;
	CGGCCATGACGGTAACCA
Sost	CGAGCCTCCTCCTGAGAAC;
	CTGTCAGGAAGCGGGTGTAG
12S-RNA	TACCGCCATCTTCAGCAAAC;
	CCCATTTCATTGGCTACACC
Vegf	ACCAGACCTCTCACCGGAAA;
	GATGGCGTGGTGGTGACA

Standard primer for plasmid PCR

Primer name	**Nucleotide sequence (5' → 3')**
Sp6	CATTTAGGTGACACTATAG
T7	TAATACGACTCACTATAGGG

2.9 Size markers for analyses

Size marker	**Provider**
Western Blot	
Precision Plus Protein Standards	Bio-Rad
Agarose gel electrophoresis	
100 bp DNA ladder	Fermentas

2.10 Antibodies

The following overview shows all primary and secondary antibodies used for western blots (WB), whole mount *in situ* hybridisation (WM) and immunochemistry (IC).

Antigen	Application, dilution	Species	Provider
Primary antibodies			
Actin	WB 1:1000	rabbit	Sigma-Aldrich A5060
Akt (pan) (11e7)	WB 1:500	rabbit	Cell Signaling #4685
Ampk α	WB 1:500	rabbit	Cell Signaling #4185
BrdU	IC 1:50	sheep	Abcam
Collagen IV	IC 1:100	goat	Merck-Millipore
Creb	WB 1:500	rabbit	Cell Signaling #9197
Desmin	IC 1:100	goat	Merck-Millipore
Embryonic myosin	IC 1:500	mouse	DSHB
Fast twitch myosin heavy chain	WB 1:500	mouse	Sigma-Aldrich M1570
GFP	IC 1:100	rabbit	Merck-Millipore #AB3080
HSP60	WB 1:500	rabbit	Santa Cruz
Ki-67	IC 1:50	mouse	BD Biosciences
Laminin A	IC 1:500	chicken	Abcam
Laminin A	IC 1:500	rabbit	Abcam
Mek1 (C-18)	WB 1:500	rabbit	Santa Cruz sc-219
MyoD	IC 1:100	rabbit	Santa Cruz
Myosin heavy chain (pan)	WB 1:1000	mouse	Merck-Millipore A4.1025
$NFAT_{c1}$	WB 1:1000	mouse	Thermo Scientific
$NFAT_{c3}$	WB 1:200	mouse	Santa Cruz
p44/42 (ERK1/2)	WB 1:500	rabbit	Cell Signaling #9102
Pax7	IC 1:25	mouse	DSHB
phospho-Ampk α	WB 1:500	rabbit	Cell Signaling #2532
phospho-Akt1 (phospho S473)	WB 1:500	rabbit	Abcam ab18206-100
phospho-cJun	WB 1:200	mouse	Santa Cruz sc-822
phospho-Creb	WB 1:500	rabbit	Cell Signaling #9108
phospho-Mek1/2	WB 1:500	rabbit	Cell Signaling #9121
phospho-p44/42 (phospho-ERK1/2)	WB 1:500	rabbit	Cell Signaling #4370
Slow twitch myosin heavy chain	IC 1:500	mouse	Sigma-Aldrich
β-Tubulin III	WB 1:100	mouse	Sigma-Aldrich T8578
Vimentin	WB 1:100	mouse	Santa Cruz sc-5565

Secondary antibodies

Chicken, polyclonal (AlexaFluor 488)	IC 1:500	donkey	life Technologies
DIG-Fab-ALP, monoclonal	WM 1:5000	sheep	Roche # 11 093 274 910
Goat, polyclonal (Alexa Fluor 488)	IC 1:1000	donkey	life Technologies
Mouse IgG (HRP Conjugate)	WB 1:1000	goat	Merck-Millipore
Mouse, polyclonal (AlexaFluor 488)	IC 1:500	donkey	life Technologies
Mouse, polyclonal (AlexaFluor 568)	IC 1:500	donkey	life Technologies
Mouse, polyclonal (AlexaFluor 680)	IC 1:250	donkey	life Technologies
Rabbit IgG (Peroxidase Conjugate)	WB 1:1000	goat	Merck-Millipore
Rabbit, polyclonal (AlexaFluor 488)	IC 1:500	donkey	life Technologies
Rabbit, polyclonal (AlexaFluor 568)	IC 1:500	donkey	life Technologies
Sheep, polyclonal (AlexaFluor 488)	IC 1:500	donkey	life Technologies

2.11 Animals

Mice used in this work were kept and bred in the animal facility of the Max Planck Institute for Molecular Genetics by K. Reinisch under supervision of Dr. L. Hartmann. All transgenes and mutations reported here were generated and maintained in C57BL6 mice. The following founder animals have been used:

- $Nf1^{flox/flox}$ mice (Zhu et al., 2001): exon 41 and exon 42 of both *Nf1* alleles are flanked by loxP sites; provided by Prof. L. Parada
- $Lbx1^{Cre}$ mice (Vasyutina et al., 2007): a transgene is inserted carrying the Cre recombinase gene under control of the Lbx1 promotor; provided by Prof. C. Birchmeyer
- $Myf5^{Cre}$ mice (Tallquist et al., 2000): the Cre recombinase gene is inserted in the Myf5 locus and is under control of the Myf5 promotor; provided by Prof. C. Birchmeyer

- HSA^{Cre} mice (Miniou et al., 1999): a transgene is inserted carrying the Cre recombinase gene under the control of the HSA (human skeletal actin) promotor; provided by Prof. C. Birchmeyer
- $Prx1^{Cre}$ mice (Logan et al., 2002): the Cre recombinase gene is under control of the Prx1 limb enhancer; provided by Dr. A. Nagy
- mTmG mice (Muzumdar et al., 2007): conditional fluorescent indicator mice that constitutively express a conditional td-Tomato transgene (*mT*) that converts to the expression of EGFP (*mG*) following exposure to Cre recombinase, provided by Prof. A. Kispert

From these founder animals four *Nf1* knockout mouse lines have been generated: Nf1Lbx1, Nf1Myf5, Nf1HSA and Nf1Prx1. *Nf1* knockout mice were derived from crossings of $Nf1^{flox/flox}$ and $Nf1^{flox/+}$; Cre mice. The $Nf1^{flox/+}$; Cre mice were generated by breeding one of the named Cre mice ($Lbx1^{Cre}$, $Myf5^{Cre}$, HSA^{Cre} or $Prx1^{Cre}$) with $Nf1^{flox/flox}$ mice.
Control mice for each experiment were sex-matched mice taken from the same litter as mutants. They had the genotype $Nf1^{flox/+}$; Cre or $Nf1^{flox/flox}$; no Cre.

Furthermore three mTmG-Cre reporter mouse lines (mTmG-Lbx1, mTmG-Myf5 and mTmG-HSA) have been generated by breeding mice from one of the Cre lines ($Lbx1^{Cre}$, $Myf5^{Cre}$ or HSA^{Cre}) with mTmG mice.

2.12 Computer Software

Application	Software program	Producer
Agarose gel documentation	E.A.S.Y Win 32	Herolab
Data documentation and calculation	Excel 2007	Microsoft
Digital microscopic photography	AxioVision 4.6	Zeiss
Digital microscopic photography	ZEN pro 2011	Zeiss
Digital microscopic scanning photography	BZ-II Viewer	Keyence
Image analysis software	Image J	NIH, public domain
Image enhancing software	Photoshop CS6	Adobe
Image processing	BZ-II Analyzer	Keyence
Image processing	CoralDraw X5	Adobe
Image quantification	AxioVision Autmess	Zeiss
Microarray data analysis	Microarray Suite 5.0	Affymetrix
Nucleotide sequence reading	SeqMan NGen	DNAStar
Oligonucleotide primer design	Primer3 (online tool)	http://primer3.ut.ee
qPCR result analysis	SDS 2.1	Applied Biosystems

3. Methods

3.1 Molecular biological methods

3.1.1 Genomic DNA isolation

From prenatal murine liver tissue

When dissecting prenatal animals liver tissue was prepared for genotyping of the investigated mice. For this purpose half of prenatal liver was isolated and digested in 500 µl of SDS (tail tip) buffer including 20 µl of freshly added proteinase K (200 µg/ml) over night. At the next day 0,25 ml of 5 M sodium chloride was added and the mixture was incubated at room temperature on a rocking device for 10 min. Afterwards, the samples were placed on ice for 10 min and centrifuged at 4 °C for another 10 min at 10000 rpm. The supernatant was transferred to a new tube containing 1 ml of chilled ethanol (100 %). The tube was smoothly shaken and centrifuged at 4 °C for 10 min at 10000 rpm. The supernatant was discarded and the DNA pellet was washed with 500 µl of ethanol (70 %) twice. After discarding the supernatant for the second time the pellet was air dried for 10 min at room temperature. At last, the pellet was re-suspended in 100 µl of A. bidest. The solution was directly used for genotyping. The DNA solution was stored at -20°C.

From postnatal murine tail tips

For genotyping of postnatal mice DNA was isolated from the tips of their tails. DNA was extracted from approximately 1 mg of tissue from tail tips of mice using QuickExtract DNA Extraction Solution. The tail tips were incubated for 20 min with 50 µl of the QuickExtract DNA Extraction Solution at 65 °C in the thermo mixer and shaken at 500 rpm. Afterwards, the samples were incubated for two minutes at 98° C. The solution was directly used for genotyping. The DNA solution was stored at -20°C.

3.1.2 Total RNA isolation from muscle tissue

About 100 mg of muscle tissue was isolated from prenatal or postnatal mice and directly snap frozen in liquid nitrogen. The tissue was quickly taken from the nitrogen and wrapped in chilled laboratory aluminium foil. The tissue was crushed with a hammer while still frozen. Afterwards, pieces were collected in a tube containing 1 ml of peqGold TriFast and homogenised with a disperser (UltraTurrax). The homogenisate was left at room temperature for five minutes. Autoclaved grinding beads were added to the samples and the samples were homogenised again with a bead mill (TissueLyser LT). In the bead mill samples were shaken three times at 60 Hz for 30 sec. In between, samples were placed on ice for 30 sec. To get rid of big tissue pieces and grinding beads samples were centrifuged at 12000 rpm in a cooled centrifuge (4 °C) for 10 min. The supernatants were transferred into new tubes which contained 200 µl of chloroform and shaken vigorously for 15 sec. Then, the samples were incubated at room temperature for 15 min

and subsequently centrifuged for 15 min at 12000 rpm in a cooled centrifuge (4 °C). Three phases appeared and the upper layer was carefully isolated with a pipette and transferred into a new tube containing 500 µl isopropanol and left for 10 min at room temperature. Afterwards the mixture was centrifuged for 10 min at 12000 rpm (4 °C). The supernatant was carefully discarded and 1 ml of 75 % ethanol (diluted in DEPC-H_2O) was added to wash the RNA pellet. The pellet was suspended by mixing vigorously and centrifuged for 5 min at 12000 rpm (4 °C). The washing step was repeated once using 100 % ethanol. Following this, the supernatant was discarded and the pellet was air dried for 10 min at 37 °C. At last, the pellet was suspended in 50 µl of DEPC-H_2O. The RNA quality was controlled via gel electrophoresis by using 1,5 µg RNA and a 1 % agarose gel (see section 3.1.8). RNA solution was stored at -80 °C.

3.1.3 Total RNA isolation from enriched osteocytes

Tibiae from mice were dissected. Joints, cartilage and periosteum were removed with sterile scalpels. Bone marrow was flushed with 1 x PBS (diluted in DEPC-H_2O) using sterile syringes. For enriching cortical osteocytes tibiae were incubated in 2 mg/ml collagenase type 4 solution (2 tibiae per 1 ml solution) in a thermo shaker (700 rpm) at 37 °C for 60 min. Afterwards tibiae were transferred into fresh tubes and snap frozen in liquid nitrogen. Tibiae were quickly taken from the nitrogen, wrapped in chilled laboratory aluminium foil and crushed by striking it with a hammer while still frozen. Afterwards pieces were collected in a tube containing 1 ml of peqGold TriFast and homogenised with a disperser (UltraTurrax). The homogenisate was left at room temperature for five minutes. Autoclaved grinding beads were added and the samples were homogenised again with a bead mill (TissueLyser LT). In the TissueLyser, the samples were shaken three times at 60 Hz for 30 sec. In between the samples were placed on ice for 30 sec. To get rid of big tissue pieces and the grinding beads samples were centrifuged at 12000 rpm in a cooled centrifuge (4 °C) for 10 min. The supernatant was transferred in new tubes which contained 200 µl of chloroform and shaken vigorously for 15 sec. The samples were incubated at room temperature for 15 min and subsequently centrifuged for 15 min at 12000 rpm in a cooled centrifuge (4 °C). Three phases appeared and the upper layer was carefully isolated with a pipette. 1 ml of peqGold TriFast and 200 µl chloroform were added and phase separation was performed again. The upper phase was transferred into a new tube containing 700 µl isopropanol and left for 10 min at room temperature. Afterwards the mixture was centrifuged for 10 min at 12000 rpm and 4 °C. The supernatant was carefully discarded and 1 ml of 75 % ethanol (diluted in DEPC-H_2O) was added to wash the pellet. The sample was mixed vigorously and centrifuged for 5 min at 12000 rpm at 4 °C. The washing step was repeated using 100 % ethanol. Following this, the supernatant was discarded and the pellet was air dried for 10 min at 37 °C. At last, the pellet was suspended in 50 µl of DEPC-H_2O. The RNA quality was controlled via gel electrophoresis of 1,5 µg RNA in a 1 % agarose gel (see section 3.1.8). RNA solution was stored at -80 °C.

3.1.4 Generation of cDNA

Complementary DNA (cDNA) was generated via reverse transcription of total RNA from muscle tissue and osteocytes, respectively. Concentration of isolated RNA was measured with the help of an UV-Vis spectrophotometer using 1 µl of total RNA. Reverse transcription reaction was performed using the TaqMan Reverse Transcription Reagents Kit with random hexamer oligonucleotides according to the supplier's protocol. Reverse transcription is based on the activity of the enzyme reverse transcriptase (RNA dependent DNA polymerase) which synthesizes DNA from RNA templates. The new synthesized DNA strand is complementary to the RNA template and is called cDNA. The generated cDNA was stored at -20°C.

3.1.5 Polymerase chain reaction (PCR) on genomic DNA

To determine the genotype of the investigated mice, PCRs were performed on isolated genomic DNA from liver of prenatal mice and tail tips of postnatal mice, respectively. According to each mouse line a specific combination of genotyping PCRs was performed according to the overview below.

Mouse line	**Genotyping PCRs**
Nf1Lbx1	Nf1 PCR 1, Nf1 PCR 2, Nf1 PCR 3, $Lbx1^{Cre}$ PCR
Nf1Myf5	Nf1 PCR 1, Nf1 PCR 2, Nf1 PCR 3, $Myf5^{Cre}$ PCR
Nf1HSA	Nf1 PCR 1, Nf1 PCR 2, Nf1 PCR 3, $Unspecific^{Cre}$ PCR
Nf1Prx1	Nf1 PCR 1, Nf1 PCR 2, Nf1 PCR 3, $Unspecific^{Cre}$ PCR
mTmG-Lbx1	mTmG PCR, $Lbx1^{Cre}$ PCR
mTmG-Myf5	mTmG PCR, $Myf5^{Cre}$ PCR
mTmG-HSA	mTmG PCR, $Unspecific^{Cre}$ PCR

Nf1 PCR 1, 2 and 3

Performing Nf1 PCR 1, 2 and 3 it was possible to detect whether the Nf1 allele of the investigated mice was excised by Cre mediated recombination (Nf1 PCR 1), not excised and unfloxed (Nf1 PCR 2) or not excised but floxed (Nf1 PCR 3).

PCR mix for one reaction

Amount	**Reagent**
1 µl	Genomic DNA
16,5 µl	A. bidest
2,5 µl	PCR buffer 10x
3,5 µl	dNTPs 1.25 mM
1 µl	Primer fw (Nf1_P1) 10 pmol/µl
1 µl	Primer rev 10 pmol/µl
0,5 µl	Taq polymerase

Program for the thermal PCR cycler

Temperature	**Time**	**Cycles**
94 °C	5 min	1
94 °C	30 sec	35
50 °C	30 sec	
72 °C	1:10 min	
72 °C	7 min	1
4 °C	∞	1

The reverse primer were Nf1_P2 (PCR1), Nf1_P3 (PCR 3) and Nf1_P4 (PCR 3), respectively. The expected specific PCR products had a size of 280 bp (PCR 1), 480 bp (PCR 2) and 350 bp (PCR 3).

Lbx1^{Cre} PCR

For identifying Nf1Lbx1 mutant mice, the Lbx1^{Cre} allele had to be identified via the Lbx1^{Cre} PCR. The expected specific PCR product had a size of 432 bp.

PCR mix for one reaction

Amount	Reagent
1 µl	Genomic DNA
7,2 µl	Sucrose solution 1M
0,19 µl	β-mercaptoethanol 10 %
2 µl	PCR buffer GS 10x
3,5 µl	PCR buffer "dilute"
1,4 µl	DMSO 50 %
1 µl	Lbx1_Cre_fw 10 pmol/µl
1 µl	Lbx1_Cre_rev 10 pmol/µl
0,2 µl	dNTPs 12,5 mM
0,5 µl	Taq polymerase
2,01 µl	A. bidest

Program for the thermal PCR cycler

Temperature	Time	Cycles
95 °C	5 min	1
95 °C	30 sec	40
55 °C	30 sec	
72 °C	1:00 min	
72 °C	7 min	1
4 °C	∞	1

Myf5^{Cre} PCR

For identifying Nf1Myf5 mutant mice, the specific PCR product for the Myf5^{Cre} allele (400 bp) and the specific product for the Myf5 allele without Cre transgene (603 bp) had to be identified by the Myf5^{Cre} PCR.

PCR mix for one reaction

Amount	Reagent
2 µl	Genomic DNA
13 µl	A. bidest
2,5 µl	PCR buffer 10x
2 µl	dNTPs 1.25 mM
2 µl	Myf5_Cre_fw 10 pmol/µl
1 µl	Myf5_Cre_WT_rev 10 pmol/µl
1 µl	Myf5_Cre_KO_rev 10 pmol/µl
0,5 µl	Taq polymerase
1 µl	Magnesium chloride 1,5 mM

Program for the thermal PCR cycler

Temperature	Time	Cycles
95 °C	5 min	1
95 °C	40 sec	35
59 °C	1:00 min	
72 °C	1:00 min	
72 °C	7 min	1
4 °C	∞	1

Unspecific^{Cre} PCR

For identifying Nf1HSA and Nf1Prx1 mutant mice, the Cre alleles were identified via the Unspecific^{Cre} PCR. The expected PCR product had a size of 650 bp.

PCR mix for one reaction

Amount	Reagent
1 µl	Genomic DNA
17 µl	A. bidest
2,5 µl	PCR buffer 10x
2 µl	dNTPs 1.25 mM
1 µl	Unspecific_Cre_fw 10 pmol/µl
1 µl	Unspecific_Cre _rev 10 pmol/µl
0,5 µl	Taq polymerase

Program for the thermal PCR cycler

Temperature	Time	Cycles
94 °C	5 min	1
94 °C	30 sec	35
55 °C	30 sec	
72 °C	1:00 min	
72 °C	7 min	1
4 °C	∞	1

mTmG PCR

By performing the mTmG PCR it was possible to detect whether the mTmG allele of the investigated mice was recombined by Cre activity or not. If the allele was recombined, the expected specific PCR products had a size of 200 bp. If the allele was not recombined, the expected specific PCR products had a size of 350 bp.

PCR mix for one reaction

Amount	Reagent
1 µl	Genomic DNA
13 µl	A. bidest
2,5 µl	PCR buffer 10x
2 µl	dNTPs 1.25 mM
2 µl	mTmG_fw 10 pmol/µl
1 µl	mTmG_WT_rev 10 pmol/µl
1 µl	mTmG_KO_rev 10 pmol/µl
0,5 µl	Taq polymerase
2 µl	Magnesium chloride 1,5 mM

Program for the thermal PCR cycler

Temperature	Time	Cycles
95 °C	5 min	1
95 °C	1:00 min	35
66 °C	1:00 min	
72 °C	1:00 min	
72 °C	10 min	1
4 °C	∞	1

3.1.6 Semi-quantitative polymerase chain reaction (PCR) on genomic DNA

Semi-quantitative PCR was performed to determine the relative quantity of the recombined *Nf1* allele in relation to the not recombined *Nf1* allele in $Nf1^{flox/flox}$, Cre mice. Two PCR reactions are set up in parallel in one tube: the expected specific size of the PCR products was 280 bp (primer Nf1_P1 and Nf1_P2) for the recombined *Nf1* allele (*R*) and 350 bp (primer Nf1_P1 and Nf1_P4) for the not recombined *Nf1* allele (*Non*R). The relation between the relative quantities of the *R* PCR product to the *Non*R PCR product was an indication for the efficiency of Cre recombination activity in the investigated samples. Before performing the PCR the concentration of genomic DNA was measured with an UV-Vis spectrophotometer and adjusted to 50 ng/µl. The PCR reaction was stopped during the exponential phase of amplification which was previously determined by a PCR pre-test.

PCR mix for one reaction

Amount	Reagent
4 µl	Genomic DNA 50 ng/µl
12,1 µl	A. bidest
2,5 µl	PCR buffer 10x
2 µl	dNTPs 1.25 mM
2 µl	Nf1_P1 10 pmol/µl
1 µl	Nf1_P2 10 pmol/µl
1 µl	Nf1_P4 10 pmol/µl
0,4 µl	Taq polymerase

Program for the thermal PCR cycler

Temperature	Time	Cycles
94 °C	5 min	1
94 °C	30 sec	32
50 °C	30 sec	
72 °C	1:10 min	
72 °C	7 min	1
4 °C	∞	1

3.1.7 Quantitative polymerase chain reaction (qPCR) on cDNA

The relative quantification of RNA transcripts in the tissue samples was performed according to the SYBR Green based method (Morrison et al., 1998; Pfaffl, 2001). For this purpose cDNA was diluted 1 in 10 in A. bidest. For each single reaction 6 µl SYBR Green PCR Master Mix, 4 µl cDNA (diluted 1 in 10) and 2 µl of primer mix were used. The primer mix is a solution of forward (1, 5 pmol/µl) and reverse primer (1,5 pmol/µl) in A. bidest. All primers used were designed with Primer3 software (Koressaar and Remm, 2007; Untergasser et al., 2012). The genes Acta1 (skeletal muscle actin alpha 1) or β-Actin were used as a standard for normalisation to calculate the relative expression of genes of interest. All reactions were performed in triplicates for each gene using the 7900HT Fast Real-Time PCR Cycler. The data was analysed with the SDS 2.1 analysis program. The relative expression calculation was done according to algorithm described by Pfaffl (Pfaffl, 2001).

PCR mix for one reaction

Amount	Reagent
4 µl	cDNA, diluted 1:10
2 µl	Primer mix, 1,5 pmol/µl each
6 µl	SYBR Green PCR Master Mix

Program for the thermal PCR cycler

Temperature	Time	Cycles
50 °C	2 min	1
95 °C	10 min	1
95 °C	15 sec	40
60 °C	1:00 min	
95 °C	15 sec	1
60 °C	15 sec	1
95 °C	15 sec	1
4 °C	∞	1

3.1.8 Agarose gel electrophoresis

After PCR on genomic DNA the amplified PCR products got separated by agarose gel electrophoresis. For evaluation of genotyping 1 % agarose gels were used and for semi-quantitative PCR 2,5 % agarose gels were used. For gel preparation 1 g or 2,5 g, respectively, of agarose powder were solved in 100 ml of 1 x TAE buffer, boiled and cooled down to 60 °C. 3 µl of ethidium bromide were added for DNA visualisation. After the gels got polymerised, 6 x loading dye was added to each PCR sample and they were loaded on the gels. The electrophoresis

was performed with a constant voltage of 100V for 45 min. PCR products were detected and photographed with the E.A.S.Y transluminator device. For semi-quantitative PCR the PCR product signal intensity was evaluated with the Analyze Gels function of Image J.

3.1.9 Microarray gene expression analysis

RNA was isolated from tibiae like described in section 3.1.3. The cRNA (complementary RNA, RNA derived from cDNA through standard RNA synthesis) generation and microarray hybridization was done according to the standard protocols applied in the Laboratory of Functional Genome Research Charité - Core Facility. A total of 10 high density oligonucleotide mouse GENE 1.0 ST arrays (Affymetrix) were used in this study. Samples from each animal (5 Nf1Prx1 mutants and 5 control animals) were applied individually to each array. All the procedures and hybridization were performed according to the Gene Chip Expression Technical Manual (Affymetrix) as reported by Gross et al., 2007. Raw data were quantified with Microarray Suite 5.0 software by the Laboratory of Functional Genome Research. Expression data were normalized using the Genespring settings for Affymetrix gene chip arrays. Results from probe sets on each array were subjected to one way ANOVA analysis (see section 3.5.3) to reveal the genes significantly deregulated in the *Nf1* deficient tibiae.

3.1.10 Generation of RNA antisense probes for WM-ISH

WM-ISH (whole mount *in situ* hybridisation) was performed using a DIG labelled antisense riboprobe against MyoD mRNA transcripts. The probe was generated through *in vitro* transcription. The probe sequence already existed in the laboratory as an insert cloned in the pTAgfp plasmid vector (4.362 kb), which contained SP6 and T7 promoters flanking the probe sequence. The MyoD (MyoD1) probe has been designed according to Sassoon et al., 1989.

Sequencing

Sequencing reaction was performed with, above mentioned, pTAgfp plasmid with the MyoD insert. For the prior sequencing PCR reaction SP6 and T7 primers and the BigDye Terminator Sequencing Kit were used. Sequencing PCR reaction was performed the following way:

Sequencing mix for one reaction

Amount	Reagent
100 ng	Plasmid DNA
2 µl	Primer SP6 or T7 10 pmol/µl
1 µl	BigDye
2 µl	5 x sequencing buffer
Ad 10 µl	A. bidest

Program for the thermal PCR cycler

Temperature	Time	Cycles
96 °C	1 min	1
96 °C	10 sec	25
50 °C	5 min	
60 °C	4 min	
4 °C	∞	1

After PCR 1 µl of 2 % SDS was added to the reaction mix and incubated at 98 °C for 10 min. Afterwards, the reaction was precipitated by adding 25 µl of 100 % ethanol to the samples and

centrifugation at 4 °C and 4000 rpm for 1 h. Subsequently, 150 µl of 70 % ethanol was added and the mixture was centrifuged at 4 °C and 4000 rpm for 30 min and the pellet was dried by upside-down centrifugation. The analyses of the reaction products were performed in the core facility of the Institute for Medical Genetics - Charité, using the Sequence Analyser 3100 AB sequencing machine. Sequences were checked with the SeqMan software of DNAStar. After sequence confirmation, the RNA antisense probe was generated from the sequenced pTAgfp plasmid.

PCR on pTAgfp plasmid vector

For generating a template for the WM-ISH probe, the MyoD insert of the pTAgfp plasmid was amplified by PCR using SP6 and T7 primers according to the following protocol:

PCR mix for one reaction

Amount	Reagent
1 µl	Plasmid DNA
17 µl	A. bidest
2,5 µl	PCR buffer 10x
2 µl	dNTPs 1.25 mM
1 µl	Primer Sp6 10 pmol/µl
1 µl	Primer T7 10 pmol/µl
0,5 µl	Taq polymerase

Program for the thermal PCR cycler

Temperature	Time	Cycles
94 °C	5 min	1
94 °C	30 sec	35
55 °C	30 sec	
72 °C	1:00 min	
72 °C	7 min	1
4 °C	∞	1

After PCR reaction the product (approximately 800 bp) was separated by agarose gel electrophoresis on a 1 % gel according to section 3.1.9. The PCR product was cleaned by isolation from the agarose gel using the Gel-Out Gel Extraction Kit according to manufacturer's instructions. DNA concentration was measured by taking 1 µl of the clean PCR product and measuring the optical absorbance at 260 nm with an UV-Vis spectrophotometer.

***In vitro* transcription of RNA probes**

The antisense RNA riboprobe was generated by *in vitro* transcription of 200 ng of the cleaned PCR product in presence of DIG labelled nucleotides, using T7 polymerase according to the MyoD insert orientation in the pTAgfp vector. The *in vitro* probe transcription and DIG labelling was performed with the DIG RNA Labelling kit according to the manufacturer's protocol. After stopping the reaction, the RNA was precipitated by adjusting the reaction volume to 100 µl with DEPC-H_2O and adding 10 µl lithium chloride and 300 µl ice cold 100 % ethanol. The precipitation mix was incubated at -80 °C for at least 1 h. After centrifugation at 13000 rpm for 30 min the pellet was washed twice with 70 % ethanol. Afterwards the pellet was dissolved in 100 µl of DEPC-H_2O. 5 µl of the transcribed probe was checked up to purity by gel electrophoresis (see section 3.1.9). The positive and pure probe was stored at -80 °C.

3.1.11 RNA whole mount *in situ* hybridisation (WM-ISH)

For WM-ISH embryos at the stage E14.5 were dissected in 1 x PBS (DEPC- H_2O) and fixed over night in 4 % PFA/PBS. The following day embryos were washed twice in PBST for 30 min on ice and dehydrated through 25 %, 50 % and 75 % methanol in PBST (DEPC-H_2O) and twice in 100 % methanol for 10 min. Each step was performed on ice. Storage of embryos was possible in 100 % methanol at -20 °C for several weeks. For hybridisation embryos got rehydrated through 75 %, 50 % and 25 % methanol in PBST (DEPC-H_2O) and washed twice with 1 x PBS (DEPC-H_2O) on ice. Afterwards embryos got bleached with 6 % hydrogen peroxide in PBST for 1 h on ice. After washing the embryos three times 10 min with PBST they got treated with proteinase K (20 µg/ml) in proteinase K buffer on a shaker at room temperature for 12 min. After several washes with PBST, PBST/glycine and RIPA buffer the embryos got fixed in 4 % PFA/0,2 % glutaraldehyde for 20 min and washed again several times in PBST, PBST/hybridisation buffer and hybridisation buffer. After a pre-hybridisation at 65 °C for 3 h the embryos got incubated with the MyoD probe at 65 °C over night. For the preparation of the probe solution tRNA (100 µg/ml) was diluted in hybridisation buffer (in relation 1 in 100). 1 ml of that solution got mixed with 10 µl probe (end concentration 0,25 µg/ml). To denaturise the probe the solution was incubated at 80 °C for 5 min. Then, the solution was applied to the embryos and incubated at 65 °C over night. An excess of probe molecules was washed away the next day by two washes with freshly made hybridisation buffer at 65 °C for 30 min. Afterwards embryos got cooled down to room temperature and digested twice with RNaseA at 37 °C for 30 min. Several washes with formamide buffer at 65 °C ensued. Initially formamide buffer was mixed with RNase solution (in relation 1 in 1) and later diluted with MABT (also 1 in 1), followed by two washing steps with MABT. For saturation of unspecific RNAs the embryos were incubated in blocking solution for 1 h and subsequently incubated with anti DIG-Fab antibody in 1 % BBR/MABT (1 in 5000) at 4 °C over night. The next day unbound antibody was removed by several washes with PBST/tetramisol all day long. For detection of antibody signals the embryos got equilibrated three times in ALP buffer for 20 min and afterwards embryos got transferred into BM purple AP substrate. The incubation took place at room temperature until a distinct colour signal was visible on the embryos. For signal conservation the embryos got washed three times with ALP buffer and fixed in 4 % PFA/PBS. Documentation of results was performed with a binocular and the AxioVision 4.6 software. Measurement and quantification of $MyoD^+$ stained area was performed with the Autmess function of AxioVision 4.6.

3.2 Primary cell culture

3.2.1 Isolation of primary myoblasts and fibroblasts

A pregnant mouse was killed by exposure to high concentrations of carbon dioxide gas at day 18.5 of pregnancy. Fetuses (E18.5) were isolated and killed via decapitation. A piece of liver was collected for DNA isolation (see section 3.1.1) and genotyping (see section 3.1.6). Limbs were removed with sterile scissors and the muscle tissue was dissected away from the skin and bones with sterile forceps. The muscle tissue was homogenized with forceps and scalpels. The

homogenisate was transferred into HBSS buffer (500 µl per fetus) which has been supplemented with 2 mM magnesium sulphate and 2 mM calcium chloride. Collagenase NB4 G was added to the solution (20 µl of 15 % collagenase in DPBS per 200 µl HBSS). The mixture was pipetted up and down and incubated on a thermo mixer at 37 °C and 1000 rpm for 20 min. Subsequently, the homogenisate was vortexed rigorously and put back on the thermo mixer for another 20 min. 1 ml of growing medium was added to each sample and mixed via pipetting up and down. Afterwards, the sample was pipetted through a 20 µM cell strainer into 15 ml tubes. The strainer was flushed with 1 ml of additional growing medium. From now on, the samples were treated under sterile cell culture conditions. The 15 ml tubes were centrifuged at room temperature and 2000 rpm for 5 min. The supernatant was discarded and the pellet was re-suspended in 200 µl growing medium and plated in 6-well cell culture plates. The plates were incubated at 37 °C for 2 h. Fibroblasts were expected to attach to the plastic surface of the cell culture wells and myoblasts were expected to remain unattached in the supernatant. The supernatant was finally transferred to 12-well cell culture plates that had been covered with 10 % matrigel before. 2 ml of growing medium was added to the uncovered 6-well plates. After 2 h of incubation at 37 °C 2 ml of growing medium was added to the 12-well plates.

3.2.2 Culturing of primary myoblasts and fibroblasts

Primary myoblasts were expected to be enriched in the matrigel covered 12-well plates and primary fibroblasts were expected to be enriched in the uncovered 6-well plates. Cells were incubated at 37 °C and 5 % carbon dioxide. Every 24 hours after plating the used growing medium was discarded from all cell culture plates, cells were washed with DPBS and 2 ml of fresh growing medium were added to the cells. Confluence of cells was controlled every day. If fibroblasts were nearly confluent, old medium was discarded, cells were washed with DPBS and 0,5 ml of trypsin was added to each well. A 3 min incubation step at 37 °C ensued and 3,5 ml of fresh growing medium was added to each well. After flushing up and down 2 ml of cell suspension were plated into a new cell culture well. This passaging process was repeated twice during the next days to ensure a clean population of fibroblasts. The primary myoblasts, however were not passaged as they proliferated significantly slower than the fibroblasts.
For harvesting of fibroblasts the growing medium was discarded and cells were washed with DPBS. 0,5 ml of trypsin were added to the cells and they were incubated at 37 °C for 3 min. 1, 5 ml fresh growing medium was added and flushed up and down. The medium was transferred to 15 ml tubes afterwards. The tubes were centrifuged at 2000 rpm for 5 min. The supernatant was discarded and the pellet was washed with DPBS. After removal of DPBS the tubes were shock frozen in liquid nitrogen and stored at -80 °C until isolation of genomic DNA. The DNA isolation was performed according to the tail tip protocol of section 3.1.1 and a semi-quantitative PCR was performed (see section 3.1.7).
For harvesting of myoblasts growing medium was removed and the layer of cells on the matrigel was washed three times with ice cold DPBS for 5 min. 2 ml of Cell Recovery Solution (DB Bioscience) were added to each of the matrigel covered cell culture wells. The gel and cell layers were scraped into cold 50 ml tubes sitting on ice. The wells were rinsed again with 3 ml of cell recovery solution which was afterwards also transferred to the 50 ml tubes. The tubes were inverted a few times and left on ice until the matrigel was dissolved completely. Afterwards, the

tubes were centrifuged at 4 °C and 5000 rcf for 5 min. The supernatant was discarded and the cell pellet was washed by gentle re-suspension in 1 ml of ice cold DPBS and another centrifugation step. After removal of DPBS the tubes were shock frozen in liquid nitrogen and stored at -80 °C until isolation of genomic DNA. The DNA isolation was performed according to the tail tip protocol of section 3.1.1 and a semi-quantitative PCR was performed (see section 3.1.7).

3.2.3 Immunocytochemistry (ICC) of primary cells

Primary fibroblasts were prepared for immunocytochemistry by taking 50 µl of growing medium from each well directly after the last passaging step (see section 3.2.2; before cells could get attached to the well). The medium was pipetted on a round glass cover slide (10 mm diameter) which was placed in a well of a cell culture plate. The plate was incubated at 37 °C for 2 h.
Primary myoblasts were prepared for immunocytochemistry by taking 50 µl of growing medium at the first plating step right before myoblasts attach to the matrigel surface (see section 3.2.2). The medium was pipetted on a round glass cover slide (10 mm diameter) which has been covered by 10 % matrigel before. The slides were placed in a well of a cell culture plate which was incubated at 37 °C for 2 h for the cells to attach.
After incubation at 37 °C the glass slides with the fibroblasts and the myoblasts were washed three times with DPBS for 5 min. Then, cells were fixed for exactly 10 min with 4 % PFA/PBS at room temperature. Afterwards, they were washed three times with 1 x PBS for 10 min. The PBS was removed and the glass slides were incubated with 500 µl of TSA blocking buffer at room temperature for 1 h. Afterwards, staining solution containing the primary antibodies against desmin (goat) and vimentin (rabbit) in a dilution of 1 in 100 each were applied to the glass slides in a humid chamber at 4 °C over night. The next day glass slides were washed 4 times with PBX on a shaker at room temperature. Then, fluorescent secondary antibodies against goat and rabbit in a dilution of 1 in 500 each as well as DAPI (1 in 1000) were applied to the glass slides in a humid chamber at room temperature for 2 h. Finally, glass slides were washed four times with 1 x PBS at room temperature and mounted on microscope glass slides with Fluoromount G. Microscopic evaluation was performed with the fluorescence microscope Axiovert 200M and the AxioVision 4.6 software.

3.2.4 Isolation, culturing and ICC of primary myotubes

Isolation of primary myotubes was performed according to the protocol of primary myoblast isolation (see section 3.2.1) but instead of using 20 µM cell strainers tissue homogenisate was filtered through a 100 µM cell strainer. Culturing was according to the protocol for myoblasts of section 3.2.2 and immunocytochemistry was according to the protocol in section 3.2.3. But for myotubes the primary antibodies against MyoD (rabbit) and myosin heavy chain (mouse) as well as fluorescent secondary antibodies against rabbit and mouse were used.

3.3 Biochemical methods

3.3.1 Protein isolation from muscle tissue

About 100 mg of muscle tissue was isolated from postnatal mice and directly snap frozen in liquid nitrogen. The tissue was quickly taken from the nitrogen and wrapped in chilled laboratory aluminium foil. Tissue was crushed in frozen state by striking it with a hammer. 250 µl of membrane lyses buffer were added to the tissue. An autoclaved grinding bead was added per sample and the mixture was homogenised with a bead mill (TissueLyser LT). In the TissueLyser samples were shaken three times at 60 Hz for 30 sec. In between, samples were placed on ice for 30 sec. The lysates were vortexed and subsequently transferred into new 1,5 ml tubes and sonificated four times for four cycles of 30 sec with low power. To get rid of big tissue pieces samples were centrifuged at 10000 rpm in a cooled centrifuge (4 °C) for 10 min. The supernatants were transferred to new tubes and the protein concentration was determined.

3.3.2 Determination of protein concentration

Protein concentrations were determined using the BCA Protein Assay Reagent Kit following the supplier's instructions. With an ELISA reader protein light absorption was measured at 562 nm. With the help of a protein (BSA) standard dilution row and standard curve the unknown concentrations of the protein samples could be calculated.

3.3.3 SDS-PAGE according to Laemmli

For protein separation SDS polyacrylamide gel electrophoresis (SDS-PAGE) was used. A polyacrylamide gel consisted of an assembling and a separation part which are passed by the proteins in that order. In this work, 10 % polyacrylamide gels were used for proteins separation and prepared according to the following instructions:

Assembling gel
- 6,8 ml A. bidest
- 1,7 ml 30 % Acrylamid
- 1,25 ml 0,5 M Tris (pH 6.8)
- 0,1 ml 10 % SDS
- 0,1 ml 10 % APS
- 0,01 ml TEMED

Separation gel (10 %)
- 15,9 ml A. bidest
- 13,3 ml 30 % Acrylamid
- 12,5 ml 1,5 M Tris (pH 8.8)
- 0,5 ml 10 % SDS
- 0,5 ml 10 % APS
- 0,02 ml TEMED

After adding combs for sample insertion in the assembling gel and polymerisation at room temperature, the gel running chambers were assembled and running buffer was added. 20 µg of each protein sample was loaded on the polyacrylamide gels. Before, protein lysates were diluted in membrane lyses buffer. 4 x protein loading buffer was added to each sample and the samples were heated at 95 °C for 5 min and placed on ice. In parallel to the samples a standard size

marker was loaded on the gel for estimating protein sizes in the western blot. After sample loading a voltage of 80 V was applied for about 2 h at room temperature.

3.3.4 Western blot (WB)

Protein transfer on a nitrocellulose membrane

With the help of a western blot it is possible to detect proteins from tissue lysates with the help of specific antibodies. After separation via SDS-Page (see section 3.3.3) proteins were transferred on a nitrocellulose membrane. Therefore, a nitrocellulose membrane of the size of a polyacrylamide gel was activated in methanol for 2 min. Afterwards, the membrane as well as the gel got incubated in 1 x transfer buffer for 15 to 30 min. The protein transfer from the gel to the membrane was realized by the *semi dry* blotting technique in a special blot chamber (assembly from the upper side [negative pole] to the lower side [positive pole]: Whatman paper - gel - nitrocellulose membrane - Whatman paper). Blotting was performed with 20 V for 40 min.

Detection of proteins with antibodies

After blotting, the membrane was washed in 1 x TBST for 5 min and then blocked in 5 % BSA (in TBST) for 2 h at room temperature to cover unspecific binding sites. Afterwards, the membrane was washed again in 1 x TBST and finally incubated with the primary antibody (in 5 % BSA solution) at 4 °C over night. At the next day, the membrane was washed several times with 1 x TBST at room temperature for 10 min. Then, the membrane was incubated with the peroxidase-coupled secondary antibody (in 5 % BSA solution). Primary and secondary antibodies were diluted as described in section 2.10. The membrane was washed again in 1 x TBST. Finally, it was possible to detect the antibodies and proteins, respectively, with the help of an enzymatic reaction.

Detection of proteins

The detection of the secondary antibodies and consequently the proteins of interest were performed with *enhanced chemiluminescence* (ECL) according to the supplier's protocol. Signals were detected through exposure of the activated membrane to an X-ray film. The developed X-ray film was digitalised by scanning it with a laser scanner.

Re-usage of nitrocellulose membranes

It was possible to re-use a western blot membrane as proteins are stably bound to the membrane. It was only necessary to remove the applied antibodies. Therefore, an already used membrane was incubated three times in stripping buffer at room temperature for 10 min. To make sure that no antibody was left on the membrane *enhanced chemiluminescence* (ECL) was applied to the membrane and a new X-ray film was developed. After successful removal of antibodies the membrane was blocked again with 5 % BSA solution to incubate with a new primary antibody.

3.4 Histology

3.4.1 Animal sample preparation

For preparation of fetal tissue samples for histological staining a pregnant mouse was killed by exposure to high concentrations of carbon dioxide gas at day 18.5 of pregnancy (E18.5). Fetuses were isolated and killed via decapitation. A piece of liver was collected for DNA isolation (see section 3.1.1) and genotyping (see section 3.1.6). Limbs were dissected completely with sterile scissors and collected for cryo conservation. For preparation of postnatal tissue, animals were killed by exposure to high concentrations of carbon dioxide gas. A piece of the tail tip was collected for DNA isolation (see section 3.1.1) and genotyping (see section 3.1.6). Limbs were dissected with sterile scissors, skin and fur was removed and limbs were collected for cryo conservation.
Isopentane was cooled down in a 50 ml tube which has been placed into a container with liquid nitrogen. Isopentane was cooled down until frozen completely, removed from the liquid nitrogen container and placed at room temperature. After a sufficient volume (in regard to sample size) of isopentane melted, the dissected mouse limbs were inserted into the melted fraction with the help of forceps for 10 sec. Afterwards samples were quickly transferred into labelled container and placed into liquid nitrogen. If samples were not processed directly they were stored at -80 °C until sectioning.

3.4.2 Cryo sectioning of limb tissue

Cryo preserved mouse limbs were transferred to a cryotome for sectioning. The cryotome and the cryotome sectioning blade were cooled down to -20 °C. The mouse limbs were attached to metal disc sample holders with TissueTek freezing medium. The part of the limb to be investigated was orientated in right angle to the sample holder. Then, the sample holder was attached to the cryotome and cooled down to -20 °C. Cross sections were taken of the upper forelimb at the distal end of the tuberositas deltoidea, of the lower hindlimb at the maximal dilatation of the tibial crest and at the upper hindlimb at the middle of femur. For mTmG reporter mice further sections were taken sagital through the brain and transversal trough the torso. Sections had a thickness of 12 µM and were collected on Superfrost glass slides which were pre-warmed at 37 °C. Sections were tried at a 37 °C warm heating plate for 30 min. Sections of mTmG mice, however, were dried in a dark chamber at room temperature for preserving the internal fluorescence signals. Sections were processed directly or stored at - 80°C in sealed boxes containing silica beads for humidity resorption.

3.4.3 Immunohistochemistry (IHC)

Fixation of tissue sections

Frozen sections of cryo preserved tissue were defrosted for 4 h at room temperature and washed for five minutes in 1 x PBS to remove any TissueTek residues. The sections were fixed using 4% PFA/PBS for five minutes. The slides were washed three times in A. bidest for 3 min to remove PFA residues.

Antigen retrieval

Sections were treated with DAKO citrate buffer with a pH of 6 when staining against Ki-67 and BrdU, respectively. DAKO citrate buffer with a pH of 9 was used for all other stainings. For antigen retrieval, the sections were immersed in 200 ml 1 x DAKO citrate buffer and cooked in the microwave for 1 min at 700 W, then left to cool down at room temperature for 5 min and heated again for 90 s at 700 W. For staining against Pax7 sections were cooked for 30 min in a water bath at 80 °C instead. Afterwards, sections were allowed to cool down at room temperature for 30 min. The citrate buffer was washed off the slides by immersing them in 1 x PBS three times for 10 min.

Blocking of unspecific antigens

The tissue sections were blocked in a humid chamber using 300 µl of TSA blocking buffer per slide at room temperature for 1h.

Incubation with primary antibodies

The sections were incubated with 300 µl of staining buffer (per slide) containing the respective primary antibodies in a humid chamber over night at 4 °C on a rotating device (30 rpm). Antibodies were diluted in staining buffer as described in section 2.10. After incubation slides were washed 4 times with PBX for 10 min (5 times for Pax7, Ki-67 and BrdU) to remove unbound and non-specifically bound antibodies.

Incubation with secondary antibodies

The tissue sections were incubated with 300 µl (per slide) of the staining buffer containing the respective secondary antibodies in a humid chamber at room temperature for 2 h. Antibodies were diluted in staining buffer as described in section 2.10. DAPI was also added to the staining solution diluted 1 in 1000. After incubation the slides were washed four times in PBS for 10 min to remove unbound and non-specifically bound antibodies. Finally, sections were mounted with Fluoromount G and covered with cover slides. Sections were stored at 4 °C, protected from light.

Microscopy and image acquisition

After immunohistochemical staining the results were evaluated with the help of fluorescence microscopy. All images used for morphometric analysis of individual myofibres (myofibre size

and circularity) and the quantification of $Pax7^+$, $Ki\text{-}67^+$ and $BrdU^+$ cells were acquired with the Axiovert 200M microscope and the AxioVision 4.6 software. All images for measurement of muscle cross sectional area (CSA), total myofibre count, slow twitch myofibre and embryonic myofibre quantification were acquired with the Biorevo BZ9000 microscope and the BZ-II Viewer software. Images of myotubes of mTmG mice were taken with the LSM700 microscope and the ZEN pro software.

Image processing

All images taken with the Axiovert 200M microscope were initially processed with the AxioVision 4.6 software. All images taken with the LSM700 microscope were initially processed with the ZEN pro software. Further image enhancing, merging and cropping was performed using the software Photoshop CS6. All images taken with the Biorevo BZ9000 microscope were merged, enhanced and cropped exclusively with the BZ-II Analyzer software.

Determination of muscle cross sectional area

For the measurement of muscle cross sectional area, wide view images of cross sectional muscle sections were taken with the Biorevo BZ9000 microscope using the Merge and Z-stack functions (10 x objective for the TB, TA, and EDL muscles and with the 20x objective for the soleus muscle). The AreaMeasure function of the BZ-II Analyzer software was used to determine the cross sectional area (CSA) of these muscles. The average CSA of every muscle was calculated for each animal using the measurements from at least three sections of different section planes per animal.

Determination of the total myofibre number

Wide view images of the muscles triceps brachii (TB), tibialis anterior (TA) and extensor digitorum longus (EDL) were taken with the Biorevo BZ9000 microscope using the merge and Z-stack functions with the 10 x objective. The soleus muscle was photographed using the 20 x objective also using the merge and Z-stack functions. The total number of myofibres was determined using the Hybrid cell count function of the BZ-II Analyzer software. The counting of every section with the hybrid cell count function was performed manually. At least three sections were counted for each animal and averaged to determine the mean myofibre number in all four muscles in all animals. The mean myofibre number was for control and mutant mice.

Quantification of myofibres expressing the slow twitch or embryonic myosin

TB, TA and EDL muscles were photographed with the 10 x objective using the merge and Z-stack functions of the BZ-II Analyzer software. For the soleus muscle the 20 x objective was used. The total number of fibres was determined using the Hybrid cell count function of the BZ-II Analyzer software (see section 3.4.5). Myofibres expressing slow twitch myosin (MySlow) or were counted with the Hybrid cell count function, too. Fibres positive for embryonic myosin were counted using the Cell Counter function of Image J. The relative number of fibres expressing a myosin isoform was calculated for each animal. The mean percentage of MySlow

and MyEmb expressing fibres was determined by averaging the fibre populations of all controls and all mutants for each investigated muscle, respectively.

Measurement of the slow myosin heavy chain positive area

TB, TA, and EDL muscles were photographed with the 10 x objective of the Keyence Biorevo BZ9000 microscope using the Merge and Z-stack functions. The soleus muscle was photographed with the 20 x objective. The images were analysed with the Autmess function of the AxioVision 4.6 software from Zeiss. The connective tissue area of each muscle was determined and subtracted from the total CSA to calculate the muscle tissue area. The MySlow$^+$ area and MyEmb$^+$ area, respectively, was divided by the muscle tissue area to determine the percentage of area expressing MySlow. One section per animal per muscle was measured. To determine the mean values the data from all controls and all mutants were averaged.

Measurement of myofibre cross sectional area, Feret's diameter and circularity

Images of the internal (Region I), medial (Region II), and external (Region III) regions of TB as well as from the internal region of TA, the external region of EDL and the internal region of soleus were taken using the Axiovert 200M microscope with the 20 x objective for this measurement. A macro programmed to recognize individual myofibres as well as measure their CSA, ferret's minimum diameter and circularity was generated using the Autmess function form the AxioVision 4.6 software from Zeiss. As the ability of the macro to recognize individual myofibres is limited, the results of every counted section were corrected manually with the Autmess function. At least 210 fibres were measured for every section. One section per muscle was counted for each animal. For TB every region (I, II and III) was counted separately. All the measured fibres from each muscle were averaged to calculate the mean values for the CSA, Feret's minimum diameter and circularity for every animal.

Quantification of Pax7$^+$, Ki-67$^+$ and BrdU $^+$ cell numbers

Images of the distinct regions of TB were taken using the 20 x objective of the Axiovert 200M microscope. For soleus the whole muscle was photographed using the 20 x objective and individual images were merged using Adobe Photoshop CS6. The Pax7, Ki-67 and BrdU signals were counted with the Cell Counter function of Image J. The myofibres in each picture were also counted with this function. The numbers of Pax7$^+$, Ki-67$^+$ or Pax7$^+$/BrdU$^+$ cells per one hundred myofibres were calculated for each region individually in the TB and averaged to get the mean for the whole muscle. For the soleus all signals and all myofibres of the whole muscle were counted as well as the number of Pax7$^+$ or Ki-67$^+$ cells. The mean values of controls and mutant animals were averaged.

3.4.4 Sdh staining

Sdh (succinate dehydrogenase) is a soluble iron flavoprotein that catalyzes the oxidation of succinate acid to fumaric acid. It is an enzyme (complex II) of the mitochondrial electron

transport chain and can be found in myofibres. It produces the reduced form of NADH, but for Sdh staining a different electron acceptor is used. The used electron acceptor chemically reacts with nitro blue tetrazolium (NBT), a purple salt, to visualize the reaction.
For Sdh staining limb tissue was prepared, sectioned and preserved as described in sections 3.4.1 and 3.4.2. The tissue sections were shortly defrosted at room temperature and incubated with Sdh incubation medium (see section 4.2) at 37 °C for 3 h. Afterwards, sections were rinsed shortly in 30 % acetone, 60 % acetone, 30 % acetone and A. bidest. Finally, sections were mounted with Hydromatrix and a coverslip was added. Sections were photographed with the Leica DMR HC microscope and the AxioVision 4.6 software. Sdh staining intensity was quantified with the Autmess function of AxioVision 4.6.

3.4.5 Single fibre isolation and processing

Animal preparation
For preparation of single muscle fibres, adult mice were killed by exposure to high concentrations of carbon dioxide gas. A piece of the tail tip was collected for DNA isolation (see section 3.1.1) and genotyping (see section 3.1.6).

Muscle dissection and digestion
Mouse hindlimbs were sprayed with 70% ethanol. The animal was pinned (face up) to a support board to have a better grasp of the hind limb during the procedure. With the help of scissors, the skin was cut through along the entire length of the limb and the underlying muscles were exposed. The skin was removed as well as any hair or fur. The muscle fascia was cut through with fine scissors without damaging the underlying muscles. Then, the EDL, which can be found in the anterior compartment of the hind limb underneath the TA muscle, was visually localized. With the help of two forceps, the distal tendons of TA and EDL were cut with sharp scissors at their ends. With the help of forceps TA and EDL muscles were hold by their tendons and the muscles were delicately pull up towards the proximal end. Then, the EDL was separated from the TA muscle by pulling the two tendons in opposite directions. The EDL tendon was exposed and the TA muscle was removed. The proximal EDL tendon was cut and the EDL was gently removed. By holding the muscle through its tendons, the EDL was transferred in 1 x PBS for washing. After dissecting both EDL muscle of an animal, the muscles were transferred to 2 ml of previously prepared collagenase solution (0,2 % collagenase type I in DMEM). They were incubated at 37 °C in a water bath. The incubation time needed to be adjusted at each experiment depending on collagenase activity. The average digestion time was 1 h. During the digestion the muscle was regularly checked to avoid over-digestion. The digestion was stopped when muscles started to loosen up and myofibres became visible. To stop the digestion, muscles were carefully transferred to a pre-warmed Petri dish (pre-coated with normal horse serum) with 4 ml of DMEM (dissociation dish) with a large bore size pipette. This pipette must be prepared previously by cutting the end of a Pasteur pipette with a diamond pen and heat polish to smooth pipette's edges.

Single myofibre dissociation

To release single myofibres from the muscles, the large bore glass pipette was used to flush the muscle with warm medium until fibres naturally start being released. The muscle was not triturated as this would have resulted in damaged fibres. This step and the following steps were performed under a microscope. Flushing the muscles was continued until the desired number of myofibres was reached. After 10 min at room temperature the muscles were allowed to incubate for 5 min at 37 °C and 5 % carbon dioxide to re-equilibrate the medium. Afterwards, the myofibres were transferred to a new pre-warmed dish (pre-coated with normal horse serum) containing washing medium (see section 2.7). Each myofibre was handled individually instead of transferring a bulk of myofibres at once. If necessary, fibres were incubated at 37 °C and 5 % carbon dioxide for 10 - 15 min to re-equilibrate the medium. This washing step was repeated once. Only live myofibres were transferred. Dead myofibres appeared as short and hyper-contracted under the microscope light. Then, fibres were transferred into pre-warmed 4 % PFA/PBS for 5 min and afterwards washed 3 times with 1 x PBS for 10 min.

Immunostaining and visualisation

Fibres were incubated in 1 % glycine in 1 x PBS to minimize PFA background staining. Myofibres were permeabilised with 0,5 % Triton X-100 in 1 x PBS for 10 min followed by a 5 min washing step in 1 x PBS. Then, fibres were transferred to TSA blocking solution and were blocked at 4 °C over night. The next day, fibres were washed once in 1 x PBS for 5 min and incubated with the primary antibody (MyFast) diluted 1 in 500 in staining solution for 1 hr at room temperature. Afterwards, fibres were washed three times for 5 min in 1 x PBS to remove any unbound antibody. Then, fibres were incubated with the fluorescent secondary antibody (donkey anti mouse; 1 in 500) and DAPI (1 in 1000) in staining solution for 1 h at room temperature. Fibres were washed three times in 1 x PBS for 5 min. All procedures were carried out with floating fibres. Then, each fibre was transferred to a glass slide separately with a Pasteur pipette. Any excess of PBS or medium was carefully removed from the glass slide. Mounting medium (Fluoromount G) was applied on the fibres and a cover slip was added. Myofibres were visualized and photographed under the fluorescence microscope Axiovert 200M with the help of the AxioVision 4.6 software.

3.4.6 Sample preparation for electron microscopy on muscle tissue

The protocol was developed by and performed with the help of the Microscopy & Cryo Electron Microscopy Group of the Max Planck Institute for Molecular Genetics. For preparation of muscle tissue for electron microscopy, mice were killed by exposure to high concentrations of carbon dioxide gas. A piece of the tail tip was collected for DNA isolation (see section 3.1.1) and genotyping (see section 3.1.6). Mouse hindlimbs were sprayed with 70 % ethanol, skinned and cut off. Further dissection was performed in 1 x PBS. Muscle fascia was removed from lower hindlimbs. Little pieces (approximately 1 mm x 1 mm) of the lateral TA muscle were cut out in the area of the maximal dilatation of the tibial crest with sharps scalpels. The pieces were directly transferred into EM fixing solution and incubated on a shaker at 4 °C over night. For subsequent washing and neutralisation samples were incubated in 50 mM sodium cacodylate buffer/ 50 mM

sodium chloride on a shaker for 5 days. Afterwards, samples were transferred into 0,5 % osmium tetroxide in 50 mM sodium cacodylate buffer/ 50 mM sodium chloride. After an incubation of 3 h, samples were washed four times in A. bidest for 20 min and afterwards incubated in 0,1 % tannin in 100 mM HEPES. After four washing steps (the last one over night), samples were stained in 2 % uranyl acetate for 2 h, shortly washed in A. bidest and dehydrated through 70 %, 90 %, 96 % ethanol and three times 100 % ethanol. To remove ethanol, samples were washed in 50 % propylene oxide/50 % ethanol for 5 min and 100 % propylene oxide for 30 min. Subsequently, the muscle samples were incubated in 50 % propylene oxide/50 % SPURR (Spurr Low-Viscosity Embedding Kit) for 1 h and in 100 % SPURR over night at 4 °C. SPURR was refreshed twice the next day and samples were embedded in SPURR, which polymerised during incubation at 60 °C for 3 days and incubation at room temperature for another 3 days. Afterwards, ultra-thin (75 nm) transversal muscle sections were performed from the embedded material using a diamond knife and the Ultracut E ultramicrotome. Sections were dried over night and contrasted with 2 % uranyl acetate (20 sec) and Reynold's lead citrate solution (20 sec) with short washes in between and afterwards (using A. bidest). Sections were analysed and photographed with the electron microscope Tecnai Spirit and the corresponding microscope software.

3.4.7 Sample preparation for electron microscopy on cortical bone

The protocol was developed by and performed with the help of the Microscopy & Cryo Electron Microscopy Group of the Max Planck Institute for Molecular Genetics. For preparation of bone tissue for electron microscopy, mice were killed by exposure to high concentrations of carbon dioxide gas. A piece of the tail tip was collected for DNA isolation (see section 3.1.1) and genotyping (see section 3.1.6). The hindlimbs were sprayed with 70 % ethanol, skinned and cut off. Further dissection was performed in 1 x PBS. Tibiae from mice were exposed by removing muscle tissue, connective tissue and periosteum with sterile forceps and scalpels. Little pieces (maximum 1mm x 1mm) of cortical bone were cut out in the area of the maximal dilatation of the tibial crest. The pieces were directly transferred into EM fixing solution and incubated on a shaker at 4 °C over night. Afterwards, bone pieces were decalcified by incubation in Osteosoft solution (Merck-Millipore) for three days. Osteosoft was replaced every day by fresh solution. For subsequent washing and neutralisation samples were incubated in 50 mM sodium cacodylate buffer/ 50 mM sodium chloride on a shaker for 5 days. Afterwards, samples were transferred into 0,5 % osmium tetroxide in 50 mM sodium cacodylate buffer/ 50 mM sodium chloride. After incubation for 3 h, bone samples were washed four times in A. bidest for 20 min and afterwards incubated in 0,1 % tannin in 100 mM HEPES. After four washing steps (the last one over night), samples were stained in 2 % uranyl acetate for 2 h, shortly washed in A. bidest and dehydrated through 70 %, 90 %, 96 % ethanol and 3 times 100 % ethanol. To remove ethanol, samples were washed in 50 % propylene oxide/50 % ethanol for 5 min and 100 % propylene oxide for 30 min. Subsequently, samples were incubated in 50 % propylene oxide/50 % SPURR (Spurr Low-Viscosity Embedding kit) for 1 h and in 100 % SPURR over night at 4 °C. SPURR was refreshed twice the next day and samples were embedded in SPURR, which polymerised at 60 °C for 3 days and another 3 days at room temperature. Afterwards, ultra-thin (75 nm) bone cross sections were performed from the embedded material using a diamond knife and the Ultracut E

ultramicrotome. Sections were dried over night and contrasted with 2 % uranyl acetate (20 sec) and Reynold's lead citrate solution (20 sec) with short washes in between and afterwards (using A. bidest). Sections were analysed and photographed with the electron microscope Tecnai Spirit and the corresponding microscope software.

3.5 Statistical evaluation

3.5.1 Standard error calculation

For all performed experiment the standard error was calculated. This error is reflected in the error bars seen in the bar diagrams. The standard error SE is a measure of how variable the mean of an experiment was, as it was repeated with a certain number (n) of biological replicates (mice). SE is calculated by dividing the standard deviation SD by the square root of the number of replicates n:

$$SE = \frac{SD}{\sqrt{n}}$$

The standard deviation SD refers to the average difference between the measured data points X of each replicate and their mean M (Cumming et al., 2007).

$$SD = \sqrt{\frac{\Sigma(X - M)^2}{n - 1}}$$

The number of biological replicates (mice) used in the experiments are indicated in figure legends.

3.5.2 Student's t-test

For all performed experiments significance of the results was determined by calculating the probability p using an unpaired Student's t-test. P is the probability that a calculated difference (M1-M2) between mutant and control animals would be achieved by chance, whereby n1 was the number of mutant animals and n2 was the number of control animals. S1 and S2 were the respective variances between the animals of a group.

$$p = \frac{M1 - M2}{\sqrt{(\frac{s1^2}{n1} + \frac{s2^2}{n2})}}$$

Significance is indicated in the diagrams by stars. Two stars (**) indicate high significance of the result; $p \leq 0{,}01$. One star (*) indicates a significant result; $p \leq 0{,}05$. No star indicates a not significant result.

3.5.3 ANOVA analysis for microarray evaluation

In gene expression microarray analysis significant gene regulations were determined with one-way analysis of variance (abbreviated one-way ANOVA). Genes found to be significantly deregulated (ANOVA F-factor ≥ 20) in mutant muscles as compared to controls have been investigated. The rationale of ANOVA is to check whether there is more variation between the animal groups than within them. That ratio (ANOVA F-factor) was calculated by using the mean squares of the 'between-groups' variance (MSB) as the numerator and the 'within-groups' variance (MSW) as the denominator.

$$F = \frac{MSB}{MSW}$$

ANOVA calculation was performed by the Laboratory of Functional Genome Research Charité - Core Facility.

4. Results

Neurofibromatosis I patients suffer from a reduction of muscle size, force and tone (Stevenson et al., 2005; Souza et al., 2009; Stevenson et al., 2012; North, 1998) due to a loss of *Nf1*. To identify the pathomechanism in muscle cells, the consequences of a loss of *Nf1* in skeletal muscle were investigated with the help of mouse models. Three different models have been generated by crossing Nf1flox mice (Zhu et al., 2001) with one of the three deleter lines Lbx1_Cre (Vasyutina et al., 2007), Myf5_Cre (Tallquist et al., 2000) or HSA_Cre (Miniou et al., 1999), respectively. This approach allowed studying the effect of *Nf1* knockout in three different muscle precursor cell types. The resulting knockout models Nf1Lbx1, Nf1Myf5 and Nf1HSA were investigated at four stages of development (Tab. 4.1) referring to the four stages of myogenesis: embryonic (until E14.5), fetal (until E18.5), perinatal (until P21) and adult (until death). Nf1Lbx1 mice die after birth due to the inability of food absorbance showed by the absence of milk in stomach and intestines (probably a consequence of *Nf1* recombination in swallowing muscles). Nf1Myf5 mice die around day P170 due to muscular weakness and exhaustion. Nf1HSA show the same viability as control animals.

Table 4.1 Overview of analysed mouse models

	Nf1Lbx1	Nf1Myf5	Nf1HSA
Cells affected by *Nf1* knockout	Embryonic muscle precursor cells and their descendants	Myoblasts and Myf5^{+} muscle pre-cursor cells and their descendants	Myotubes and myofibres
Investigated stages of development	· Embryonic E14.5 · Fetal E18.5 — —	· Embryonic E14.5 · Fetal E18.5 · Perinatal P21 · Adult P156	— · Fetal E18.5 · Postnatal P21 —
Viability	Not viable (die after birth)	Viable until P160	Normal viability

4.1 Generation of knockout mice for a skeletal muscle specific loss of *Nf1*

4.1.1 mTmG mice show tissue specific activity of Lbx1_Cre, Myf5_Cre and HSA_Cre

To study the consequences of a loss of *Nf1* in skeletal muscle, three conditional *Nf1* knockout mouse models have been generated using the Cre/loxP system (Lobe and Nagy, 1998). To ensure that *Nf1* is specifically and exclusively deleted in skeletal muscle tissue mTmG reporter mouse lines (Muzumdar et al., 2007) have been generated for each model. The mTmG reporter mice carry a transgenic mTmG allele with Cre recombination sites. They express a red fluorescent

Tomato protein in cells without Cre activity and a green GFP protein in cells with Cre activity. By breeding mTmG mice with one of the three delete lines Lbx1_Cre (Vasyutina et al., 2007), Myf5_Cre (Tallquist et al., 2000) or HSA_Cre (Miniou et al., 1999), three specific reporter lines have been generated: mTmG-Lbx1, mTmG-Myf5 and mTmG-HSA. Histological sections of these animals were taken from tissue essential for investigation of skeletal muscles and analysed via fluorescent microscopy. For better visualization specific sections were stained with DAPI (cell nuclei) or immunohistochemistry using antibodies against β tubulin III (neurons) and Pax7 (fetal precursor cells). It could be observed that mTmG-Lbx1, mTmG-Myf5 and mTmG-HSA show Cre activity in all skeletal muscles of forelimb and hindlimb at embryonic day E18.5 (Fig. 4.1). Adjacent tissues, e.g. bone, cartilage, vascular cells and skin, did not show Cre activity. Myotubes showed Cre activity whereas muscle connective tissue cells and neurons did not show Cre activity on limb cross sections. Transverse sections of torsi showed no Cre activity in spinal cords of mTmG-Lbx1, mTmG-Myf5 and mTmG-HSA. Dorsal root ganglia of mTmG-Lbx1 and mTmG-HSA did not show Cre activity. In mTmG-Myf5, however, some cells (between 1 % and 10 %) displayed Cre activity. As dorsal root ganglia only contain afferent and no motor neurons, only an influence on sensory abilities is expected by Cre recombination of *Nf1* in Nf1Myf5. Furthermore, neurons in muscle tissue of the limbs did not show Cre activity. Therefore, the Myf5_Cre deleter line was considered as suitable. Cerebral motor cortex of mTmG mice also did not show Cre activity.

To ensure that all postnatal myofibres have been targets of Cre recombinase activity, forelimb and hindlimb muscles of mTmG-Myf5 and mTmG-HSA have been analysed at day P21. Histological cross section have been performed and analysed via fluorescent microscopy. The investigated muscles showed a complete staining for Cre activity in myofibres (Fig. 4.2). No mTmG-Lbx1 mice were investigated as Nf1Lbx1 animals were not viable (see Tab.4.1). The analyses showed that the three delete lines Lbx1_Cre, Myf5_Cre and HSA_Cre are suitable for generation of muscle specific *Nf1* knockout models

4.1.2 *Nf1* is excised by Cre mediated recombination in Nf1Myf5, Nf1Lbx1 and Nf1HSA

In order to validate the three *Nf1* knockout models Nf1Lbx1, Nf1Myf5 and Nf1HSA the Cre recombination efficiency should be tested in skeletal muscle taken from embryos at day E18.5. For this purpose, genomic DNA was isolated from muscle tissue of forelimb and hindlimb muscles. A semi-quantitative PCR for the *Nf1* allele was performed using specific primer pairs for amplification of the non recombinant *Nf1* allele (P1 and P4) and the recombinant *Nf1* allele (P1 and P2) in one reaction in parallel. Results showing a recombination rate of 52,2 % and 50,1 % in Nf1Lbx1 forelimb and hindlimb, a recombination rate of 45,6 % and 48,6 % in Nf1Myf5 forelimb and hindlimb and a recombination rate of 50,4 % and 30,9 % in Nf1HSA forelimb and hindlimb, respectively (Fig. 4.3A). The prepared muscle tissue consisted of muscle and connective tissue cells (fibroblasts). In this work it was important to delete *Nf1* in muscle cells only. Therefore primary myoblasts and fibroblasts were isolated from E18.5 limb muscles and plated separately in cell culture wells.

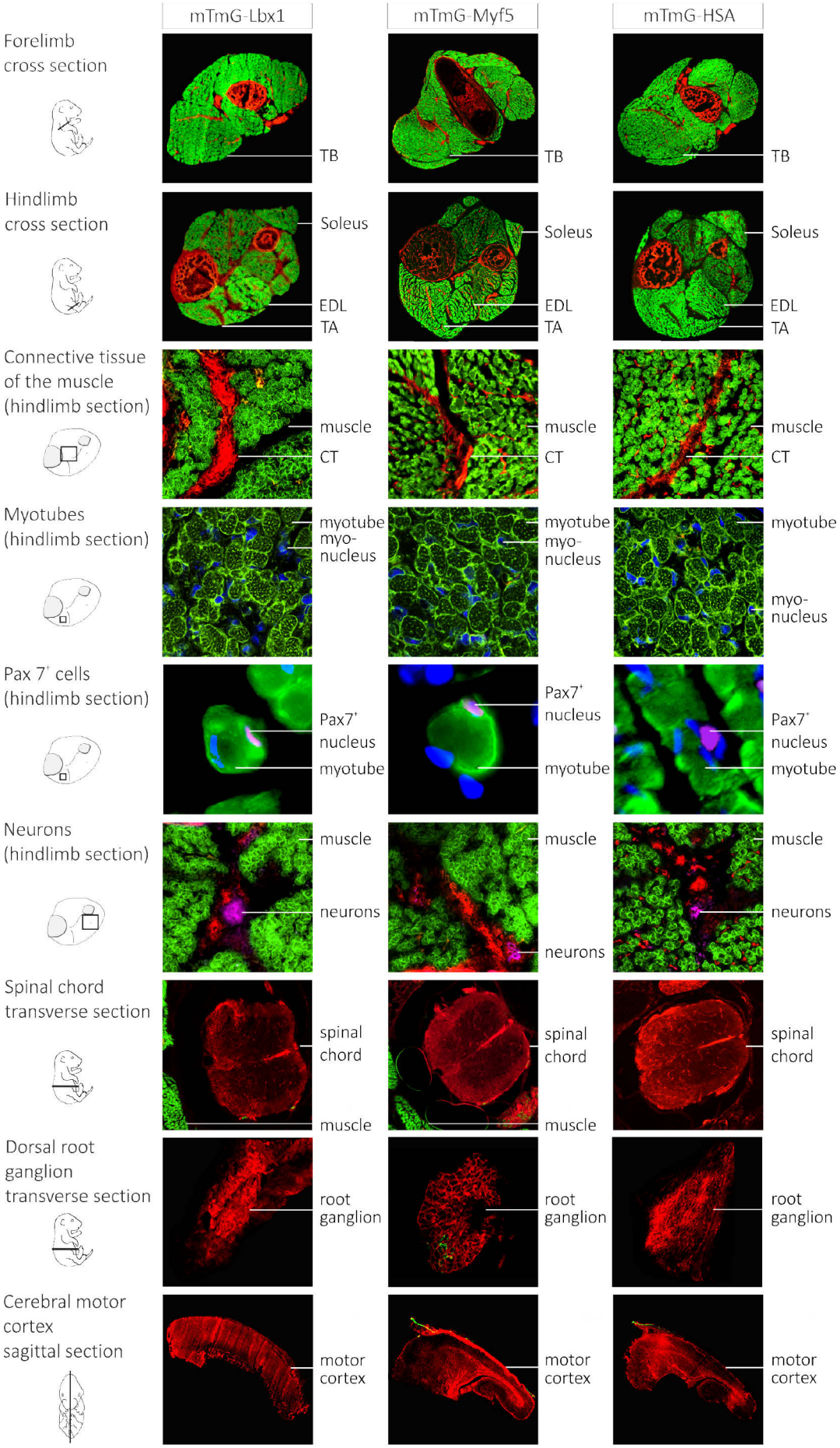

Figure 4.1 Histological analyses of mTmG-Lbx1, mTmG-Myf5 and mTmG-HSA mice at E18.5

Legend for figure 4.1: Histological sections of mTmG-Lbx1, mTmG-Myf5 and mTmG-HSA mice showing endogenous tomato protein (mT) in red and endogenous GFP (mG) in green. Sections are partly stained with DAPI (blue; nuclei) or via immunohistochemistry against Pax7 (fetal precursor cell nuclei; magenta) and β tubulin III (neurons; magenta). During Pax7 staining internal mTmG signal was lost due to antigen retrieval. Therefore, GFP was immunolabelled with a GFP antibody.

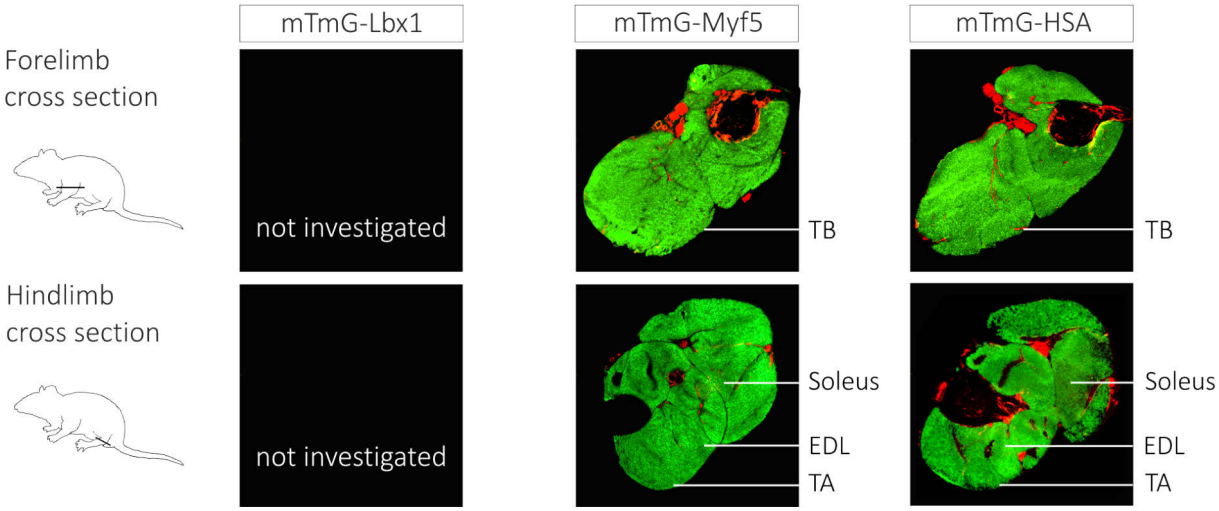

Figure 4.2 Histological analyses of mTmG-Myf5 and mTmG-HSA reporter mouse lines at P21
Histological sections of mTmG-Myf5 and mTmG-HSA mice showing the endogenous tomato protein (mT) in red and the endogenous GFP (mG) in green. Cre activity was detected in myofibres of all muscle areas.

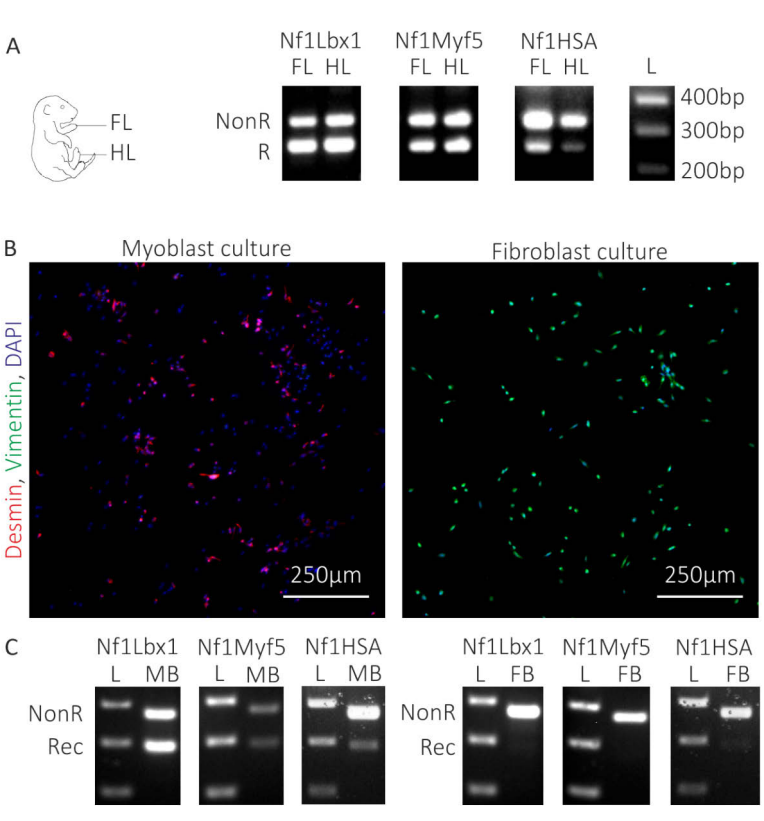

Figure 4.3 Confirmation of specific knockout of *Nf1* in muscle cells of knockout mice at E18.5
A PCR analysis on genomic DNA isolated from forelimb (FL) and hindlimb (HL) muscles of E18.5 mice. Left side: Scheme of location of tissue isolation for DNA isolation. Right side: Results of semi-quantitative PCR for the *Nf1* locus shows two products: *NonR* (not recombinant allele) and *R* (recombinant allele). **B** Immuno-cytochemistry of cultured primary cells isolated from forelimb and hindlimb muscles of E18.5 mice. Fibroblasts (right side) have been isolated from myoblasts (left side) via attachment to the plastic surface. **C** Results of PCR on genomic DNA isolated from primary myoblasts (MB) and primary fibroblasts (FB) of E18.5 mice. Images showing results of semi-quantitative PCR for the *Nf1* locus on genomic DNA: *NonR* (not recombinant *Nf1* allele) and *R* (recombinant *Nf1* allele). L = 100 bp DNA ladder.

After attachment of cells to the well surface, immunocytochemistry with antibodies against cell specific markers was performed to confirm the purity of cell populations. Specific antibodies against Desmin for myoblasts and Vimentin for fibroblasts were applied in parallel (Fig. 4.3.B). Genomic DNA from pure cell populations was isolated for semi-quantitative PCR. Specific primer pairs for amplification of the non recombinant *Nf1* allele (P1 and P4) and the recombinant *Nf1* allele (P1 and P2) were used. The myoblasts showed PCR products for both, the non recombinant and recombinant *Nf1* allele. The recombination efficiency was 53,6 % for Nf1Lbx1, 51,4 % for Nf1Myf5 and 43 % for Nf1HSA. Contrary, no recombination could be detected in isolated fibroblasts (Fig. 4.3.C). The results showed an exclusive Cre activity in myoblasts but not in fibroblasts confirming a muscle cell specific *Nf1* knockout.

Conclusion:

The analysis of mTmG reporter mice and *Nf1* knockout efficiency in E18.5 mice showed that the three mouse lines Nf1Lbx1, Nf1Myf5 and Nf1HSA are suitable models to study the consequences of a muscle cell specific *Nf1* knockout.

4.2 Loss of *Nf1* results in a growth defect of skeletal muscles

4.2.1 Embryonic muscles of *Nf1* knockout mice do not show a growth defect

4.2.1.1 Embryonic Nf1Myf5 mice show no muscle patterning or growth defect

Neurofibromatosis I patients suffer from a reduction of muscle size (Stevenson et al., 2005; Souza et al., 2009) due to a loss of *Nf1*. It should be tested whether the generated *Nf1* knockout models show a growth defect, too, and when the putative growth retardation starts. For chronological analysis embryonic muscles were investigated first. A possible role for *Nf1* in muscle patterning was suggested previously (Kossler et al., 2011). Muscle patterning should be studied in a muscle specific *Nf1* knockout model via whole mount RNA *in situ* hybridization. For this purpose E14.5 Nf1Myf5 and control embryos were stained with a labelled probe against MyoD transcripts (a transcription factor expressed in early myoblasts). The MyoD probe stains muscle anlagen (Fig. 4.4A). All skeletal muscle anlagen could be detected in Nf1Myf5 indicating no muscle patterning defect. The relative size of the MyoD positive area in an embryo was not significantly altered in Nf1Myf5 compared to controls (Fig. 4.4B). The same is true for the size of the single muscle anlagen of triceps brachii (TB), tibialis anterior (TA) and extensor digitorum longus (EDL; Fig. 4.4C). The whole mount RNA *in situ* hybridization indicated no effect of a muscle specific *Nf1* knockout on muscle patterning and embryonic muscle growth.

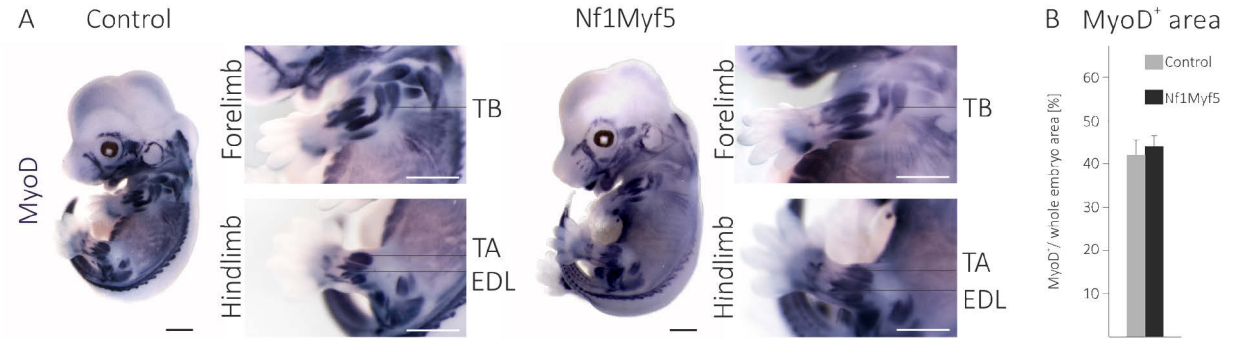

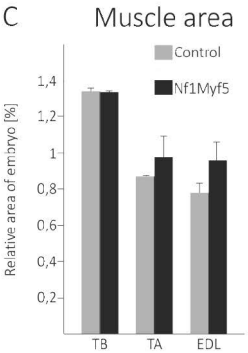

Figure 4.4 A muscle specific *Nf1* knockout does not cause a defect in muscle patterning and embryonic muscle growth

A Whole mount RNA *in situ* hybridization of E14.5 embryos with a labelled probe against MyoD mRNA transcripts (blue staining). Left side showing control embryo and magnifications of forelimb and hindlimb. Right side showing Nf1Myf5 embryo and magnifications of forelimb and hindlimb. Scale bars = 10 mm. Muscle patterning is not affected by *Nf1* knockout in muscle cells since all muscles show normal appearance in Nf1Myf5 mice. **B** Quantification of total MyoD stained ($MyoD^+$) area does not show a significant difference between Nf1Myf5 (n = 2) and control (n = 2) animals. **C** Quantification of single $MyoD^+$ muscle areas does not show a significant difference between Nf1Myf5 (n = 2) and control (n = 2) animals for TB, TA and EDL. TB = triceps brachii, TA = tibialis anterior, EDL = extensor digitorum longus.

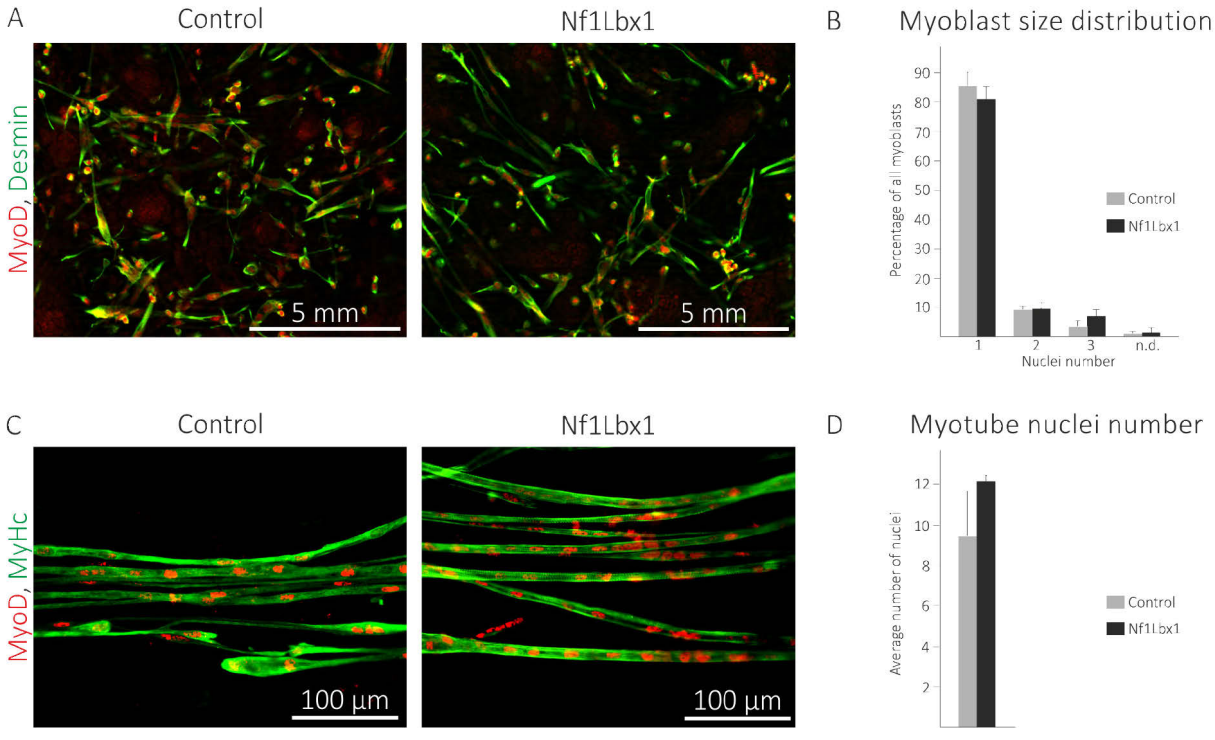

Figure 4.5 *Nf1* depleted embryonic myoblasts do not show a fusion defect

A Immunocytochemistry of cultured primary myoblasts isolated from limbs of E14.5 embryos. Desmin (green) labels the myoblast cytoskeleton and MyoD (red) labels myonuclei. **B** Quantification of myoblasts and fused myoblasts according to the number of nuclei of a cell. No significant difference of relative cell numbers was detected between controls (n = 2) and Nf1Lbx1 (n = 2). **C** Immunocytochemistry of cultured primary myotubes isolated from limbs of E14.5 embryos. MyHc (green) labels myofibrils and MyoD (red) labels myonuclei. **D** Quantification of myonuclei number per myotube shows no significant difference in nuclei number between controls (n = 3) and Nf1Lbx1 (n = 3).

4.2.1.2 Embryonic myoblasts of the Nf1Lbx1 model do not show a reduced fusion rate

Additionally to muscle patterning (see section 4.2.1.1), the behaviour of *Nf1* depleted myoblasts was studied *in vitro*. As prenatal muscles mainly grow through myoblasts fusion and generation of multinucleated cells (Duprez, 2010), the fusion rate of myoblasts was analysed. Primary myoblasts from E14.5 embryonic limbs of Nf1Lbx1 and control mice were cultured and immunolabelled with antibodies against MyoD (transcription factor expressed in early myoblasts) and Desmin (cytoskeleton component of myoblasts; Fig. 4.5A). Determination of nuclei number showed no significant difference in the number of myoblasts with one, two or three nuclei between Nf1Lbx1 and controls (Fig. 4.5B). Therefore, no fusion defect in *Nf1* depleted embryonic myoblasts was assumed. Myotubes from E14.5 embryos were also isolated, plated and immunolabelled with antibodies against MyoD and myosin heavy chain (MyHc, component of myofilaments). Determination of nuclei numbers per myotube did not show a significant alteration in Nf1Lbx1 compared to controls suggesting no effect of *Nf1* knockout on embryonic myotube growth.

4.2.2 Fetal muscles of *Nf1* knockout mice show a growth defect

4.2.2.1 The size of fetal muscles in Nf1Lbx1 and Nf1Myf5 is decreased

Embryonic Nf1Myf5 and Nf1Lbx1 mice did not show a reduction of muscle size. For chronological detection of putative effects fetal muscles were analysed next. At day E18.5 histological cross sections through the forelimb of Nf1Lbx1, Nf1Myf5 and Nf1HSA mice were prepared. Sections were immunolabelled with a specific antibody against myosin heavy chain (MyHc, a component of myofilaments; stains myotubes) and analysed via fluorescence microscopy (Fig. 4.6B and C). The histological parameters of triceps brachii were measured (Fig. 4.6D to I). A decrease of triceps cross sectional area could be detected for Nf1Lbx1 and Nf1Myf5 (Fig 4.6D). The decrease was accompanied by a significant reduction of myotube diameters (Fig. 4.6E) and increased numbers of central nuclei - a characteristic of immature myotubes. However, Nf1HSA did not show any significant alterations suggesting a role for *Nf1* in fetal myoblasts (affected by *Nf1* knockout in Nf1Lbx1 and Nf1Myf5) rather than in myotubes (affected by *Nf1* knockout in Nf1HSA). The results show an overlapping phenotype between Nf1Lbx1 and Nf1Myf5 and propose a role for *Nf1* in fetal muscle growth. To confirm the phenotypic findings of the forelimbs hindlimbs of Nf1Myf5 mice were analysed as well. Histological cross sections were prepared and stained with DAPI and a specific antibody against myosin heavy chain (MyHc). Vastus medialis (Vm), tibialis anterior (TA), extensor digitorum longus (EDL) and soleus (S) muscles were investigated (Fig. 4.7A,B and C). As seen in triceps brachii, cross sectional areas of vastus medialis, tibialis anterior, extensor digitorum longus and soleus were decreased, but only the size reduction of tibialis anterior was significant (Fig.4.7E). As detected in triceps, vastus medialis and tibialis anterior of Nf1Myf5 showed a significant increase in myotubes with central nuclei (Fig. 4.7G). This indicates a delay in myotube maturation. Additionally, the number of myotubes per muscle was determined. No significant decrease in myotube number could be detected in Nf1Myf5 (Fig. 4.7F) suggesting no defect in hyperplasic growth. Fetal hindlimb muscles were affected in the same way by *Nf1* knockout as the forelimb muscle triceps brachii.

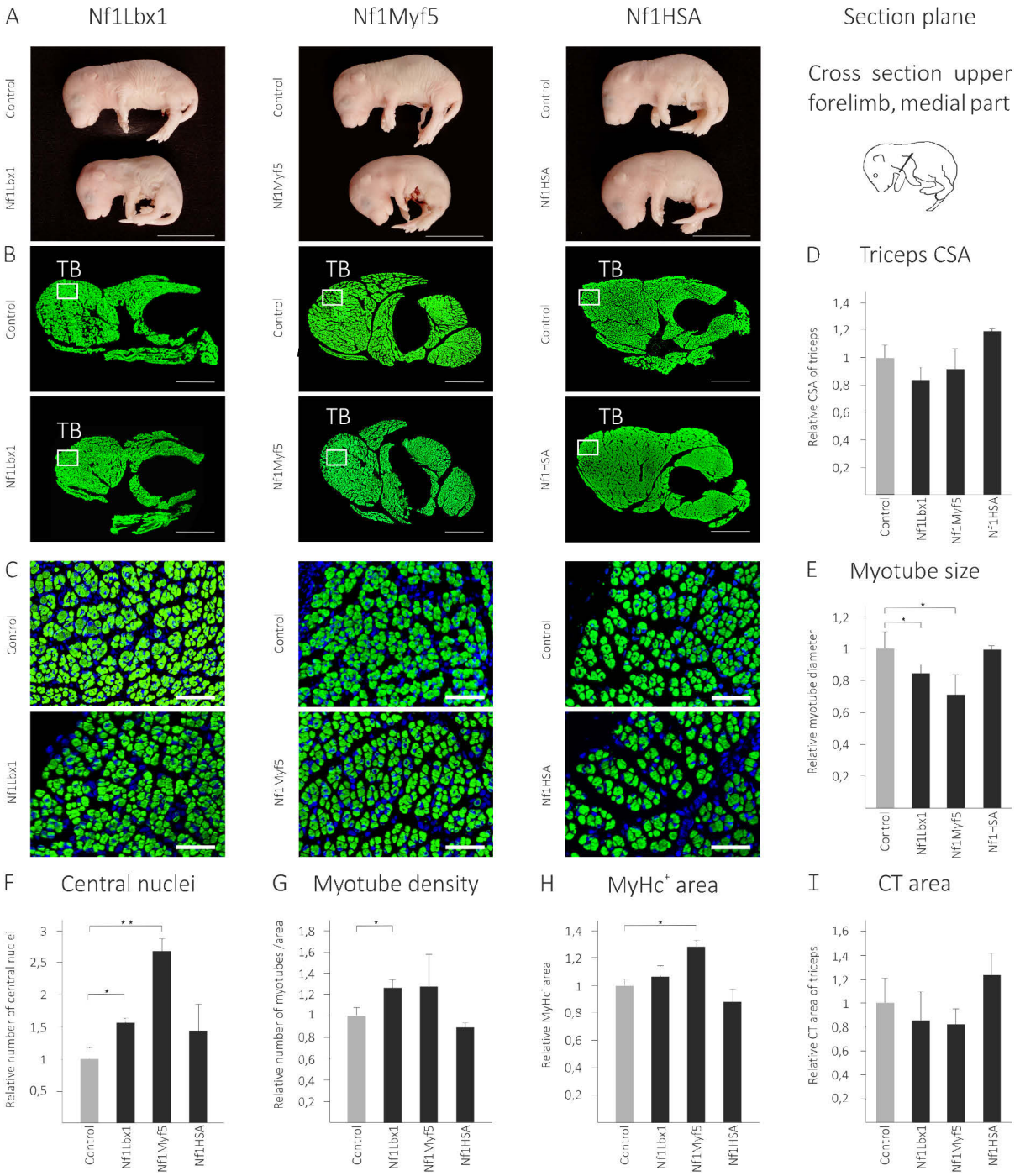

Figure 4.6 *Nf1* depleted fetal muscles showed a growth defect

A Photographs show Nf1Lbx1, Nf1Myf5 and Nf1HSA mice and control litter mates at E18.5. The scheme on the right side shows the section plane through the forelimb for histological analysis. **B** Histological cross sections through forelimbs immunolabelled against MyHc (green) for indication of myotubes. Scale bars = 1 mm. White boxes mark areas of magnification shown in C. **C** Magnification of myotubes of TB immunolabelled against MyHc (green) and DAPI (blue; nuclei). Scale bars = 50 µm. **D to I** Diagrams showing quantifications of TB muscles parameters of mutants (n = 3) relative to the respective controls (n = 3). **D** Triceps CSA is reduced in Nf1Lbx1 and Nf1Myf5, but not in Nf1HSA. **E** The size of myotubes was determined by measuring the diameter on cross sections. Nf1Lbx1 ($p = 0,022$) and Nf1Myf5 ($p = 0,02$) showed a significant decrease of myotube size whereas Nf1HSA myotubes remained unchanged. **F** Relative numbers of central nuclei were significantly increased in Nf1Lbx1 ($p = 0,039$) and Nf1Myf5 ($p = 0,004$), but not in Nf1HSA. **G** Density of myotubes was increased in Nf1Lbx1 ($p = 0,011$) and not significantly changed in Nf1Myf5 and Nf1HSA mutants. **H** Relative $MyHc^+$ area was significantly increased in Nf1Myf5 ($p = 0,047$). No significant change in Nf1Lbx1 and Nf1HSA could be detected. **I** Relative area of connective tissue (CT) was not significantly changed in Nf1Lbx1, Nf1Myf5 and Nf1HSA mice. CSA = cross sectional area, MyHc = myosin heavy chain, TB = triceps brachii, CT = connective tissue.

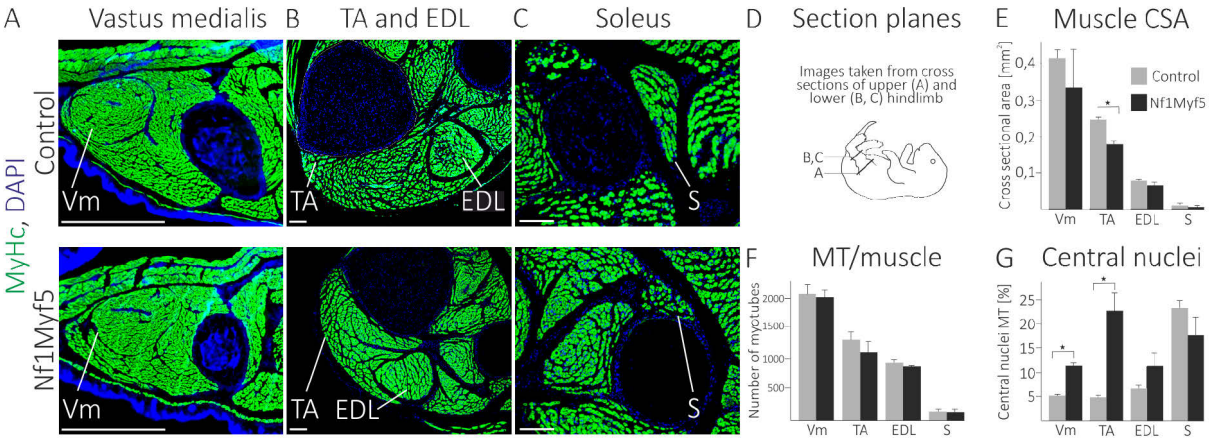

Figure 4.7 Hindlimb muscles of Nf1Myf5 show a growth defect

A, B and **C** Immunohistochemistry of hindlimb cross sections of E18.5 embryos stained with a specific antibody against MyHc (green; myotubes) and DAPI (blue; nuclei). **A** Section through upper hindlimb showing vastus medialis. **B** Section through lower hindlimb showing tibialis anterior (TA) and extensor digitorum longus (EDL). **C** Section through lower hindlimb showing soleus (S). All scale bars = 100 µM. **D** Scheme of an E18.5 embryo with section planes used in A, B and C. Quantifications of muscle parameters: **E** All investigated muscles of Nf1Myf5 (n = 2) showed a decrease in muscle size compared to control animals (n = 2), which was only significant for TA (p = 0,034). **F** The number of myotubes per muscle was not significantly decreased in all investigated muscles. **G** The number of central nuclei myotubes was significantly increased in Nf1Myf5 in vastus medialis (p = 0,05) and tibialis anterior (p = 0,013) but not significantly changed in EDL and soleus. CSA = cross sectional area, Vm = Vastus medialis, TA = tibialis anterior, EDL = extensor digitorum longus, S = soleus, MT = myotubes.

4.2.3 Postnatal muscles of *Nf1* knockout mice show a growth defect

Neurofibromatosis I patients present a reduction of muscle size from childhood on (Stevenson et al., 2005). In order to validate the mouse models as an accurate representation of the muscular defects of Neurofibromatosis I, it should be determined whether the size reduction observed in the patients was also present in young postnatal *Nf1* knockout mice. Therefore mice at the end of perinatal development (day P21) were analysed. Since Nf1Lbx1 mice die after birth only Nf1Myf5 and Nf1HSA could be analysed and were investigated one after another.

4.2.3.1 The size of muscles is decreased in NfMyf5 mice at P21

To investigate muscle growth in perinatal development of Nf1Myf5, the cross sectional area of four skeletal muscles was measured at P21: triceps bracchii (TB), tibialis anterior (TA), extensor digitorum longus (EDL) and soleus (S). Cross sections of whole limbs from three weeks old (P21) mice were performed, labelled with DAPI (nuclei), immunostained against Collagen IV (component of muscle connective tissue) and photographed (Fig. 4.8A,B). For measurements of TB, sections of the upper forelimb were used; for TA, EDL and soleus, sections of the lower hindlimb were analysed. Nf1Myf5 mutants showed a decrease in muscular size between 30 % and 60 % in all analysed muscles (Fig. 4.8D). Triceps bracchii (TB) showed a reduction of cross sectional area of 39.5 %, tibialis anterior (TA) a reduction of 48.7 %, extensor digitorum longus (EDL) a reduction of 31.6 % and soleus a reduction of 59.7 % in Nf1Myf5 mutants. The

knockout of *Nf1* leads to a significant growth defect at the perinatal stage of development. Therefore, the situation in the mouse model is comparable to the syndromes of young Neurofibromatosis I patients.

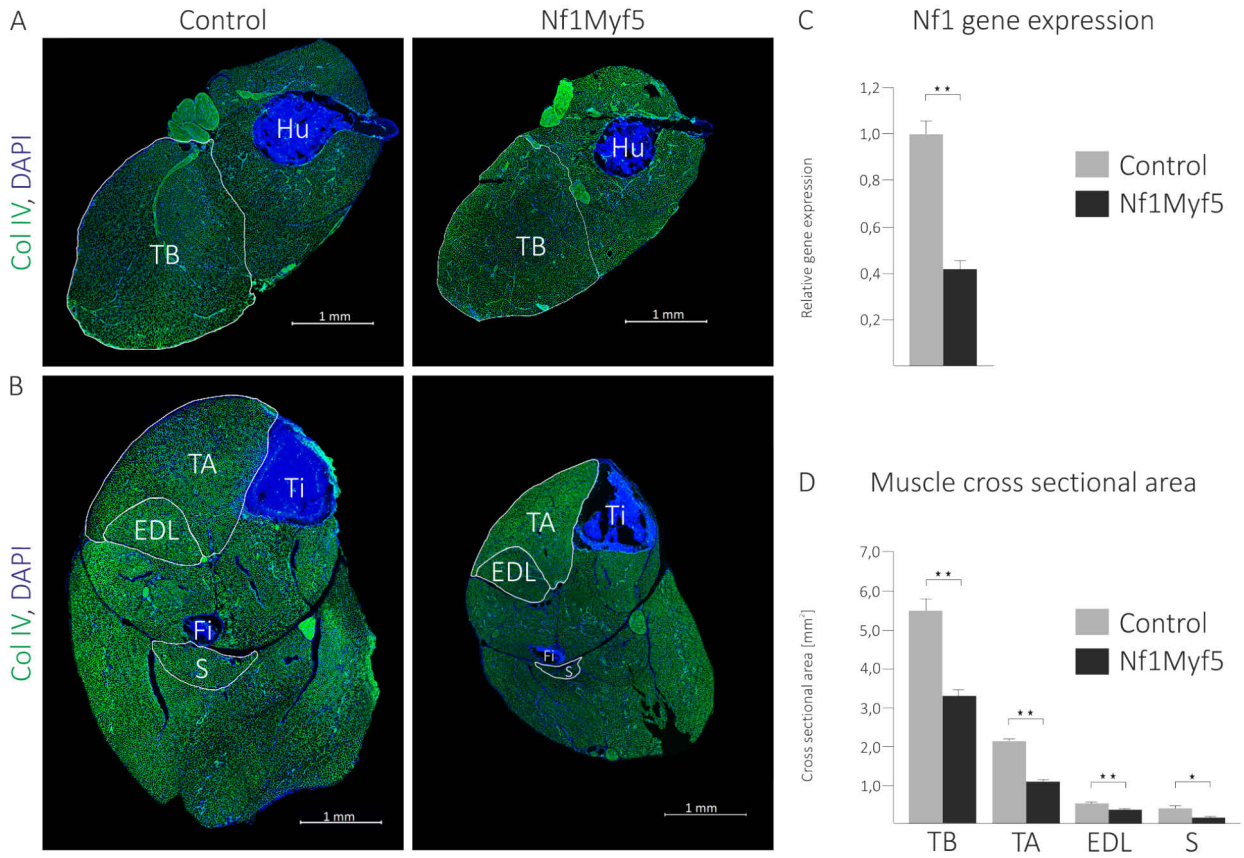

Figure 4.8 Loss of *Nf1* causes a decrease in cross sectional area of skeletal muscles at P21

A Cross sections of P21 upper forelimbs (upper panel) and **B** lower hindlimbs (lower panel) immunostained against Collagen IV (Col IV) and DAPI. **C** The expression of the *Nf1* gene is significantly (p=0,008) decreased in whole muscle tissue of Nf1Myf5 (n = 4) compared to controls (n = 3). **D** Quantification of the cross sectional area of skeletal muscles from control and mutant mice. Nf1Myf5 mutants show a significant decrease in muscle size (TB: p = 0,000, TA: $p = 5 \cdot 10^{-5}$, EDL: $p = 2 \cdot 10^{-3}$; S: p = 0.03; forelimbs: controls n = 4 and mutants n = 5; hindlimbs: controls n=3 and mutants n=3). Hu = humerus, Ti = tibia, Fi = fibula, TB = triceps bracchii, TA = tibialis anterior, EDL = extensor digitorum longus, S = soleus.

4.2.3.2 Size reduction of Nf1Myf5 muscles is not caused by a decrease in myofibre number

Nf1Myf5 mutants show a decrease in muscle area at P21. As muscle anlagen are formed correctly in these animals (see section 4.2.1.2) size reduction might be due to defects in perinatal hyperplasic or hypertrophic growth. A defect in hyperplasic growth is characterized by reduced total cell numbers. Therefore, total numbers of myofibres of TB, TA, EDL and S muscles were determined in order to establish whether any difference in the number of myofibres could, at least partially, account for the size decrement in Nf1Myf5 mice. To mark the individual myofibres, the muscle connective tissue surrounding them was stained in cross sections of whole limbs using an antibody against Collagen IV (Col IV; Fig. 4.9A). All myofibres in each muscle

were counted. The numbers of fibres in TB, TA and soleus were slightly reduced, but no significant decrease in total fibre number could be seen (Fig. 4.9B). The fibre number of EDL was nearly unaltered in Nf1Myf5 mice. Therefore, a hyperplasic growth defect does not or only negligibly contributes to the muscle size reduction in Nf1Myf5.

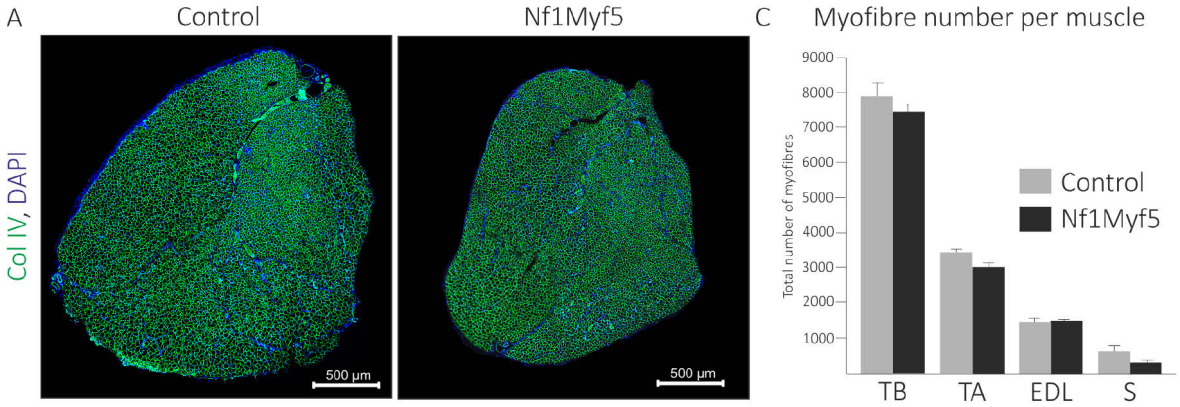

Figure 4.9 Loss of *Nf1* causes no significant alteration in the total number of myofibres in skeletal muscles
A Cross sections of P21 triceps stained with an antibody against Collagen IV (Col IV) and DAPI. **B** Quantification of total myofibre numbers of control (n = 4 for TB; n = 3 for TA, EDL and S) and mutant (n = 5 for TB; n = 4 for TA and EDL, n = 3 for S) P21 mice. TB = triceps brachii, TA = tibialis anterior, EDL = extensor digitorum longus, S = soleus.

4.2.3.3 Size reduction of Nf1Myf5 muscles is caused by a decrease in myofibre size

Nf1Myf5 mice showed a muscle size reduction like Neurofibromatosis I patients. The defect is not caused by fibre number reduction. Therefore, it was studied whether a reduction of the size of individual myofibres contributes to the decrease in muscle size (defect in hypertrophic growth). The size of myofibres was measured by determining the Feret's minimum diameter of each fibre. The CSA (cross sectional area) of the myofibres was also measured to ensure differences measured in the Feret's minimum diameter were not caused by a change in fibre shape. However, the CSA was not directly used to estimate the size of the myofibres due to its high susceptibility to changes in the cutting angle of the analysed tissue (Briguet et al., 2004). The TB is a large muscle with different functional parts. It possesses a certain degree of myofibre size heterogeneity. For measurement it was divided into three more homogeneous regions: the innermost region (in close proximity to the humerus bone; region I), the medial region (region II) and the outermost (lateral; region III; Fig.4.10A and B). The individual myofibres were made visible on cross sections of P21 mice by staining the connective tissue surrounding them with an antibody against Collagen IV (Col IV). It could be shown that the total Feret's minimum diameter of all myofibres in the TB muscle was reduced by approximately 25 % in Nf1Myf5 compared to controls (Fig.4.10C). Analysing each region individually, a decrease in myofibre size throughout all regions could also be observed. This reduction, however, was only significant in region III (Fig. 4.10E). Control mice showed a size gradient of the myofibres, where a gradual outwardly increment in size is seen from the smallest fibres in region I to the biggest in region III. This gradient was distorted in the Nf1Myf5 mutants. The size of the myofibres in all regions

was more homogeneous in the mutants than in controls (Fig. 4.10E and F). The reduction of TB size in Nf1Myf5 seems to be due to a defect in growth of myofibres which are smaller and more uniform in size throughout the TB muscle.

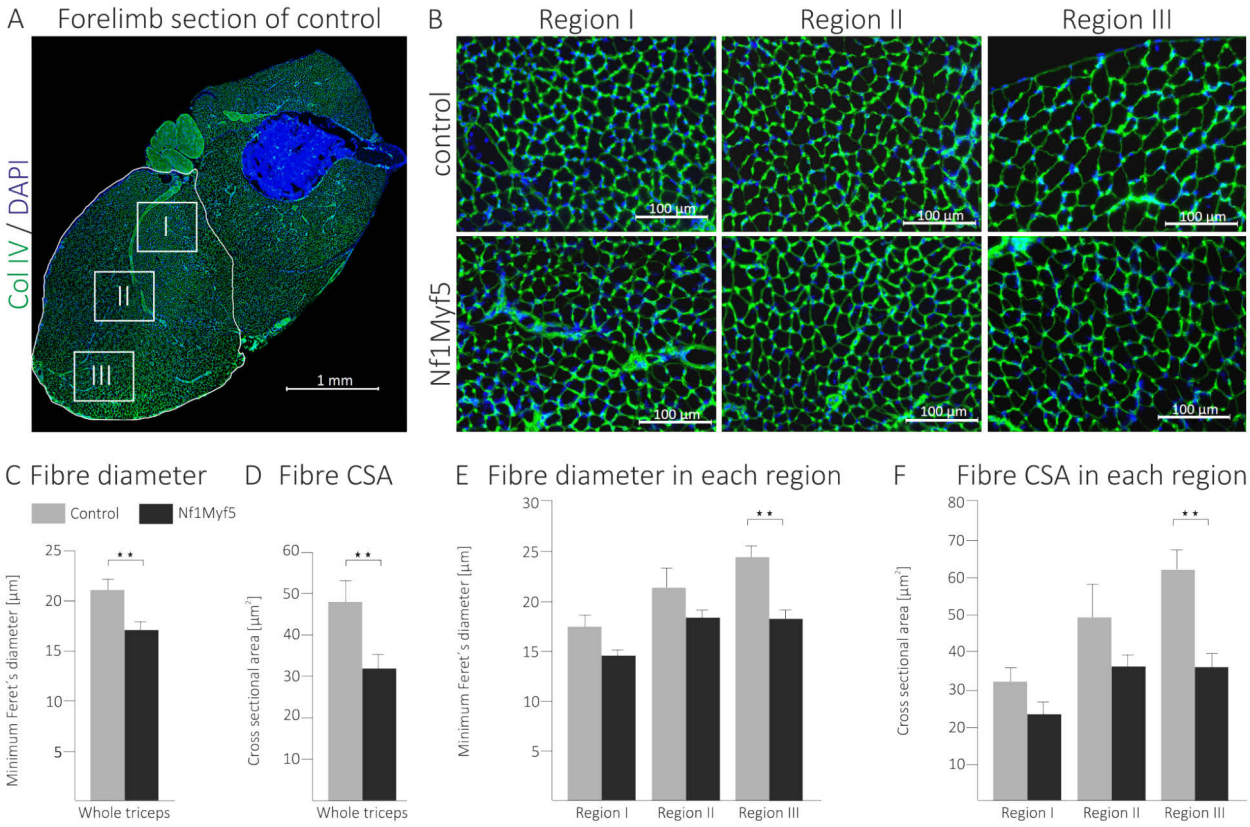

Figure 4.10 Loss of *Nf1* causes a decrease in myofibres size in triceps brachii at P21
A Cross section through the upper forelimb of a control mouse at P21 stained with DAPI and an antibody against Collagen IV (Col IV) with the TB muscle outlined. The three functionally different regions I, II and III are marked by white boxes. **B** 40 x magnification of cross sections of Regions I, II and III of the TB muscle of P21 control and Nf1Myf5 mutant mice stained with DAPI and an antibody against Collagen IV (Col IV). **C** Mean Feret's minimum diameter and **D** CSA of all the myofibres of the TB muscle of P21 control and Nf1Myf5 mice ($p = 0.004$; control n = 4, mutant n = 5). **E** Feret's minimum diameter and **F** CSA of the myofibres of control and Nf1Myf5 mutant mice in the three regions. The size difference is only significant in region III (region I: $p > 0.05$; region II: $p > 0.05$; region III: $p < 0.01$; controls n = 4, mutants n = 5). CSA = cross sectional area, TB = triceps brachii.

Myofibre size in triceps brachii is reduced at P21. Therefore, also myofibres of hindlimb muscles were analysed. Histological cross sections of lower hindlimb were performed and individual myofibres were made visible by staining the connective tissue surrounding them with an antibody against Collagen IV (Col IV; Fig. 4.11A). It could be shown that the total Feret's minimum diameter of all myofibres in the TB muscle was reduced by approximately 25 % in Nf1Myf5 compared to controls (Fig. 4.11C). For the TA muscle the fibre size was significantly reduced in Nf1Myf5 mutants, as shown by the reduction of the Feret's minimum diameter, by 32 %. The EDL showed a significant decrease in myofibre diameter of 25 % and soleus showed a not significant decrease of 20 % in Nf1Myf5 (Fig. 4.11E). The growth defect does affect hindlimb myofibres in the same way as forelimb myofibres. It seems that all limb muscles are affected.

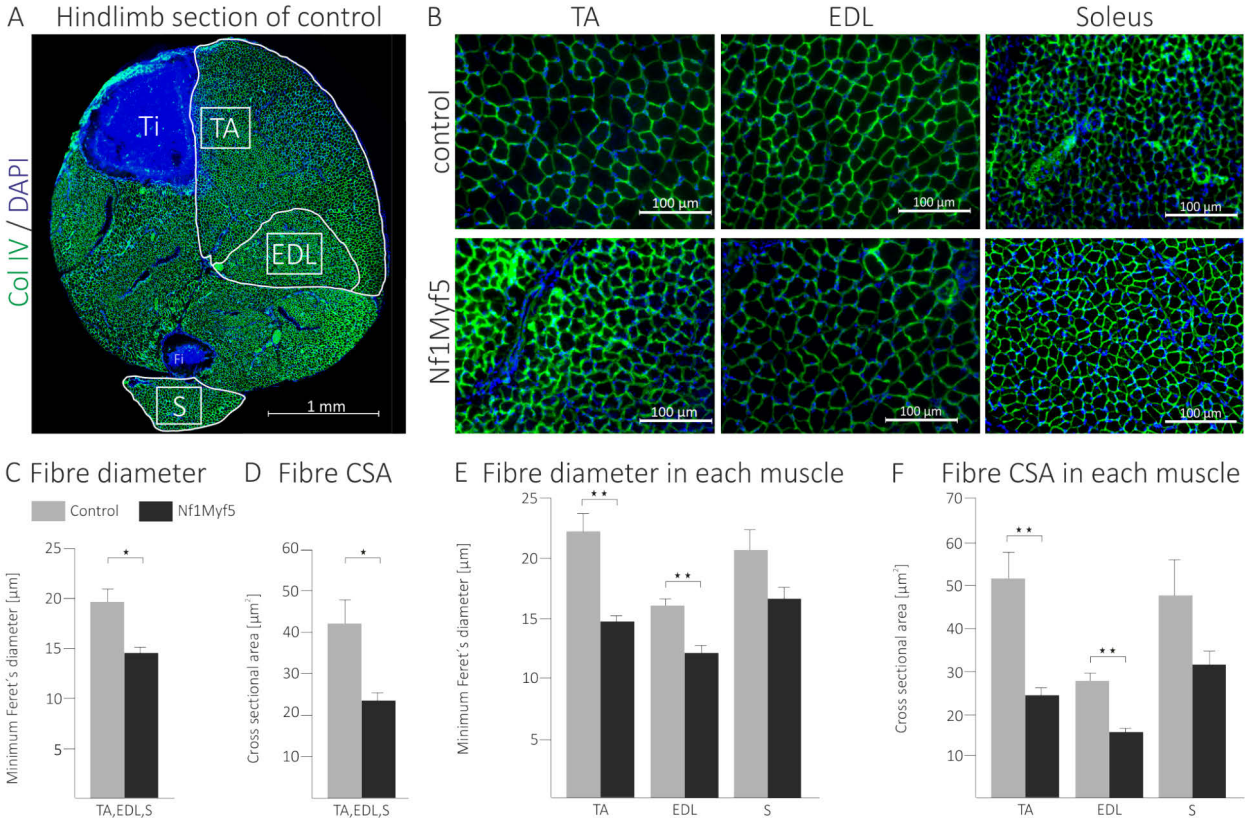

Figure 4.11 Loss of *Nf1* causes a decrease in myofibre size in hindlimb muscles at P21

A Cross section through the lower hindlimb of control mice at P21 stained with DAPI and an antibody against Collagen IV (Col IV) with TA, EDL and S muscles outlined. The white boxes show the location of the respective magnifications of each muscle in B. **B** 40 x magnification of cross sections of TA, EDL and soleus (S) stained with DAPI and an antibody against Collagen IV (Col IV). **C** Mean Feret's minimum diameter (p = 0,01) and **D** CSA (p = 0,01) of all myofibres of TA, EDL and S muscles of control and Nf1Myf5 mice. **E** Mean Feret's minimum diameter of the myofibres of the TA, EDL and S muscles separately of control and Nf1Myf5 mice (TA: p = 0.008; EDL: p = 0.003). **F** Myofibre CSA of the TA, EDL and S muscles separately of control and Nf1Myf5 mice (TA: p = 0.0024; EDL: p = 0.003). TA and EDL: control n = 3, mutant n = 4; S: control n = 3, mutant n = 3. CSA = cross sectional area, TA = tibialis anterior, EDL = extensor digitorum longus, S = soleus.

4.2.3.4 Myofibre size reduction in Nf1Myf5 mice is dependent on the myofibre type

Nf1Myf5 mice show a muscle size reduction due to a decrease in myofibre size. A significant change in hindlimb myofibre size could only been shown for TA and EDL (Fig. 4.11E,F). EDL is a so called fast muscle, nearly exclusively consisting of fast twitch fibres. TA consists of fast and slow twitch fibres, but mainly fast twitch fibres. Soleus did not show a significant fibre size reduction. Soleus is a so called slow twitch muscle, nearly exclusively consisting of slow twitch fibres. In triceps brachii (forelimb) only muscle region III showed a significant decrease in myofibre size (Fig. 4.10E,F). Compared to regions I and II, it consists nearly exclusively of fast twitch fibres. Region I and II have a high percentage of slow twitch fibres. Slow twitch fibres are a subclass of myofibres also called endurance fibres characterized by the expression of Slow myosin heavy chain (MySlow^{+}). Fast twitch fibres are the second big subclass of fibres, also called rapid movement fibres, which do not express Slow myosin heavy chain (MySlow^{-}). To investigated putative differences between fibre types, cross sections of forelimb and hindlimb of

P21 mice were immunolabelled for Collagen IV (connective tissue) and Slow myosin heavy chain (MySlow) to distinguish fibres (Fig. 4.12A). The Feret's minimum diameter of the slow (MySlow$^+$) and fast twitch (MySlow$^-$) myofibres of the TB, TA, EDL and S muscles were measured separately. The slow twitch myofibres in the Nf1Myf5 mutants are not significantly reduced in size in all four analysed muscles. Only fast twitch fibres show a significant decrease in size in all four analysed muscles (Fig. 4.12B,C,D and E). Loss of *Nf1* in Nf1Myf5 animals seems to have differential effects on slow twitch and fast twitch fibres.

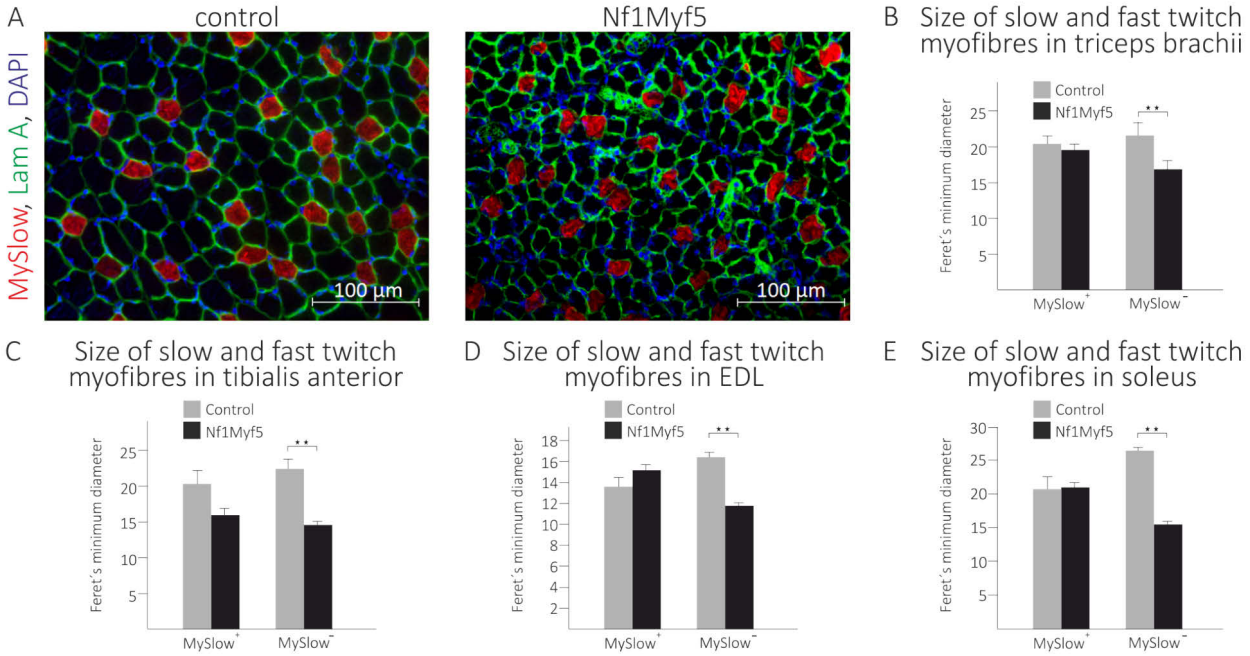

Figure 4.12 Fast twitch myofibres show a stronger size reduction than slow twitch fibres in Nf1Myf5
A Cross section of the TA muscle of P21 old control and Nf1Myf5 mice immunostained against Slow myosin heavy chain (MySlow), Laminin A (Lam A) and DAPI. Quantification of Feret's minimum diameter of slow (Slow$^+$) and fast (Slow$^-$) twitch myofibres of triceps brachii (**B**), tibialis anterior (**C**), extensor digitorum longus (**D**) and soleus (**E**) muscles. Only the fast twitch fibres (Slow$^-$) are significantly smaller in the Nf1Myf5 mutants. TB: controls n = 4, mutants n = 5, p = 0.004; TA: controls n = 3, mutants n = 4, p = 0.005; EDL: controls n = 3 mutants n = 4, p = 0.001; S: controls n = 3, mutants n = 3, p = 0.05. MySlow = Slow twitch myosin heavy chain, TB = triceps brachii, TA = tibialis anterior, EDL = extensor digitorum longus, S = soleus.

4.2.3.5 Nf1Myf5 mice do not show characteristics of degeneration and regeneration processes

Nf1Myf5 mutants show a decrease in muscle area at P21. Size reductions can be due to defects in hyperplasic or hypertrophic growth. Hyperplasic growth does not seem to be significantly affected (see section 4.2.3.2). A decreased fibre size seems to be the cause of muscle size reduction (see section 4.2.3.3). However, a decreased fibre size is not necessarily a hypertrophy defect. In skeletal muscles aberrant processes of cell degeneration and regeneration can disturb fibre growth, too. This can be seen by an increased heterogeneity of fibre sizes in the cross sectional view (Briguet et al., 2004). For an overall estimation of fibre size distribution myofibres of triceps brachii, tibialis anterior, extensor digitorum longus and soleus were classified according to their minimum Feret´s diameter. Fig. 4.13 shows the size distribution diagram for control and Nf1Myf5 mice. A negative shift is visible for Nf1Myf5 mice showing maximum myofibre

numbers at a diameters between 13 and 15 µm whereas controls show maximum myofibre numbers at diameters between 17 and 19 µm. Nf1Myf5 mutants have the same overall size range as controls (5 to 41 µm). Therefore, increased degeneration and regeneration processes can be excluded for Nf1Myf5 at P21. Like shown in triceps brachii (see section 4.2.3.3), Nf1Myf5 myofibres showed a tendency of more uniform diameters in comparison to controls. Most (about 58 %) of Nf1Myf5 myofibres were found in a size range of 8 µm (diameters between 11 and 19 µm) whereas 58 % of control myofibres were found in a size range of 10 µm (diameters between 15 and 25 µm). A further sign of aberrant degeneration and regeneration are central nuclei in myofibres. An increase in central nuclei in Nf1Myf5 mutants was not detected (data not shown). Therefore, the decrease in muscle size in Nf1Myf5 was not caused by fibre degeneration or regeneration defects.

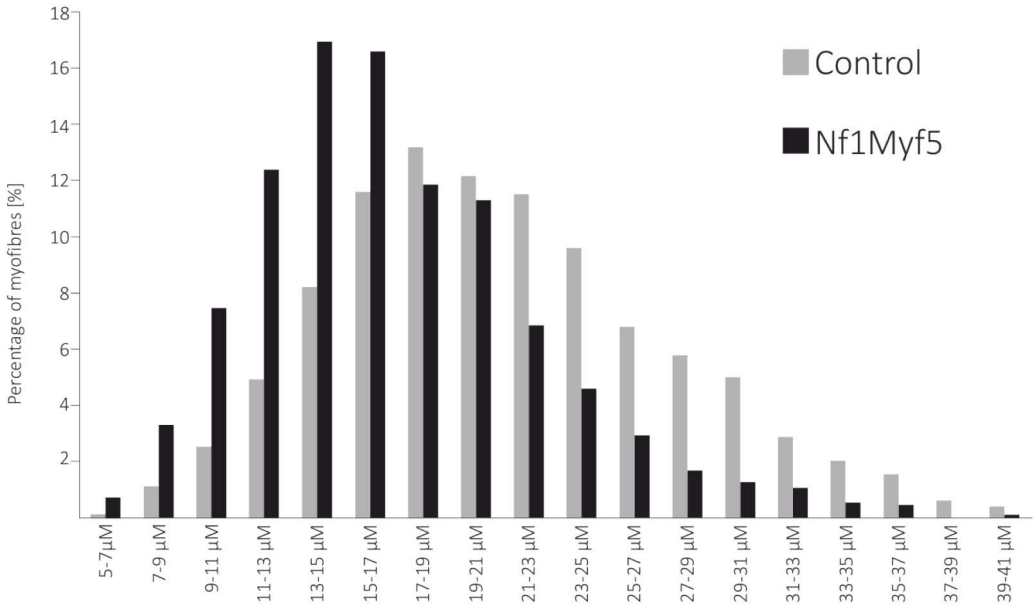

Figure 4.13 Myofibres of Nf1Myf5 mice show a shift in size distribution
The diagram shows the distribution of myofibre numbers according to their Feret's minimum diameter. A shift is visible in Nf1Myf5 mutants showing maximum myofibre numbers at diameters of 13 - 15 µm whereas controls show maximum myofibres numbers at diameters of 17 - 19 µm. Nf1Myf5 myofibres show a tendency of more uniform diameters compared to controls: Nf1Myf5 myofibres can be preferentially found in a size range between 11 and 19 µm (57,7 % of all fibres) whereas control myofibres have a broader range around their maximum (58,0 % of fibres between 15 and 25 µm diameter). Numbers have been calculated by merging data of triceps brachii (control n = 4, Nf1Myf5 n = 5), tibialis anterior (control n = 3, Nf1Myf5 n = 4), extensor digitorum longus (control n = 3, Nf1Myf5 n = 4) and soleus muscle (control n = 3, Nf1Myf5 n = 3).

4.2.3.6 Muscle and myofibre size reduction is persistent throughout age in Nf1Myf5 mice

Muscle and myofibre size of Nf1Myf5 is significantly reduced at P21. To analyse whether size reduction is a developmental delay or a persistent phenotype, muscles of Nf1Myf5 at P156 have been analysed. Day P156 represents the adult phase of muscle development. Muscles of mice not exposed to exercise do not gain size any more. Histological cross sections of Nf1Myf5 limbs were immunolabelled with antibodies against Collagen IV (connective tissue) and myosin heavy

chain (myofibres; Fig. 4.14A). Measurements showed that the muscle cross sectional area was significantly decreased for triceps brachii (TB) and tibialis anterior (TA) which consists of mixed fibre types. A not significant decrease was detected for extensor digitorum longus (EDL), which nearly exclusively consists of fast twitch fibres. Surprisingly, the size of soleus was slightly but not significant increased in Nf1Myf5 mice (Fig 4.14B). Soleus mainly consists of slow twitch fibres. The results suggest that additional growth mechanisms in slow and fast Nf1Myf5 muscles exist. These might be secondary, maybe compensatory, hyperplasic growth mechanisms as the size of myofibres was reduced in all muscles (Fig. 4.14C). The strongest fibre size reduction was detected in EDL which was surprising regarding the fact that EDL only shows a slight muscle size reduction. Therefore the myofibre number was analysed. TB and TA muscles showed a decrease of total fibre numbers indicating a progression of phenotype compared to P21 animals (see Fig. 4.9). Surprisingly, EDL showed the contrary effect. Fibre numbers were significantly increased in Nf1Myf5 animals which could account for the very mild muscle size reduction. It indicates a possible secondary hyperplasia or myofibre branching effect in EDL compensating for fibre hypoplasia or a possible performance decrease.
A sign of aberrant muscle development and degeneration processes are increased numbers of myofibres with central nuclei. An increase in central nuclei in Nf1Myf5 mutants could not be detected (data not shown). The results show a persistence of muscle defects induced by a loss of *Nf1* with possible secondary effects in the adult stage of development. The defects are not due to a pure developmental delay.

4.2.3.7 The Nf1Myf5 muscle phenotype is progressive with age of mice

Neurofibromatosis I is a progressive disorder (Korf, 2002). In order to test whether the muscle phenotype in Nf1Myf5 mice was also progressive, relative muscle sizes were compared between mice at E18.5 (fetal), P21 (perinatal) and P156 (adult). A gradual decrease of relative muscle size of NfMyf5 with age could be detected. At E18.5 the size difference was small in TB (92 % of the control size) and moderate in TA (73 % of the control size). By P21 TB and TA were only 60.5 % and 51.3 % of control sizes and at P156 the sizes of TB and TA had decreased further to only 50.9 % and 43.1 % of the normal size seen in control littermates (Fig. 14B). The same tendency could be detected for myofibres: At E18.5 myofibres of Nf1Myf5 mice reached only a size of 71,2 % (TB) and 69,4 % (TA). At day P21 Nf1Myf5 relative myofibre size decreased to 66,6 % (TB) and 46,5 % (TA) in relation to control (100 %). At P156 relative myofibre size decreased further to 63,4 % (TB) and 44,9 % (TA; Fig. 14C).
Neurofibromatosis I patients additionally show a short body stature (North, 1998). The same could be seen in postnatal Nf1Myf5 mice: Nf1Myf5 mice at day P21 reached a body size of 71 % of control mice and Nf1Myf5 mice at day P156 reached a body size of 63 % of control mice (Fig. 4.15A). The observed phenotype is progressive with age like in patients. This indicates ongoing defects in postnatal muscle homeostasis.

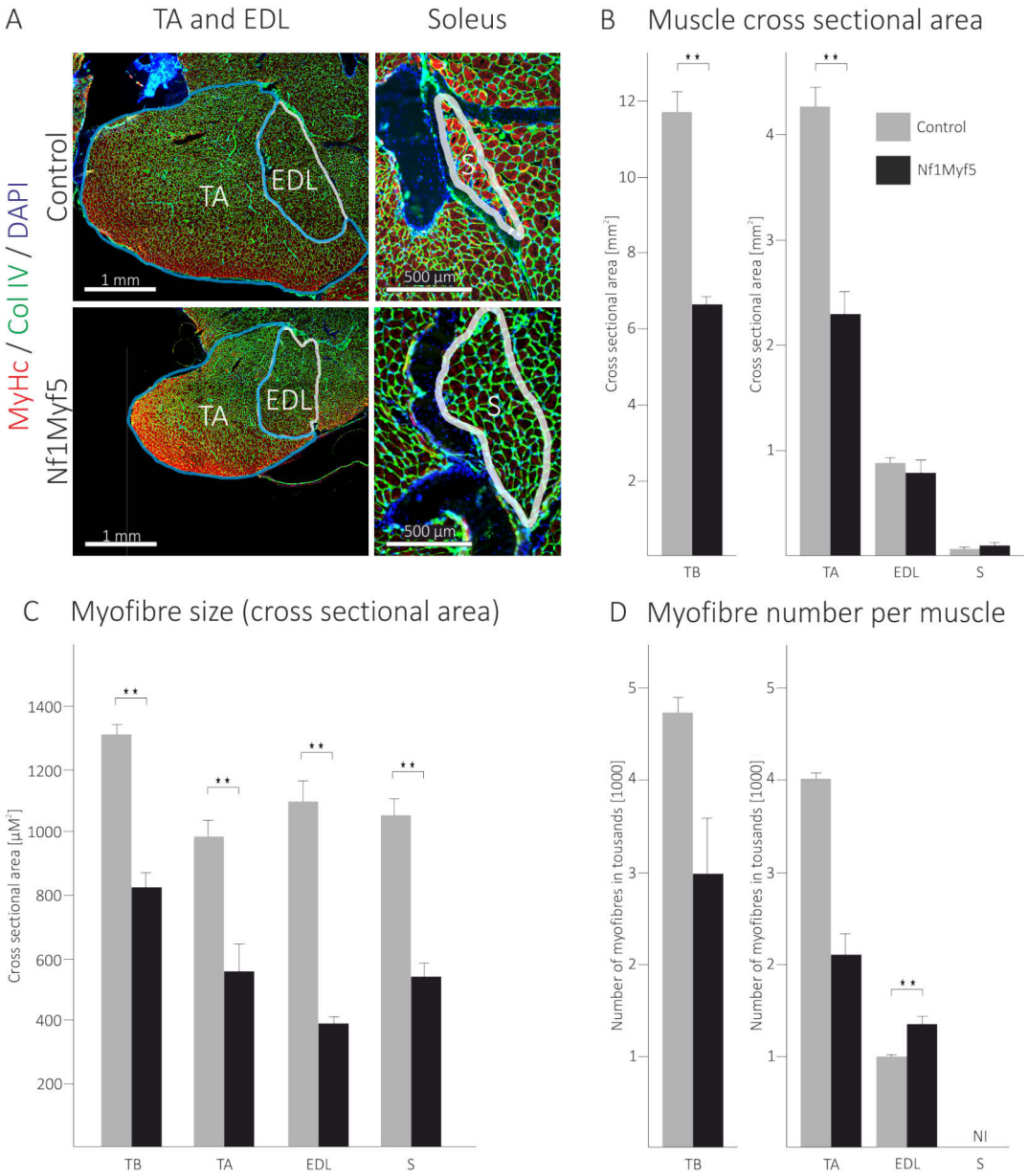

Figure 4.14 Muscles of Nf1Myf5 show a size reduction at P156

A Cross sections through the lower hindlimb of P156 control and Nf1Myf5 mice immunostained with specific antibodies against myosin heavy chain (MyHc), Collagen IV (Col IV) and DAPI with the TA, EDL and soleus (S) outlined. **B** Quantification of muscle cross sectional area (CSA) for control (n = 3) and NfMyf5 mice (n = 3). A significant size reduction could be detected for TB (p = 0,008) and TA ($p = 4{,}8 \cdot 10^{-6}$) muscles of Nf1Myf5 animals. **C** Quantification of myofibre cross sectional area (CSA) for each muscle. Nf1Myf5 mutants showed significant size reduction in TB (p = 0,0007), TA (p = 0,003), EDL ($p = 1{,}8 \cdot 10^{-9}$) and S ($p = 7{,}5 \cdot 10^{-6}$). **D** Quantification of myofibre number per muscle showed a not significant reduction of fibre number in TB (n = 3) and TA in Nf1Myf5 (n = 1). However, EDL of Nf1Myf5 (n = 2) showed a significant increase in fibre number (p = 0,003). Soleus (S) was not investigated. TA = tibialis anterior, EDL = extensor digitorum longus, S = soleus muscle, NI = not investigated.

4.2.3.8 Fast twitch myofibre size reduction is due to a decreased myonuclear domain

Nf1Myf5 mice showed size reduction of myofibres which is persistent and progressive with age (see section 4.2.3.7). Myofibres grow by two mechanisms: myonuclear accretion and protein syn-

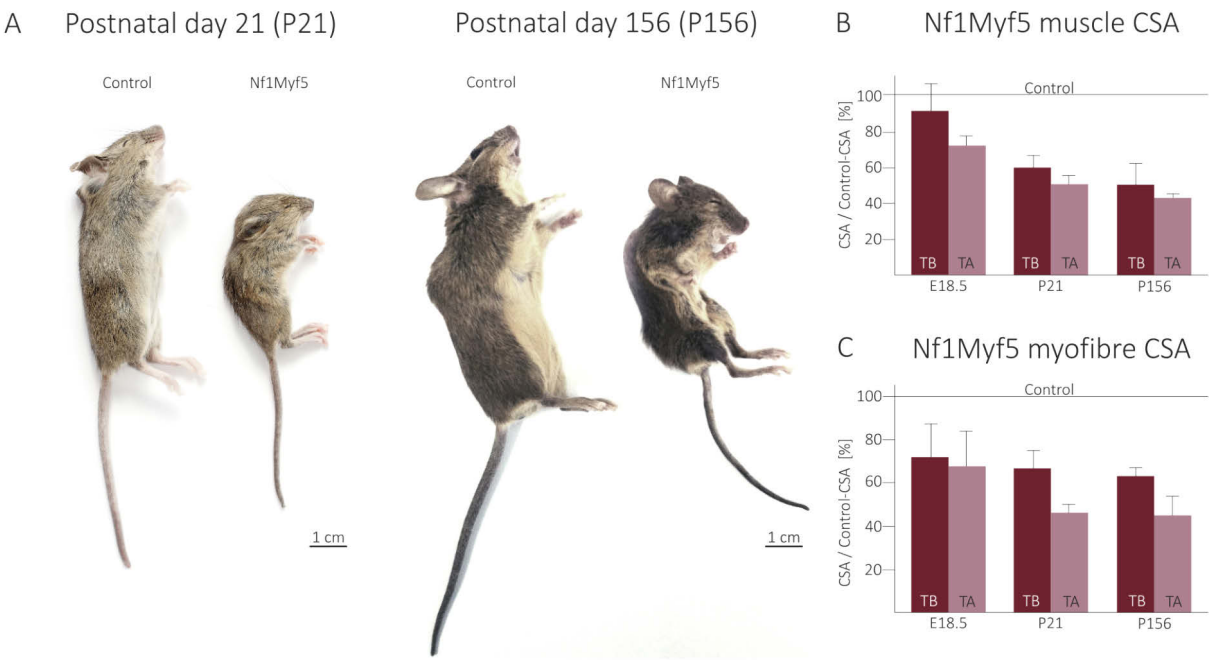

Figure 4.15 The Nf1Myf5 muscle phenotype is progressive
A Photographs taken from control and Nf1Myf5 mice at postnatal days P21 and P156. **B** and **C** Representation of progression of the Nf1Myf5 muscle phenotype. Bars showing the percental size of Nf1Myf5 muscles (**B**) and Nf1Myf5 myofibres (**C**) in comparison to control mice which correspond to 100% of size. Dark red bars: TB muscle. Light red bars: TA muscle. The bars show a progressive size reduction in Nf1Myf5 animals with age. CSA = cross sectional area, TB = triceps brachii, TA = tibialis anterior.

thesis (hypertrophy). During postnatal growth $Pax7^+$ muscle precursors proliferate and give rise to new myoblasts that will differentiate and fuse with their associated myofibres in a process called myonuclear accretion. During postnatal growth fibres also undergo myonuclear accretion independent hypertrophy characterized by increased protein synthesis leading to enlargement of the myonuclear domain. The myonuclear domain is defined as the cytoplasmic volume per nucleus in a cell. It is thought to remain constant in fully grown muscles not exposed to varying physical demands or nutrition conditions (White et al., 2010). As fast twitch fibres of Nf1Myf5 mice showed significant size reduction (see section 4.2.3.4), it was studied whether defects occur in myonuclear accretion or hypertrophy. For this purpose, single myofibres were isolated from extensor digitorum longus (EDL) of Nf1Myf5 mice at P105. Fibres of EDL show the strongest sizes reduction in the adult stage (see Fig. 4.14). The fibres were stained with DAPI and immunolabelled with an antibody against Fast myosin heavy chain (MyFast) to mark fast twitch fibres (Fig. 4.16A). To determine the rate of myonuclear accretion nuclei of myofibres were counted. Nuclei number per fibre was not significantly decreased in Nf1Myf5 (Fig. 4.16C). To determine the size of the myonuclear domain the fibre volume was calculated. The ratio of fibre volume to myonuclei number gave the size of the myonuclear domain. A significant decrease in domain size could be detected for Nf1Myf5 mice which only showed 72,8 % of control domain size. This range of reduction corresponds approximately with the size reduction of fast twitch fibres of EDL. They showed a relative size of 66,4 % of control fibres (see Fig. 4.12D). With this experiment it could be shown that a decrease of hypertrophic growth rather than a defect in myonuclear accretion contributes the most to the fibre size reduction.

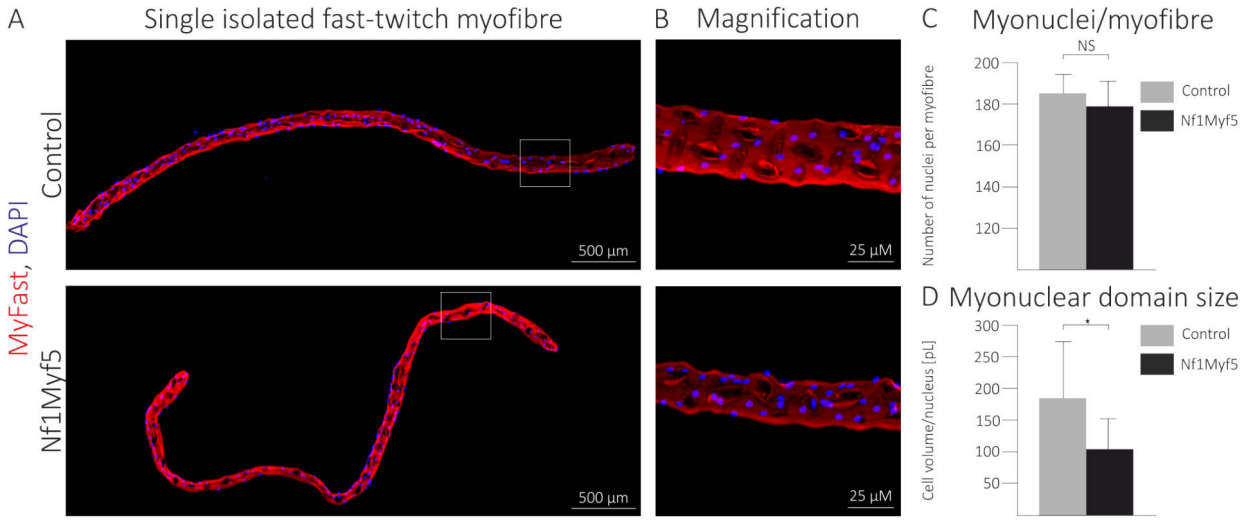

Figure 4.16 Nf1Myf5 mice show reduction of their myonuclear domain in fast twitch fibres

A Isolated fast twitch myofibres of EDL immunolabelled against MyFast (red) and stained with DAPI (nuclei, blue). White boxes indicating region showed in B. **B** Magnification of myofibres. **C** Quantification of myonuclei number per fast twitch fibre. No significant decrease of nuclei number could be detected in Nf1Myf5 (n = 3) in comparison to control (n = 3). **D** Quantification of the myonuclear domain (cell volume/myonucleus). Nf1Myf5 mutants show a significant decrease in myonuclear domain size (44 fibres, 2 animals) in comparison to control (36 fibres, 2 animals). EDL = extensor digitorum longus, MyFast = Fast twitch myosin heavy chain, pL = pico litre.

4.2.3.9 Postnatal Nf1HSA mice do not show muscle size reduction

Nf1Myf5 mice showed a decrease in postnatal muscle size. It was determined whether the observed size reduction was also present in postnatal Nf1HSA mice, which carry a *Nf1* knockout in myotubes and myofibres, but not in myoblasts and precursor cells. Nf1HSA mice do not show a reduction of body size (Fig. 4.17A). Cross sections of whole forelimbs of Nf1HSA were made, immunostained against Collagen IV (component of the muscle connective tissue) and photographed (Fig. 4.17B and C). Nf1HSA mutants did not show a significant decrease in size of triceps brachii (Fig. 4.17D) nor in mean size of myofibres (Fig. 4.17E). The TB is a large muscle with different functional parts. It possesses a certain degree of fibre size heterogeneity. For measurement it was divided into three more homogeneous regions: the innermost region (in close proximity to the humerus bone; region I), the medial region referred to as region II and the outermost (lateral) part referred to as region III (Fig. 4.17F). Analysing each region individually, no significant decrease in myofibre size throughout all regions could be observed like in Nf1Myf5 mice. Nf1HSA mice also did not show significant muscle and fibre size alterations in hindlimb muscles (data not shown). Furthermore, a decrease of body size, muscle size or myofibre size was not detected in adult Nf1HSA at P156 (data not shown). Since no size reduction in Nf1HSA could be detected, a knockout of *Nf1* in myotubes and myofibres does not have significant effects on muscle growth and cannot recapitulate the phenotype of Neurofibromatosis I patients. Therefore no further studies were performed on Nf1HSA mice.

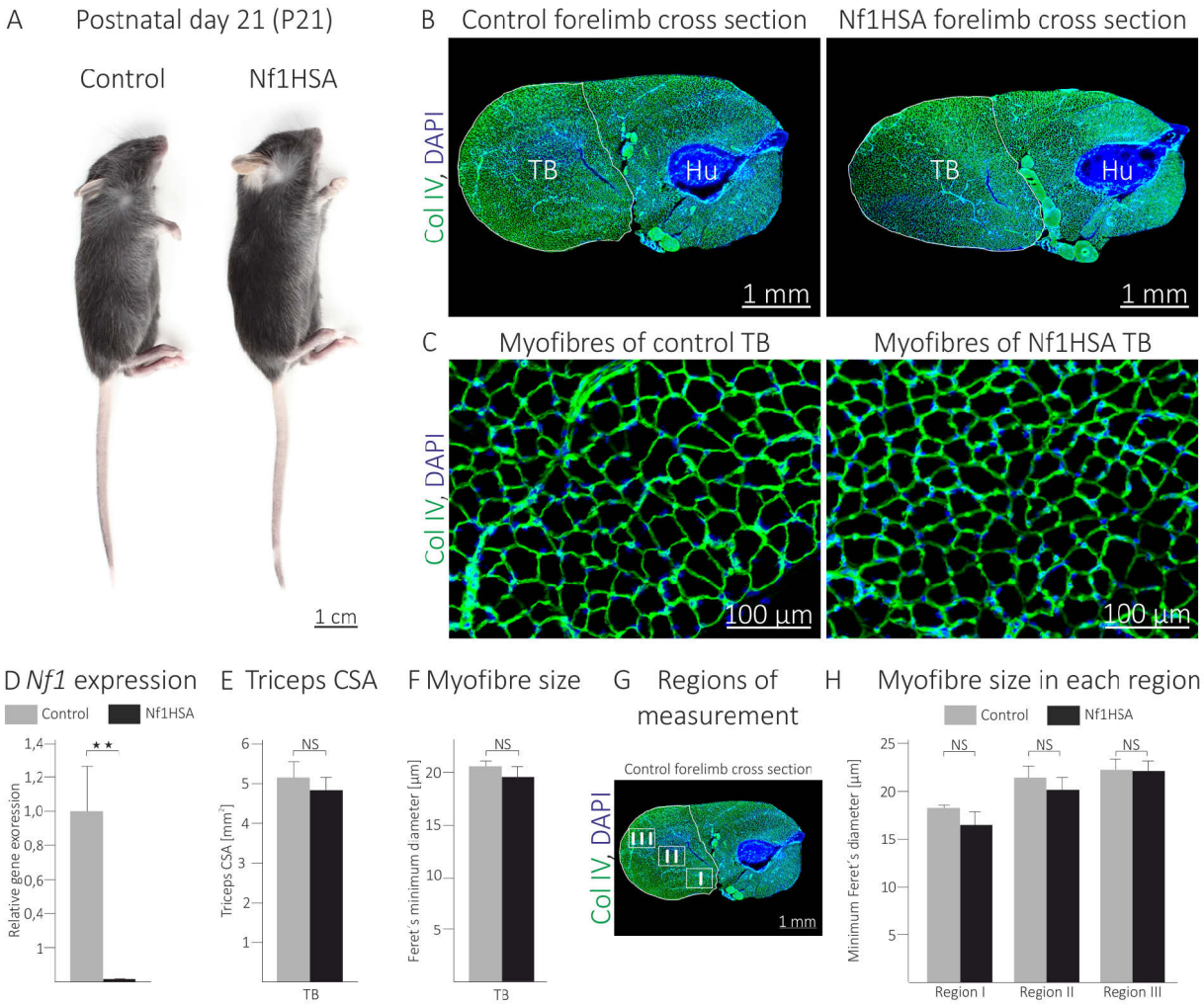

Figure 4.17 Nf1HSA mice do not show reduction of muscle or myofibre size at P21
A Photographs of control and Nf1HSA at postnatal day 21. No difference in size or appearance was detectable. **B** Cross sections of P21 upper forelimbs were immunostained against Collagen IV (Col IV) and DAPI with TB muscle outlined. **C** 40x magnification of cross sections of Region III (referred to the image in G) of the TB muscle of P21 control and Nf1HSA mutant mice stained with DAPI and an antibody against Collagen IV (Col IV). **D** Quantification of *Nf1* gene expression in whole muscle lysates from controls (n = 3) and Nf1HSA (n = 1). A significant decrease in *Nf1* expression was detected in the mutant (p = 0,01). **E** Cross sectional area of triceps brachii of control and mutant mice. Nf1HSA mice do not show a significant decrease in muscle size. **F** Quantification of the mean Feret´s minimum diameter of myofibres of triceps brachii of control and mutant mice. Nf1HSA mice did not show a significant decrease in myofibre size. **G** Cross section through the upper forelimb of a control mouse at P21 stained with DAPI and an antibody against Collagen IV (Col IV) with TB muscle outlined. The three functionally different regions I, II and III are marked by white boxes. **H** Feret's minimum diameter of control and Nf1Myf5 mutant mice separately for myofibres of each region. The size difference is not significant in any region. CSA = cross sectional area, Hu = humerus, TB = triceps bracchii.

Conclusions:

Knockout of *Nf1* in myoblasts and Myf5^{+} precursor cells and their descendents leads to muscle growth defect in Nf1Myf5 from fetal stage of development on. A strong additional effect could be detected in perinatal and adult muscle development when a stronger muscle size reduction was detected. This effect mainly consists of reduction of hypertrophic growth in fast twitch myofibres.

Knockout of *Nf1* in myotubes and myofibres leads to no significant growth defect in Nf1HSA mice. These mice do not show an altered phenotype. It seems that only a knockout of *Nf1* in myoblasts and Myf5$^+$ precursor cells is capable of changing developmental processes throughout entire muscle development. Therefore, Nf1Myf5 mice are subject of further functional analyses.

4.3 Loss of *Nf1* leads to defective Pax7$^+$ cell development

4.3.1 Loss of *Nf1* leads to altered numbers of Pax7$^+$ cells in Nf1Myf5

Knockout of *Nf1* in the myoblasts and Myf5$^+$ precursor cells leads to a muscle growth defect in Nf1Myf5 mice from fetal development on (see section 4.2). In the fetal stage of development a muscle mainly grows through proliferation of Pax7$^+$ cells and their fusion with myotubes through the process of myonuclear accretion. During postnatal growth the number of Pax7$^+$ cells declines until it reaches a constant level at the end of the perinatal stage (P21). From this point on, all Pax7$^+$ cells are supposed to have occupied their characteristic position beneath the basal lamina of the myofibre and were referred to as satellite cells. They are responsible for myofibre repair and regeneration during further life. Pax7$^+$ cells are affected by *Nf1* knockout in Nf1Myf5 mice as soon as they express Myf5 (Pax7$^+$/Myf5$^+$). These cells can be referred to as fetal myoblasts. Analyses of mTmG reporter mice showed a recombination activity (green fluorescence) of Myf5_Cre in Pax7$^+$ cells (see Fig. 4.1). The number of Pax7$^+$ cells in E18.5 Nf1Myf5 mice was quantified in triceps brachii (TB) and vastus medialis (Vm) muscles. Histological cross sections of muscles were labelled with DAPI, immunostained with an antibody against Pax7 and an antibody against Laminin A (LamA) for basal lamina to make the myotubes visible (Fig. 4.18A). In triceps brachii a significant decrease of Pax7$^+$ cells could be detected in cross sections. Nf1Myf5 had approximately 45 % more Pax7$^+$ cells than control mice. A not significant increase of Pax7$^+$ cell numbers could be detected in vastus medialis (Fig. 4.18B). Pax7$^+$ cell numbers were also significantly decreased in Nf1Lbx1 mice, but not in Nf1HSA mice (Fig. 4.18C). Once again it could be shown that only the *Nf1* knockout in precursor cells and myoblasts (Nf1Lbx1, Nf1Myf5), not myotubes and myofibres (Nf1HSA) is sufficient to cause significant defects.
To confirm the results gene expression of *Pax7* was determined using quantitative RT-PCR on whole muscle lysates from E18.5 mice. Nf1Myf5 mice showed a significant upregulation of *Pax7* expression by more than fivefold (Fig. 4.18D). Elevated Pax7$^+$ cell numbers might be due to increased proliferation or defects in cell differentiation. To test for proliferation gene expression of *Cyclin D1*, a regulator of cell cycle progression, was analysed. The expression was significantly upregulated in Nf1Myf5 mice by approximately 1,4 fold (Fig. 4.18E) suggesting an elevated proliferation of fetal myoblasts. Differentiation marker expression analysis showed a significant decrease of *MyoD*, an early myoblast differentiation marker, expression by about 60 % (Fig. 4.18F). However, the late myoblast differentiation marker *Myogenin* and *Maz* (Myc-associated zinc finger protein) showed an increased expression of approximately 50 % and 30 %, respectively (Fig. 4.18G). These data suggest a tendency of increased differentiation rates towards mature myoblasts and a decrease in the pool of early fetal myoblasts. Expression of *Myf5*, however, is not

significantly altered (Fig. 4.18H), although the genomic *Myf5* locus is heterozygously disrupted in Nf1Myf5 by Cre insertion.

During healthy postnatal development the number of Pax7$^+$ cells declines until it reaches a constant level at the end of the perinatal stage. From this point on the Pax7$^+$ cells are referred to as satellite cells. The number of Pax7$^+$ cells in 21 days old Nf1Myf5 mice was quantified in triceps brachii (TB) and soleus (S). The TB muscle was selected as an example for a mixed fibre type muscle and soleus for a slow twitch muscle. It has been suggested that different fibre types differ in the number of Pax7$^+$ cells and their rate of nuclear accretion (White et al., 2010).

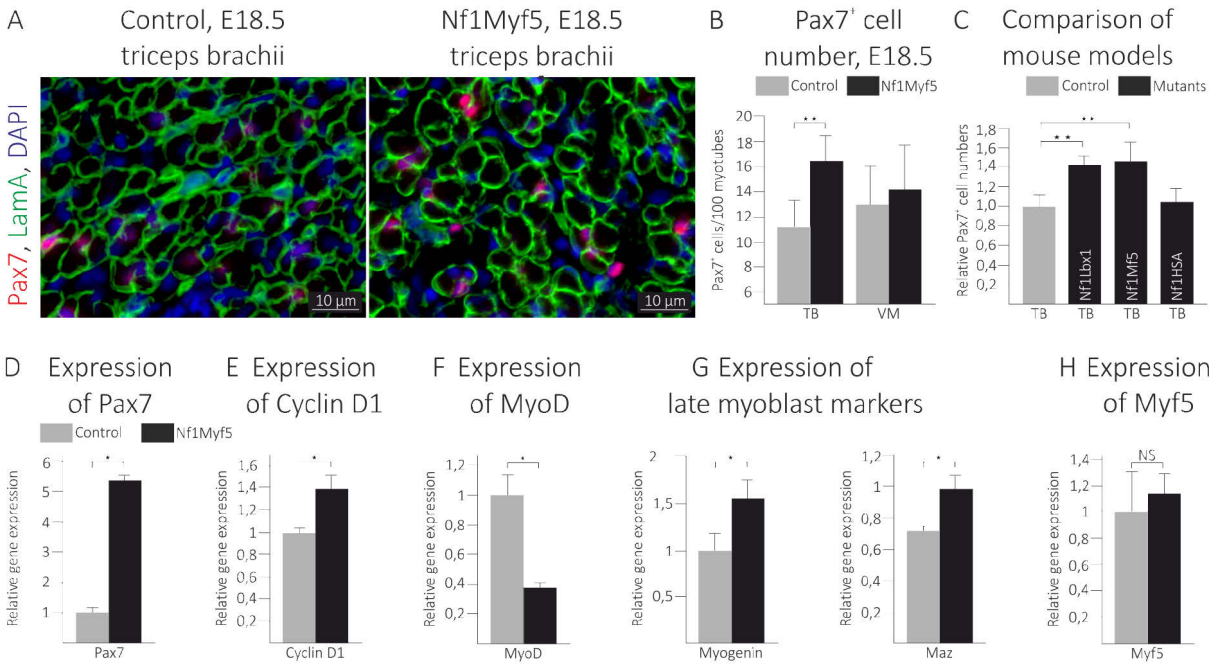

Figure 4.18 Nf1Myf5 show an increase in Pax7$^+$ cell numbers at E18.5

A Cross sections of the TB muscle of E18.5 control and Nf1Myf5 mutant mice stained with DAPI and antibodies against Pax7 and Laminin A (Lam A). **B** Quantification of Pax7$^+$ cells per 100 myotubes in TB and Vm muscles. The increase in Pax7$^+$ cells in Nf1Myf5 mice was significant for TB (n = 3; p = 0,009). **C** Quantification of Pax7$^+$ cell numbers for the Nf1Lbx1, Nf1Myf5 and Nf1HSA model in relation to their respective controls at E18.5. Bar diagram showing relative cell numbers. A significant increase could be detected for Nf1Lbx1 (n = 2; p = 0,042) and Nf1Myf5 (n = 3; p = 0,009). **D** to **H** Gene expression analysis using quantitative RT-PCR showing altered gene expression in muscle (whole muscle lysates) of Nf1Myf5 mice at E18.5. **D** Expression of *Pax7* is significantly increased in Nf1Myf5 (n = 3; p = 0,036). **E** Expression analyses of *Cyclin D1* indicates an elevated level of myoblast proliferation in Nf1Myf5 mice (n = 3; p = 0,036). **F** Expression of *MyoD*, an early myoblast differentiation marker, is significantly decreased in Nf1Myf5 (n = 3; p = 0,026).**G** Expression of the late myoblast differentiation marker *Myogenin* (n = 3; p = 0,017) and *Maz* (n = 3; p = 0,013), however, is significantly increased in Nf1Myf5 in comparison to control. **H** Myf5 gene expression is not significantly altered in Nf1Myf5 (n = 3). TB = triceps brachii, VM = Vastus medialis.

Histological cross sections of muscles were immunostained with DAPI and antibodies against Pax7 and Laminin A (LamA; basal lamina; Fig. 4.19A). In contrast to fetal Nf1Myf5 mice (E18.5), postnatal Nf1Myf5 mice (P21) showed a decrease of Pax7$^+$ cells. Pax7$^+$ cell numbers in triceps brachii were even significantly reduced by 44 % in mutants compared to controls (Fig. 4.19B). Triceps possesses a certain degree of myofibre size heterogeneity. For measurement it was divided into three more homogeneous regions: the innermost region (in close proximity to

the humerus bone; region I), the medial region referred to as region II and the outermost (lateral) part referred to as region III (according to Fig. 4.10A). Analysis of the different regions of triceps revealed that the difference in $Pax7^+$ cells was biggest in region III where slow twitch myofibres are not present. The decrease of $Pax7^+$ cell numbers was also only significant in region III (Fig. 4.19C). This result is in accordance with the fibre size measurements which revealed a significant size reduction in Nf1Myf5 mice only occurs in region III (see Fig. 4.10E). It seems that fast fibres are affected the most by *Nf1* knockout.

At E18.5 the increase in $Pax7^+$ cell numbers is accompanied by an increased expression of the proliferation marker *Cyclin D1*. Therefore, proliferation marker analysis was also performed in mice at P21. The proliferative status of the triceps and soleus was assessed by quantifying the amount of $Ki\text{-}67^+$ cells. Ki-67 is an antigen expressed during all active phases of the cell cycle (Scholzen and Gerdes, 2000). Triceps was used as an example of mixed fibre type muscles and soleus as an example of slow muscles. Cross sections of the upper forelimb and the lower hindlimb were immunostained against Laminin A to make the individual myofibres visible. Proliferating cells were marked using an antibody against Ki-67 (Fig. 4.19D). The results of quantification showed a significant decrease in proliferation in both muscles of Nf1Myf5 mutants. The reduction in proliferation was more pronounced in soleus (around 18 fold) than in triceps (around 3 fold; Fig. 4.19E). Afterwards, each region of the triceps (see Fig. 4.10E) was analysed separately. The decrease of $Ki\text{-}67^+$ cell numbers was only significant in region III (Fig. 4.19F). This result is in accordance with the $Pax7^+$ cell count which showed a significant decrease of $Pax7^+$ cells only in region III of Nf1Myf5 mice (see Fig. 4.19C). The gradual increase in differences between control and Nf1Myf5 mice from region I to III can be seen for $Pax7^+$ and $Ki\text{-}67^+$ cell numbers. This correlation suggests an association between decreasing $Pax7^+$ cell numbers and proliferation although this experiment cannot be seen as a proof as the identity of $Ki\text{-}67^+$ cells is not clarified. They might be $Pax7^+$ cells, connective tissue or endothelial cells, for example.

In summary, an increased number of $Pax7^+$ cells could be detected in Nf1Myf5 mice and NfLbx1 mice at the fetal stage (E18.5). Surprisingly, a decreased number of $Pax7^+$ cells could be detected in Nf1Myf5 mice at perinatal stage (P21). That means that the $Pax7^+$ cell pool is decreased perinatal much stronger in Nf1Myf5 than in controls. Aberrant proliferation and differentiation processes might play a role in this process.

4.3.2 Fetal $Pax7^+$ cells of Nf1Myf5 mice show altered proliferation behaviour

Nf1Myf5 mice show a significantly increased number of $Pax7^+$ cells in triceps brachii at E18.5 (see Fig. 4.18). To analyse the causes, proliferation rates of $Pax7^+$ cells were investigated. For this purpose a BrdU assay was performed. BrdU (5-bromo-2'-deoxyuridine) is a labelled nucleotide which incorporates in newly synthesized DNA in proliferating cells. After application of BrdU to a pregnant female, embryos are dissected and histological sections of upper forelimbs were performed. Sections were stained with DAPI and immunolabelled with antibodies against BrdU and Pax7. To determine myotube numbers, Laminin A (basal lamina) was labelled as well. The assay was performed at day E17.5 to find the cause for the $Pax7^+$ cell increase at day E18.5. Surprisingly, only a slight, not significant increase in $Pax7^+$ and proliferating $Pax7^+$ ($Pax^+/BrdU^+$) cells was detected (Fig. 4.20A) which could not account for the $Pax7^+$ cell increase at E18.5. As

triceps brachii is a large muscle, it was divided into two regions: A (inner region, close to humerus bone) and B (outer, lateral region). The distribution of cells between these regions was determined. Whereas $Pax7^+$ and $Pax7^+/BrdU^+$ cells were evenly distributed in control mice (Fig. 4.20C and D, upper panels), a significant change of cell distribution was detected in Nf1Myf5 mice (Fig. 4.20C and D, lower panels). Nf1Myf5 mice showed significantly more $Pax7^+$ cells in the inner region (A) than in the outer region (B) and significantly more $Pax7^+/BrdU^+$ in the outer region (B) than in the inner region (A). This might be due to a disturbance in $Pax7^+$ proliferation if $Pax7^+$ cells have a consecutive locally proliferation behaviour. This has not been reported yet. Nevertheless, it would be conceivable to assume that in Nf1Myf5 mutants $Pax7^+$ proliferation is delayed and has already taken place in region A (high $Pax7^+$ cell numbers), but not in region B (low $Pax7^+$ numbers). In region B the transient burst of proliferation is currently taking place visible in the high numbers of $Pax7^+/BrdU^+$ cells. This could mean that mutant mice will reach the step of even distribution later in development than controls and therefore show a delay in development.

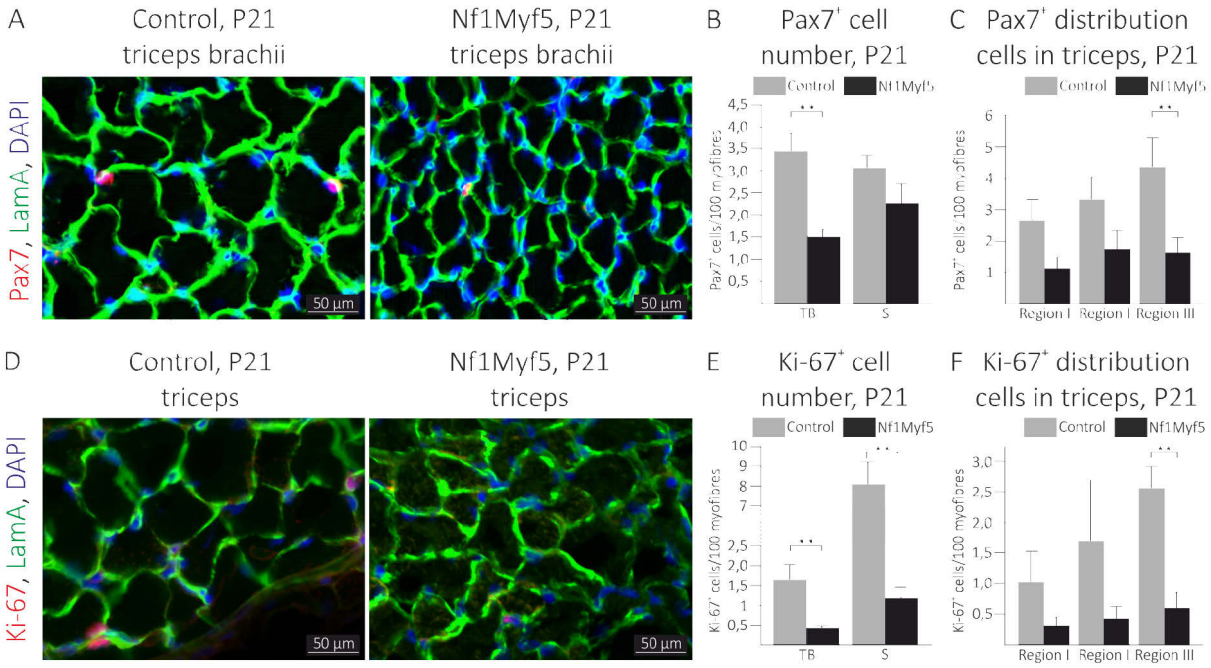

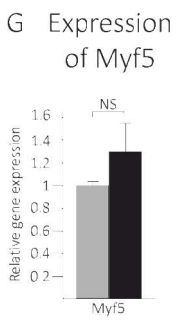

Figure 4.19 Nf1Myf5 show a decrease in $Pax7^+$ cell numbers at P21

A Cross sections of TB of Nf1Myf5 mutant and control mice at P21, stained with DAPI and antibodies against Pax7 and Laminin A (LamA). **B** Quantification of $Pax7^+$ cells in the TB (controls n = 4, mutants n = 5; p = 0.0008) and soleus (controls n = 3, mutants n = 3) showed a decrease of $Pax7^+$ cells in TB at P21. **C** Quantification of $Pax7^+$ cell numbers in each region of the TB muscle separately (regions refer to figure 4.10A). Only region III (lateral part of the TB muscle) showed a significant decrease of $Pax7^+$ cell numbers (controls n = 4, mutants n = 5; p = 0.028). **D** Cross sections of the TB muscle of control and Nf1Myf5 mice immunostained with antibodies against Ki-67, Laminin A (LamA) and DAPI. **E** Quantification of proliferating cells ($Ki\text{-}67^+$ cells) in TB and soleus. The diagram shows the average of the whole muscles. A significant decrease in $Ki\text{-}67^+$ cells could be detected in both muscles (TB: controls n = 4, mutants n = 5; p = 0.0008 and S: controls n = 3, mutants n = 3; p = 0.004). **F** Quantification of $Ki\text{-}67^+$ cell numbers in each separate region of the TB muscle (regions refer to figure 4.10A). Only region III (lateral part of TB muscle) showed a significant decrease of $Ki\text{-}67^+$ cell numbers (p = 0.002; controls n = 4, mutants n = 5). **G** Myf5 gene expression is not significantly altered in Nf1Myf5 mice (n = 4) compared to controls (n = 3). TB = triceps brachii, S = soleus, NS = not significant.

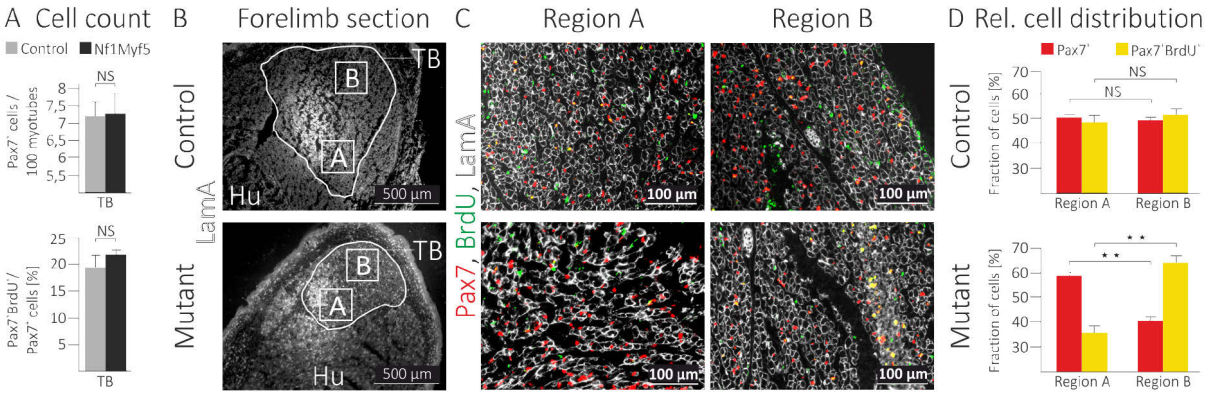

Figure 4.20 Nf1Myf5 show altered Pax7$^+$ cell proliferation

A Upper diagram: Quantification of Pax7$^+$ cell numbers per 100 myotubes in TB of Nf1Myf5 mice at E17.5. A significant increase in total Pax7$^+$ cell numbers could not be detected. Lower diagram: Quantification of proliferating Pax$^+$ cells (Pax7$^+$/BrdU$^+$) per 100 myotubes in TB of Nf1Myf5 at E17.5. No significant increase in total Pax7$^+$/BrdU$^+$ cell numbers could be detected in Nf1Myf5. **B** Cross sections of TB muscle of E17.5 Nf1Myf5 and control mice stained with an antibody against Laminin A (LamA) with the TB muscle outlined. The two investigated regions A and B are marked by white boxes. **C** 20 x magnification of cross sections of regions A and B of the TB muscle of control and Nf1Myf5 mutant mice immunostained with antibodies against Pax7, BrdU and Laminin A (LamA). **D** Quantification of relative Pax7$^+$ cell numbers and Pax7$^+$/BrdU$^+$ cell numbers separately for control (n = 4, upper diagram) and Nf1Myf5 mice (n = 3, lower panel). Relative cell numbers are determined for region A (left side) and region B (right side). Diagrams show percental distribution of cell populations within the regions of the triceps. An even distribution of Pax$^+$ and Pax7$^+$/BrdU$^+$ cells within the two regions could be detected in controls (numbers for each measurement approximately 50 %) indicating a stage of even proliferation rates. An uneven distribution of Pax7$^+$ and Pax7$^+$/BrdU$^+$ cells within the two regions could be detected in Nf1Myf5 mutants: The Pax7$^+$ cells are mainly (about 60 %) located in region A suggesting a stage of incomplete Pax7$^+$ cell formation in region B (about 40 % of Pax7$^+$ cells; p = 1,3·10^{-5}). The proliferating cells are mainly located in region B (about 64 %) indicating the process of compensatory proliferation in region B in comparison to region A (about 36 %; p = 0,0005). TB = tibialis anterior, Hu = humerus, Rel = relative.

4.3.3 Nf1Myf5 myofibres show characteristics of a disturbed differentiation process

In fetal Nf1Myf5 mice a disturbed differentiation process of fetal muscle progenitor cells could be observed (see sections 4.3.1 and 4.3.2). Fetal progenitor cells proliferate and give rise to new myoblasts which will differentiate and fuse with their associated myofibres (myonuclear accretion). To analyse whether Nf1Myf5 myofibres also show characteristics of a differentiation defect, expression of the early myosin isoform MyEmb (embryonic myosin) was examined at the end of perinatal development. The expression of the embryonic isoform of myosin can be used to estimate the degree of maturation of muscle fibres since its expression gradually recedes as the myofibres mature. To estimate the degree of maturation of the myofibres in Nf1Myf5 mutants the percentage of myofibres expressing embryonic myosin (MyEmb) was determined. Cross sections of muscles were immunolabelled with a specific antibody against embryonic myosin (Fig. 4.21A). All muscles showed an increased MyEmb expression in Nf1Myf5 (Fig. 4.21B) but the increase was only significant for tibialis anterior (TA) and soleus (S).

A second characteristic of myofibre maturity is their cross sectional shape. Mature myofibres display a polygonal shape in cross sections. It has been postulated that immature myofibres are circular and become polygonal as they mature (Nilwik et al., 2013). The circularity of the myofibres can be mathematically expressed with the circle form factor CFF, which is the ratio of

the cross sectional area (CSA) of a myofibre to its perimeter p (CFF = $[4\pi \cdot CSA]/p^2$). The circle form factor equals 1.0 for perfect circles and approaches zero as the shape becomes more polygonal. To estimate if a delay in the development of the myofibres of Nf1Myf5 mutants was present the from circle factor was calculated for fibres of TB, TA, EDL and soleus. Cross sections of forelimbs and hindlimbs were immunolabelled with antibodies against Collagen IV (Col IV, connective tissue) and MyHc (myosin heavy chain, myofibre filaments) to make the myofibres visible (Fig. 4.21C). A trend is recognizable showing that the myofibres of the mutants are more circular (Fig. 4.21D). The increase in circularity in Nf1Myf5 is only significant for soleus, a so called 'slow' muscle suggesting a differentiation delay in slow twitch fibres. The results point towards more immature myofibres in the Nf1Myf5 mutants. This is an interesting fact as immature muscle characteristics are associated with muscle hypotonia (Farkas-Bargeton et al., 1978), which is a symptom of neurofibromatosis I (North, 1998).

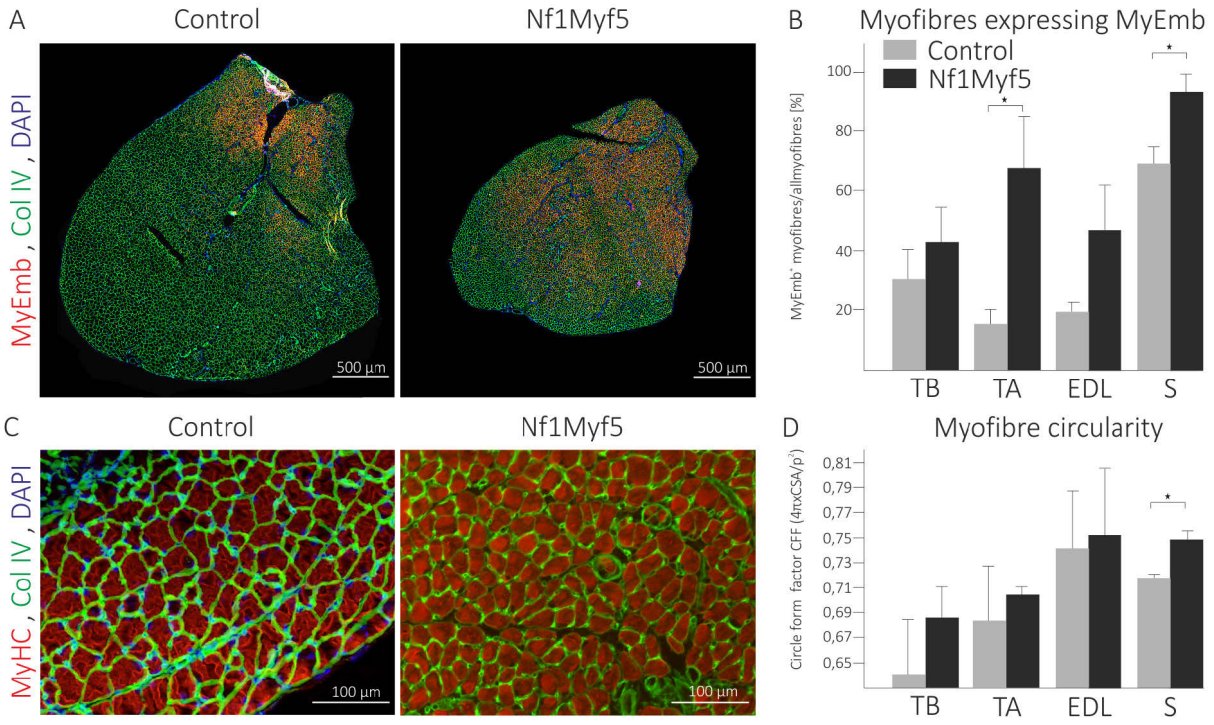

Figure 4.21 Nf1Myf5 show characteristics of immature myofibres at P21

A Triceps cross sections of P21 control and Nf1Myf5 mutant mice immunolabelled against embryonic myosin (MyEmb), Collagen IV (Col IV) and DAPI. **B** Quantification of the percentage of myofibres expressing MyEmb in TB, TA, EDL and soleus (S). Nf1Myf5 mice showed an increase of fibres expressing MyEmb. TB: controls n = 4, mutants n = 5; TA: controls n = 3, mutants n = 4, p = 0.05; EDL: controls n = 3, mutants n = 4; S: controls n = 3, mutants n = 3, p = 0,05. **C** Cross sections of the TB of P21 control and Nf1Myf5 mutant mice stained against myosin heavy chain (MyHc), Collagen IV (Col IV) and DAPI. **D** Quantification of myofibre circularity: Mean form circle factor (CFF) of myofibres of TB, TA, EDL and S of P21 control and Nf1Myf5 mutant mice. Nf1Myf5 mice showed an increase in circularity, which is only significant for soleus (p = 0,019). TB: controls n = 4, mutants n = 5; TA: controls n = 3, mutants n = 4; EDL: controls n=3, mutants n = 4; S: controls n = 3, mutants n = 3. Nf1Myf5 mice showed a not significant increase in myofibre circularity in all muscle. The circularity is defined by the circle form factor CFF = $(4\pi \cdot CSA/p^2)$. MyEmb = embryonic myosin, TB = triceps brachii, TA = tibialis anterior, EDL = extensor digitorum longus, S = soleus, CSA = cross sectional area of a myofibre, p = perimeter.

Conclusions

The Nf1Myf5 model could recapitulate the muscle growth defect seen in Neurofibromatosis I patients (see section 4.2). In this section putative causing mechanism should be revealed. The Nf1Myf5 muscle size reduction is accompanied by severe defects in development of $Pax7^+$ cells and myofibre differentiation. These defects have been described to be a primary cause of muscle growth defects (Relaix et al., 2005; Minetti et al., 2014; Boyer et al., 2014) and therefore could account for the size reduction. Myofibre identity and functionality is determined by the expression of special myosin isoforms. A shift towards more MyEmb (embryonic myosin) expressing fibres in Nf1Myf5 was observed. A distorted composition of myosin isoforms can cause muscular disorders (DeChene et al., 1993). Therefore, the expression of other myosin isoforms was investigated subsequently (see section 4.4.1.1).

4.4 Loss of *Nf1* leads to a metabolic muscle defect in postnatal mice

4.4.1 Loss of *Nf1* results in a switch of fibre specific gene expression and metabolism

4.4.1.1 Nf1Myf5 mice show a switch in myofibre specific protein and gene expression

Myofibre identity, which is, among others, determined by expression of specific myosin isoforms, is essential for proper muscle function and metabolism. Myofibres can differentiate into two main types: slow twitch and fast twitch myofibres. They differ in function, kinetics and cell metabolism. To determine if the differentiation defect seen in Nf1Myf5 mice (see section 4.3.3) has an influence on fibre type composition, myofibre marker expression was analysed in Nf1Myf5 mice. Cross sections of forelimbs and hindlimbs were immunostained with an antibody against Slow myosin heavy chain (MySlow) to identify the slow twitch fibres. The connective tissue was stained with an antibody against Collagen IV (Col IV; Fig. 4.22A). The total number of myofibres and the number of myofibres expressing MySlow was determined. The percentage of slow twitch ($MySlow^+$) myofibres in triceps brachii (TB) and extensor digitorum longus (EDL) was not significantly altered in the Nf1Myf5 mice compared to controls. Tibialis anterior (TA) showed a significant increase in slow twitch fibres from 4,0 % in controls to 5,7 % in mutants. Surprisingly, in soleus the amount of slow twitch fibres significantly decreased from 37 % in controls to 29 % in Nf1Myf5 mice (Fig. 4.22B). Soleus is the only so called slow muscle which was investigated. The percentage of muscle area positive for the MySlow staining was also calculated. For this measurement, the total CSA, the area expressing MySlow and the connective tissue area were determined. The area of the connective tissue was subtracted from the total CSA to establish the muscle tissue area. The MySlow expressing ($MySlow^+$) area of the muscle was then compared to the total muscle tissue area. Relative $MySlow^+$ area was increased significantly in TB, TA and EDL in Nf1Myf5 mice (about 12 %) compared to controls (about 5 %). However, the slow muscle soleus presented a decrease in the muscle area expressing MySlow from 37 % to 29 % (Fig. 4.22C). To confirm the immunohistochemical results quantitative RT-PCR analysis was performed on whole muscle tissue lysates. The expression of marker genes for each fibre

type was investigated. A significant increase in expression of *MySlow* (*Myh7*) by about fourfold in Nf1Myf5 mice was detected. *Calsarcin-1* (*CS-1*), a z-disc protein in slow twitch fibres, is upregulated by about fivefold in Nf1Myf5. The myosin isoform of fast twitch oxidative myofibres *MyFastOx* (*Myh2*) is also upregulated (about fourfold) in Nf1Myf5. But on the other hand, the myosin isoform of fast twitch glycolytic myofibres *MyFastGl* (*Myh4*) is downregulated by approximately 60 % in Nf1Myf5 mice (Fig. 4.22D). These results suggest a general shift in myofibre identity towards the oxidative type at expense of the glycolytic type.

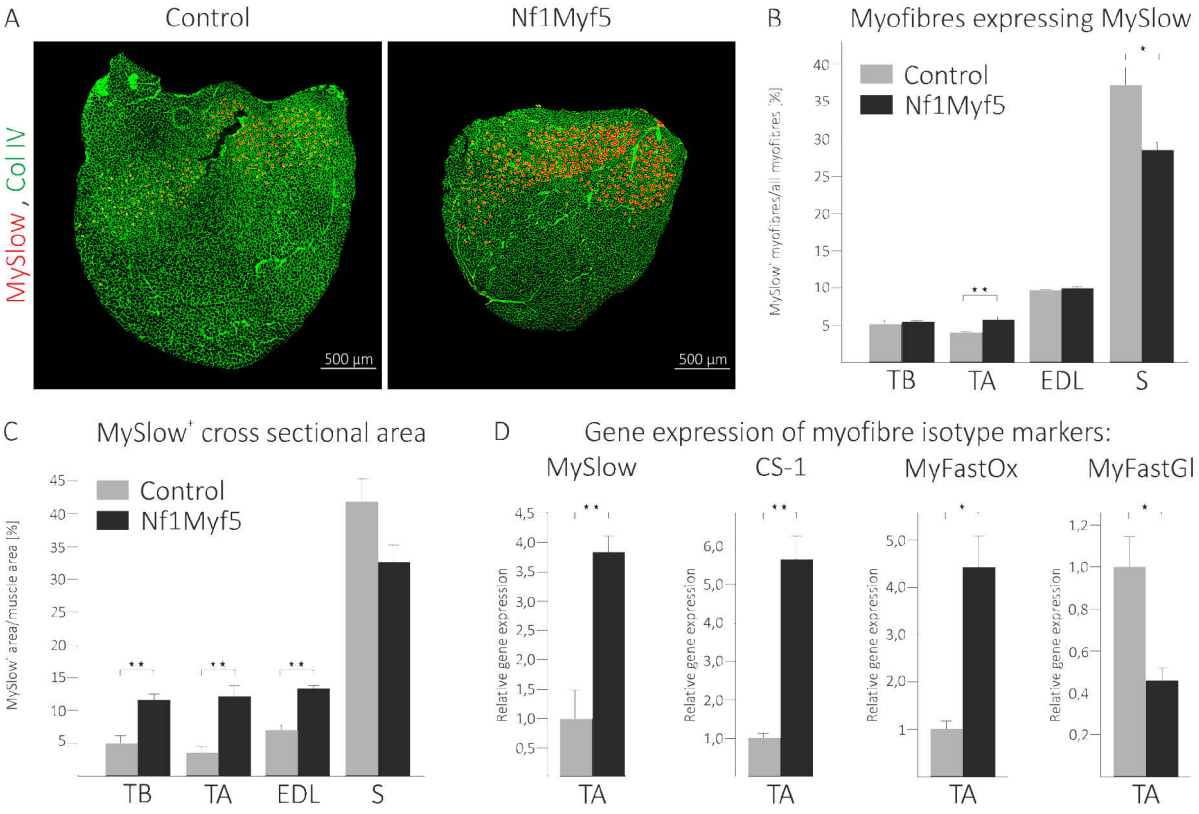

Figure 4.22 Nf1Myf5 show a switch in myosin isoform expression

A Triceps cross sections of control and Nf1Myf5 mice at P21 stained for MySlow (red) and Col IV (green). Nf1Myf5 mice show a more intensive MyEmb staining. **B** Quantification of relative MySlow$^+$ fibre numbers. Nf1Myf5 mice showed a not significant increase of MySlow$^+$ fibres in TB and EDL, a significant increase in TA ($p = 0{,}0003$) and a significant decrease in soleus ($p = 0{,}02$). TB: controls n = 4, mutants n = 5; TA: controls n = 3, mutants n = 4; EDL: controls n = 3, mutants n = 4; S: controls n = 3, mutants n = 3. **C** Quantification of the percentage of muscle area (CSA) expressing MySlow in TB, TA, EDL and S. Nf1Myf5 mice show a significant increase of muscle area (CSA) expressing MySlow in TB muscle ($p = 0{,}001$), TA ($p = 0{,}006$), and EDL ($p = 0{,}0004$) and a not significant decrease in S muscle. TB: controls n = 4, mutants n = 5; TA: controls n = 3, mutants n = 4; EDL: controls n = 3, mutants n = 4; S: controls n = 3, mutants n = 3. **D** Gene expression analysis in TA showed a significant increase in gene expression of the exclusive slow twitch myofibre proteins MySlow (*Myh7*; $p = 0{,}015$) and CS-1 (*Myoz2*; $p = 0{,}004$). A significant increase in gene expression was also detected for *MyFastOx* (*Myh2; p = 0,015*), which is only expressed in fast oxidative fibres. However, gene expression of *MyFastGl* (*Myh4; p = 0,028)*, a marker for fast glycolytic fibres is significantly decreased in Nf1Myf5. Controls n = 4, mutants n = 5. Col IV = Collagen IV, MySlow = Slow myosin heavy chain, TB = triceps brachii, TA = tibialis anterior, EDL = extensor digitorum longus, S = soleus muscle. CSA = cross sectional area.

4.4.1.2 Nf1Myf5 mice show a shift towards mitochondrial oxidative metabolism

Nf1Myf5 mice show a shift in myofibre type identity (see section 4.4.1.1). Myofibre types differ in their specific metabolism. Metabolic parameters influence muscle performance (Conley et al., 2001) as well as muscle differentiation (Jang et al., 2011) and can cause muscular weakness (Cruz Guzmán et al., 2012). Therefore metabolic parameters were investigated in the Nf1Myf5 model. Nf1Myf5 mice have a darker (redder) muscle colour and strongly diminished adipose tissue compared to controls (Fig. 4.23A). These observation point toward an increase in myofibres with high oxidative capacity (oxidative metabolism mainly in slow twitch fibres, so called red fibres) and an increase in fat catabolism. Oxidative metabolism takes place in mitochondria. To test the activity of mitochondrial respiratory chain in myofibres histological cross sections of lower hindlimbs were stained for succinate dehydrogenase (Sdh) activity. Nf1Myf5 mutants showed a more intense staining in tibialis anterior (TA), extensor digitorum longus (EDL) and surrounding muscles (Fig. 4.23B) indicating an increase in oxidative phosphorylation. Quantification of staining intensities taken together for TB, TA, EDL and soleus showed an increase of muscle area with high Sdh activity in Nf1Myf5 (59,2 %) compared to control mice (37,4 %). Furthermore, muscle area with low Sdh activity is severely reduced in Nf1Myf5 mice (20,7 %) in comparison to control mice (40,1 %). To confirm the hypothesis of increased mitochondrial oxidative phosphorylation gene expression of metabolic marker enzymes was measured via quantitative RT-PCR. Cytochrom-c-oxidase (Cox1) and NADH dehydrogenase (Nd1) are, like Sdh, components of the oxidative phosphorylation chain. In Nf1Myf5 mice expression of these genes is upregulated by 1,6 fold each. Mitochondrial citrate synthase (m-Cs) is an enzyme of the citrate cycle (TCA cycle). *M-Cs* expression is also upregulated by 1.6 fold in Nf1Myf5 mice in comparison to controls. M-CS is a marker for oxidative metabolism (Leek et al., 2001). On the other hand, expression of *Gapdh*, an enzyme of glycolysis, is downregulated by 30 % in Nf1Myf5. Glycolysis and glyconeogenesis are reciprocally regulated (Berg et al., 2002). If glycolysis is downregulated, glyconeogenesis is upregulated. In Nf1Myf5 mutants the expression of the glyconeogenesis marker *Pepck* is significantly upregulated (by approximately tenfold). Also upregulated was glycogen synthesis as seen by the upregulation of *Gsk3b* expression in Nf1Myf5 mutants (Fig. 4.23D). A major regulator of cellular metabolic processes is AMP-activated protein kinase α (Ampk). Ampk is an important sensor of cellular energy status in skeletal muscles (Winder, 2001) and increases mitochondrial enzymes in muscle (Winder et al., 2000). Therefore activation status of Ampk was tested in skeletal muscle lysates of Nf1Myf5 mice via western blot analysis. Ampk is active when it is phosphorylated (P). Nf1Myf5 mutants show an increase in activated Ampk (P-Ampk) protein levels in muscle. A constitutive activation of Ampk is supposed to cause an increased uptake of glucose and oxidation of fatty acids (O'Neill, 2013). The results show that myofibre identity shift is associated with a metabolic switch in Nf1Myf5 mutants.

4.4.1.3 Nf1Myf5 mice show an increase in fatty acid beta oxidation

Muscle metabolism has a strong influence on muscle performance (Conley et al., 2001) and needs to be investigated in order to describe the symptoms of a myopathy. An increased activation of Ampk as described in section 4.4.1.2 changes cellular metabolism. Activated Ampk can elevate

levels of fatty acid beta oxidation (O'Neill, 2013). Muscular fatty acid depots can be found in the sarcoplasm of a myofibre adjacent to mitochondria. Electron microscopy revealed a drastic decrease of fatty acid storage units in myofibres of TA muscle. In control mice single lipid depots in the size of 0,5 µm to 1 µm could be found. However, no such depots could be seen in Nf1Myf5 (Fig. 4.24A). Gene expression analysis on whole muscle lysates via quantitative RT-PCR showed an upregulation of beta oxidation marker genes in Nf1Myf5.

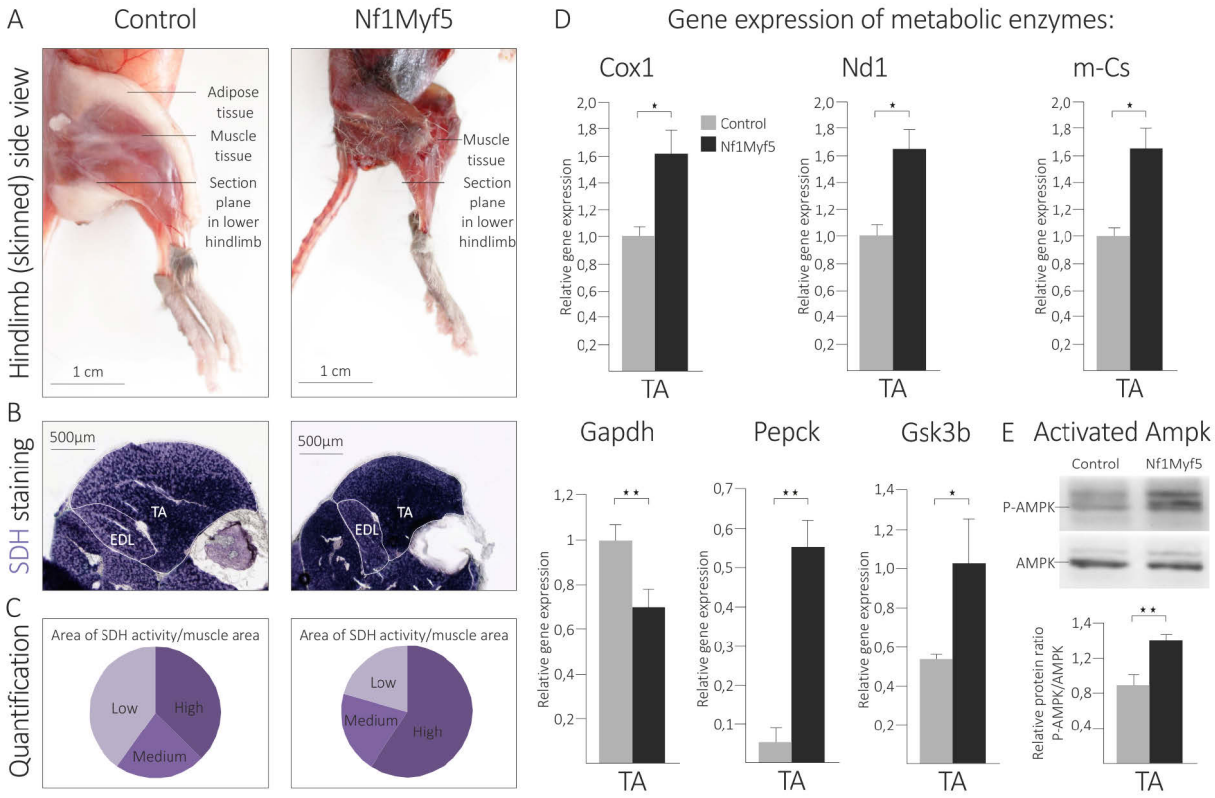

Figure 4.23 Nf1Myf5 show a shift towards mitochondrial metabolism

A Photographs of skinned hindlimbs of control and Nf1Myf5 mice at P21. Muscles of Nf1Myf5 mice show a darker, redder colour than control muscles. Black lines indicate section planes for images shown in B. **B** Histological Sdh staining of hindlimb muscles of control and Nf1Myf5 mice. Violet colour indicates Sdh enzyme activity. **C** Quantification of relative muscle area with low, medium and high Sdh activity. Results combine data from TB, TA, EDL and S muscles. Nf1Myf5 mice showed an increase in high Sdh activity muscle area (59,2 %) compared to control mice (37,4 %). Area with medium Sdh activity stays approximately unaltered (control: 22,5 %, mutant 20,2 %). Area with low Sdh activity is decreased in Nf1Myf5 mice (20,7 %) compared to controls (40,1 %). **D** Quantification of gene expression analysis via quantitative RT-PCR on metabolic enzymes in muscle tissue of TA (control n = 3, Nf1Myf5 n = 4). Nf1Myf5 showed a significant increase in gene expression of markers of mitochondrial metabolism (*Cox1*: p = 0,046; *Nd1*: p = 0,028; *m-Cs*: p = 0,012). Expression of the glycolysis enzyme Gapdh is significantly decreased (p = 0,005) in Nf1Myf5 (p = 0,012). *Pepck* (enzyme of glyconeogenesis) expression is significantly increased (p = 0,0007) in Nf1Myf5 as well as expression of *Gsk3b* (p = 0,093; enzyme of glycogen synthesis). **E** Western blot analysis on muscle tissue of controls and Nf1Myf5. Images showing specific antibody-detected western blot signals. Upper panel: activated Ampk (P-Ampk). Lower panel: inactivated Ampk (Ampk) as reference. Diagram shows quantification of western blot results: Relative amount of P-Ampk is significantly increased in Nf1Myf5 (n = 4) compared to controls (n = 3; p = 0,004). TB = triceps brachii, TA = tibialis anterior, EDL = extensor digitorum longus, S = soleus. CSA = cross sectional area. Sdh = succinate dehydrogenase, Cox1 = cytochrome oxidase subunit I, Nd1 = NADH dehydrogenase 1, m-Cs = mitochondrial citrate synthase, Gapdh = glyceraldehyde 3-phosphate dehydrogenase, Pepck = phosphoenolpyruvate carboxykinase, Gsk3b = glycogen synthase kinase 3 beta, Ampk = 5' AMP-activated protein kinase α.

The transport protein Fabp4 is required to provide fatty acids for beta oxidation. *Fabp4* gene expression was significantly upregulated (by threefold) in Nf1Myf5. The expression of *Acadl*, which catalyses the initial step of beta oxidation, was significantly upregulated by more than twofold. Hadh catalyses the third step of mitochondrial beta oxidation. Its expression is also significantly upregulated (by threefold) in Nf1Myf5. It could be shown that not only mitochondrial oxidative phosphorylation but also mitochondrial beta oxidation is upregulated in Nf1Myf5 mutants.

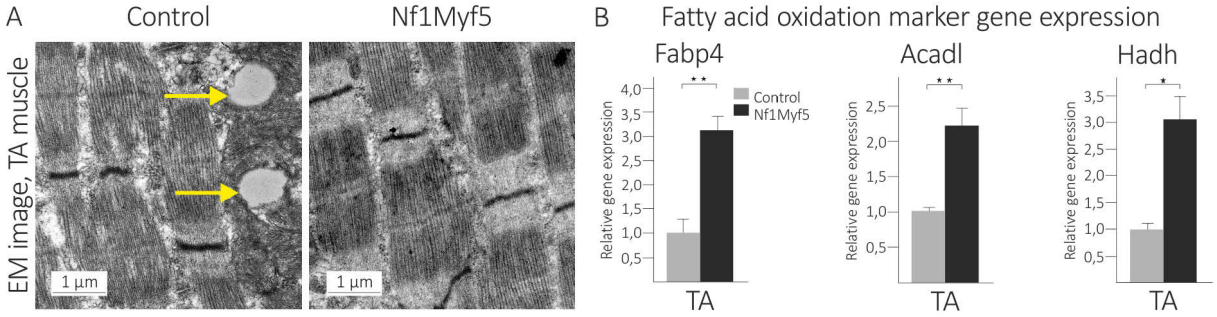

Figure 4.24 Nf1Myf5 show an increase in fatty acid beta oxidation

A Electron microscopy images of longitudinal sections of TA muscles of control and Nf1Myf5 at postnatal day P21. Images showing intracellular myofilaments. Only in controls intramyocellular lipid storages with a diameter between 0,5 and 1 µm could be detected (yellow arrows). Nf1Myf5 did not show such lipid storages. **B** Quantification of gene expression analysis of muscle tissue of TA in P21 mice. Nf1Myf5 (n = 4) show a significant increase in gene expression of marker enzymes of beta oxidation in comparison to control (n = 3): *Fabp4* p = 0,005; *Acadl* p = 0,005; *Hadh* p = 0,008. TA = tibialis anterior, Fabp4 = fatty acid binding protein 4, Acadl = acyl-CoA dehydrogenase long chain, Hadh = hydroxyacyl-CoA dehydrogenase.

4.4.2 Loss of *Nf1* causes an increased activity of Ras downstream pathways in Nf1Myf5

Nf1 is deleted in muscle cells of Nf1Myf5. Its gene product neurofibromin is a so called GAP, a GTPase activating protein, that facilitates hydrolysis of Ras-GTP and therefore induces deactivation of Ras signalling. Loss of *Nf1* causes constitutive Ras signalling (Mayes et al., 2013). It is not yet clear which Ras downstream pathways are essential in developing myofibres. As severe muscle alteration could be seen in Nf1Myf5 at P21, muscle tissue from these animals was tested regarding Ras pathway activation. An upregulation of three Ras downstream pathways - the Akt pathway, the Mek/Erk pathway and the Nfat pathway (Fig 4.25A) - was detected. Pathway components are activated by phosphorylation (Akt, Mek, Erk) or dephosporylation (Nfat) events. Whole muscle protein lysates were taken from Nf1Myf5 and controls and western blots were performed using specific antibodies against activated Akt (P-Akt) and Akt, activated Creb (P-Creb) and HSP60, activated Erk1/2 (P-Erk1/2) and Erk1/2, activated cJun (P-cJun) and HSP60, activated $Nfat_{c3}$ (dephosphorylated $Nfat_{c3}$) and HSP60, activated $Nfat_{c1}$ (dephosphorylated $Nfat_{c1}$) and HSP60 (Fig. 4.25B). Quantitative evaluation of protein levels revealed a significant increase in activated Akt, Creb, Mek, Erk, cJun and $Nfat_{c3}$. $Nfat_{c1}$ was only mildly and not significantly over-activated. This might be a hint to a more essential role of $Nfat_{c3}$. Nfat signalling induces the expression of embryonic myosin (MyEmb) whereby $Nfat_{c1}$ and $Nfat_{c3}$ preferentially regulate the *MyEmb* gene (Daou et al., 2013). Increased expression of *MyEmb* was found in muscles of Nf1Myf5 (see Fig. 4.21A). Slow myosin (*MySlow*) expression is also elevated

in Nf1Myf5 mice (see Fig. 4.22A,B,C and D). *MySlow* expression is also induced by Nfat (Delling et al., 2000). Another prominent Nfat transcriptional target is *Rcan1* (Shin et al., 2011), which has a role in calcium signalling (Genescà et al., 2003) and was upregulated in Nf1Myf5 mice (Fig. 4.25D). Nfat proteins positively regulate their own gene expression (Chuvpilo et al., 2002). *Nfat* gene expression was increased for all isoforms in Nf1Myf5 at P21 (Fig. 4.25D). As Nfat signalling has an essential role in early muscle differentiation (Messina et al., 2010), it was also analysed in muscle lysates of E18.5 mice. Nf1Myf5 mice showed upregulated gene expression of all *Nfat* isoforms, which was significant for $Nfat_{c1}$ and $Nfat_{c4}$ (both upregulated by around 1,6 fold; Fig. 4.25F). This points towards a common mechanism that could cause postnatal metabolic defects as well as prenatal differentiation defects. Nfat signalling is regulated by cJun (Ikeda et al., 2004) which was found to be stronger activated in Nf1Myf5 than in control mice. The transcription factor Creb was also activated in Nf1Myf5. Creb regulates the transcription of mitochondrial genes like *12S-RNA* (De Rasmo et al., 2009) and nuclear genes like *Mc2-R*. These genes were significantly upregulated in Nf1Myf5 (Fig. 4.25D). Mc2-R is an adrenocorticotropic hormone receptor normally very weakly expressed in skeletal muscle. Its ligand is a potent lipolytic hormone (Xue et al., 1998). Mc2-R might additionally magnify the effect of increased fatty acid oxidation in muscle tissue of Nf1Myf5 (see section 4.4.1.3). Creb is also the transcription factor of *Pgc-1*. Pgc-1 is a metabolic regulator that stimulates mitochondrial oxidative metabolism and fibre type switching towards slow twitch fibres (Puigserver and Spiegelman, 2003), which could be observed in Nf1Myf5 mice (see section 4.4.1.2 and 4.4.1.1). *Pcg-1* gene expression was significantly increased in Nf1Myf5 by twofold (Fig. 4.25D). The gene product Pcg-1 interacts with the nuclear receptor Ppar g. Both cooperate in transcriptional control of nuclear genes encoding mitochondrial fatty acid oxidation enzymes (Vega et al., 2000). Among others, Ppar g is a transcription factor for *Fabp4* (fatty acid binding protein 4; see Fig. 4.24B). *Ppar g* expression itself was significantly upregulated in Nf1Myf5 by more than threefold (Fig. 4.25D). Taken together, *Nfat*, *Pcg-1* and *Ppar g*, which are transcriptional targets of the Ras downstream pathways Akt, Mek/Erk and Nfat, are strong candidates responsible for the developmental and metabolic phenotype of Nf1Myf5.

4.4.3 *Nf1* depletion in osteocytes leads to defects similar to *Nf1* depletion in muscles: Evidence for a pleiotropic effect

Neurofibromatosis I patients suffer from muscular defects (Stevenson et al., 2005; Souza et al., 2009; Stevenson et al., 2012; North, 1998). Additionally, skeletal defects are reported in approximately 50 % of patients including low bone mass, mineralisation defects and long bone bowing (Stevenson et al., 2006). Disorders with musculoskeletal symptoms often have pleiotropic causes (Karasik and Kiel, 2008). It means that deregulation of one molecular factor causes muscle and bone defects at the same time. In the Nf1Myf5 model *Nf1* is exclusively deleted in skeletal muscle cells. It is therefore not suitable for studying effects of *Nf1* knockout in bone. Another *Nf1* knockout model is the Nf1Prx1 mouse. In this model *Nf1* is deleted, among others, in bone cells. The Nf1Prx1 mouse recapitulates skeletal symptoms of Neurofibromatosis I patients (Kolanczyk et al., 2007).

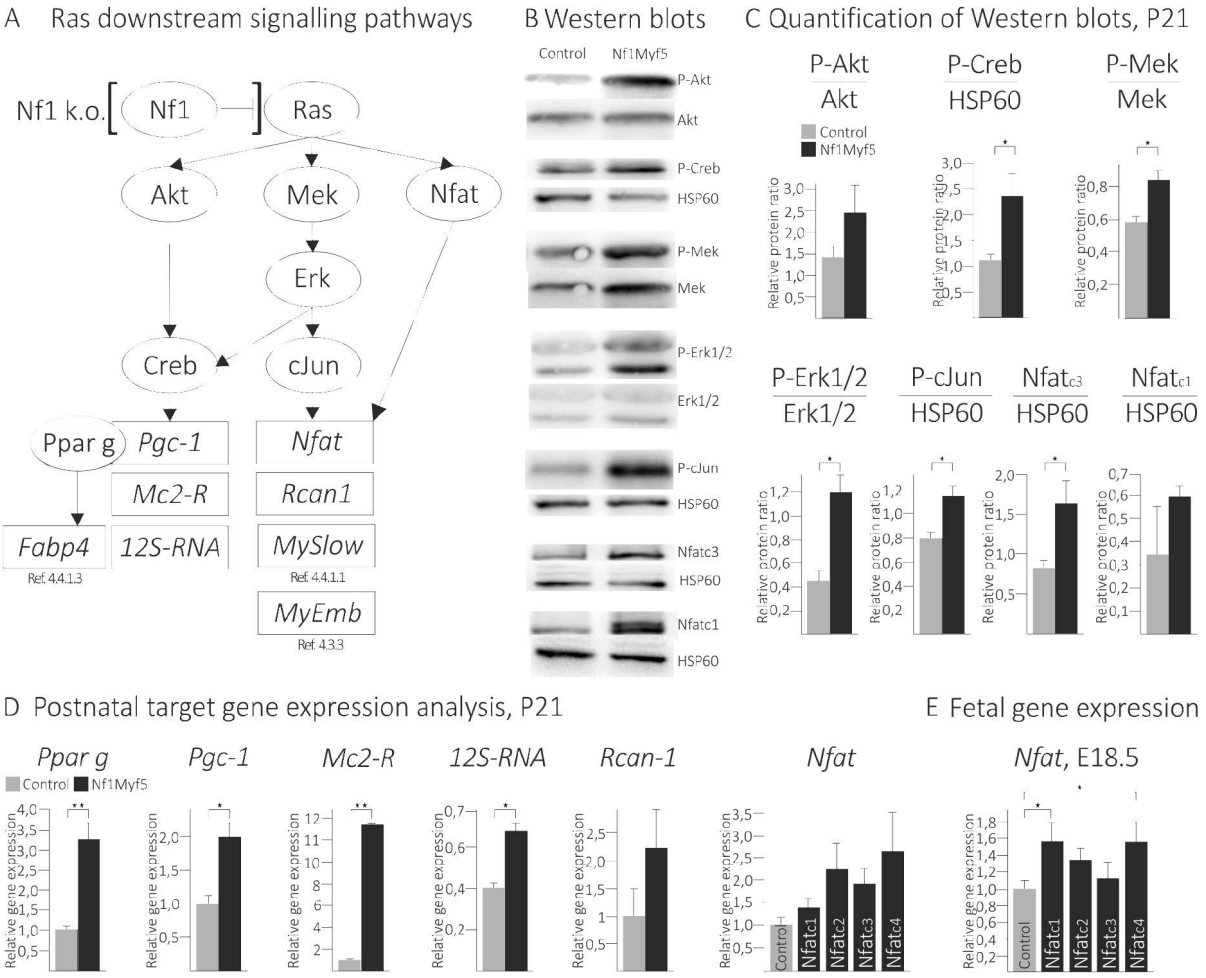

Figure 4.25 Nf1Myf5 mice show an increased activation of the Akt, Mek/Erk and Nfat pathways in muscle
A Scheme showing Ras downstream pathways that were activated in muscle tissue of Nf1Myf5. Ellipses marking pathway protein components. Rectangles marking pathway target genes. **B** Western blot analysis on whole muscle protein lysates from control and Nf1Myf5 mice. Images showing specific antibody-detected western blot signals with reference proteins below specific bands. **C** Diagrams show quantification of western blot results performed on whole muscle lysates: Relative protein level of activated pathway components in reference to not activated proteins. Nf1Myf5 (n = 4) showed an increase in the activated Ras downstream signalling proteins in comparison to control (n = 3) mice at P21. P-Creb/HSP60: p = 0,043. P-Mek/Mek: p = 0,029. P-Erk1/2/Erk1/2: p = 0,047, P-cJun/HSP60: p = 0,032, $Nfat_{c3}$/HSP60: p = 0,049. **D** Quantification of gene expression analysis at P21 performed on whole muscle lysates. Nf1Myf5 (n = 4) show a significant increase in expression of target genes of Ras signalling in comparison to control (n = 3) mice: *Pgc-1* (p = 0,047) and its interaction partner *Ppar g* (p = 0,01), *Mc2-R* (p = 0,00007), *12S-RNA* (p = 0,016) and *Rcan1*. Expression of Nfat proteins is also increased indicating a positive self regulation of Nfat signalling. **E** Quantification of gene expression analysis at embryonic day E18.5 performed on whole muscle lysates. Expression of *Nfat* was increased significantly for $Nfat_{c1}$ (p = 0,022) and $Nfat_{c4}$ (p = 0,031) in Nf1Myf5 (n = 3) in comparison to control (n = 3). Pcg-1 = peroxisome proliferator-activated receptor gamma coactivator 1, Ppar g = peroxisome proliferator-activated receptor gamma, Mc2-R = melanocortin receptor 2, Rcan1 = regulator of calcineurin 1, Nfat = nuclear factor of activated T-cells.

It seems likely that in Nf1Myf5 mice the upregulation of Akt and Mek/Erk signalling leads to increased expression of *Pcg-1* and *Ppar g* (see Fig. 4.25). Pcg-1 and Ppar g are described as pleiotropic factors that can cause muscle and bone defects (Abreu et al., 2012; Karasik and Kiel, 2010). On the other hand, Nfat signalling is increased in Nf1Myf5 muscles (see Fig. 4.25). Nfat is

also a regulator of bone mass (Winslow et al., 2006). Therefore the expression of *Nfat*, *Pcg-1* and *Ppar g* was investigated in bones of Nf1Prx1.

Cortical bone of tibiae was investigated in Nf1Prx1 since tibiae are affected in many Neurofibromatosis I patients (Stevenson et al., 2006). Bone is a multi cellular tissue. Mineralisation defects refer to cortical bone and cells of cortical bone are osteocytes. To prevent false results, adjacent cell populations had to be excluded in the experiment. Therefore, osteocytes had to be enriched. Tibiae were isolated from mice at P21. Joints, bone marrow and periosteum were removed and a collagenase digest was applied to bone. With this procedure superficial cell populations could be removed. The process of digestion was monitored via gene expression analysis (Fig 4.26A). Relative expression of cell population marker gene was measured before collagenase digest, after 30 min of digest and after 60 min of digest. Cell marker expression of peripheral chondrocytes (*Col II*) and endothelial cells (*Vegfr*) decreased over time. *Vegfr* expression decreased very mildly which was supposed to be no issue as endothelial cells are not affected by *Nf1* knockout in Nf1Prx1 mice. Gene expression of early (*Runx2*) and active osteoblasts markers (*Akp2*) decreased as well whereby the expression of osteocyte marker genes (*E11* and *Sost*) increased over time showing an enrichment of osteocytes.

Tibiae of control and Nf1Prx1 were prepared by 60 min collagenase digest and RNA was isolated. Quantitative RT-PCR revealed a significant increase of *Pgc-1* and *Ppar g* expression in Nf1Prx1 by fourfold and fivefold, respectively (Fig. 4.26B). Pgc-1 is a metabolic regulator that stimulates mitochondrial oxidative metabolism (Puigserver and Spiegelman, 2003). RNA microarray expression analysis showed that mitochondrial components of respiration chain were actually upregulated in Nf1Prx1 osteocytes like in Nf1Myf5 muscle, e.g. succinate dehydrogenase *Sdh* and NADH dehydrogenase *Nd* (Fig. 4.26C). Like in Nf1Myf5 *m-Cs* (mitochondrial citrate synthase) and enzymes of fatty acid beta oxidation were upregulated in Nf1Prx1. Glycolytic enzyme expression is decreased and the glycogen synthesis enzyme *Gsk3b* is upregulated like in Nf1Myf5 (Fig. 4.26C). Furthermore, RNA microarray results were analysed for Nfat signalling. *Nfat* transcription was upregulated between 1,25 fold and 1,7 fold in Nf1Prx1 mutants (Fig. 4.26C) similar to its upregulation in Nf1Myf5 muscles (see Fig. 4.25D).

Ppar g upregulation in cortical bone leads to death of osteocytes (Mieczkowska et al., 2012) which can cause mineralization defects (Knothe Tate et al., 2004) like seen in Neurofibromatosis I patients. Osteocyte cell morphology was investigated using electron microscopy on cross sections of tibiae bone of control and Nf1Prx1 mice. Osteocytes lay in wholes called lacunae embedded in extracellular matrix (Fig. 4.26D). Cell morphological characteristics were investigated and cells classified according to their developmental stage. Three main stages could be distinguished: immature, mature (resorptive) and dying (degenerative) osteocytes. Dead osteocytes could also be observed with only cell debris or nothing (empty) left in lacunae. Quantification of cells showed nearly a doubling of degenerative osteocytes in Nf1Prx1 (38 % of all osteocytes) compared to controls (20 % of all osteocytes). Also increased was the amount of lacunae with cell debris (mutants 12 %, controls 7 %). On the other hand the percentage of resorptive osteocytes was decreased in Nf1Prx1 mice (48 %) compared to controls (67 %) (Fig. 4.26E). The severe shift towards dying or death osteocytes in Nf1Prx1 may account for the *Nf1* associated bone mineralization defects.

Pcg-1, Nfat and Ppar g are possible pleiotropic factors in *Nf1* depleted muscles and bone. These factors can account for muscular symptoms as well as for bone defects in *Nf1* knockout mice.

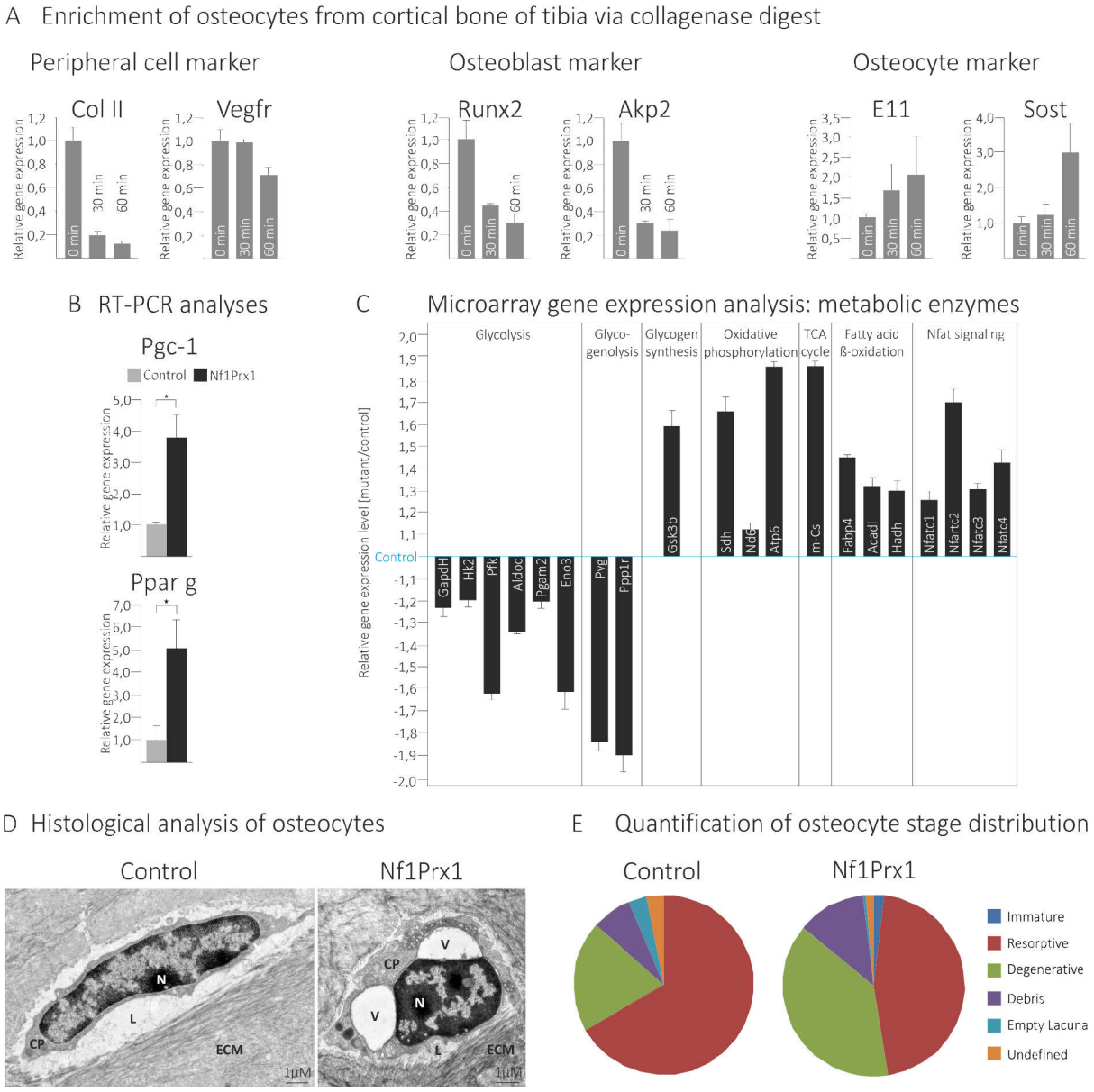

Figure 4.26 A possible pleiotropic effect in *Nf1* depleted osteocytes of Nf1Prx1 mice

A Quantitative RT-PCR analysis on gene marker before and after collagenase digest of isolated tibiae of control bone at P21. Diagrams showing a decrease of peripheral cell markers with time of digest (*Col II* for chondrocytes and *Vegfr* for endothelial cells) as well as osteoblast markers (*Runx2* for differentiating osteoblasts and *Akp2* for active osteoblasts). However, relative osteocyte marker (*E11* and *Sost*) expression increased with time of digest. **B** Quantification of gene expression in enriched osteocytes (60 min collagenase digest of tibiae) at P21. Nf1Prx1 mice (n = 4) showed a significant increase in gene expression of *Pcg-1* (p = 0,016) and *Ppar g* (p = 0,046) in comparison to controls (n = 4). **C** Microarray gene expression analysis on enriched osteocytes (60 min collagenase digest of tibiae) at P21 reveals differentially expression profiles of metabolic marker enzymes in Nf1Prx1 (n = 5) in comparison to controls (n = 5). Enzymes of glycolysis were downregulated in Nf1Prx1 mice as well as *Pyg*, an enzyme of glycogenolysis. On the other hand, enzymes of oxidative phosphorylation, the TCA cycle and fatty acid beta oxidation were upregulated in Nf1Prx1. As in Nf1Myf5 muscle tissue, *Nfat* expression is upregulated in Nf1Prx1 osteocytes. **D** Electron microscopy images of cross sections of tibiae of control and Nf1Prx1 mice at P21. Images show osteocytes of cortical bone. In control tibiae mainly resorptive (mature) osteocytes could be found. As displayed in the image they showed a long elliptic shape, a big nucleus with a big portion of euchromatin (light areas) in comparison to heterochromatin (dark areas). Resorptive osteocytes are surrounded by a wide, well-defined lacuna. Nf1Prx1 tibiae showed an increased number of osteocytes with degenerative characteristics: the typical long elliptic shape is lost, most of the chromatin in the nucleus is condensed (dark areas) and big cytoplasmic vacuoles can be seen. The lacuna is smaller and partly filled with

bone and cell breakdown products. **E** Quantification of relative osteocyte numbers belonging to each developmental stage of control (n = 3) and Nf1Prx1 mice (n = 3) at P21. The main difference was the increased portion of degenerative osteocytes (38 %) and decreased portion of resorptive osteocytes (46 %) in Nf1Prx1 mice in comparison to control animals (20 % and 67 %, respectively). CP = cytoplasm, L = lacuna, N = nucleus, ECM = extracellular matrix, V = cytoplasmic vacuole, Col II = Collagen II; Vegfr = vascular endothelial growth factor, Runx2 = runt-related transcription factor 2, Akp2 = alkaline phosphatase 2, E11 = podoplanin, Sost = sclerostin, Pcg-1 = peroxisome proliferator-activated receptor gamma coactivator 1, Ppar g = peroxisome proliferator-activated receptor gamma, Gapdh = glyceraldehyde 3-phosphate dehydrogenase, Hk2 = hexokinase 2, Pfk = phosphofructokinase, Aldoc = aldolase c, Pgam2 = phosphoglycerate mutase 2, Eno3 = beta-enolase, Pyg = glycogen phosphorylase, Ppp1r = glycogen-associated regulatory subunit of protein phosphatase, Gsk3b = glycogen synthase kinase 3 beta, Sdh = succinate dehydrogenase, Nd6 = NADH dehydrogenase 6, Atp6 = ATP synthase 6, Cs = citrate synthase, Fabp4 = fatty acid binding protein 4, Acadl = acyl-CoA dehydrogenase, long chain, Hadh = hydroxyacyl-CoA dehydrogenase, Nfat = nuclear factor of activated T-cells.

Conclusions

Nf1Myf5 mice showed an upregulation of slow and oxidative myofibre characteristics at P21. On the other hand, fast and glycolytic fibre markers were downregulated. This shift was accompanied by increased Ras signalling seen by an over-activation of its downstream components Akt, Mek/Erk and Nfat and their gene targets *Pcg-1*, *Ppar g* and *Nfat*. The expression of these factors was also found to be upregulated in *Nf1* depleted osteocytes of the Nf1Prx1 model. Pcg-1, Nfat and Ppar g are candidate pleiotropy factors that could account for metabolic and differentiation defects in muscles and also for bone mineralization defects. It could be shown that a deletion of *Nf1* can cause deregulation of the same factors in muscle and skeleton.

5. Discussion

5.1 Generation of knockout mice for a muscle cell specific loss of *Nf1*

5.1.1 Distinction of muscle specific models to the Nf1Prx1 model

It was the aim of this work to generate a suitable mouse model for investigation of the muscle cell endogenous role of *Nf1*. Therefore a conditional knockout approach using the Cre/lox system (Lobe and Nagy, 1998) was chosen. Previous studies on the conditional Nf1Prx1 model in our laboratory showed that a loss of *Nf1* causes a fibrosis associated myopathy primarily caused by a patterning and differentiation defect of early embryonic myoblasts (Kossler et al., 2011). However, this model was not suitable to study the muscle cell endogenous role of *Nf1* as the knockout concerns several different cell populations originating from embryonic mesenchymal cells (Kolanczyk et al., 2007). This includes, among muscle cells, osteocytes, chondrocytes, stromal cells, tenocytes and fibroblasts (Andrades et al., 2011). Correct muscle development strongly depends on proper function of bone and tendon cells (Schweitzer et al., 2010), which are affected by loss of *Nf1*. Also, fibroblasts of muscle connective tissue strongly interact with muscle cells during development and homeostasis (Kardon et al., 2002, Murphy et al., 2011). In the Nf1Prx1 model it has been shown that the Ras downstream component Mek is over-activated in muscle connective tissue, but not in muscle cells themselves (Kossler et al., 2011). This increased signalling might affect muscle development, e.g. by altered secretion of signalling molecules or matrix components. Possible consequences cannot be distinguished from muscle cell endogenous effects in Nf1Prx1. It concerns, for example, the muscle patterning defect seen in this model. Taking into account that such a severe patterning defect has not been described for NF1 patients (Stevenson et al., 2005), it is questionable whether Nf1Prx1 as a suitable model for NF1 associated muscular defects. Furthermore, studies performed so far left open questions concerning mechanistic consequences of prenatal deregulations on postnatal muscles. The adult muscle cells (myofibres and satellite cells) have not been characterized yet. Therefore, with this work gaps of knowledge should be filled. The endogenous role of *Nf1* in muscle cells should be determined by a structured approach investigating chronologically the four stages of muscular development: embryonic, fetal, perinatal and adult myogenesis.

5.1.2 Cell specificity of the investigated mouse models

Three muscle cell specific *Nf1* knockout models were generated using the Cre/lox system (Lobe and Nagy, 1998). They differ in the cell stage of initial *Nf1* knockout to get an idea of stage specific functions of *Nf1*. This was approached via crossing Nf1flox mice (Zhu et al., 2001) with one of the three well established deleter lines Lbx1_Cre, Myf5_Cre and HSA_Cre, respectively.
In the Lbx1_Cre deleter line the *Cre* gene is inserted into the genome as a transgene at an unknown position. Mice hemizygous for this transgene are phenotypically normal. Recombinase activity is seen in migrating embryonic muscle progenitors that generate hypaxial muscles of the limbs, tongue, and diaphragm (Vasyutina et al., 2007). Lbx1 also plays a role in neuronal determination processes

and its involvement in cardiogenesis has been postulated (Schmitteckert et al., 2011). The Lbx1_Cre deleter line used in this work, however, is designed to only target muscle progenitor cells (Vasyutina et al., 2007). Myf5_Cre mice express Cre recombinase from the endogenous Myf5 locus. The *Cre* gene is inserted in one of the *Myf5* alleles deleting it at the same time (Tallquist et al., 2000). Mice heterozygous for this *Cre* "knockin" do not display any abnormalities. When crossed with a strain containing a loxP site flanked sequence of interest Cre-mediated recombination results in tissue specific deletion of the target, primarily in skeletal muscle cells. Myf5 is essential for the specification of myogenic cell fate that act upstream of the terminal differentiation program of myoblasts (Buchberger et al., 2003). Furthermore Myf5_Cre activity is described for dermis, adipose tissue, skeletal elements of thorax (ribs, vertebrae) and neuronal cells (Tallquist et al., 2000). Still, Myf5_Cre was considered to be a suitable deleter line as a direct external influence on limb muscles development could be excluded via mTmG reporter mouse analysis. The genomic HSA_Cre locus is a transgene inserted into the mouse genome. Mice hemizygous for this transgene do not display any abnormalities. These transgenic mice have the Cre gene driven by the human alpha-skeletal actin (HSA or ACTA1) promoter. Cre activity is restricted to adult striated muscle fibres and embryonic striated muscle cells of the somites and heart (Miniou et al., 1999).
To proof Cre recombinase specificity for each knockout mouse line Nf1Lbx1, Nf1Myf5 and Nf1HSA specific mTmG reporter mouse lines were generated. These mice express special fluorescent proteins in cells with Cre activity. Of particular interest was Cre expression in muscle cells of the limbs, muscle connective tissue and in the neurons associated with the muscular system. Skeletal muscle development and function strongly depends on its interaction with the neuronal system. A failure in stimuli processing or forwarding by a putative loss of *Nf1* could cause developmental defects. For all models it was shown that skeletal muscle cells at E18.5 have been targeted completely by Cre recombinase. Adjacent tissue like muscle connective tissue, bone, skin and cartilage have not been targeted. In spinal cord and cerebral motor cortex no recombinase activity of Lbx1_Cre, Myf5_Cre or HSA_Cre was found. Dorsal root ganglia showed no activity of Lbx1_Cre and HSA_Cre. However, Myf5_Cre recombinase activity was seen in 1 % to 10 % of dorsal root ganglia cells. Dorsal root ganglia mainly consist of sensory nerve cell bodies. These nerve cells innervate for example limb musculature. But as nerve cells in limbs did not show Myf5_Cre activity, Cre positive cells might be neurons not innervating investigated limb areas or might be satellite glial cells. A loss of *Nf1* in satellite glial cells is associated with tumour formation (Rizvi et al., 2002) but tumours could not be seen in Nf1Myf5 mice.

5.1.3 Critical evaluation of investigated mouse models

The Lbx1_Cre and HSA_Cre alleles are transgenes which do not interfere with internal expression of Lbx1 or Acta1, respectively. Myf5_Cre is a knockin construct deleting the function of the endogenous Myf5 gene. All Nf1Myf5 mutants are heterozygous for the Myf5_Cre knockin allele. Still, Nf1Myf5 mice were considered to be suitable for investigation as no effect of haploinsufficiency of the *Myf5* allele has been reported. Furthermore, Myf5_Cre heterozygous control animals did not show any phenotypic aberrations. However, it has been reported that postnatal *Myf5* heterozygous muscle stem cells are more primed for myogenic commitment and have higher self-renewal capacity compared with wild-type muscle stem cells (Gayraud-Morel et al., 2012). Nf1Myf5 mice did not show these defects. Additionally, Nf1Myf5 mice did not show a down-

regulation of *Myf5* gene expression at day E18.5 and P21 (seen by quantitative RT-PCR analysis). Therefore, all defects of Nf1Myf5 mice were attributed to the loss of *Nf1*.
Cre efficiency was also tested in the mouse models themselves. Nf1Lbx1, Nf1Myf5 and Nf1HSA showed recombinase efficiency of approximately 50 % in muscle tissue at E18.5. Regarding the fact that a muscle also consists of connective tissue, neuronal and endothelial cells, the recombination rates were considered to be sufficient.
The advantage of the used mouse models is the muscle cell specificity which allows studying the consequences of *Nf1* knockout *in vivo* independent from effects of *Nf1* deletion in other cell populations, like fibroblasts or neurons. Of course, this bears the limitation that it recapitulates only a part of the situation in NF1 patients. In patients multiple organs are affected by a depletion of *NF1* (Holt, 1987). A second advantage of the *Nf1* knockout models used here is the early embryonic time point of *Nf1* knockout. Myotome differentiation takes place at day E9.5 until E10.5 dpc in mouse. The migration of muscle precursors into the limb occurs at E10.5. During migration Lbx1 expression is initiated. This should be the initial time point of *Nf1* knockout in the Nf1Lbx1 model. The first hypaxial differentiation process takes place at day E11.5: precursor cells differentiate to myoblasts which express Myf5. This is the initial time point of *Nf1* knockout in limb muscles of Nf1Myf5 (Laclef et al., 2003). Some pre-fusion myoblasts at E11.5 and E12.5 display the first immature myofibrils. After fusion of myoblasts to myotubes at E13.5 and E14.5 all resulting myotubes show myofibrils (Fürst et al., 1989). Myofibrils mark the initial time point of *Nf1* knockout in Nf1HSA.
With the Nf1Lbx1 model it is possible to study effects of *Nf1* loss from an early differentiation stage on. The knockout efficiency is the highest as all limb muscle precursor cells are affected. However, Nf1Lbx1 mice die after birth due to the inability of food intake (probably due to consequences of *Nf1* knockout in swallowing muscles) which makes it impossible to study postnatal development. In the fetus the Nf1Lbx1 phenotype is overlapping to the Nf1Myf5 phenotype. Nf1Myf5 animals show a smaller knockout efficiency as not all precursor cells express Myf5 (Günther et al., 2013). The advantage of Nf1Myf5 is their viability until P170 in the adult stage and the formation of a significant muscle phenotype. Nf1HSA mice have a normal viability and do not show a detectable phenotype although *Nf1* expression is significantly decreased in Nf1HSA muscles (shown by RT-qPCR at P21). Taken together, the Nf1Myf5 model is most suited for an extensive phenotype analysis. Nf1Lbx1 and Nf1HSA were used to confirm results and a more exactly distinction of cellular and molecular causes.

5.2 Loss of *Nf1* results in a growth defect of skeletal muscles

5.2.1 Embryonic muscles do not show a growth defect at E14.5

First *in vivo* studies on the role of *Nf1* on muscle development have been performed on the Nf1Prx1 model. In Nf1Prx1 mice *Nf1* is deleted in embryonic mesenchymal cells resulting in a severe myopathy phenotype. It is primarily caused by muscle patterning defects and a differentiation defect of early embryonic myoblasts. Isolated myoblasts from Nf1Prx1 show a reduced fusion rate in cell culture (Kossler et al., 2011). Isolated embryonic myoblasts of Nf1Lbx1, however, do not show a fusion defect. Furthermore, Nf1Myf5 embryos did not show a muscle patterning or growth defect at

E14.5. A not significant increase is detectable in muscle sizes of Nf1Myf5 and fusion rates of Nf1Lbx1 in comparison to controls. Investigation of older Nf1Lbx1, Nf1Myf5 and Nf1HSA mice additionally showed that the location, shape and identity of all limb muscles were not altered by loss of *Nf1*. Contrary to the deletion in mesenchymal cells (Nf1Prx1), a muscle cell specific *Nf1* knockout does not affect embryonic myogenesis. It is possible that patterning defects were due to *Nf1* knockout in other tissues, probably muscle connective tissue as it is critical for muscle formation (Kardon et al., 2002). *Nf1* seems to have no essential role in embryonic muscle precursor cells. Only a mild, not significant growth promoting effect was detectable.

5.2.2 Fetal muscles show first signs of growth retardation at E18.5

First signs of Nf1 associated muscle size reduction could be found in the fetal stage of development. Nf1Lbx1 and Nf1Myf5 showed a slight reduction of triceps cross sectional area and a significant reduction of myotube diameters. Myotubes are the predecessors of myofibres and grow by fusion with myoblasts (myonuclear accretion). Nf1Lbx1 and NfMyf5 show a significant increase in myotubes with central nuclei. This is a sign for delayed growth and differentiation processes. Nf1Lbx1 and Nf1Myf5 mice showed a strong overlap in their muscle phenotype suggesting a role for *Nf1* in myoblasts. Nf1HSA mice did not show any significant alterations of muscle parameters at E18.5 suggesting that *Nf1* knockout in myotubes does not influence muscle growth at this stage.

5.2.3 Postnatal muscles of Nf1Myf5 show a growth reduction at P21

Nf1Lbx1 mice were not viable. Therefore, only Nf1Myf5 and Nf1HSA were investigated postnatally. Nf1HSA, however, did not show muscle defects at this stage. Nf1Myf5 mutants showed a significant decrease in muscular cross sectional area at P21 as observed in paediatric neurofibromatosis I patients (Stevenson et al., 2005). This size reduction is starting at the fetal stage and progressing until the adult stage of development. But the main effect could be seen during the so called perinatal stage of myogenesis. At E18.5 the size difference is virtually undetectable between Nf1Myf5 and control in the TB (92 % of the normal size) and mild, but significant, in the TA (73 % of the normal size). By P21 the TB and the TA are only 60.5 % and 51.3 % their normal sizes and at P156 the sizes of the TB and TA have decreased further to 50.9 % and 43.1 % of the normal size seen in control littermates. Furthermore, Nf1Myf5 animals seemed healthy and did not show any signs of weakness or limitations in muscle mobility at P21.
This size reduction is due to a size reduction of myofibres and not in the number of myofibres. In contrary, Nf1Prx1 mice showed a reduction of myofibre numbers by 30 to 40 % (Kossler et al., 2011). This also might to be due to aberrant signalling from adjacent tissues, like connective tissue. *Nf1* in muscle cells does not seem to have a role in the basic myotube and myofibre formation process.

5.2.4 Adult muscles of Nf1Myf5 show a progressive size reduction

Nf1HSA mice did not show a muscle defect in the perinatal stage. Furthermore adult Nf1HSA animals had a normal phenotypical appearance at P156; therefore only Nf1Myf5 animals were investigated in the adult stage. The phenotype of Nf1Myf5 in the adult stage recapitulates the phenotype in the perinatal stage. The effects were even more pronounced. The relative muscle size and myofibre size decreased further in comparison to animals at P21. Furthermore, Nf1Myf5 animals now displayed signs of weakness, exhaustion and limitations in movement of undetermined origin. So, the phenotype seen at P21 is not only a delay in development as it lasts and progresses until P156 in the adult stage of development.

5.2.5 The size reduction in Nf1Myf5 is due to a fibre size reduction

Since the fibre number in all analysed muscles was essentially unaltered in the Nf1Myf5 mutants at P21, the muscle size reduction can be attributed to the decrease in myofibre size. Only the fast twitch fibres seem to be affected by size reduction in Nf1Myf5 at P21 since no significant size reduction was detectable in slow twitch fibres at this stage. A main reason seems to be the reduction of the myonuclear domain, i.e. mutant myofibres produce less protein than controls. The difference between the fibre types might be due to differential transcriptional control of fibre type specific protein synthesis. It has been reported that the expression of the slow myosin gene *Myh7* and the fast, oxidative myosin gene *Myh2* is stimulated by $Nfat_{c3}$ (Allen et al., 2001; Delling et al., 2000). Nf1Myf5 mutants show a significant increase in the $Nfat_{c3}$ protein at P21 which could explain the upregulation of *Myh7* and *Myh2* also seen in these animals. On the other hand, *Myh4*, which is expressed in fast, glycolytic fibres is regulated by different mechanisms (Allen et al., 2001).
Another cause for differential effects on different fibre types might be a secondary effect. Possibly all fibres are affected by a growth defect. But there might be compensatory effects in slow fibres, e.g. Akt or Nfat signalling induced hypertrophy (Lai et al., 2004; Hudson and Price, 2013). The Akt/mTOR signalling is a downstream pathway of Ras and has been shown to induce muscle hypertrophy without myonuclear accretion (Bodine et al., 2001) making it a good candidate to be affected by the loss of *Nf1*. Calcineurin/Nfat signalling has also been implicated in slow twitch fibre specific hypertrophy (Hudson and Price, 2013).
If hypertrophic pathways were indeed upregulated in the slow twitch fibres of Nf1Myf5 mutants this should be noticeable in an increased myonuclear domain in comparison to fast twitch fibres. The myonuclear domain describes the cytoplasmic volume per myonucleus. The existence of a threshold at which no further hypertrophy can occur without the accretion of new myonuclei has been postulated (Van der Meer et al. 2011). It means that the slow twitch fibres would not be able to undergo hypertrophic processes without limitations. At some point they would reach their maximum size (White et al., 2010). From that point on their relative size would decrease as seen in fast twitch fibres. A significant size decrease of the slow twitch fibres in Nf1Myf5 mutants should be detectable in the adult stage at P156. This has not been investigated yet. A hint to a possible size decrease is the significant reduction of the mean fibre diameter in soleus of Nf1Myf5 at P156. The majority of soleus fibres are slow twitch fibres. The myonuclear domain of slow twitch fibres needs to be determined as well, because another hypothesis is an increased fusion of $Pax7^+$ cells with slow, but not fast twitch fibres. It has been described that $Pax7^+$ cell numbers can be influenced by the fibre

that they are attached to, with more cells being associated with fibres that are predominantly oxidative (slow, type I fibres) than with fibres that rely primarily on glycolysis (fast, type IIb fibres; Christov et al., 2007; Manzano et al., 2011). In Nf1Myf5 mutants there might be a facilitated fusion mechanism for slow twitch $Pax7^+$ cells.
In summary, it seems apparent that *Nf1* and putative downstream (Ras) pathways have a different role in different myofibre types.

5.2.6 Postnatal Nf1HSA mice do not show a muscle size reduction

The effect of size reduction can be seen initially in the fetal stage of development in Nf1Lbx1 and Nf1Myf5 mice. Nf1HSA do not show a size reduction of muscles throughout development. This is surprising as the main reason for size reduction seems to be a decrease of myofibre protein synthesis (decrease in myonuclear domain). This leads to the hypothesis that only a loss of *Nf1* in precursor cells (as in Nf1Lbx1) or myoblasts (as in Nf1Myf5) is capable to cause growth defects in myofibres. A possible explanation would be the determination of the fibre growth program in myoblasts. This would be possible by long-term modifications of gene transcriptional activity. Long-term effects can be achieved by direct DNA modifications via nucleotide methylation or demethylation (Handy et al., 2011). If DNA is methylated it gets transcriptional inactive. DNA methylation is catalysed by DNA methyltransferases (Dnmt). The Ras/Mek/Erk pathway is described as the upstream activator of DNA methyltransferase I (Dnmt1; Molognoni et al., 2013). Furthermore, reactive oxygen species are described to activate Dnmts (Kowluru et al., 2013). High concentrations of reactive oxygen species are generated by a stimulated oxidative metabolism like seen in Nf1Myf5 mice. If Dnmt1 is over-activated in myoblasts of Nf1Lbx1 and Nf1Myf5 it might permanently down-regulate genes that initiate muscle protein synthesis or myofibre protein genes themselves. When myoblasts fuse to myofibres, these genes would not be transcribed and myofibres develop a defect of hypertrophic growth. However, it seems to be a balanced effect as animals do not have movement problems and no structural aberration could be found in myofibres via electron microscopy. In Nf1HSA myoblast do not carry the *Nf1* deletion. Therefore there is no putative over-activation of Dnmts. It has been shown that actively transcribed genes employ a defence mechanism against Dnmt1 mediated silencing (Di Ruscio et al., 2013). Thus, one can hypothesize that genes involved in myofibre protein synthesis would not be affected by Dnmt1 in growing myofibres, where those genes are actively transcribed. This would explain the normal size of myofibres in Nf1HSA although *Nf1* is deleted in these fibres. In myogenic progenitors, however, these genes are not active yet and could be subject to methylation and thus permanent silencing.

5.3 Loss of *Nf1* leads to defects in $Pax7^+$ cell development

During fetal and early postnatal development myotube growth is driven by myonuclear accretion. Therefore, the most likely cause for myotube size decrease in Nf1Myf5 mice would be an impaired myonuclear accretion. The main events involved in myonuclear accretion are emergence of new myoblasts from $Pax7^+$ progenitor cells, differentiation to fusion competent cells and the fusion with

existing myotubes. This does not only increase myotube size but also the number of nuclei in myotubes and consequently in myofibres. As postnatal myofibres in Nf1Myf5 do not show a significant decrease in nuclei number, it is possible that size decrease at E18.5 is caused by a delay in fusion with fetal myoblasts ($Pax7^+$). Another indication is the increased number of myotubes with central nuclei in Nf1Myf5 which is a sign for immature myotubes. Increased numbers of $Pax7^+$ cells in muscle of Nf1Myf5 at E18.5 also argue for a delay in fusion and development, respectively. However, surprisingly in postnatal Nf1Myf5 mice $Pax7^+$ cell numbers were significantly decreased in comparison to control animals. Such a tremendous depletion of the $Pax7^+$ cell pool cannot only be explained by delayed development. Muscles of Nf1Myf5 at E18.5 also show increased gene expression of the proliferation marker Cyclin D1. Muscle cells undergoing proliferation at this stage are $Pax7^+$ cells meaning the $Pax7^+$ proliferation rate seems to be increased. At the same time expression of MyoD, an early myoblast marker, is significantly decreased in Nf1Myf5 and the expression of Myog and Maz, markers of terminally differentiated myoblasts, is upregulated. This indicates a disturbed balance between early and late myoblasts and increased differentiation rate of $Pax7^+$ myoblasts. Once terminally differentiated $Pax7^+$ cells cannot contribute to the pool of residual postnatal stem cells (satellite cells) as they would do normally (Yablonka-Reuveni, 2011).

The exact mechanism regulating the balance between proliferation and differentiation of muscle progenitors is not very well understood. During fetal development two co-existing populations of resident muscle progenitors have been identified: a slow-cycling $Pax7^+/Myf5^-$ population and a fast-cycling $Pax7^+/Myf5^+$ population (Picard and Marcelle, 2013). The *Nf1* knockout would only concern the fast-cycling $Pax7^+/Myf5^+$ population in Nf1Myf5. $Pax7^+/Myf5^-$ satellite cells have never expressed Myf5 (Kuang et al., 2007). The resident $Pax7^+$ progenitors give rise to satellite cells in adults as they become gradually less proliferative during the course of development until reaching quiescence in adulthood. The heterogeneity remains among adult satellite cells showed by the existence of a fast- and a slow-cycling population upon activation of these cells (Ono et al., 2012). The proportion of $Pax7^+/Myf5^+$ cells (90 %) to $Pax7^+/Myf5^-$ cells (10 %) is about the same in adults (Kuang et al., 2007) as in fetuses (Picard and Marcelle, 2013). The $Pax7^+/Myf5^-$ satellite cells have been shown to both self-renew and give rise to $Pax7^+/Myf5^+$ cells through asymmetrical division. In accordance to these findings, it is believed that like in many self-renewing tissues in the adult, muscles maintain homeostasis through two cell populations: the less differentiated slow-cycling and the fast-cycling transit-amplifying population. Since both populations are present from the embryonic stage on, it is possible that growth is also regulated by them. Possibly the fast-cycling $Pax7^+/Myf5^+$ cells start dividing while becoming more differentiated through the expression of MyoD, thus creating a large population of myoblasts. The slow-cycling progenitors proliferate to self-renew and give rise to new fast-cycling muscle progenitors in order to maintain a steady pool of transit amplifying progenitor cells. The myoblasts produced by the differentiation of the fast-cycling cells can then terminally differentiate and fuse with the existing fibres.

The differentiation process of the transit amplifying $Pax7^+/Myf5^+$ cells that gives rise to myoblasts could be accelerated in the Nf1Myf5 mutants. This would diminish the size of the fast-cycling cell pool since these cells would differentiate faster than the slow-cycling cells can replenish them. As a result the total number of $Pax7^+$ cells would decline faster in the Nf1Myf5 mutants as they grow older.

The Ras pathway has been implicated in all three involved processes: proliferation, differentiation and fusion (Jones et al., 2005, Hindi et al., 2013). A well investigated pathway in $Pax7^+$ cells is the p38α/ß Mapk pathway downstream of Ras. It has been shown to activate satellite cells and induce them to differentiate (Jones et al., 2005). Aberrant Ras/Mapk signalling caused by the loss of *Nf1*

could increase the activation of p38α/ß Mapk and thereby accelerate the differentiation of the $Pax7^+/Myf5^+$ muscle progenitors. On the other hand, Sprouty1, an inhibitor of Ras signalling, has been shown to inhibit differentiation of satellite cells and induce their return to quiescence (Shea et al. 2010). This suggests that increased Ras activation leads to an upregulation of progenitor differentiation and interferes with maintenance of stemness. Interestingly, also the Calcineurin/Nfat, the MAPK (mitogen activated protein kinase) and the PI3K (phosphatidylinositol-3-OH kinase)/Akt pathways have been implicated in satellite cell proliferation. Igf I-stimulated satellite cell differentiation appears to be mediated through the PI3K/Akt pathway (Hawke and Garry, 2001). These pathways are candidates which were investigated in this work. They were found to be upregulated during perinatal development in Nf1Myf5.
The resemblance of the Nf1Myf5 myopathy to the muscular phenotype of Pax7 knockout mice ($Pax7^{-/-}$) should also be noted at this point. $Pax7^{-/-}$ mice have an unaltered perinatal myofibre number but the fibres are extremely reduced in size. They display a complete lack of satellite cells as the population of satellite cells is depleted due to cell cycle defects during postnatal growth (Seale et al., 2000; Zammit et al., 2006). The effects were milder in Nf1Myf5 mutants but still very similar to those in the $Pax7^{-/-}$ mutants thus suggesting that premature differentiation of the $Pax7^+/Myf5^+$ muscle progenitors in the Nf1Myf5 mutants could cause a net loss of $Pax7^+$ cells and thus generating a similar phenotype.

5.4 Loss of *Nf1* leads to metabolic muscle defects

5.4.1 Loss of *Nf1* results in an alteration of fibre specific gene expression

The fibre type composition was altered in all analysed muscles in Nf1Myf5 mice. All fast and mixed fibre type muscles seemed more "slow like" as the $MySlow^+$ cross sectional area was increased. The opposite was observed in the slow muscle soleus which seemed more "fast like" as, in contrast to the other muscles, the relative number of slow twitch fibres was reduced. The distinction between fast and slow muscles became less sharp in Nf1Myf5 mutants. This phenomenon could attribute to the reduced muscle force production reported in NF1 patients (Johnson et al., 2012; Stevenson et al., 2012). Fast muscles might lose their ability to produce strong contractions because of the size reduction of the fast twitch fibres. Slow muscles, like soleus, might be more prone to fatigue due to the loss of slow twitch fibres. Muscular endurance abilities of NF1 patients have not been tested yet, but exhaustion, fatigue and tiredness are among NF1 symptoms (North, 1998).
Fibre type conversion from fast to slow twitch could cause increased numbers of slow twitch fibres and thus aggravating the "slow like" phenotype of fast muscles. Molecular signalling via the Nfat transcription factors has been shown to repress fast related genes and enhance the expression of slow related genes (Rana et al., 2008; Mu et al., 2007). Nfat is dephosphorylated and activated by Calcineurin upon increase of cytosolic Ca^{2+} levels. A deletion of *Nf1* could cause an over-activation of Akt, a Ras downstream component. Akt signalling is capable of inducing Ca^{2+} channel trafficking to the plasma membrane and increasing Ca^{2+} uptake (Viard et al., 2004) which could further activate Nfat signalling. Since Ca^{2+} regulates many essential physiological functions like muscle contraction (Szent-Gyorgyi, 1975) further studies on Ca^{2+} signalling could provide useful information about the muscular phenotype present in the Nf1Myf5 mutants.

5.4.2 Loss of *Nf1* results in a shift towards mitochondrial oxidative metabolism

Due to its essential role in movement, insulating the internal organs, generating heat to maintain core body temperature and acting as a major energy storage depot, any impairment to skeletal muscle structure and function may lead to an increase in morbidity and mortality. Alterations in muscle metabolism are directly associated with numerous pathologies and disorders, including, diabetes, obesity, Pompe's disease, McArdle disease and numerous mitochondrial disorders (Angelini and Semplicini; 2010, Russell et al., 2014; Raben et al., 2012). On the other hand many skeletal muscle pathologies have secondary changes in metabolism, including cancer cachexia, sarcopenia (muscle weakness), age-related muscle wasting and muscular dystrophies (Ryall et al., 2008; Russell et al., 2014; Koopman et al., 2014). In Nf1Myf5 mice myofibre composition is changed which was a hint towards an altered muscle metabolism. The investigation of muscle tissue showed that marker genes for main metabolic pathways were differentially regulated in Nf1Myf5 mutants. The generation of ATP used for muscle movement predominantly occurs in the mitochondria via oxidative phosphorylation (OXPHOS) or in the cytoplasm via glycolysis (Ryall, 2013). Different myofibre types have different preferential ways of ATP generation according to their specific function. In Nf1Myf5 mice a significant upregulation was detected for genes involved in mitochondrial OXPHOS and citric acid cycle. OXPHOS rates were increased in Nf1Myf5 as shown by elevated Sdh activity. Furthermore, fatty acid beta oxidation enzymes were upregulated and myofibrillar lipid storages as well as muscle adjacent adipose tissue were not detectable. These findings point towards a switch in usage of catabolic pathways in Nf1Myf5 muscles. As metabolism is essential for muscular performance, a switch in metabolism can cause a myopathy (Cruz Guzmán et al., 2012). Metabolic myopathies are genetic defects that interfere with the energy generating processes in skeletal muscles. When these defects interfere with muscle function and energy production, muscle cells cannot work properly. Metabolic myopathies can cause progressive muscle weakness, fatigue, episodes of pain and cramps after exercise and breakdown of muscle tissue. As neurofibromatosis I (NF1) patients suffer from symptoms of myopathy of unknown causes it might be possible that metabolic changes also affect patients. However, most described metabolic myopathies are characterised by defects in mitochondrial function (Berardo et al., 2010) and not an increase in OXPHOS activity. The Nf1Myf5 mouse would be the first model to describe negative long term consequences of increased oxidative metabolism in the context of a myopathy.

Recently, alterations in metabolism were described in a mouse model with a conditional *Nf1* deletion under control of the endogenous MyoD promoter (Nf1MyoD). Controversial to the results presented here, these mice did not show increased OXPHOS activity at day P2 (Sullivan et al., 2014). Assuming a progressive phenotype, effects might not be obvious at the age of P2. Again contrary to Nf1Myf5 mice, Nf1MyoD mutants showed a severe increase in myofibrillar lipid storages. However, detection of lipids was performed on histological sections via bright field overview microscopy that showed signals obviously larger than size of intracellular lipid storages causing doubts in origin of detected lipids. Furthermore the MyoD_Cre mouse line used in this study shows recombinase activity in the liver (Chen et al., 2005), a fact that was neglected by the authors. As liver plays a key role in body lipid metabolism (Nguyen et al., 2008) this might be a confounding effect and thus the Nf1MyoD line appears not suitable for studying lipid metabolism.

Concerning the Nf1Myf5 mouse, it is not entirely clear whether all types of myofibres undergo, in some degree, a switch towards oxidative metabolism or if a relative increase in slow oxidative and fast oxidative fibre portion causes the increase in mitochondrial enzymes. But independent from the cause, the effect is a severe change in muscular energy conversion. Differential metabolic pathway

usage could lead to aberrant accumulation of intermediates in muscle, i.e. reactive oxygen species, which can cause severe cell damage. Accumulated or depleted intermediates could be used as a disease marker in NF1 patients. An absent increase of blood lactate to pyruvate ratio during exercise would be an indicator for an insufficient switch to anaerobic metabolism (Wasserman et al., 1985). The elevated level of activated AMP-activated protein kinase α (Ampk) in muscles of Nf1Myf5 suggests an energy deficiency (elevated AMP to ATP ratio) despite of increased OXPHOS activity. The deficiency could be caused by an induction of uncoupling proteins by Ras (Porras et al., 1996) or an ATP wastage, for example by an increased ATP-dependent transport of Ca^{2+}, as Ras signalling has been linked to Ca^{2+} signalling (Pierro et al., 2014). ATP-dependent transport of Ca^{2+} in muscle is regulated by Sarcolipin, which is described to play a role in thermogenesis by promoting the uncoupling of SERCA (sarcoplasmic reticulum Ca^{2+}-ATPase) ATP hydrolysis activity from its Ca^{2+} transport function (Sahoo et al., 2013). Sarcolipin expression is upregulated in muscles (Kossler et al., 2011) and osteocytes of Nf1Prx1 mice (microarray data not shown) and should be tested for Nf1Myf5 muscles as well.

Peripheral fatigue, exhaustion and tiredness are among NF1 symptoms (North, 1998). Peripheral fatigue is a decline in muscle function associated with over-activity that originates in tissues or organ systems other than the brain or spinal cord. Perceptions of tiredness or weariness are typical symptoms (Keyser, 2010). Mitochondrial metabolic pathways are aerobic. It means they use oxygen to convert nutrients (carbohydrates, lipids and protein) to ATP. If NF1 patients show, like Nf1Myf5 mice, a higher level of mitochondrial metabolism at rest, they would have severely increased substrate utilization as well as a severely increased oxygen demand. Intracellular concentrations of fatigue mediating metabolites would be increased as well. Utilized oxygen might not be available for quick force muscle movements. It could be possible that higher oxygen consumption at rest leads to lower blood oxygen concentrations and fatigue. However, studies performed in this work do not exactly recapitulate the situation in patients as they do not carry a homozygous *NF1* deletion muscle cells. All NF1 patients are heterozygous for a loss of *NF1*. Some of their symptoms emanate from haploinsufficency, others are caused by second-hit mutations in the second *NF1* allele and a loss of heterozygosity during development or at later points in life (Cichowski and Jacks, 2001). This situation cannot be exactly reflected in the mouse, since haploinsufficiency of *Nf1* does not lead to significant muscle alterations (Sullivan et al., 2014). Therefore, it is certainly necessary to investigate muscle metabolism and its consequences for muscle performance and body metabolism directly in NF1 patients. A suitable start experiment would be to test endurance muscle performance in addition to already existing muscle force measurements (Johnson et al., 2012; Souza et al., 2009).

5.4.3 The putative influence of metabolic shift on muscle mass and myogenesis in Nf1Myf5

Metabolic defects do not only affect muscle proficiency, but also development of myoblasts and stem cells as well as muscle mass and regeneration (Koopman et al., 2014; Ryall, 2013). The breakdown of ATP into ADP or AMP and inorganic phosphate is the predominant source of cellular energy. Under normal conditions, substrate (carbohydrates, lipids and proteins) and oxygen availability, as well as energy demand, dictate the pathway used for ATP generation (Ryall, 2013). The investigation of Nf1Myf5 showed that marker genes of glycolysis were downregulated. Glycolysis is an inefficient method of generating ATP, as each molecule of glucose generates a net gain of two ATP molecules. In the OXPHOS pathway 32 to 36 molecules of ATP are generated.

Although it is relatively inefficient, glycolysis provides a number of important advantages, including the ability to rapidly generate ATP in response to acute changes in energy demand (Pfeiffer et al., 2001), as well as generating the necessary glycolytic intermediates for the biosynthesis of new macromolecules via the pentose phosphate pathway (Ryall, 2013). Thus, down-regulation of glycolysis might cause severe defects in myogenesis. During development a switch to glycolysis is believed to allow both: the generation of ATP by catabolic mechanisms and the production of nucleotides, proteins and phospholipids needed for the anabolic processes required for cell growth (Folmes et al., 2012; Ryall, 2013). The best studied energy sensor in skeletal muscle is the 5'-AMP-activated protein kinase α (Ampk). In Nf1Myf5 mice Ampk is significantly stronger activated than in control mice at P21. Ampk is a negative regulator of skeletal muscle mass as it can inhibit mTOR signalling. By this inhibition protein synthesis can be reduced (Steinberg and Kemp, 2009). Interestingly, mTOR has been shown to be activated in *Nf1* deficient cells (Johannessen et al., 2005). But, putative mTOR activation in Nf1Myf5 muscles seems to be nullified by the activation of Ampk. Nevertheless, it needs to be proofed whether mTOR signalling is activated in Nf1Myf5, for example by western blot analyses of activated mTOR or target proteins like S6K and 4EBP1. Interesting is also the contrary effect of activated Ampk and activated Akt proteins. Both have been shown to be activated in Nf1Myf5. These proteins can phopshorylate the TSC (tuberous sclerosis complex) 1-TSC2 complex, an inhibitor of mTOR. By phosphorylation Ampk activates TSC1-TSC2 whereas Akt inactivates it (Huang and Manning, 2009). Testing for specific phosphorylation events in TSC1-TSC2, could reveal whether Ampk or Akt play the prevalent role in Nf1Myf5.

Importantly, cellular metabolism does not only play a role in hypertrophic growth but also in the determination of cell fate. In the C2C12 muscle cell line a clear reliance upon glycolysis in proliferating myoblasts could be shown. An increase in mitochondria number and OXPHOS activity could be detected after their differentiation (Leary et al., 1998; Lyons et al., 2004; Kraft et al., 2006). Glucose restriction could be shown to significantly impair the differentiation of C2C12 cells, and this defect could not be overcome by incubation with another substrate used for ATP generation. It suggests that glycolytic by-products may be required for successful differentiation and growth (Fulco et al., 2008). The inhibition of differentiation by glucose restriction was dependent on Ampk. Ampk has been found to regulate *Pgc-1* (peroxisome proliferator-activated receptor-γ coactivator 1α) transcription (Ryall, 2013). Pgc-1 is believed to be a master regulator of mitochondrial biogenesis. Increased Pgc-1 activity has been shown to inhibit C2C12 differentiation (Williamson et al., 2009). In Nf1Myf5 mice transcription of *Pgc-1* is significantly increased at P21. It is possible that Pgc-1 is also involved in differentiation of fetal myoblasts. Therefore Pcg-1 expression should be investigated in Nf1Myf5 muscles at E18.5, too.

In contrast to myoblast differentiation the importance of metabolism in satellite cell (muscle stem cells) biology is not well characterised yet. Recently, metabolic changes have been identified as regulators of stem cell specification and differentiation through a process called "metabolic reprogramming" (Lunt and Vander Heiden, 2011; Ryall, 2013; Koopman et al., 2014). However, little is known about the energy demands and metabolic status of stem cells during their life cycle. Compared to proliferating stem cells, quiescent stem cells are small in size and primarily composed of the nucleus with little cytoplasm. Like many stem cell populations (Facucho-Oliveira and St John, 2009), satellite cells only contain few tightly packed mitochondria (Latil et al., 2012). After differentiation and fusion into myofibres, mitochondrial density, complexity and organization increases drastically (Ryall, 2013). Studies in embryonic and induced pluripotent stem cells revealed that these populations strongly rely upon glycolysis and show reduced levels of OXPHOS compared to differentiating cells (Folmes et al., 2012; Zhang et al., 2012). In summary, the demands for energy

and new biomass differ for stem cells during periods of quiescence, proliferation and differentiation. Thus, stem cells must reprogram their metabolic profile to match these altered conditions. The metabolic state of a cell reflects its intracellular energy demands and the extracellular environment conditions. Alterations to either can lead to changes in metabolite balances (NAD^+/NADH, ADP/ATP, GDP/GTP), cellular pH, oxygen availability, concentrations of small molecules (acetyl-CoA, methionine), voltage gradients and many more. All of these metabolically regulated changes can lead to differential regulation of transcription and changes in cell identity (Lu and Thompson, 2012). It seems that Ras is involved in stem cell life cycle regulation as the RTK inhibitor Sprouty1 is essential for both, maintenance of quiescence and promotion of the self-renewal capacity of stem cells (Shea et al., 2010). Sprouty1 is, like Nf1, a negative regulator of Ras signalling.

During the muscle regeneration processes, muscle stem cells get activated upon muscle damage. The space that surrounds the stem cells is called the stem cell niche (Lander et al., 2012) and several studies have proposed that stem cell behaviour can be regulated via changes to the niche environment (Chakkalakal et al., 2012; Gilbert et al., 2010). That might happen through muscle damage and might lead to changes in stem cell metabolism and nutrient uptake (Ryall, 2013). A damage induced increase of mitochondrial activity could, for example, diminish the capability of a stem cell to give rise to new stem cells (Rocheteau et al., 2012).

Furthermore, it was shown that the numbers of stem cells is dependent on the myofibre type they are attached to. More stem cells are attached to predominantly oxidative fibres than to glycolytic fibres (Christov et al., 2007; Manzano et al., 2011) raising the question whether fibre metabolism plays a role in stem cell development. Surprisingly, it has been shown that with age the number of oxidative fibres increases (Ryall et al., 2007; Ryall et al., 2008), but the number of stem cells decreases (Chakkalakal et al., 2012). The same tendency could be described for young (P21) Nf1Myf5 in comparison to control mice. Therefore Nf1Myf5 could be a suitable model for studying the correlation between stem cells and fibre type, for example by studying if the metabolic status of a fibre influences stem cell numbers. Furthermore, pathways and mechanism involved in metabolic reprogramming during development could be very well investigated with the Nf1Myf5 mouse.

On the other hand, it has not been proven yet that the metabolic switch seen in perinatal Nf1Myf5 might also occur in myoblasts and satellite cells. To differentiate between effects on myofibres and mononucleated muscle cells, it would be necessary to isolate fetal myoblasts and postnatal satellite cells separately and determine their metabolic status by testing for expression of metabolic markers and analyzing cell metabolites (e.g. lactate to pyruvate ratio, free fatty acids and reactive oxygen species). Differentiation and proliferation defects detected in fetal Nf1Myf5 mice might be due to direct or indirect consequences of increased Ras/Mek/Erk or p38 MAPK signalling and not to changes in metabolism. Therefore, expression and activation of candidate regulators like Pcg-1, Ampk and mTOR should be tested. These analyses should be combined with studies on the proliferation and differentiation potential of isolated cells. Additionally satellite cell proliferation, differentiation and fusion potential should be monitored in muscle damage experiments in Nf1Myf5 mice. If a correlation between a metabolic imbalance towards mitochondrial metabolism and an impaired differentiation could be detected, Nf1Myf5 would be the first *in vivo* model to proof that metabolic defects can cause both differentiation and growth defects in skeletal muscle. If these results could be transferred to the situation in NF1 patients it would mean that metabolic pathways could be main candidates for medical intervention in early development and further life. Steady therapy of metabolic imbalance in skeletal muscles could also have positive influence on the symptoms of peripheral fatigue, exhaustion and tiredness in patients. Local metabolic treatment of

satellite cells could be beneficial for muscle regeneration after injury which improves healing of bone fractures, another NF1 symptom (Stevenson et al., 2005).
With the Nf1Myf5 model it is possible to study effects of metabolism on skeletal muscle stem cells and myofibre development. However, the influence of metabolism of stem cells on muscle development could be best studied by deleting *Nf1* in satellite cells only, for example by using the Pax7_Cre recombinase (von Maltzahn et al., 2013).

5.5 Loss of *Nf1* causes an increased activity of Ras downstream pathways

In postnatal Nf1Myf5 mice an increased activation of three Ras downstream signalling pathways could be detected. This concerns the PI3K/Akt, the Mek/Erk and the Calcineurin/Nfat pathway. Activation of these pathways in Nf1Myf5 mice could explain the main phenotypic characteristics: the proliferation and differentiation defect of progenitor cells, the hypertrophic growth defect in myofibres, the increased fraction of slow twitch myosin in postnatal muscles and the increase in mitochondrial oxidative metabolism. The three pathways are therefore candidates of causing both, fetal developmental defects and postnatal functional aberrations. The Mek/Erk pathway has been described to have a role in myoblast proliferation and myotube differentiation (Jo et al., 2009). In a C2C12 cell culture model it was shown that Erk/Mek signalling prevents MyoD expression in myoblasts (Mitin et al., 2001). The Mek/Erk pathway is often simultaneously activated with the PI3K-Akt pathway and it has been proposed that these two pathways exert opposing effects (Rommel et al., 1999). Manipulation of these pathways during muscle differentiation indicates that the Mek/Erk pathway inhibits differentiation, whereas the PI3K/Akt pathway stimulates differentiation (Bennett and Tonks, 1997; Coolican et al., 1997; Jiang et al., 1998). Furthermore, it was shown that the Erk/Mek pathway inhibits hypertrophy in muscle cells (Rommel et al., 1999). A defect in hypertrophic growth could be detected in Nf1Myf5 which therefore might be attributed to increased Erk/Mek signalling. However, the PI3K/Akt pathway has been described to stimulate hypertrophic growth. This pathway would be a candidate to explain the normal size of slow twitch fibres in Nf1Myf5 mice by inducing a secondary hypertrophy effect in these fibres. Furthermore induction of Akt in skeletal muscle has been shown to reduce adipose tissue (Lai et al., 2004), an effect also seen in limbs of perinatal Nf1Myf5 mice.
As already described in section 5.4.3 Nf1 and Ras downstream pathways can have opposing effects. Ampk activation was described to be Ras dependent (Ríos et al., 2013) and could be shown to be increased in Nf1Myf5. Ampk and Akt, however have a contrary influence on mTOR by differentially regulating TSC1-TSC2, an inhibitor of mTOR. Ampk activates TSC1-TSC2 by phosphorylation whereas Akt inactivates it (Huang and Manning, 2009). mTOR stimulates protein synthesis (Bodine et al., 2001). However, hypertrophy by possible mTOR activation in Nf1Myf5 seems to be compensated by another effect, for example the activation of Ampk. The effect might be different in slow and fast twitch fibres as only fast fibres are reduced in size in Nf1Myf5. Nevertheless, mTOR activation needs to be tested in fast and slow fibres of Nf1Myf5 in comparison to control mice. Testing for Ampk and Akt specific phosphorylation events in TSC1-TSC2 could reveal which pathway plays the prevalent role.
Akt signalling is also capable to induce an increased Ca^{2+} uptake (Viard et al., 2004). This would activate Nfat signalling. Hypertrophy of myofibres is positively regulated by Nfat signalling (Schulz

et al., 2004). This was described to mainly refer to slow twitch myofibres (Hudson and Price, 2013). Nfat is activated by Calcineurin. Although the downstream effectors of Calcineurin have not been fully elucidated, it is known to be essential for proper function of skeletal muscle. Calcineurin participates in a variety of processes including myoblast recruitment, myotube differentiation, fibre type specification and recovery from injury and dystrophic muscle damage (Hudson and Price, 2013; Friday et al., 2000; Naya et al., 2000; Horsley et al., 2001; Horsley et al., 2003; Parsons et al., 2003; Stupka et al., 2006). Although no direct proof for a correlation between *Nf1* deletion and Calcineurin exists, it could be shown that Nfat activation is increased in *Nf1* depleted endothelial cells (Gitler et al., 2003). As there is also no description of Nfat activating signalling pathways in skeletal muscles *in vivo* (Schiaffino and Serrano, 2002) the Nf1Myf5 model could be the first model for pathway analysis.

It is also possible that myofibre type specific size reductions in Nf1Myf5 are mediated by nerve activity-dependent Ras signalling. Nerve activity can induce long-lasting, transcription-dependent changes in skeletal muscle fibres and affect muscle growth and fibre-type specification. Calcineurin signalling has been implicated in the transcriptional regulation of slow muscle fibre genes. It has been shown that Calcineurin function in muscle fibres and not in motor neurons is responsible for nerve-dependent specification of slow muscle fibres (Serrano et al., 2001). However, in NF1 patients neurons do also show *NF1* haplodeficiency which might cause a secondary effect on neuron-myofibre interactions which cannot be detected in the Nf1Myf5 model. Nevertheless, with the three investigated pathways Akt, Mek/Erk and Calcineurin/Nfat, specific candidates for treatment of NF1 associated muscle defects have been proposed. For NF1 treatment it seems to be an advantage to target specific downstream pathways instead of Ras. Unwanted side effects like blockade of further Ras pathways influencing intracellular trafficking or actin organization as well as induction of compensatory pathway activation could be limited. For a time specific treatment, however, further research has to be done. It is not clear whether different cell populations (e.g. myofibres and satellite cells) at different developmental stages show different pathway activation. Therefore, myoblasts, myotubes, myofibres and satellite cells have to be isolated from each stage of development and pathway analysis should be performed on each cell type separately. Also, possible Ras pathway feedback inhibition mechanisms were neglected in this study. It has been reported that endogenous protein-protein interactions regulate Ras pathways and that they contribute to coordinate activation steps, sub-cellular redistribution, substrate phosphorylation and cross-talk with other signalling pathways (Kolch, 2000; Pan et al., 2007; Menges and McCance; 2008). The present study was also not designed to unreveal muscular Ras or Nf1 associated pathways that are not described yet, but the Nf1Myf5 model would be suitable for that, too. It might be further helpful to constitutively activate each of the Ras downstream pathways separately in a mouse or cell culture model to differentiate between different pathway effects.

Jo et al. described a biphasic activation profile of Erk in cultured C2C12 cells. They detected Erk activation during myoblast proliferation which inhibited differentiation. During a subsequent Erk inactivation phase, Mek becomes activated and stimulates the formation of myotubes. After its inactivation phase, Erk is activated again and stimulates the differentiation of myotubes (Jo et al., 2009). Thus, myoblasts have a unique biphasic requirement for Erk activity. Erk1/2 is critical for growth factor-induced cellular proliferation, inhibitory to myoblast differentiation and later required for myoblast fusion; or at least Erk2 appears critical to this last process (Knight and Kothary, 2011). Correct cell development depends on accurately timed pathway component activation. In the Nf1Myf5 model Ras is constitutively activated by the deletion of its inhibitor Nf1. In the embryonic stage no defect in muscle development could be detected in Nf1Myf5. If at all, a small advantage in

growth was detectable in mutant embryos. It is possible that in the phase between *Nf1* knockout in embryonic myoblasts (E11.5) and phenotype investigation at E14.5, Ras pathway is activated in muscle precursors to its limit anyway and that the loss of *Nf1* in mutants does not show additional effects on signalling. It is, however, possible that after the embryonic stage Ras signalling would be downregulated normally to facilitate generation and migration of fetal progenitor cells. In Nf1Myf5 this process might be disturbed and in consequence an endogenous feedback inhibition might down-regulate Ras pathways which would later enable proliferation of fetal myoblasts ($Pax7^{+}$) which is probably delayed in Nf1Myf5.
Ras signalling consists of complex pathways and feedback inhibition mechanisms. In this work the first *in vivo* candidate pathways for NF1 associated muscular defects could be shown. These pathways might be candidates for testing targeted treatment of the muscular defects via pathway inhibition.

5.6 *Nf1* depleted osteocytes show a pleiotropic effect to *Nf1* depleted muscles

Bone and muscle development are strictly dependent on each other. The two organs evolve as a functional unit. Therefore it is not surprising that if one of these organs is disturbed in its development, the other organ is as well. Musculoskeletal diseases include back pain, arthritis and osteoporosis and occur more frequently as people age. Congenital defects like RASopathies also cause musculoskeletal defects (Stevenson and Yang, 2011). RASopathies are developmental syndromes caused by germline mutations that alter cellular Ras signal transduction, including Noonan syndrome, Costello syndrome and neurofibromatosis I (NF1). For studying NF1 muscle and bone defects two models have been investigated in detail: the muscle cell specific knockout mouse Nf1Myf5 and the Nf1Prx1 mouse showing a *Nf1* knockout in multiple tissues of the limbs, e.g. bone (Kolanczyk et al., 2007). After mouse investigation the question arose whether muscle and bone phenotypes are induced by deregulation of the same molecular factors (pleiotropy). Pleiotropic factors already described in the musculoskeletal context are Gdf-8, Mef-2c, Pgc-1 and Ppar g (Abreu et al., 2012; Wan, 2010). Pleiotropy effects are explained as being dependent on "cellular context" meaning that common signalling mechanisms are interpreted differently by different cell types (Hunter, 1997; Marshall, 1995a). Phenotypical differences between different cell types are very likely. Therefore, an identical behaviour of *Nf1* depleted muscle and bone cells (osteocytes) is not expected. As *Pcg-1* and *Ppar g* were upregulated in Nf1Myf5 muscle, they were analysed in bone as well and an upregulated expression of both factors could be seen in osteocytes of Nf1Prx1. Also maker genes of oxidative metabolism were upregulated, which might be mediated by Pcg-1 in both cell types as Pgc-1 is described as a metabolic regulator (Ehrenborg and Krook, 2009). Ppar g interacts with Pcg-1 but was also described to cause osteocyte death (Mieczkowska et al., 2012). Osteocyte death was also shown to be increased in Nf1Prx1 in the context of this work. This might explain for mineralisation defects (Kolanczyk et al., 2007) and fracture healing defects reported in Nf1Prx1 (Kolanczyk et al., 2008). Furthermore, Nfat (nuclear factor of activated T cell) expression is elevated in Nf1Myf5 muscle as well as Nf1Prx1 bone indicating increased Nfat signalling in both tissues. Contrary to Pgc-1 (Abreu et al., 2012) and Ppar g (Wan, 2010), Nfat is not described as pleiotropic factor in the musculoskeletal context, yet. Therefore results presented here might unreveal an undiscovered function of Calcineurin/Nfat signalling. Calcineurin is a protein

phosphatase, also known as protein phosphatase 3, and Ca^{2+}-dependent serine-threonine phosphatase (Liu et al., 2005). Calcineurin activates Nfat by dephosphorylation. The activated Nfat is then translocated into the nucleus, where it upregulates the expression of target genes. Calcineurin and Nfat have been described as important regulators of bone homeostasis in both osteoclast differentiation and osteoblastic bone formation (Takayanagi, 2006). Mice expressing a constitutively active $Nfat_{c1}$ ($Nfat_{c1}^{nuc}$) variant were described to have a less organized osteoblasts appearance and increased osteoblasts numbers (Winslow et al., 2006) which was also seen in Nf1Prx1 (Kolanczyk et al., 2007; Kühnisch et al., 2014). Furthermore $Nfat_{c1}^{nuc}$ showed an increase in bone volume in embryonic and perinatal mice. In Nf1Prx1 only an increase in the not mineralized osteoid fraction could be shown and furthermore a decrease in cortical bone mass (Kolanczyk et al., 2007). This difference might be due to Nfat isoform dependency of the phenotype. Contrary to $Nfat_{c1}^{nuc}$, in Nf1Prx1 $Nfat_{c1}$ is markedly less upregulated than the other isoforms, especially $Nfat_{c2}$. Also other deregulated molecular factors might cause the bone mass decrease in Nf1Prx1 (Kolanczyk et al., 2007; Kühnisch et al., 2014). Nevertheless, Nfat is a candidate pleiotropic factor for mediating *Nf1* deficiency associated muscle and bone defects and should be further investigated as it would have a strong indication for treatment of neurofibromatosis I patients. One kind of recent medical treatment of bone defects in NF1 is supplementation of calcium (Elefteriou et al., 2009; Hogan et al., 1986; information on treatment in "Neurofibromatose-Ambulanz Hamburg" on www. bv-nf.de, 2014). However, studies investigating the efficiency of calcium showed that calcium gavages did not increase bone mass in patients (Petramala et al., 2012; Brunetti-Pierri et al., 2008). Regarding the results of the recent work, it is possible that calcium substitution even has a negative effect on *Nf1* depleted muscle cells and osteocytes. Calcium ion (Ca^{2+}) uptake by cells stimulates Calcineurin (Li et al., 2012) which activates Nfat. It has already been shown that Nfat activation is specific to stimulation by Ca^{2+} (Srinivasan et al., 2010). As Nfat is already over-activated in *Nf1* depleted muscle cells and osteocytes a further calcium supplementation would rather worsen the NF1 phenotype. At least calcium application should be accompanied by application of an inhibitor of Calcineurin/Nfat signalling. However, first of all, Calcineurin activation on protein level should be investigated in muscle of Nf1Myf5 and bone of Nf1Prx1. Again, it is necessary to point out that the situation in the mouse models does not fully recapitulate the situation in NF1 patients as they are heterozygous for the loss of *NF1* (Ismat et al., 2006). That means one would expect heterogeneous effects between different organs and even cells of one organ. Interaction between them could cause secondary effects that cannot be detected in mice. Nevertheless, patients' muscle and bone biopsies should be investigated for aberrant pathway activation with a focus on Calcineurin/Nfat, Ppar g and Pgc-1. Preferentially samples should be isolated from areas which were affected by bone fractures.

Taken together, the neurofibromatosis I associated musculoskeletal phenotype seems to be a combined result of several deregulated pathways. The ones described here, have not been described in context of *Nf1* depleted muscle-bone interaction before, but are capable of explaining aspects of severe NF1 symptoms.

6. Summary

The aim of this work was to describe the role of the protein neurofibromin in skeletal muscle cells. Loss of neurofibromin function causes neurofibromatosis I (NF1) - one of the most common genetic disorders worldwide. Although the most prominent symptoms of NF1 are tumours of neuroectodermal origin, a high fraction of patients suffers from pathological changes of the musculoskeletal system. These symptoms mostly appear in early childhood and include bone malformations, decreased bone density and a high predisposition to fractures. An additional reduction of muscular strength and coordination skills increases the risk of falls and injuries which altogether contributes to tremendous restrictions of patients' health and life quality.

Neurofibromatosis I is caused by mutations in the gene *NF1*. The gene encodes for the RAS GTPase activating protein neurofibromin, which is described as a tumour suppressor and histogenesis control gene. Although considerable research was performed on tumourgenesis and skeletogenesis in NF1 patients, the aspect of putative muscular defects has not been investigated yet. However, in respect to skeletal malformations it seems most likely that a combination of skeletal and muscular defects causes the clinical picture. Therefore, basic pathomechanisms of NF1 in muscle cells were studied in this work. For this purpose, three mouse models were generated using a conditional knockout approach allowing a muscle cell specific *Nf1* knockout. In each model *Nf1* was deleted in a specific stage of embryonic development. In the first model (Nf1Lbx1) *Nf1* was deleted in muscle precursor cells. In the second model (Nf1Myf5) myoblasts were targeted and in the third model (Nf1HSA) *Nf1* was deleted in myotubes. The mice were analysed using histological, immunochemical, molecular biological and biochemical methods. Thereby, the four phases of muscle development were analysed: embryonic, fetal, perinatal and adult myogenesis.

It could be shown that loss of *Nf1* causes a decrease in muscle fibre growth. This decrease was first detected in the fetal phase of myogenesis at embryonic day E18.5. It was detected only if *Nf1* was deleted in precursor cells or myoblasts, but not if deleted in myotubes. The fibre size reduction was mainly due to reduction of the myonuclear domain (cellular protein content per nucleus). Furthermore, it was detected that the number of $Pax7^+$ progenitor cells showed a transient increase in the fetal stage upon deletion of *Nf1*. However, postnatally the *Nf1* deletion resulted in strong depletion of $Pax7^+$ progenitor cell numbers. That leads to a diminished cell pool of muscle stem cells, so called satellite cells, which are responsible for muscle regeneration. Also, it seems that *Nf1* has a role in fibre type determination and regulation of metabolic parameters as loss of *Nf1* caused a shift towards oxidative fibre characteristics. Investigations of molecular pathways in muscle tissue showed that deletion of *Nf1* leads to significant over-activation of the Ras downstream components Erk/Mek, Akt and Nfat as well as transcriptional upregulation of their downstream targets which might be responsible for the detected growth and metabolism defects.

The results show that *Nf1* has several roles in skeletal muscle cells, including differentiation of $Pax7^+$ precursor cells, fibre growth and regulation of metabolic characteristics. The described mouse models recapitulated aspects of neurofibromatosis I associated muscle defects like the decrease of muscle size. Therefore, they are suitable for further studies and therapy testing in the process of neurofibromatosis I research.

Zusammenfassung

Das Ziel der vorliegenden Arbeit war es, die Rolle des Proteins Neurofibromin in skelettalen Muskelzellen zu beschreiben. Ein Verlust von Neurofibromin ist die Ursache von Neurofibromatose I (NF1) - eine der häufigsten Erbkrankheiten weltweit. Die bekanntesten Krankheitssymptome sind Tumore neuroektodermalen Ursprungs. Eine große Zahl der Patienten leidet darüber hinaus an schweren Defekten des muskuloskelettalen Systems. Diese Defekte treten häufig bereits im Kindesalter auf und führen zu Knochendeformationen, einer verminderten Knochendichte und einer erhöhten Prädisposition für Frakturen. Außerdem erhöht eine Reduktion von Muskelkraft und Koordinationsfähigkeit das Risiko für Stürze und Verletzungen und beeinträchtigt die Patienten zusätzlich.

Neurofibromatose I wird durch Mutationen im *NF1*-Gen hervorgerufen. Dieses Gen kodiert für das RAS-GTPase-aktivierende Protein Neurofibromin, welches als Tumorsupressor und Histogenese-Kontrollgen beschrieben wurde. Tumor- und Knochenentwicklung stehen im Mittelpunkt der NF1-Forschung. Die Ursachen verringerter Muskelleistungen wurden bisher allerdings nicht untersucht. In Anbetracht der skelettalen Missbildungen stellt sich jedoch die Frage, ob nicht skelettale und muskuläre Defekte zusammen das klinische Bild hervorrufen.
Die vorliegende Arbeit widmet sich der Erforschung des NF1-Pathomechanismus in Muskelzellen. Dafür wurden drei Mausmodelle mithilfe einer konditionellen Knockout-Technik erzeugt. Die Technik erlaubte eine Muskelzell-spezifische Deletion des *Nf1*-Gens zu ausgewählten Zeitpunkten der Embryonalentwicklung. Im ersten Model (Nf1Lbx1) wurde *Nf1* in Muskel-Vorläuferzellen ausgeschaltet. Im zweiten Model (Nf1Myf5) sind Myoblasten und im dritten Model (Nf1HSA) Myotuben vom *Nf1*-Knockout betroffen. Alle Modelle wurden mithilfe von histologischen, immunochemischen, molekularbiologischen und biochemischen Methoden hinsichtlich der vier Phasen der Muskelentwicklung - embryonale, fetale, perinatale und adulte Myogenese - untersucht.

Es konnte gezeigt werden, dass ein Verlust von *Nf1* ein reduziertes Muskelfaser-Wachstums hervorruft. Diese Reduktion konnte erstmalig im fetalen Stadium der Myogenese bei Tag E18.5 detektiert werden. Sie wird durch den *Nf1*-Verlust in Muskel-Vorläuferzellen beziehungsweise Myoblasten, nicht jedoch in Myotuben, ausgelöst. Die Größenreduktion der Muskelfasern geht hauptsächlich auf eine Verminderung der myonukleären Domäne (zellulärer Proteingehalt pro Zellkern) zurück. Der Verlust von *Nf1* löst zudem einen transienten Anstieg der Zahl $Pax7^+$ Vorläuferzellen im fetalen Stadium aus. Nach der Geburt nimmt deren Zahl wiederum verstärkt ab, wahrscheinlich durch eine Erschöpfung des Zellpools. Dadurch verringert sich die Anzahl sogenannter Satellitenzellen, residenter Muskelstammzellen.
Es wurde ebenfalls gezeigt, dass *Nf1* maßgeblich an der Regulation von Muskelfaser-Identität und metabolischen Parametern beteiligt ist. Die Untersuchung von Nf1- und Ras-assoziierten Signalwegen ergab eine erhöhte Aktivierung der Akt-, Mek/Erk- und Nfat-Signalkaskaden durch einen *Nf1*-Knockout. Eine Reihe von transkriptionellen Zielgenen dieser Signalwege konnte als möglicher Auslöser der beschriebenen Wachtums- und Metabolismusdefekte identifiziert werden.

Die Ergebnisse zeigen, dass *Nf1* wichtige Funktionen in skeletalen Muskelzellen übernimmt, dies schließt die Differenzierung von $Pax7^+$ Vorläuferzellen, das Faserwachstum und die Regulation metabolischer Prozesse ein. Die hier etablierten Mausmodelle rekapitulieren Aspekte des Neurofibromatose I-Krankheitsbildes. Sie sind daher geeignete Forschungsobjekte für weitere Studien zum Pathomechanismus sowie für die Durchführung therapeutischer Tests.

7. References

Abreu, E.L., Stern, M., and Brotto, M. (2012a). Bone-muscle interactions: ASBMR Topical Meeting, July 2012. IBMS BoneKEy *9*.

Allen, D.L., Sartorius, C.A., Sycuro, L.K., and Leinwand, L.A. (2001). Different Pathways Regulate Expression of the Skeletal Myosin Heavy Chain Genes. J. Biol. Chem. *276*, 43524–43533.

Alwan, S., Tredwell, S.J., and Friedman, J.M. (2005). Is osseous dysplasia a primary feature of neurofibromatosis 1 (NF1)? Clin. Genet. *67*, 378–390.

Andrades, J., Claros, S., Jimenez-Palomo, P., Ma, J., ZamoraNavas, P., Guerado, E., Monleon, M., C., M., and Becerr, J. (2011). Skeletal Regeneration by Mesenchymal Stem Cells: What Else? In Regenerative Medicine and Tissue Engineering - Cells and Biomaterials, D. Eberli, ed. (InTech), p. 10.5772/20889.

Angelini, C., and Semplicini, C. (2010). Metabolic myopathies: the challenge of new treatments. Curr. Opin. Pharmacol. *10*, 338–345.

Aravind, L., Neuwald, A.F., and Ponting, C.P. (1999). Sec14p-like domains in NF1 and Dbl-like proteins indicate lipid regulation of Ras and Rho signaling. Curr. Biol. CB *9*, R195–197.

Bennett, A.M., and Tonks, N.K. (1997). Regulation of distinct stages of skeletal muscle differentiation by mitogen-activated protein kinases. Science *278*, 1288–1291.

Bentzinger, C.F., Wang, Y.X., and Rudnicki, M.A. (2012). Building muscle: molecular regulation of myogenesis. Cold Spring Harb. Perspect. Biol. *4*.

Berardo, A., DiMauro, S., and Hirano, M. (2010). A Diagnostic Algorithm for Metabolic Myopathies. Curr. Neurol. Neurosci. Rep. *10*, 118–126.

Berg, J.M., Tymoczko, J.L., and Stryer, L. (2002). Biochemistry.

Bernards, A., Snijders, A.J., Hannigan, G.E., Murthy, A.E., and Gusella, J.F. (1993). Mouse neurofibromatosis type 1 cDNA sequence reveals high degree of conservation of both coding and non-coding mRNA segments. Hum. Mol. Genet. *2*, 645–650.

Bodine, S.C., Stitt, T.N., Gonzalez, M., Kline, W.O., Stover, G.L., Bauerlein, R., Zlotchenko, E., Scrimgeour, A., Lawrence, J.C., Glass, D.J., et al. (2001). Akt/mTOR pathway is a crucial regulator of skeletal muscle hypertrophy and can prevent muscle atrophy in vivo. Nat. Cell Biol. *3*, 1014–1019.

Bollag, G., Clapp, D.W., Shih, S., Adler, F., Zhang, Y.Y., Thompson, P., Lange, B.J., Freedman, M.H., McCormick, F., Jacks, T., et al. (1996). Loss of NF1 results in activation of the Ras signaling pathway and leads to aberrant growth in haematopoietic cells. Nat. Genet. *12*, 144–148.

Bonni, A., Brunet, A., West, A.E., Datta, S.R., Takasu, M.A., and Greenberg, M.E. (1999). Cell survival promoted by the Ras-MAPK signaling pathway by transcription-dependent and -independent mechanisms. Science *286*, 1358–1362.

Bothe, I., and Dietrich, S. (2006). The molecular setup of the avian head mesoderm and its implication for craniofacial myogenesis. Dev. Dyn. Off. Publ. Am. Assoc. Anat. *235*, 2845–2860.

Boyer, J.G., Deguise, M.-O., Murray, L.M., Yazdani, A., Repentigny, Y.D., Boudreau-Larivière, C., and Kothary, R. (2014). Myogenic program dysregulation is contributory to disease pathogenesis in spinal muscular atrophy. Hum. Mol. Genet. ddu142.

Brannan, C.I., Perkins, A.S., Vogel, K.S., Ratner, N., Nordlund, M.L., Reid, S.W., Buchberg, A.M., Jenkins, N.A., Parada, L.F., and Copeland, N.G. (1994). Targeted disruption of the neurofibromatosis type-1 gene leads to developmental abnormalities in heart and various neural crest-derived tissues. Genes Dev. *8*, 1019–1029.

Briguet, A., Courdier-Fruh, I., Foster, M., Meier, T., and Magyar, J.P. (2004). Histological parameters for the quantitative assessment of muscular dystrophy in the mdx-mouse. Neuromuscul. Disord. NMD *14*, 675–682.

Brunetti-Pierri, N., Doty, S.B., Hicks, J., Phan, K., Mendoza-Londono, R., Blazo, M., Tran, A., Carter, S., Lewis, R.A., Plon, S.E., et al. (2008). Generalized metabolic bone disease in Neurofibromatosis type I. Mol. Genet. Metab. *94*, 105–111.

Buchberger, A., Nomokonova, N., and Arnold, H.-H. (2003). Myf5 expression in somites and limb buds of mouse embryos is controlled by two distinct distal enhancer activities. Development *130*, 3297–3307.

Buckingham, M., Bajard, L., Chang, T., Daubas, P., Hadchouel, J., Meilhac, S., Montarras, D., Rocancourt, D., and Relaix, F. (2003). The formation of skeletal muscle: from somite to limb. J. Anat. *202*, 59–68.

Chakkalakal, J.V., Jones, K.M., Basson, M.A., and Brack, A.S. (2012). The aged niche disrupts muscle stem cell quiescence. Nature *490*, 355–360.

Chen, J.C.J., Mortimer, J., Marley, J., and Goldhamer, D.J. (2005). MyoD-cre transgenic mice: a model for conditional mutagenesis and lineage tracing of skeletal muscle. Genes. N. Y. N 2000 *41*, 116–121.

Christ, B., and Ordahl, C.P. (1995). Early stages of chick somite development. Anat. Embryol. (Berl.) *191*, 381–396.

Christov, C., Chrétien, F., Abou-Khalil, R., Bassez, G., Vallet, G., Authier, F.-J., Bassaglia, Y., Shinin, V., Tajbakhsh, S., Chazaud, B., et al. (2007). Muscle satellite cells and endothelial cells: close neighbors and privileged partners. Mol. Biol. Cell *18*, 1397–1409.

Chuvpilo, S., Jankevics, E., Tyrsin, D., Akimzhanov, A., Moroz, D., Jha, M.K., Schulze-Luehrmann, J., Santner-Nanan, B., Feoktistova, E., König, T., et al. (2002). Autoregulation of

NFATc1/A expression facilitates effector T cells to escape from rapid apoptosis. Immunity *16*, 881–895.

Cichowski, K., and Jacks, T. (2001). NF1 tumor suppressor gene function: narrowing the GAP. Cell *104*, 593–604.

Clark, E.A., and Hynes, R.O. (1996). Ras activation is necessary for integrin-mediated activation of extracellular signal-regulated kinase 2 and cytosolic phospholipase A2 but not for cytoskeletal organization. J. Biol. Chem. *271*, 14814–14818.

Condon, K., Silberstein, L., Blau, H.M., and Thompson, W.J. (1990). Development of muscle fiber types in the prenatal rat hindlimb. Dev. Biol. *138*, 256–274.

Conley, K.E., Kemper, W.F., and Crowther, G.J. (2001). Limits to sustainable muscle performance: interaction between glycolysis and oxidative phosphorylation. J. Exp. Biol. *204*, 3189–3194.

Coolican, S.A., Samuel, D.S., Ewton, D.Z., McWade, F.J., and Florini, J.R. (1997). The mitogenic and myogenic actions of insulin-like growth factors utilize distinct signaling pathways. J. Biol. Chem. *272*, 6653–6662.

Cruz Guzmán, O.D.R., Chávez García, A.L., and Rodríguez-Cruz, M. (2012). Muscular dystrophies at different ages: metabolic and endocrine alterations. Int. J. Endocrinol. *2012*, 485376.

Cumming, G., Fidler, F., and Vaux, D.L. (2007). Error bars in experimental biology. J. Cell Biol. *177*, 7–11.

D'Angelo, I., Welti, S., Bonneau, F., and Scheffzek, K. (2006). A novel bipartite phospholipid-binding module in the neurofibromatosis type 1 protein. EMBO Rep. *7*, 174–179.

Daou, N., Lecolle, S., Lefebvre, S., della Gaspera, B., Charbonnier, F., Chanoine, C., and Armand, A.-S. (2013). A new role for the calcineurin/NFAT pathway in neonatal myosin heavy chain expression via the NFATc2/MyoD complex during mouse myogenesis. Dev. Camb. Engl. *140*, 4914–4925.

Dasgupta, B., and Gutmann, D.H. (2003). Neurofibromatosis 1: closing the GAP between mice and men. Curr. Opin. Genet. Dev. *13*, 20–27.

DeChene, E.T., Kang, P.B., and Beggs, A.H. (1993). Congenital Fiber-Type Disproportion. In GeneReviews(®), R.A. Pagon, M.P. Adam, H.H. Ardinger, T.D. Bird, C.R. Dolan, C.-T. Fong, R.J. Smith, and K. Stephens, eds. (Seattle (WA): University of Washington, Seattle),.

Delling, U., Tureckova, J., Lim, H.W., De Windt, L.J., Rotwein, P., and Molkentin, J.D. (2000a). A Calcineurin-NFATc3-Dependent Pathway Regulates Skeletal Muscle Differentiation and Slow Myosin Heavy-Chain Expression. Mol. Cell. Biol. *20*, 6600–6611.

Dimitrova, V., Pavlova, V., Valtchev, V., Yordanova, I., and al. (2008). A case of neurofibromatosis type 1. JoFIMAB *14*, 63–67.

Dunglison, G.F., Scotting, P.J., and Wigmore, P.M. (1999). Rat embryonic myoblasts are restricted to forming primary fibres while later myogenic populations are pluripotent. Mech. Dev. *87*, 11–19.

Duprez, D. (2002). Signals regulating muscle formation in the limb during embryonic development. Int. J. Dev. Biol. *46*, 915–925.

Duprez, D. (2010). Muscle development and regeneration. In McGraw Hill Encyclopedia of Science & Technology, (Paris, France: AccessScience), pp. 2–6.

Ehrenborg, E., and Krook, A. (2009). Regulation of Skeletal Muscle Physiology and Metabolism by Peroxisome Proliferator-Activated Receptor δ. Pharmacol. Rev. *61*, 373–393.

Elefteriou, F., Kolanczyk, M., Schindeler, A., Viskochil, D.H., Hock, J.M., Schorry, E.K., Crawford, A.H., Friedman, J.M., Little, D., Peltonen, J., et al. (2009). Skeletal abnormalities in neurofibromatosis type 1: approaches to therapeutic options. Am. J. Med. Genet. A. *149A*, 2327–2338.

Erwin, D.H., Laflamme, M., Tweedt, S.M., Sperling, E.A., Pisani, D., and Peterson, K.J. (2011). The Cambrian conundrum: early divergence and later ecological success in the early history of animals. Science *334*, 1091–1097.

Facucho-Oliveira, J.M., and St John, J.C. (2009). The relationship between pluripotency and mitochondrial DNA proliferation during early embryo development and embryonic stem cell differentiation. Stem Cell Rev. *5*, 140–158.

Farkas-Bargeton, E., Aicardi, J., Arsenio-Nunes, M.L., and Wehrle, R. (1978). Delay in the maturation of muscle fibers in infants with congenital hypotonia. J. Neurol. Sci. *39*, 17–29.

Feldkamp, M.M., Angelov, L., and Guha, A. (1999). Neurofibromatosis type 1 peripheral nerve tumors: aberrant activation of the Ras pathway. Surg. Neurol. *51*, 211–218.

Ferner, R.E., Huson, S.M., Thomas, N., Moss, C., Willshaw, H., Evans, D.G., Upadhyaya, M., Towers, R., Gleeson, M., Steiger, C., et al. (2007). Guidelines for the diagnosis and management of individuals with neurofibromatosis 1. J. Med. Genet. *44*, 81–88.

Folmes, C.D.L., Dzeja, P.P., Nelson, T.J., and Terzic, A. (2012). Metabolic plasticity in stem cell homeostasis and differentiation. Cell Stem Cell *11*, 596–606.

Francis-West, P.H., Antoni, L., and Anakwe, K. (2003). Regulation of myogenic differentiation in the developing limb bud. J. Anat. *202*, 69–81.

Friday, B.B., Horsley, V., and Pavlath, G.K. (2000). Calcineurin activity is required for the initiation of skeletal muscle differentiation. J. Cell Biol. *149*, 657–666.

Friedman, J.M., Gutmann, D.H., MacCollin, M., and Riccardi, V.M. (1999). Neurofibromatosis: phenotype, natural history, and pathogenesis (Baltimore: 1-25: Johns Hopkins University Press).

Fulco, M., Cen, Y., Zhao, P., Hoffman, E.P., McBurney, M.W., Sauve, A.A., and Sartorelli, V. (2008). Glucose restriction inhibits skeletal myoblast differentiation by activating SIRT1 through AMPK-mediated regulation of Nampt. Dev. Cell *14*, 661–673.

Fürst, D.O., Osborn, M., and Weber, K. (1989). Myogenesis in the mouse embryo: differential onset of expression of myogenic proteins and the involvement of titin in myofibril assembly. J. Cell Biol. *109*, 517–527.

Galler, S., Schmitt, T.L., and Pette, D. (1994). Stretch activation, unloaded shortening velocity, and myosin heavy chain isoforms of rat skeletal muscle fibres. J. Physiol. *478 Pt 3*, 513–521.

Gayraud-Morel, B., Chrétien, F., Jory, A., Sambasivan, R., Negroni, E., Flamant, P., Soubigou, G., Coppée, J.-Y., Di Santo, J., Cumano, A., et al. (2012). Myf5 haploinsufficiency reveals distinct cell fate potentials for adult skeletal muscle stem cells. J. Cell Sci. *125*, 1738–1749.

Genescà, L., Aubareda, A., Fuentes, J.J., Estivill, X., De La Luna, S., and Pérez-Riba, M. (2003). Phosphorylation of calcipressin 1 increases its ability to inhibit calcineurin and decreases calcipressin half-life. Biochem. J. *374*, 567–575.

Gilbert, P.M., Havenstrite, K.L., Magnusson, K.E.G., Sacco, A., Leonardi, N.A., Kraft, P., Nguyen, N.K., Thrun, S., Lutolf, M.P., and Blau, H.M. (2010). Substrate elasticity regulates skeletal muscle stem cell self-renewal in culture. Science *329*, 1078–1081.

Gille, H., and Downward, J. (1999). Multiple ras effector pathways contribute to G(1) cell cycle progression. J. Biol. Chem. *274*, 22033–22040.

Gillies, A.R., and Lieber, R.L. (2011). Structure and function of the skeletal muscle extracellular matrix. Muscle Nerve *44*, 318–331.

Gitler, A.D., Zhu, Y., Ismat, F.A., Lu, M.M., Yamauchi, Y., Parada, L.F., and Epstein, J.A. (2003). Nf1 has an essential role in endothelial cells. Nat. Genet. *33*, 75–79.

Gross, J., Machulik, A., Amarjargal, N., Moller, R., Ungethüm, U., Kuban, R.-J., Fuchs, F.-U., Andreeva, N., Fuchs, J., Henke, W., et al. (2007). Expression of apoptosis-related genes in the organ of Corti, modiolus and stria vascularis of newborn rats. Brain Res. *1162*, 56–68.

Günther, S., Kim, J., Kostin, S., Lepper, C., Fan, C.-M., and Braun, T. (2013). Myf5-positive satellite cells contribute to Pax7-dependent long-term maintenance of adult muscle stem cells. Cell Stem Cell *13*, 590–601.

Gutmann, D.H., Wood, D.L., and Collins, F.S. (1991). Identification of the neurofibromatosis type 1 gene product. Proc. Natl. Acad. Sci. U. S. A. *88*, 9658–9662.

Handy, D.E., Castro, R., and Loscalzo, J. (2011). Epigenetic modifications: basic mechanisms and role in cardiovascular disease. Circulation *123*, 2145–2156.

Hawke, T.J., and Garry, D.J. (2001). Myogenic satellite cells: physiology to molecular biology. J. Appl. Physiol. Bethesda Md 1985 *91*, 534–551.

Hindi, S.M., Tajrishi, M.M., and Kumar, A. (2013). Signaling mechanisms in mammalian myoblast fusion. Sci. Signal. *6*, re2.

Hogan, D.B., Anderson, C., MacKenzie, R.A., and Crilly, R.G. (1986). Hypophosphatemic osteomalacia complicating von Recklinghausen's neurofibromatosis: increase in spinal density on treatment. Bone *7*, 9–12.

Holt, G.R. (1987). Von Recklinghausen's neurofibromatosis. Otolaryngol. Clin. North Am. *20*, 179–193.

Hölzel, M., Huang, S., Koster, J., Ora, I., Lakeman, A., Caron, H., Nijkamp, W., Xie, J., Callens, T., Asgharzadeh, S., et al. (2010). NF1 is a tumor suppressor in neuroblastoma that determines retinoic acid response and disease outcome. Cell *142*, 218–229.

Horsley, V., Friday, B.B., Matteson, S., Kegley, K.M., Gephart, J., and Pavlath, G.K. (2001). Regulation of the growth of multinucleated muscle cells by an NFATC2-dependent pathway. J. Cell Biol. *153*, 329–338.

Horsley, V., Jansen, K.M., Mills, S.T., and Pavlath, G.K. (2003). IL-4 acts as a myoblast recruitment factor during mammalian muscle growth. Cell *113*, 483–494.

Huang, J., and Manning, B.D. (2009). A complex interplay between Akt, TSC2 and the two mTOR complexes. Biochem. Soc. Trans. *37*, 217–222.

Hudson, M.B., and Price, S.R. (2013). Calcineurin: a poorly understood regulator of muscle mass. Int. J. Biochem. Cell Biol. *45*, 2173–2178.

Hunter, T. (1997). Oncoprotein networks. Cell *88*, 333–346.

Ikeda, F., Nishimura, R., Matsubara, T., Tanaka, S., Inoue, J., Reddy, S.V., Hata, K., Yamashita, K., Hiraga, T., Watanabe, T., et al. (2004). Critical roles of c-Jun signaling in regulation of NFAT family and RANKL-regulated osteoclast differentiation. J. Clin. Invest. *114*, 475–484.

Ingalls, C.P. (2004). Nature vs. nurture: can exercise really alter fiber type composition in human skeletal muscle? J. Appl. Physiol. Bethesda Md 1985 *97*, 1591–1592.

Ismat, F.A., Xu, J., Lu, M.M., and Epstein, J.A. (2006). The neurofibromin GAP-related domain rescues endothelial but not neural crest development in Nf1 mice. J. Clin. Invest. *116*, 2378–2384.

Izawa, I., Tamaki, N., and Saya, H. (1996). Phosphorylation of neurofibromatosis type 1 gene product (neurofibromin) by cAMP-dependent protein kinase. FEBS Lett. *382*, 53–59.

Jang, Y.C., Sinha, M., Cerletti, M., Dall'Osso, C., and Wagers, A.J. (2011). Skeletal muscle stem cells: effects of aging and metabolism on muscle regenerative function. Cold Spring Harb. Symp. Quant. Biol. *76*, 101–111.

Jiang, B.H., Zheng, J.Z., and Vogt, P.K. (1998). An essential role of phosphatidylinositol 3-kinase in myogenic differentiation. Proc. Natl. Acad. Sci. U. S. A. *95*, 14179–14183.

Jo, C., Jang, B.G., and Jo, S.A. (2009). MEK1 plays contrary stage-specific roles in skeletal myogenic differentiation. Cell. Signal. *21*, 1910–1917.

Johannessen, C.M., Reczek, E.E., James, M.F., Brems, H., Legius, E., and Cichowski, K. (2005). The NF1 tumor suppressor critically regulates TSC2 and mTOR. Proc. Natl. Acad. Sci. U. S. A. *102*, 8573–8578.

Johnson, B.A., MacWilliams, B.A., Carey, J.C., Viskochil, D.H., D'Astous, J.L., and Stevenson, D.A. (2010). Motor proficiency in children with neurofibromatosis type 1. Pediatr. Phys. Ther. Off. Publ. Sect. Pediatr. Am. Phys. Ther. Assoc. *22*, 344–348.

Johnson, B.A., Macwilliams, B., Carey, J.C., Viskochil, D.H., D'Astous, J.L., and Stevenson, D.A. (2012). Lower extremity strength and hopping and jumping ground reaction forces in children with neurofibromatosis type 1. Hum. Mov. Sci. *31*, 247–254.

Jones, N.C., Tyner, K.J., Nibarger, L., Stanley, H.M., Cornelison, D.D.W., Fedorov, Y.V., and Olwin, B.B. (2005). The p38alpha/beta MAPK functions as a molecular switch to activate the quiescent satellite cell. J. Cell Biol. *169*, 105–116.

Jorge, A.A.L., Malaquias, A.C., Arnhold, I.J.P., and Mendonca, B.B. (2009). Noonan syndrome and related disorders: a review of clinical features and mutations in genes of the RAS/MAPK pathway. Horm. Res. *71*, 185–193.

Kaneko, J.J., Harvey, J.W., and Bruss, M. (1997). Clinical Biochemistry of Domestic Animals (Gulf Professional Publishing).

Karasik, D., and Kiel, D.P. (2008). Genetics of the musculoskeletal system: a pleiotropic approach. J. Bone Miner. Res. Off. J. Am. Soc. Bone Miner. Res. *23*, 788–802.

Karasik, D., and Kiel, D.P. (2010). Evidence for pleiotropic factors in genetics of the musculoskeletal system. Bone *46*, 1226–1237.

Kardon, G., Campbell, J.K., and Tabin, C.J. (2002). Local extrinsic signals determine muscle and endothelial cell fate and patterning in the vertebrate limb. Dev. Cell *3*, 533–545.

Kettelhut, I.C., Wing, S.S., and Goldberg, A.L. (1988). Endocrine regulation of protein breakdown in skeletal muscle. Diabetes. Metab. Rev. *4*, 751–772.

Keyser, R.E. (2010). Peripheral fatigue: high-energy phosphates and hydrogen ions. PM R *2*, 347–358.

Knight, J.D., and Kothary, R. (2011). The myogenic kinome: protein kinases critical to mammalian skeletal myogenesis. Skelet. Muscle *1*, 29.

Knothe Tate, M.L., Adamson, J.R., Tami, A.E., and Bauer, T.W. (2004). The osteocyte. Int. J. Biochem. Cell Biol. *36*, 1–8.

Kolanczyk, M., Kossler, N., Kühnisch, J., Lavitas, L., Stricker, S., Wilkening, U., Manjubala, I., Fratzl, P., Spörle, R., Herrmann, B.G., et al. (2007). Multiple roles for neurofibromin in skeletal development and growth. Hum. Mol. Genet. *16*, 874–886.

Kolanczyk, M., Kühnisch, J., Kossler, N., Osswald, M., Stumpp, S., Thurisch, B., Kornak, U., and Mundlos, S. (2008). Modelling neurofibromatosis type 1 tibial dysplasia and its treatment with lovastatin. BMC Med. *6*, 21.

Kolch, W. (2000). Meaningful relationships: the regulation of the Ras/Raf/MEK/ERK pathway by protein interactions. Biochem. J. *351 Pt 2*, 289–305.

Koopman, R., Ly, C.H., and Ryall, J.G. (2014). A metabolic link to skeletal muscle wasting and regeneration. Front. Physiol. *5*, 32.

Koressaar, T., and Remm, M. (2007). Enhancements and modifications of primer design program Primer3. Bioinforma. Oxf. Engl. *23*, 1289–1291.

Korf, B.R. (2002). Clinical features and pathobiology of neurofibromatosis 1. J. Child Neurol. *17*, 573–577; discussion 602–604, 646–651.

Kossler, N. (2010). Funktionelle Charakterisierung von Neurofibromin in der Entwicklung des muskuloskelettalen Systems. Dissertation, Freie Universität Berlin.

Kossler, N., Stricker, S., Rödelsperger, C., Robinson, P.N., Kim, J., Dietrich, C., Osswald, M., Kühnisch, J., Stevenson, D.A., Braun, T., et al. (2011a). Neurofibromin (Nf1) is required for skeletal muscle development. Hum. Mol. Genet. *20*, 2697–2709.

Kowluru, R.A., Santos, J.M., and Mishra, M. (2013). Epigenetic modifications and diabetic retinopathy. BioMed Res. Int. *2013*, 635284.

Kraft, C.S., LeMoine, C.M.R., Lyons, C.N., Michaud, D., Mueller, C.R., and Moyes, C.D. (2006). Control of mitochondrial biogenesis during myogenesis. Am. J. Physiol. Cell Physiol. *290*, C1119–1127.

Krone, W., Mao, R., Mühleck, O.S., Kling, H., and Fink, T. (1986). Cell culture studies on neurofibromatosis (von Recklinghausen). Characterization of cells growing from neurofibromas. Ann. N. Y. Acad. Sci. *486*, 354–370.

Kuang, S., Kuroda, K., Le Grand, F., and Rudnicki, M.A. (2007). Asymmetric self-renewal and commitment of satellite stem cells in muscle. Cell *129*, 999–1010.

Kühnisch, J., Seto, J., Lange, C., Schrof, S., Stumpp, S., Kobus, K., Grohmann, J., Kossler, N., Varga, P., Osswald, M., et al. (2014). Multiscale, converging defects of macro-porosity, microstructure and matrix mineralization impact long bone fragility in NF1. PloS One *9*, e86115.

Laclef, C., Hamard, G., Demignon, J., Souil, E., Houbron, C., and Maire, P. (2003). Altered myogenesis in Six1-deficient mice. Dev. Camb. Engl. *130*, 2239–2252.

Lai, K.-M.V., Gonzalez, M., Poueymirou, W.T., Kline, W.O., Na, E., Zlotchenko, E., Stitt, T.N., Economides, A.N., Yancopoulos, G.D., and Glass, D.J. (2004). Conditional activation of akt in adult skeletal muscle induces rapid hypertrophy. Mol. Cell. Biol. *24*, 9295–9304.

Lander, A.D., Kimble, J., Clevers, H., Fuchs, E., Montarras, D., Buckingham, M., Calof, A.L., Trumpp, A., and Oskarsson, T. (2012). What does the concept of the stem cell niche really mean today? BMC Biol. *10*, 19.

Larizza, L., Gervasini, C., Natacci, F., and Riva, P. (2009). Developmental abnormalities and cancer predisposition in neurofibromatosis type 1. Curr. Mol. Med. *9*, 634–653.

Latil, M., Rocheteau, P., Châtre, L., Sanulli, S., Mémet, S., Ricchetti, M., Tajbakhsh, S., and Chrétien, F. (2012). Skeletal muscle stem cells adopt a dormant cell state post mortem and retain regenerative capacity. Nat. Commun. *3*, 903.

Leary, S.C., Battersby, B.J., Hansford, R.G., and Moyes, C.D. (1998). Interactions between bioenergetics and mitochondrial biogenesis. Biochim. Biophys. Acta *1365*, 522–530.

Leek, B.T., Mudaliar, S.R., Henry, R., Mathieu-Costello, O., and Richardson, R.S. (2001). Effect of acute exercise on citrate synthase activity in untrained and trained human skeletal muscle. Am. J. Physiol. Regul. Integr. Comp. Physiol. *280*, R441–447.

Li, C., Cheng, Y., Gutmann, D.A., and Mangoura, D. (2001). Differential localization of the neurofibromatosis 1 (NF1) gene product, neurofibromin, with the F-actin or microtubule cytoskeleton during differentiation of telencephalic neurons. Brain Res. Dev. Brain Res. *130*, 231–248.

Li, L., Stefan, M.I., and Le Novère, N. (2012). Calcium input frequency, duration and amplitude differentially modulate the relative activation of calcineurin and CaMKII. PloS One *7*, e43810.

Lindquist (2011). PAG-RasGAP, http://informatik.med.uni-magdeburg.de /unimagdeburg /Institute /Molekulare+ und+ Klinische+ Immunologie.

Liu, L., Zhang, J., Yuan, J., Dang, Y., Yang, C., Chen, X., Xu, J., and Yu, L. (2005). Characterization of a human regulatory subunit of protein phosphatase 3 gene (PPP3RL) expressed specifically in testis. Mol. Biol. Rep. *32*, 41–45.

Lobe, C.G., and Nagy, A. (1998). Conditional genome alteration in mice. BioEssays News Rev. Mol. Cell. Dev. Biol. *20*, 200–208.

Lodish, H., Berk, A., Zipursky, S.L., Matsudaira, P., Baltimore, D., and Darnell, J. (2000). Muscle: A Specialized Contractile Machine. In Molecular Cell Biology, (New York: W.H.Freeman),.

Logan, M., Martin, J.F., Nagy, A., Lobe, C., Olson, E.N., and Tabin, C.J. (2002). Expression of Cre Recombinase in the developing mouse limb bud driven by a Prxl enhancer. Genes. N. Y. N 2000 *33*, 77–80.

Lu, C., and Thompson, C.B. (2012). Metabolic regulation of epigenetics. Cell Metab. *16*, 9–17.

Lunt, S.Y., and Vander Heiden, M.G. (2011). Aerobic glycolysis: meeting the metabolic requirements of cell proliferation. Annu. Rev. Cell Dev. Biol. *27*, 441–464.

Lyons, C.N., Leary, S.C., and Moyes, C.D. (2004). Bioenergetic remodeling during cellular differentiation: changes in cytochrome c oxidase regulation do not affect the metabolic phenotype. Biochem. Cell Biol. Biochim. Biol. Cell. *82*, 391–399.

Malhotra, R., and Ratner, N. (1994). Localization of neurofibromin to keratinocytes and melanocytes in developing rat and human skin. J. Invest. Dermatol. *102*, 812–818.

Von Maltzahn, J., Jones, A.E., Parks, R.J., and Rudnicki, M.A. (2013). Pax7 is critical for the normal function of satellite cells in adult skeletal muscle. Proc. Natl. Acad. Sci. U. S. A. *110*, 16474–16479.

Manzano, R., Toivonen, J.M., Calvo, A.C., Miana-Mena, F.J., Zaragoza, P., Muñoz, M.J., Montarras, D., and Osta, R. (2011). Sex, fiber-type, and age dependent in vitro proliferation of mouse muscle satellite cells. J. Cell. Biochem. *112*, 2825–2836.

Marchuk, D.A., Saulino, A.M., Tavakkol, R., Swaroop, M., Wallace, M.R., Andersen, L.B., Mitchell, A.L., Gutmann, D.H., Boguski, M., and Collins, F.S. (1991). cDNA cloning of the type 1 neurofibromatosis gene: complete sequence of the NF1 gene product. Genomics *11*, 931–940.

Marieb, E.N., and Hoehn, K. (2010). Human Anatomy and Physiology (Benjamin Cummings).

Marshall, C.J. (1995a). Specificity of receptor tyrosine kinase signaling: transient versus sustained extracellular signal-regulated kinase activation. Cell *80*, 179–185.

Marshall, M.S. (1995b). Ras target proteins in eukaryotic cells. FASEB J. Off. Publ. Fed. Am. Soc. Exp. Biol. *9*, 1311–1318.

Martin, G.A., Viskochil, D., Bollag, G., McCabe, P.C., Crosier, W.J., Haubruck, H., Conroy, L., Clark, R., O'Connell, P., and Cawthon, R.M. (1990). The GAP-related domain of the neurofibromatosis type 1 gene product interacts with ras p21. Cell *63*, 843–849.

Mautner, V.F., Friedrich, R.E., von Deimling, A., Hagel, C., Korf, B., Knöfel, M.T., Wenzel, R., and Fünsterer, C. (2003). Malignant peripheral nerve sheath tumours in neurofibromatosis type 1: MRI supports the diagnosis of malignant plexiform neurofibroma. Neuroradiology *45*, 618–625.

Mayes, D.A., Rizvi, T.A., Titus-Mitchell, H., Oberst, R., Ciraolo, G.M., Vorhees, C.V., Robinson, A.P., Miller, S.D., Cancelas, J.A., Stemmer-Rachamimov, A.O., et al. (2013). Nf1 loss and Ras hyperactivation in oligodendrocytes induce NOS-driven defects in myelin and vasculature. Cell Rep. *4*, 1197–1212.

Menges, C.W., and McCance, D.J. (2008). Constitutive activation of the Raf-MAPK pathway causes negative feedback inhibition of Ras-PI3K-AKT and cellular arrest through the EphA2 receptor. Oncogene *27*, 2934–2940.

Messina, G., Biressi, S., Monteverde, S., Magli, A., Cassano, M., Perani, L., Roncaglia, E., Tagliafico, E., Starnes, L., Campbell, C.E., et al. (2010). Nfix regulates fetal-specific transcription in developing skeletal muscle. Cell *140*, 554–566.

Mieczkowska, A., Baslé, M.F., Chappard, D., and Mabilleau, G. (2012). Thiazolidinediones induce osteocyte apoptosis by a G protein-coupled receptor 40-dependent mechanism. J. Biol. Chem. *287*, 23517–23526.

Minetti, G.C., Feige, J.N., Bombard, F., Heier, A., Morvan, F., Nürnberg, B., Leiss, V., Birnbaumer, L., Glass, D.J., and Fornaro, M. (2014). Gαi2 signaling is required for skeletal muscle growth, regeneration, and satellite cell proliferation and differentiation. Mol. Cell. Biol. *34*, 619–630.

Miniou, P., Tiziano, D., Frugier, T., Roblot, N., Le Meur, M., and Melki, J. (1999). Gene targeting restricted to mouse striated muscle lineage. Nucleic Acids Res. *27*, e27.

Mitin, N., Ramocki, M.B., Konieczny, S.F., and Taparowsky, E.J. (2001). Ras regulation of skeletal muscle differentiation and gene expression. Methods Enzymol. *333*, 232–247.

Mologhoni, F., de Melo, F.H.M., da Silva, C.T., and Jasiulionis, M.G. (2013). Ras and Rac1, frequently mutated in melanomas, are activated by superoxide anion, modulate Dnmt1 level and are causally related to melanocyte malignant transformation. PloS One *8*, e81937.

Morrison, T.B., Weis, J.J., and Wittwer, C.T. (1998). Quantification of low-copy transcripts by continuous SYBR Green I monitoring during amplification. BioTechniques *24*, 954–958, 960, 962.

Mu, X., Brown, L.D., Liu, Y., and Schneider, M.F. (2007). Roles of the calcineurin and CaMK signaling pathways in fast-to-slow fiber type transformation of cultured adult mouse skeletal muscle fibers. Physiol. Genomics *30*, 300–312.

Murgia, M., Serrano, A.L., Calabria, E., Pallafacchina, G., Lomo, T., and Schiaffino, S. (2000). Ras is involved in nerve-activity-dependent regulation of muscle genes. Nat. Cell Biol. *2*, 142–147.

Murphy, M., and Kardon, G. (2011). Origin of vertebrate limb muscle: the role of progenitor and myoblast populations. Curr. Top. Dev. Biol. *96*, 1–32.

Murphy, M.M., Lawson, J.A., Mathew, S.J., Hutcheson, D.A., and Kardon, G. (2011). Satellite cells, connective tissue fibroblasts and their interactions are crucial for muscle regeneration. Dev. Camb. Engl. *138*, 3625–3637.

Muzumdar, M.D., Tasic, B., Miyamichi, K., Li, L., and Luo, L. (2007). A global double-fluorescent Cre reporter mouse. Genes. N. Y. N 2000 *45*, 593–605.

Naya, F.J., Mercer, B., Shelton, J., Richardson, J.A., Williams, R.S., and Olson, E.N. (2000). Stimulation of slow skeletal muscle fiber gene expression by calcineurin in vivo. J. Biol. Chem. *275*, 4545–4548.

Nguyen, P., Leray, V., Diez, M., Serisier, S., Le Bloc'h, J., Siliart, B., and Dumon, H. (2008). Liver lipid metabolism. J. Anim. Physiol. Anim. Nutr. *92*, 272–283.

Nilwik, R., Snijders, T., Leenders, M., Groen, B.B.L., van Kranenburg, J., Verdijk, L.B., and van Loon, L.J.C. (2013). The decline in skeletal muscle mass with aging is mainly attributed to a reduction in type II muscle fiber size. Exp. Gerontol. *48*, 492–498.

North, K.N. (1998). Clinical aspects of neurofibromatosis 1. Eur. J. Paediatr. Neurol. EJPN Off. J. Eur. Paediatr. Neurol. Soc. *2*, 223–231.

O'Neill, H.M. (2013). AMPK and Exercise: Glucose Uptake and Insulin Sensitivity. Diabetes Metab. J. *37*, 1–21.

Ono, Y., Masuda, S., Nam, H.-S., Benezra, R., Miyagoe-Suzuki, Y., and Takeda, S. (2012). Slow-dividing satellite cells retain long-term self-renewal ability in adult muscle. J. Cell Sci. *125*, 1309–1317.

Ontell, M., Ontell, M.P., and Buckingham, M. (1995). Muscle-specific gene expression during myogenesis in the mouse. Microsc. Res. Tech. *30*, 354–365.

Pan, F., Sun, L., Kardian, D.B., Whartenby, K.A., Pardoll, D.M., and Liu, J.O. (2007). Feedback inhibition of calcineurin and Ras by a dual inhibitory protein Carabin. Nature *445*, 433–436.

Parsons, S.A., Wilkins, B.J., Bueno, O.F., and Molkentin, J.D. (2003). Altered skeletal muscle phenotypes in calcineurin Aalpha and Abeta gene-targeted mice. Mol. Cell. Biol. *23*, 4331–4343.

Peltonen, J., Jaakkola, S., Lebwohl, M., Renvall, S., Risteli, L., Virtanen, I., and Uitto, J. (1988). Cellular differentiation and expression of matrix genes in type 1 neurofibromatosis. Lab. Investig. J. Tech. Methods Pathol. *59*, 760–771.

Petramala, L., Giustini, S., Zinnamosca, L., Marinelli, C., Colangelo, L., Cilenti, G., Formicuccia, M.C., D'Erasmo, E., Calvieri, S., and Letizia, C. (2012). Bone mineral metabolism in patients with neurofibromatosis type 1 (von Recklingausen disease). Arch. Dermatol. Res. *304*, 325–331.

Pfaffl, M.W. (2001). A new mathematical model for relative quantification in real-time RT-PCR. Nucleic Acids Res. *29*, e45.

Pfeiffer, T., Schuster, S., and Bonhoeffer, S. (2001). Cooperation and competition in the evolution of ATP-producing pathways. Science *292*, 504–507.

Picard, C.A., and Marcelle, C. (2013). Two distinct muscle progenitor populations coexist throughout amniote development. Dev. Biol. *373*, 141–148.

Pierro, C., Cook, S.J., Foets, T.C.F., Bootman, M.D., and Roderick, H.L. (2014). Oncogenic K-Ras suppresses IP_3-dependent Ca^{2+} release through remodelling of the isoform composition of IP_3Rs and ER luminal Ca^{2+} levels in colorectal cancer cell lines. J. Cell Sci. *127*, 1607–1619.

Poole, R.M. (1986). The Incredible machine (Washington, D.C: The National Geographic Society).

Porras, A., Hernández, E.R., and Benito, M. (1996). Ras proteins mediate induction of uncoupling protein, IGF-I, and IGF-I receptor in rat fetal brown adipocyte cell lines. DNA Cell Biol. *15*, 921–928.

Puigserver, P., and Spiegelman, B.M. (2003). Peroxisome proliferator-activated receptor-gamma coactivator 1 alpha (PGC-1 alpha): transcriptional coactivator and metabolic regulator. Endocr. Rev. *24*, 78–90.

Quiat, D., Voelker, K.A., Pei, J., Grishin, N.V., Grange, R.W., Bassel-Duby, R., and Olson, E.N. (2011). Concerted regulation of myofiber-specific gene expression and muscle performance by the transcriptional repressor Sox6. Proc. Natl. Acad. Sci. U. S. A. *108*, 10196–10201.

Raben, N., Wong, A., Ralston, E., and Myerowitz, R. (2012). Autophagy and mitochondria in Pompe disease: nothing is so new as what has long been forgotten. Am. J. Med. Genet. C Semin. Med. Genet. *160C*, 13–21.

Rana, Z.A., Gundersen, K., and Buonanno, A. (2008). Activity-dependent repression of muscle genes by NFAT. Proc. Natl. Acad. Sci. U. S. A. *105*, 5921–5926.

De Rasmo, D., Signorile, A., Roca, E., and Papa, S. (2009). cAMP response element-binding protein (CREB) is imported into mitochondria and promotes protein synthesis. FEBS J. *276*, 4325–4333.

Relaix, F., Rocancourt, D., Mansouri, A., and Buckingham, M. (2005). A Pax3/Pax7-dependent population of skeletal muscle progenitor cells. Nature *435*, 948–953.

Riccardi, V.M. (2000). Histogenesis control genes: embryology, wound-healing, and NF1. Teratology *62*, 4.

Riccardi, V.M. (2010). Neurofibromatosis type 1 is a disorder of dysplasia: the importance of distinguishing features, consequences, and complications. Birt. Defects Res. A. Clin. Mol. Teratol. *88*, 9–14.

Ríos, M., Foretz, M., Viollet, B., Prieto, A., Fraga, M., Costoya, J.A., and Señarís, R. (2013). AMPK activation by oncogenesis is required to maintain cancer cell proliferation in astrocytic tumors. Cancer Res. *73*, 2628–2638.

Rizvi, T.A., Akunuru, S., de Courten-Myers, G., Switzer, R.C., 3rd, Nordlund, M.L., and Ratner, N. (1999). Region-specific astrogliosis in brains of mice heterozygous for mutations in the neurofibromatosis type 1 (Nf1) tumor suppressor. Brain Res. *816*, 111–123.

Rizvi, T.A., Huang, Y., Sidani, A., Atit, R., Largaespada, D.A., Boissy, R.E., and Ratner, N. (2002). A Novel Cytokine Pathway Suppresses Glial Cell Melanogenesis after Injury to Adult Nerve. J. Neurosci. Off. J. Soc. Neurosci. *22*, 9831–9840.

Rocheteau, P., Gayraud-Morel, B., Siegl-Cachedenier, I., Blasco, M.A., and Tajbakhsh, S. (2012). A subpopulation of adult skeletal muscle stem cells retains all template DNA strands after cell division. Cell *148*, 112–125.

Rommel, C., Clarke, B.A., Zimmermann, S., Nuñez, L., Rossman, R., Reid, K., Moelling, K., Yancopoulos, G.D., and Glass, D.J. (1999). Differentiation stage-specific inhibition of the Raf-MEK-ERK pathway by Akt. Science *286*, 1738–1741.

Ruggieri, M., Pavone, V., De Luca, D., Franzò, A., Tiné, A., and Pavone, L. (1999). Congenital bone malformations in patients with neurofibromatosis type 1 (Nf1). J. Pediatr. Orthop. *19*, 301–305.

Di Ruscio, A., Ebralidze, A.K., Benoukraf, T., Amabile, G., Goff, L.A., Terragni, J., Figueroa, M.E., De Figueiredo Pontes, L.L., Alberich-Jorda, M., Zhang, P., et al. (2013). DNMT1-interacting RNAs block gene-specific DNA methylation. Nature *503*, 371–376.

Russell, A.P., Foletta, V.C., Snow, R.J., and Wadley, G.D. (2014). Skeletal muscle mitochondria: a major player in exercise, health and disease. Biochim. Biophys. Acta *1840*, 1276–1284.

Ryall, J.G. (2013). Metabolic reprogramming as a novel regulator of skeletal muscle development and regeneration. FEBS J. *280*, 4004–4013.

Ryall, J.G., Schertzer, J.D., and Lynch, G.S. (2007). Attenuation of age-related muscle wasting and weakness in rats after formoterol treatment: therapeutic implications for sarcopenia. J. Gerontol. A. Biol. Sci. Med. Sci. *62*, 813–823.

Ryall, J.G., Schertzer, J.D., and Lynch, G.S. (2008). Cellular and molecular mechanisms underlying age-related skeletal muscle wasting and weakness. Biogerontology *9*, 213–228.

Sahoo, S.K., Shaikh, S.A., Sopariwala, D.H., Bal, N.C., and Periasamy, M. (2013). Sarcolipin protein interaction with sarco(endo)plasmic reticulum Ca2+ ATPase (SERCA) is distinct from phospholamban protein, and only sarcolipin can promote uncoupling of the SERCA pump. J. Biol. Chem. *288*, 6881–6889.

Sambasivan, R., Yao, R., Kissenpfennig, A., Van Wittenberghe, L., Paldi, A., Gayraud-Morel, B., Guenou, H., Malissen, B., Tajbakhsh, S., and Galy, A. (2011). Pax7-expressing satellite cells are indispensable for adult skeletal muscle regeneration. Dev. Camb. Engl. *138*, 3647–3656.

Samuelsson, B., and Riccardi, V.M. (1989). Neurofibromatosis in Gothenburg, Sweden. III. Psychiatric and social aspects. Neurofibromatosis *2*, 84–106.

Sanes, J.R. (2003). The basement membrane/basal lamina of skeletal muscle. J. Biol. Chem. *278*, 12601–12604.

Sassoon, D., Lyons, G., Wright, W.E., Lin, V., Lassar, A., Weintraub, H., and Buckingham, M. (1989). Expression of two myogenic regulatory factors myogenin and MyoD1 during mouse embryogenesis. Nature *341*, 303–307.

Schiaffino, S., and Serrano, A. (2002). Calcineurin signaling and neural control of skeletal muscle fiber type and size. Trends Pharmacol. Sci. *23*, 569–575.

Schindeler, A., and Little, D.G. (2008). Recent insights into bone development, homeostasis, and repair in type 1 neurofibromatosis (NF1). Bone *42*, 616–622.

Schlossberg, L., and Zuidema, G.D. (1997). The Johns Hopkins Atlas of Human Functional Anatomy (JHU Press).

Schmitteckert, S., Ziegler, C., Kartes, L., and Rolletschek, A. (2011). Transcription Factor Lbx1 Expression in Mouse Embryonic Stem Cell-Derived Phenotypes. Stem Cells Int. *2011*.

Scholzen, T., and Gerdes, J. (2000). The Ki-67 protein: from the known and the unknown. J. Cell. Physiol. *182*, 311–322.

Schweitzer, R., Zelzer, E., and Volk, T. (2010). Connecting muscles to tendons: tendons and musculoskeletal development in flies and vertebrates. Dev. Camb. Engl. *137*, 2807–2817.

Seale, P., Sabourin, L.A., Girgis-Gabardo, A., Mansouri, A., Gruss, P., and Rudnicki, M.A. (2000). Pax7 is required for the specification of myogenic satellite cells. Cell *102*, 777–786.

Seipel, K., and Schmid, V. (2005). Evolution of striated muscle: jellyfish and the origin of triploblasty. Dev. Biol. *282*, 14–26.

Serrano, A.L., Murgia, M., Pallafacchina, G., Calabria, E., Coniglio, P., Lømo, T., and Schiaffino, S. (2001). Calcineurin controls nerve activity-dependent specification of slow skeletal muscle fibers but not muscle growth. Proc. Natl. Acad. Sci. U. S. A. *98*, 13108–13113.

Serrano, M., Lin, A.W., McCurrach, M.E., Beach, D., and Lowe, S.W. (1997). Oncogenic ras provokes premature cell senescence associated with accumulation of p53 and p16INK4a. Cell *88*, 593–602.

Sharir, A., Stern, T., Rot, C., Shahar, R., and Zelzer, E. (2011). Muscle force regulates bone shaping for optimal load-bearing capacity during embryogenesis. Dev. Camb. Engl. *138*, 3247–3259.

Shea, K.L., Xiang, W., LaPorta, V.S., Licht, J.D., Keller, C., Basson, M.A., and Brack, A.S. (2010). Sprouty1 regulates reversible quiescence of a self-renewing adult muscle stem cell pool during regeneration. Cell Stem Cell *6*, 117–129.

Shin, S.-Y., Yang, H.W., Kim, J.-R., Heo, W.D., and Cho, K.-H. (2011). A hidden incoherent switch regulates RCAN1 in the calcineurin-NFAT signaling network. J. Cell Sci. *124*, 82–90.

Shwartz, Y., Farkas, Z., Stern, T., Aszódi, A., and Zelzer, E. (2012). Muscle contraction controls skeletal morphogenesis through regulation of chondrocyte convergent extension. Dev. Biol. *370*, 154–163.

Shwartz, Y., Blitz, E., and Zelzer, E. (2013). One load to rule them all: mechanical control of the musculoskeletal system in development and aging. Differ. Res. Biol. Divers. *86*, 104–111.

Souza, J.F., Passos, R.L.F., Guedes, A.C.M., Rezende, N.A., and Rodrigues, L.O.C. (2009). Muscular force is reduced in neurofibromatosis type 1. J. Musculoskelet. Neuronal Interact. *9*, 15–17.

Srinivasan, S., Ausk, B.J., Prasad, J., Threet, D., Bain, S.D., Richardson, T.S., and Gross, T.S. (2010). Rescuing loading induced bone formation at senescence. PLoS Comput. Biol. *6*.

Steelman, L.S., Franklin, R.A., Abrams, S.L., Chappell, W., Kempf, C.R., Bäsecke, J., Stivala, F., Donia, M., Fagone, P., Nicoletti, F., et al. (2011). Roles of the Ras/Raf/MEK/ERK pathway in leukemia therapy. Leukemia *25*, 1080–1094.

Steinberg, G.R., and Kemp, B.E. (2009). AMPK in Health and Disease. Physiol. Rev. *89*, 1025–1078.

Stevenson, D.A., and Yang, F.-C. (2011). The musculoskeletal phenotype of the RASopathies. Am. J. Med. Genet. C Semin. Med. Genet. *157C*, 90–103.

Stevenson, D.A., Birch, P.H., Friedman, J.M., Viskochil, D.H., Balestrazzi, P., Boni, S., Buske, A., Korf, B.R., Niimura, M., Pivnick, E.K., et al. (1999). Descriptive analysis of tibial pseudarthrosis in patients with neurofibromatosis 1. Am. J. Med. Genet. *84*, 413–419.

Stevenson, D.A., Moyer-Mileur, L.J., Carey, J.C., Quick, J.L., Hoff, C.J., and Viskochil, D.H. (2005). Case-control study of the muscular compartments and osseous strength in neurofibromatosis type 1 using peripheral quantitative computed tomography. J. Musculoskelet. Neuronal Interact. *5*, 145–149.

Stevenson, D.A., Zhou, H., Ashrafi, S., Messiaen, L.M., Carey, J.C., D'Astous, J.L., Santora, S.D., and Viskochil, D.H. (2006). Double inactivation of NF1 in tibial pseudarthrosis. Am. J. Hum. Genet. *79*, 143–148.

Stevenson, D.A., Allen, S., Tidyman, W.E., Carey, J.C., Viskochil, D.H., Stevens, A., Hanson, H., Sheng, X., Thompson, B.A., Okumura, M.J., et al. (2012). Peripheral muscle weakness in RASopathies. Muscle Nerve *46*, 394–399.

Stocker, K.M., Baizer, L., Coston, T., Sherman, L., and Ciment, G. (1995). Regulated expression of neurofibromin in migrating neural crest cells of avian embryos. J. Neurobiol. *27*, 535–552.

Stupka, N., Plant, D.R., Schertzer, J.D., Emerson, T.M., Bassel-Duby, R., Olson, E.N., and Lynch, G.S. (2006). Activated calcineurin ameliorates contraction-induced injury to skeletal muscles of mdx dystrophic mice. J. Physiol. *575*, 645–656.

Sullivan, K., El-Hoss, J., Quinlan, K.G.R., Deo, N., Garton, F., Seto, J.T.C., Gdalevitch, M., Turner, N., Cooney, G.J., Kolanczyk, M., et al. (2014). NF1 is a critical regulator of muscle development and metabolism. Hum. Mol. Genet. *23*, 1250–1259.

Szent-Gyorgyi, A.G. (1975). Calcium regulation of muscle contraction. Biophys. J. *15*, 707–723.

Takayanagi, H. (2006). Amazing multifunctionality of calcineurin and NFAT signaling in bone homeostasis. BoneKEy-Osteovision *3*, 28–31.

Tallquist, M.D., Weismann, K.E., Hellström, M., and Soriano, P. (2000). Early myotome specification regulates PDGFA expression and axial skeleton development. Dev. Camb. Engl. *127*, 5059–5070.

Termin, A., Staron, R.S., and Pette, D. (1989). Changes in myosin heavy chain isoforms during chronic low-frequency stimulation of rat fast hindlimb muscles. A single-fiber study. Eur. J. Biochem. FEBS *186*, 749–754.

Tokuo, H., Yunoue, S., Feng, L., Kimoto, M., Tsuji, H., Ono, T., Saya, H., and Araki, N. (2001). Phosphorylation of neurofibromin by cAMP-dependent protein kinase is regulated via a cellular association of N(G),N(G)-dimethylarginine dimethylaminohydrolase. FEBS Lett. *494*, 48–53.

Tonsgard, J.H. (2006). Clinical manifestations and management of neurofibromatosis type 1. Semin. Pediatr. Neurol. *13*, 2–7.

Untergasser, A., Cutcutache, I., Koressaar, T., Ye, J., Faircloth, B.C., Remm, M., and Rozen, S.G. (2012). Primer3--new capabilities and interfaces. Nucleic Acids Res. *40*, e115.

Vasyutina, E., Lenhard, D.C., Wende, H., Erdmann, B., Epstein, J.A., and Birchmeier, C. (2007). RBP-J (Rbpsuh) is essential to maintain muscle progenitor cells and to generate satellite cells. Proc. Natl. Acad. Sci. U. S. A. *104*, 4443–4448.

Vega, R.B., Huss, J.M., and Kelly, D.P. (2000). The coactivator PGC-1 cooperates with peroxisome proliferator-activated receptor alpha in transcriptional control of nuclear genes encoding mitochondrial fatty acid oxidation enzymes. Mol. Cell. Biol. *20*, 1868–1876.

Viard, P., Butcher, A.J., Halet, G., Davies, A., Nürnberg, B., Heblich, F., and Dolphin, A.C. (2004). PI3K promotes voltage-dependent calcium channel trafficking to the plasma membrane. Nat. Neurosci. *7*, 939–946.

Walker, S.M., and Schrodt, G.R. (1967). Contraction of skeletal muscle. Am. J. Phys. Med. *46*, 151–172.

Wan, Y. (2010). PPARγ in bone homeostasis. Trends Endocrinol. Metab. TEM *21*, 722–728.

Wasserman, K., Beaver, W.L., Davis, J.A., Pu, J.Z., Heber, D., and Whipp, B.J. (1985). Lactate, pyruvate, and lactate-to-pyruvate ratio during exercise and recovery. J. Appl. Physiol. Bethesda Md 1985 *59*, 935–940.

Wegener, E. (2009). Identification of a potential biomarker of Neurofibromatosis type 1 implicated in regulation of bone and cartilage metabolism. Diplomarbeit, Martin-Luther-Universität Halle-Wittenberg.

White, R.B., Biérinx, A.-S., Gnocchi, V.F., and Zammit, P.S. (2010). Dynamics of muscle fibre growth during postnatal mouse development. BMC Dev. Biol. *10*, 21.

Wigmore, P.M., and Dunglison, G.F. (1998). The generation of fiber diversity during myogenesis. Int. J. Dev. Biol. *42*, 117–125.

Williamson, D.L., Butler, D.C., and Alway, S.E. (2009). AMPK inhibits myoblast differentiation through a PGC-1alpha-dependent mechanism. Am. J. Physiol. Endocrinol. Metab. *297*, E304–314.

Wilmore, J.H., and Costill, D.L. (2005). Physiology of Sport and Exercise (Champaign, IL: Human Kinetics Publishers).

Wimmer, K. (2005). [Neurofibromatosis: the most frequent hereditary tumor predisposition syndrome]. Wien. Med. Wochenschr. 1946 *155*, 273–280.

Winder, W.W. (2001). Energy-sensing and signaling by AMP-activated protein kinase in skeletal muscle. J. Appl. Physiol. Bethesda Md 1985 *91*, 1017–1028.

Winder, W.W., Holmes, B.F., Rubink, D.S., Jensen, E.B., Chen, M., and Holloszy, J.O. (2000). Activation of AMP-activated protein kinase increases mitochondrial enzymes in skeletal muscle. J. Appl. Physiol. Bethesda Md 1985 *88*, 2219–2226.

Winslow, M.M., Pan, M., Starbuck, M., Gallo, E.M., Deng, L., Karsenty, G., and Crabtree, G.R. (2006). Calcineurin/NFAT signaling in osteoblasts regulates bone mass. Dev. Cell *10*, 771–782.

Wolkenstein, P., Durand-Zaleski, I., Moreno, J.C., Zeller, J., Hemery, F., and Revuz, J. (2000). Cost evaluation of the medical management of neurofibromatosis 1: a prospective study on 201 patients. Br. J. Dermatol. *142*, 1166–1170.

Xu, G.F., O'Connell, P., Viskochil, D., Cawthon, R., Robertson, M., Culver, M., Dunn, D., Stevens, J., Gesteland, R., and White, R. (1990). The neurofibromatosis type 1 gene encodes a protein related to GAP. Cell *62*, 599–608.

Xue, B., Moustaid-moussa, N., Wilkison, W.O., and Zemel, M.B. (1998). The agouti gene product inhibits lipolysis in human adipocytes via a Ca^{2+}-dependent mechanism. FASEB J. *12*, 1391–1396.

Yablonka-Reuveni, Z. (2011). The Skeletal Muscle Satellite Cell. J. Histochem. Cytochem. *59*, 1041–1059.

Yamamoto, L.G. (2004). Case Based Pediatrics for Medical Students and Residents (AuthorHouse).

Zammit, P.S. (2008). All muscle satellite cells are equal, but are some more equal than others? J. Cell Sci. *121*, 2975–2982.

Zammit, P.S., Relaix, F., Nagata, Y., Ruiz, A.P., Collins, C.A., Partridge, T.A., and Beauchamp, J.R. (2006). Pax7 and myogenic progression in skeletal muscle satellite cells. J. Cell Sci. *119*, 1824–1832.

Zhang, J., Nuebel, E., Daley, G.Q., Koehler, C.M., and Teitell, M.A. (2012). Metabolic regulation in pluripotent stem cells during reprogramming and self-renewal. Cell Stem Cell *11*, 589–595.

Zhu, Y., Romero, M.I., Ghosh, P., Ye, Z., Charnay, P., Rushing, E.J., Marth, J.D., and Parada, L.F. (2001). Ablation of NF1 function in neurons induces abnormal development of cerebral cortex and reactive gliosis in the brain. Genes Dev. *15*, 859–876.

8. Abbreviations

A	adenine
A. bidest	Aqua bidest
ALP	alkaline phosphatase
ANOVA	analysis of variance
bp	base pairs
BMP	bone morphogenic protein
BSA	bovine serum albumin
C	cytosine
°C	degree Celsius
Ca^{2+}	calcium ion(s)
cDNA	complementary DNA
Col IV	collagen type IV
Cre	Cre recombinase
cRNA	complementary RNA
CSA	cross sectional area
DAPI	4',6-diamidino-2-phenylindole
DEPC	diethylpyrocarbonate
DIG	digoxygenin
DMEM	Dulbecco´s modified eagle medium
DMSO	dimethylsulfoxide
DNA	deoxyribonucleic acid
dNTP	deoxyribonucleotide
dpc	days post coitum
E	embryonic stage
ECL	enhanced chemiluminescence
EDL	Extensor digitorum longus
EDTA	ethylenediaminetetraacetic acid
e.g.	for example
Erk	extracellular signal regulated kinase
EtOH	ethanol
Fab	fragment antigen-binding
FCS	fetal calf serum
Fgf	fibroblast growth factor
Fig.	figure
fw	forward
g	gram
G	guanine
GAP	GTPase activating protein
GDP	guanosine-5`-diphosphate
GEF	guanine nucleotide exchange factor
GRD	GAP-related domain
GTP	guanosine-5`-triphosphate

h	hour(s)
HRP	horse-radish peroxidase
i.e.	id est (that is)
IHC	immunohistochemistry
ISH	*in situ* hybridisation
k	kilo (prefix)
kb	kilo-bases
kDA	kilodalton
KO	knock-out
l	liter
LamA	laminin type A
loxP	locus of X-over P1
m	metre
m	milli (prefix)
M	molar
µ	micro (prefix)
MAPK	mitogen activated proteine kinase
Mb	mega-bases
MEK	MAP/ERK kinase
MeOH	methanol
min	minute(s)
mol	moles
MRF	muscle regulatory factor
mRNA	messenger RNA
mTmG	membrane-targeted tandem dimer Tomato (mT) prior to membrane-targeted green fluorescent protein (mG)
My	myosin
MyEmb	embryonic myosin
Myf	myogenic factor
MyHc	myosin heavy chain
MyoD	myogenic differentiation
Myog	myogenin
n	nano (prefix)
NBT	nitro blue tetrazolium
Nf1	neurofibromin
Nf1	murine *Nf1* gene encoding for neurofibromin
NF1	neurofibromatosis I
NF1	human *NF1* gene encoding for neurofibromin
Nfat	nuclear factor of activated T-cells
NI	not investigated
NIH	National Institutes of Health
NS	not significant
OXPHOS	oxidative phosphorylation
p	pico (prefix)
p	probability
P2	postnatal day 2

P21	postnatal day 21
P156	postnatal day 156
PAGE	polyacrylamide gel electrophoresis
Pax	paired box
PBS	phosphate-buffered saline
PCR	polymerase chain reaction
PFA	paraformaldehyde
pH	potentium hydrogenii
PI3K	phosphatidylinositol-4,5-bisphosphate 3-kinase
qPCR	quantitative PCR
RAS	rat sarcoma
rcf	relative centrifugal force
rev	reverse
RNA	ribonucleic acid
rpm	revolutions per minute
rRNA	ribosomal RNA
RT	Reverse Transkriptase
RT	room temperature
RTK	receptor tyrosine kinase
RT-PCR	reverse transcription PCR
S	soleus
SDH	succinate dehydrogenase
SDS	sodium dodecyl sulfate
sec	second(s)
SSC	saline sodium citrate buffer
T	thymine
TCA	tricarboxylic acid cycle
TA	tibialis anterior
Tab.	table
Taq	Thermus aquaticus
TB	triceps brachii
TEA	triethanolamin
Tris	tris-(hydroxymethyl-)aminoethan
TSA	tyramide signal amplification
U	units
UV	ultraviolett
V	Volt
WB	western blot
WM-ISH	whole mount *in situ* hybridisation
Wnt	wingless-related MMTV integration site
WT	wild-type

9. Appendix

9.1 Acknowledgements

I thank all the people who supported me in the course of working on this thesis!

First of all, I would like to thank Professor Roland Lauster for accepting my work for reviewing, for exceptionally friendly and helpful counselling and for helping with organising the graduation process.

Writing the thesis was only possible because I had the fantastic opportunity to work in the research group of Professor Stefan Mundlos at the Max Planck Institute. Thank you, Professor Mundlos, for allowing me to work in your group for four years! I learned a lot and had a wonderful time not least because of the helpful supervision of Professor Sigmar Stricker, who supported me with helpful advices, fruitful discussion and practical help during my last three years. For supervision in my first year, I thank Dr. Mateusz Kolanczyk, who worked me into the topic of Nf1 and histology.

I want to express my biggest acknowledgements to the research group Mundlos as the team I was working with. Thanks to all of you for the fabulous work spirit, your unlimited helpfulness and friendly ways! Seeing all of you was a great joy every day. "Schön, schön, schön!" is all that I can say. Special thanks to Sigmar, Norbert, Pedro and Saniye for teaching me patiently laboratory techniques. Thank you very much! Also, I want to mention Sinje, Hendrikje, Daniel, Till, Katerina, Ivana, Alejandro and Martin - thanks for good advices, discussions and brightening up laboratory routine!

Furthermore, I thank the Electron Microscopy Group of the Max Planck Institute for developing protocols and carefully investigating my countless tissue samples!

For "external" support I want to send my biggest thanks to my wonderful family, especially my parents who have always believed in me.

The biggest support I received from "my best friend" Victor, the greatest mental guide and mouse photographer I know. Thank you!

9.2 Publications

Multiscale, converging defects of macro-porosity, microstructure and matrix mineralization impact long bone fragility in NF1.

Kühnisch J, Seto J, Lange C, Schrof S, Stumpp S, Kobus K, **Grohmann J**, Kossler N, Varga P, Osswald M, Emmerich D, Tinschert S, Thielemann F, Duda G, Seifert W, El Khassawna T, Stevenson DA, Elefteriou F, Kornak U, Raum K, Fratzl P, Mundlos S, Kolanczyk M

PLoS One. 2014 Jan 21;9(1):e86115. doi: 10.1371/journal.pone.0086115. eCollection 2014.

Neurofibromin inactivation impairs osteocyte development in Nf1Prx1 and Nf1Col1 mouse models.

Jirko Kühnisch, Jong Seto, Claudia Lange, Sabine Stumpp, Karolina Kobus, **Julia Grohmann**, Florent Elefteriou, Peter Fratzl, Stefan Mundlos, Mateusz Kolanczyk

Bone. 2014. Published online: 2014 June 16. DOI: http://dx.doi.org/10.1016/j.bone.2014.06.012